Avulsion process : stratigraphic and lithologic records - Application to the Amazon and Zaïre turbidite systems

Sandra Mansor

THÈSE / UNIVERSITÉ DE BRETAGNE OCCIDENTALE
sous le sceau de l'Université européenne de Bretagne

pour obtenir le titre de
DOCTEUR DE L'UNIVERSITÉ DE BRETAGNE OCCIDENTALE
Mention : très honorable
École Doctorale des Sciences de la Mer - Géosciences Marines

présentée par
Sandra Mansor

UMR-CNRS 6538 "Domaines Océaniques", IUEM
Laboratoire Environnements Sédimentaires, Ifremer

Le processus d'avulsion : Enregistrement stratigraphique et sédimentologique - Application aux éventails turbiditiques de l'Amazone et du Zaïre

Avulsion process : stratigraphic and lithologic records - Application to the Amazon and Zaïre turbidite systems

Thèse soutenue le 19 novembre 2009
devant le jury composé de :

Michel Lopez, Rapporteur
Professeur à l'Université Montpellier 2
Tadeu dos Reis, Rapporteur
Professeur à l'Université d'Etat de Rio de Janeiro
Christophe Delacourt, Examinateur
Professeur à l'Université de Brest
Mike Sweet , Examinateur
Chercheur à ExxonMobil
Nathalie Babonneau , Examinateur
Maître de Conférence à l'Université de Brest
Bernard Dennielou, Tuteur
(remplacement de Bruno Savoye)
Chercheur à Ifremer
Laurence Droz, Directrice
Chercheur CNRS à l'Université de Brest

« Si on se limite à décrire la réalité, on ne rencontre aucun obstacle. Mais le problème consiste bien plus à repérer en elle ce qui a du sens pour nous, ce qui est surprenant dans l'ensemble des faits. Si les faits ne nous surprennent pas, ils n'apporteront aucun élément nouveau pour la compréhension de l'univers : autant donc les ignorer ! » (René Thom, Paraboles et catastrophes)

Acknowledgment - Remerciements - Danksagung

Mon travail présenté dans ce mémoire a été effectué au Laboratoire des Environnements Sédimentaires du département Géosciences Marines d'Ifremer (Institut français de recherche pour l'exploitation de la mer) et au Laboratoire des Domaines Océaniques - UMR 6538 - de l'IUEM (Institut Universitaire Européen de la Mer) à Plouzané en France. Cette thèse s'inscrit dans une collaboration académique et industrielle et a été cofinancée par le partenaire industriel ExxonMobil. J'ai eu également l'opportunité de passer un séjour de trois mois au sein de l'équipe « Stratigraphy Core Group » d'ExxonMobil Exploration Company à Houston, Texas aux Etats-Unis.

Je remercie les collègues, qui à divers titres et en diverses circonstances m'ont accueilli et qui ont su me faire bénéficier de leur expérience.

J'exprime mes sincères remerciements à Laurence Droz et Bruno Savoye qui m'ont permis d'apprendre, d'avancer et de réaliser cette thèse.

Je remercie aussi les membres du jury de m'avoir donné l'occasion de défendre ce travail au cours de ma soutenance de thèse.

Mes meilleures pensées et toute ma reconnaissance à tous ceux, amis ou famille, qui m'ont accompagné ou qui ont marqué mon chemin.

Un mot à Norah et Hervé : Danke.

Et des pensées particulières pour Bruno et sa famille.

Sandra

Table of contents

-Introduction-

As rivers flow across the landscape they pick up and transport sediments, ranging from pebbles to very fine sand and mud. Part of the sediments is deposited upstream, part will continue downstream and as rivers reach the sea, sediments will be deposited at the estuaries (Figure 1). Depending of the local physical conditions of currents, tides and waves, sediments will be washed away from the river mouth, moved along the coast or out to the sea, or the sediment may build up lagoons, barriers islands or deltas.

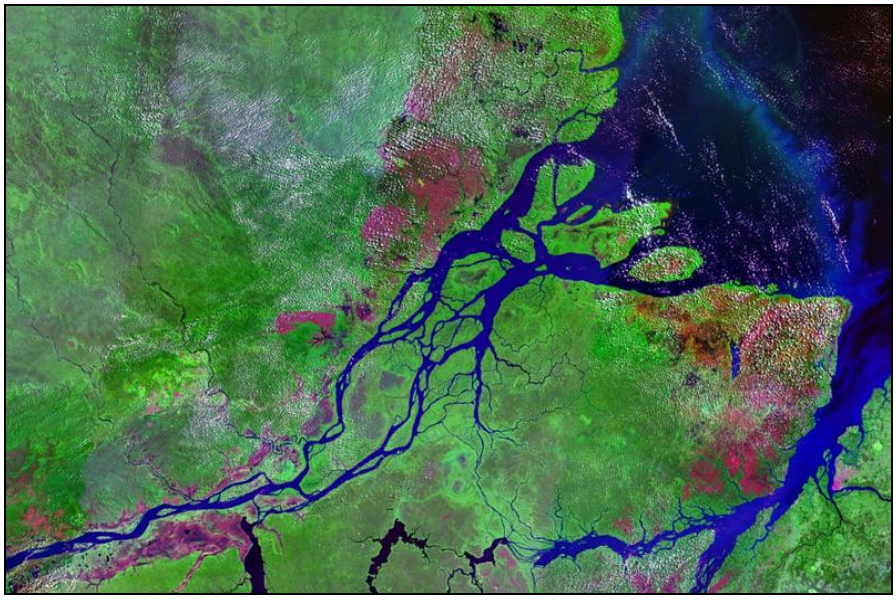

Figure 1: Amazon River estuary (source Wikipedia, screenshoot taken from NASA's globe software World Wind)

A component of the sediment will be transported further into the basin by a variety of gravity-driven processes (Figure 2) on the slope: slumps or debris flows (non-channelized systems) or avalanches or turbidity current along an incised canyon or a network of canyons (channelized systems). At the base of the continental slope, where canyons end, a deep sea fan can be formed.

Major deep-sea fans have been built from vertical and lateral stacking of the following elements with associated features, interspersed with mass-flow deposits:

- Channels, serve as pathways for turbidity currents and other sediment-gravity flows to transport and deposit sediments further in the deep-sea,
- Levees representing sediments coming from overflow currents of the channels,
- Lobes, representing sediments deposited in lobate bodies, mainly at channel-ends.

The distal lobes are the areas where sediments end their travel from the continent.

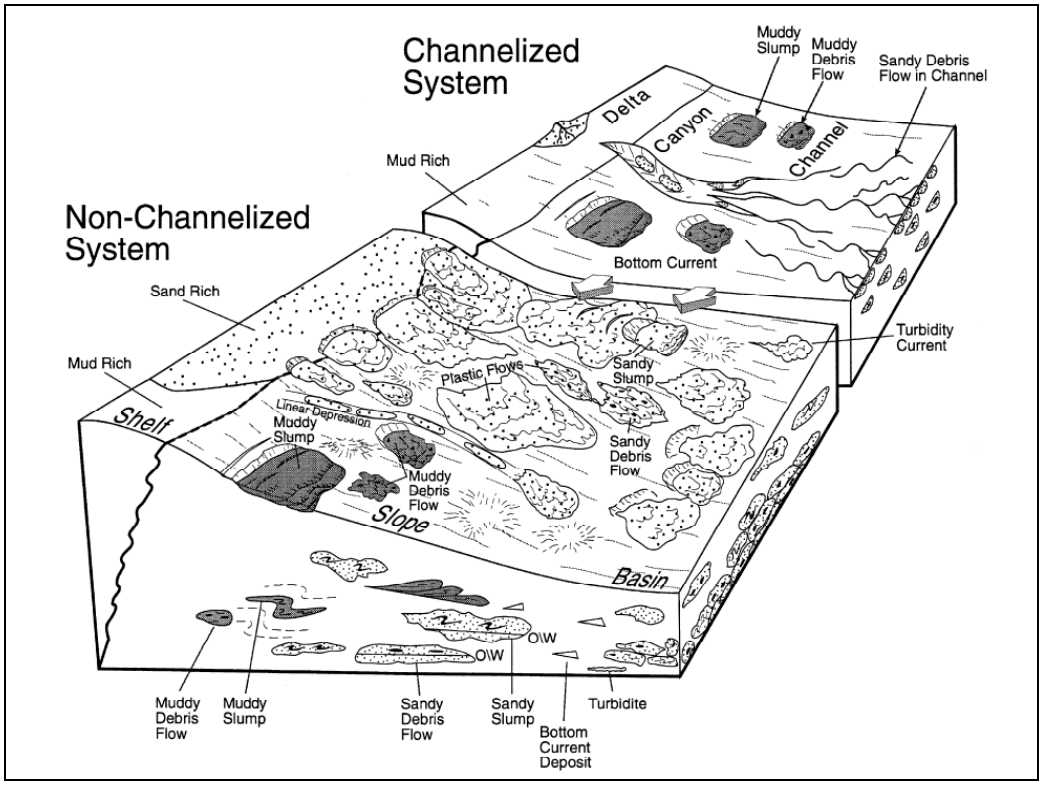

Figure 2 : Gravity processes on passive margins (Shanmugam, 2000).

This study will be focused on Avulsion, one of the “end of chain” processes of sediment transport and deposition from continent to the deep basins, explaining the distribution of depocenters and the sediment partitioning in deepwater, provoking the abandonment of a channel and the birth of a new one. This process is mentioned since the 50s, where migration of a turbidity-current channel to some less elevated sector (Figure 3) is suggested in analogy to subaerial stream channel. Low levee sides, interpreted to result from the influence of the Coriolis force, are suggested to favor the breaking out of the turbidity currents (Menard, 1955).

Beside the analogy to subaerial channels, the first true indicator of avulsions in deepwater was the detection of the HARPs, a seismic term, firstly introduced by Flood et al. (1991). HARPs are packets of high-amplitude reflectors at the base of channel-levee systems. HARPs were suggested to be sandy deposits and related to the avulsion process in deep-sea fan environments because of their disposition in lows adjacent to the breached parent channel. The avulsion process concerns the sediment distribution associated with channel shifting within channel-levee complexes.

Therefore, avulsion is an important process controlling the architecture of deepwater deposits and understanding the avulsion process in deepwater is the aim of this thesis.

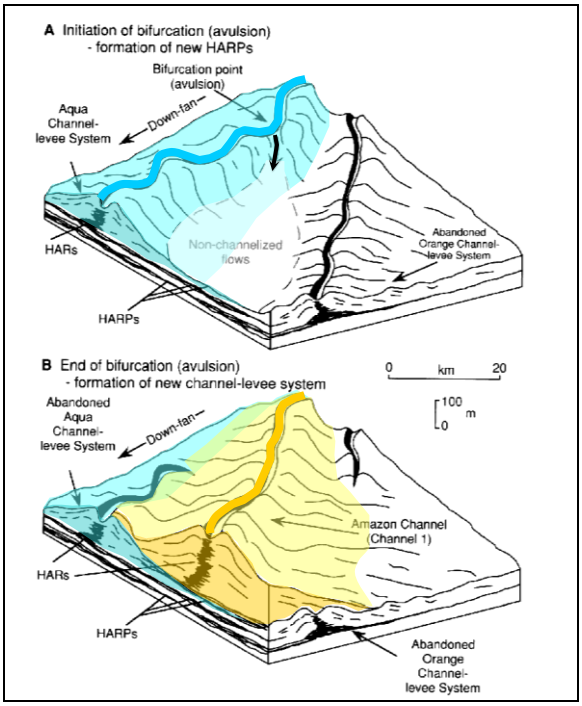

Figure 3: Diagram showing the development of a channel (channel 1) by avulsion of the parent channel (channel Aqua) (Flood et al., 1991).

Besides of their academic interest, these studies also bear an applied interest because they are potential areas for hydrocarbon reservoirs. Even though most of the world has begun a transition from conventional oil and gas energy toward alternative energy sources, it is expected that the means of world energy survival will still depend on hydrocarbon supplies for probably the next century (Halbouty, 2001).

Framework of this thesis

During the last 30 years, study of the continental margins has been one of the main research objectives of IFREMER's and Laboratoire Domaines Océaniques, while the oil industry has been increasingly focusing on deep-offshore energy resources (Pettingill and Weimer, 2002). At the end of 1997, IFREMER and TOTAL launched a 5-years research program devoted to studying the continental margin seaward of Gabon, Congo and Angola, with particular emphasis on exploring the huge submarine valley network carved in the ocean floor offshore the Congo River mouth. The ZaïAngo project, under the leadership of B. Savoye, was intended to study, at a regional scale, the recent Zaïre (Congo) fan in order to acquire an integrated regional understanding of sedimentary processes controlling the distribution and the characteristics of the reservoirs, from the river mouth to the distal areas. Different studies have been undertaken about the overall fan stratigraphy and channel avulsions (Droz et al.,

2003), the morphology of the present canyon and channel system and sedimentary processes (Migeon, 2000, Babonneau, 2002, Gervais et al., 2001, Migeon et al. 2004, Bonnel, 2005).
Based on the Zaïre experience, a new project has been realized on the Amazon Fan in 2004 (Lobestory cruise) under the responsibility of B. Savoye.
The aim was to acquire complementary data of this zone in order to find answers to questions that were addressed by the results of the Zaïre Fan and the state-of-the art knowledge about deep-sea fans in the academic world, concerning in particular: (1) the distal lobes, a domain that remained unknown at that time and has now been studied by Jégou (Jégou, 2008; Jégou et al., 2008) in the framework of her thesis, (2) the avulsion process, which is associated to the HARP deposits and is one of the main cause for the lateral distribution of sediments.
The avulsion process has been studied in my work funded by ExxonMobil, under the tutoring of B. Savoye and L. Droz.

The Amazon Fan is one of the biggest and most studied deep-sea fans of the world. But despite these works, the avulsion process remained insufficiently understood. Kolla (2007) mentioned in a paper reviewing channel avulsion patterns in some major deep-sea fans, that “in the Amazon Fan is felt that existing published ODP data (Flood and Piper, 1997) need to be re-examinated in order to evaluate whether or not extra- or intra-basinal factors affected timing of specific channel avulsions”.

The Lobestory campaign in 2004, acquired high-resolution data on the Quaternary Amazon Fan, crossing 9 ODP sites, with the aim to re-evaluate the lithostratigraphic recording of ODP and to describe at a smaller seismic scale the famous HARPs of the Amazon Fan.
The combination of the ODP drillings and the newly acquired high-resolution multichannel seismic data has made the Amazon Fan an ideal study area to refine the avulsion model proposed by Flood et al (1997).

We also studied the avulsion process in the Zaïre Fan, comparable in size to the Amazon Fan because previous studies had shown that early stages of channel avulsion were probably observed.
The two fans revealed complementary observations that allowed to highlight some new findings and to propose a refined model for the avulsion process.

-Chapter I-

A review of sediment transport in deepwater

1 TURBIDITY CURRENTS: THE MAIN MECHANISM FOR SEDIMENT TRANSPORT IN TURBIDITE SYSTEMS

Investigation of deep-sea sediments began with the voyage of the Challenger (1872-1876) which established the general morphology of the ocean basins, published by Murray and Renard (1891). Oceans were considered to have quiet, undisturbed floors where only pelagic and hemipelagic sediments were deposited. All sandstones were thought to have been deposited in shallow waters. Today we know, thanks to studies of the last century about deep-sea sedimentation, that morphologies on passive margin slopes are a result of a combination of pelagic settling, bottom currents accumulations and gravity flow deposits that are able to transport coarse sediments to the deep-sea.

1.1 TURBIDITY CURRENTS

Gravity flows have been well studied (e.g. Middleton and Hampton, 1973; Lowe, 1982; Mulder and Cochonat, 1996; Shanmugam, 2000; Stow and Mayall, 2000) and can be classified into three main groups: (1) mass movements (creeping, slides and slumps), (2) laminated or plastic flows (debris flows, grain flows, fluidized flows, liquefied flows), (3) turbulent flows (turbidity currents) that deposit turbidites. It is generally accepted that turbidites are the most common deposits in the deep-water clastic systems (Stow and Mayall, 2000). Turbidity currents are mixtures of sediment and water, which move under gravity due to the density contrast with the less dense medium of seawater or fresh water. They are also less dense than debris flows and hence have a higher Reynolds number.

The turbidity current concept was introduced by Kuenen and Magliorini (1950) in their paper “Turbidity currents as a cause of graded bedding”. Previously to the in-situ observations or records of these currents (e.g. Shepard et al., 1977), they were inferred from observations of breaks of submarine telegraph cables (Heezen and Ewing, 1952). The period from the 1950 to the 1980s was a time of conceptual model building for the deposits of turbidity currents. Models are constantly re-evaluated by new findings from deep-water sedimentology and sequence stratigraphy research.

The anatomy of gravity currents, including turbidity currents, is described in numerous studies (e.g. Allen, 1971; Britter and Simpson, 1978; Kneller and Buckee, 2000), often based

on experimental works in laboratory. Gravity currents are described as having a head, a body and in some cases a tail (Figure I.1).

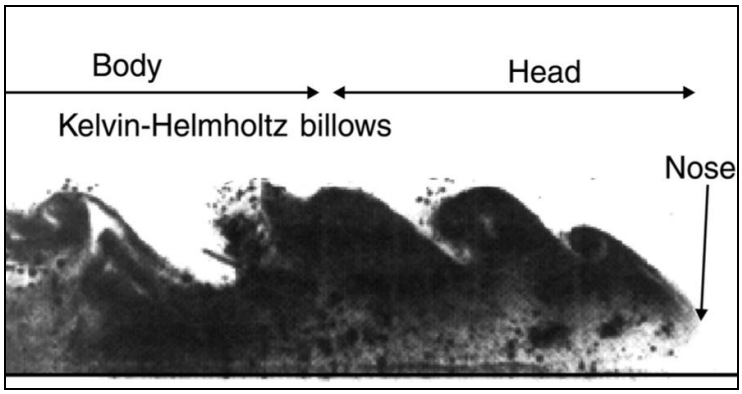

Figure I.1: 2-D image of a gravity current. In Kneller and Buckee (2000), modified from Simpson (1969).

- The head is erosional and has an overhanging nose. The head height increases with slope, as the body velocity increases and material moves more rapidly into the head. Mixing of the current with the ambient fluid is an important process that occurs at the head, primarily by the entraining of dense fluid out of the back of the head in a series of transverse vortices, identified as Kelvin-Helmholtz instabilities.
- The body is divided into a basal dense layer, and an overlying less dense region of mixed fluid that has been mixed out of the head of the current. This density stratification is indicated by the measured concentration profile inside the gravity flows (Figure I.2).

A number of models for the distribution of density in gravity currents have been proposed (e.g. Middleton, 1966; Postma et al., 1988; Garcia and Parker, 1993).

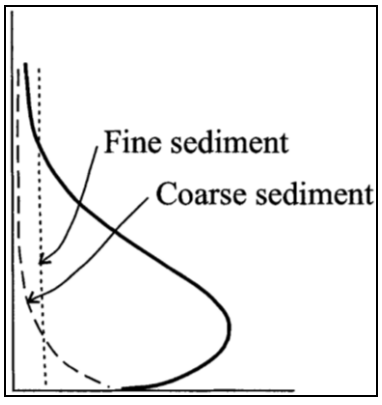

Figure I.2: Density/concentration profile (dashed line) and velocity profile (solid line) in turbidity currents. In Kneller and Buckee (2000), modified from Peakall et al. (2000) and García (1994).

Figure I.2 provides a typical distribution of sediment grain-sizes observed in turbidity currents, in which coarse material is concentrated in the lower part of the flow (high-density

turbidity current) whereas fine-grained material is distributed throughout the flow column and becomes dominant in the upper part (low-density turbidity current).

The classification of turbidity currents by Mulder and Alexander (2001), based on the cohesion of the particles, flow duration, sediment concentration and particle-support mechanism, defines a turbidity current as a non-cohesive flow, where the fluid turbulence is the main particle transport mechanism. The classification assumes that any flow may change in type with time and at any time, in both down and across flow directions. Turbidity currents can be subdivided on the basis of their flow behaviour into surge flows and surge-like turbidity flows, corresponding to very-short-duration flow events (few tens of hours in a large event), and quasi-steady hyperpycnal turbidity currents, where the flow is fed by prolonged river flow with a duration of hours to months (Mulder and Syvitski, 1995; Mulder and Alexander, 2001), (Figure I.3).

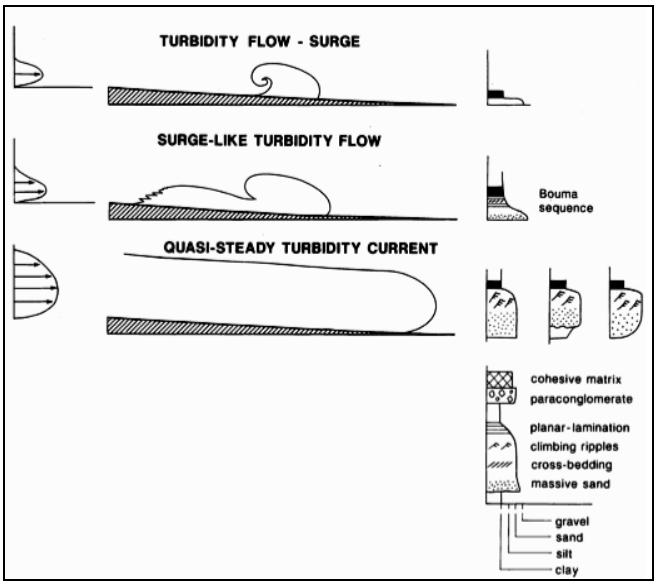

Figure I.3: Turbidity flows (middle) with corresponding velocity profile (left) and deposits (right). Detail of the classification of Mulder and Alexander (2001).

1.2 TURBIDITES

Much of our knowledge of turbidity currents is inferred from their deposits: the turbidites. The first model of turbidity current deposits was published by Bouma (1962) who proposed after the work of Kuenen and Magliorini (1950, see p.9) a vertical facies model for turbidites, which is commonly referred to as the "Bouma Sequence" or "classic turbidite" for the internal structures in individual turbidites.

The sequence represents a normally graded deposit (Ta to Te divisions, Figure I.4)

- Ta to Tc intervals are deposited from a waning flow (Harms and Fahnestock,

1965; Walker, 1965). Ta is generally structureless sand implying rapid deposition, whereas Tb and Tc imply traction of grains on the bed to form parallel lamination and ripple cross lamination in sand, respectively.

- Td and Te represent deposition of fine-grained material from suspension without traction on the bed. Td consists of thin laminae of silt and clay, and Te is pelitic, probably mainly turbidity-current mud with a small proportion of hemipelagic mud.

Stow and Shanmugam (1980) added a more detailed division for the silt-mud facies of low-density turbidity currents to the original model and Lowe (1982) expanded it for the coarse-grained turbidite fractions of high-density turbidity currents.

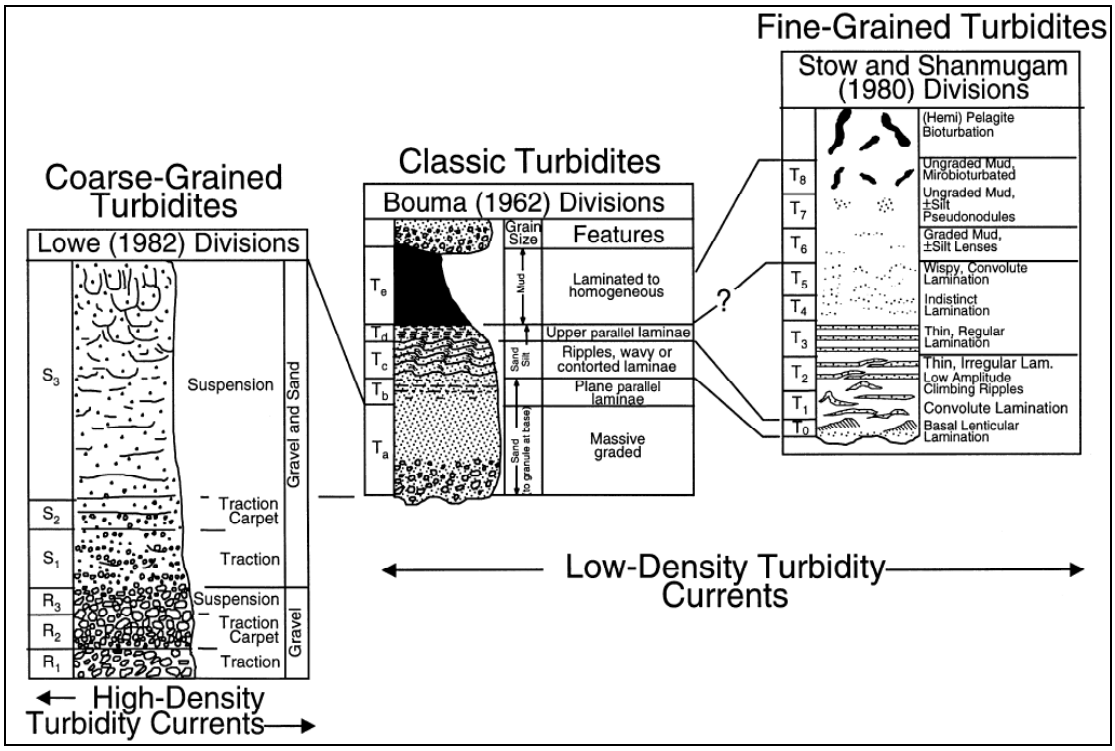

Figure I.4: Existing vertical facies models of coarse grained turbidites (Lowe, 1982), classical turbidites or Bouma Sequence (Bouma, 1962), and fine-grained turbidites (Stow and Shanmugam, 1980). In Shanmugam (2000).

2 DEEP-SEA FANS

Deep-sea fans are distinctive constructional features on the sea floor that develop seaward of a major sediment point source, such as a river, delta, alluvial fan or glacial tongue, or beyond a main cross-slope support route, such as a canyon, gully or through at the base-of-slope (Reading, 1996). They are composed of gravity flow deposits, in particular turbidites.

2.1 MODELS

In the 70s, two approaches to developing models for deepwater deposits appeared: (1) ancient fan models based on outcrop studies (Mutti and Ricci Lucchi, 1972) and (2) models based on seismic studies of modern submarine fans (suprafan model, Normark, 1970). Both approaches were combined by Walker (1978) in a single model where the main morphologic features (feeder channel, upper fan, mid-fan/suprafan lobes, lower fan, levees) are characterized by their verticale lithological successions (Figure I.5). This approach proved to be too simplistic because controlling factors, like sea level variations and the nature of the sediment supply, were not included and it was subsequently refined as more and more data from modern submarine fan systems became available.

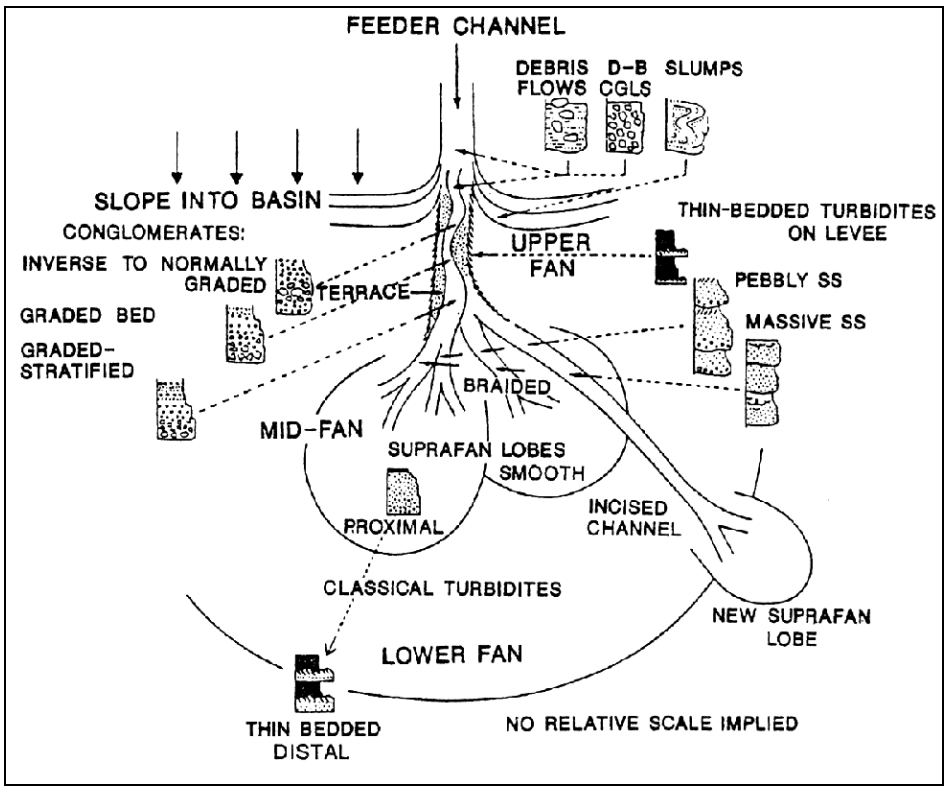

Figure I.5: Deep-sea fan model of Walker (1978).

Around the 80s, the fan models were updated with the progress of sequence stratigraphy concepts by integrating the effects of sea level fluctuations as a mechanism to get sediment across the shelf (e.g. Vail et al., 1977; Posamentier et al., 1991). At this time, seismic-based models replaced more and more the field-based models, influenced by the technologic advancement in marine geology. So, during the 80s a series of 2D-seismic study on deep-sea fans have been published (see the compilation “Seismic Facies and Sedimentary Processes of Submarine Fans and Turbidite Systems” of Weimer and Link, 1991). Many parameters such as basin size and shape, duration of activity of the source, sediment nature

etc., which are unique to a system, were taken into account to accommodate the complexity of deep-water clastic systems. For example, Reading and Richards (1994), classified the deep-water clastic systems on the basis of volume and grain size of available sediment, and the number of input points (Figure I.6).

Shanmugam (2000) explains in his paper the difficulty of a general model due in particular to the variable facies distribution "The applicability of a facies model depends on its generalization. The more general a facies model gets, the more applicable the model becomes beyond its origination point. On the other hand, the more precise a facies model gets, the less applicable the model becomes beyond its birthplace. For these reasons, generalists tend to lump and diffuse the details, whereas purists prefer to split the details (…). The challenge in constructing useful facies models has always been where to draw the line between lumping and splitting. This is particularly true for deep-water systems because of their highly complex and variable facies distribution."

Posamentier (2007) accents that any attempts at modelling of turbidite systems must incorporate information of four different types and scales: processes (flume experimental scale as well as modern fan scale), 3-D seismic studies, ancient rock descriptions and numerical models. He thinks, that future fan models will evolve as more work is done relating experimental studies to ancient rocks and relating the geometry of large outcrops to 3-D seismic data. As the seismic studies evolve, the large-scale processes of fan development will be better understood, and the future conceptual basis for modelling will be better established.

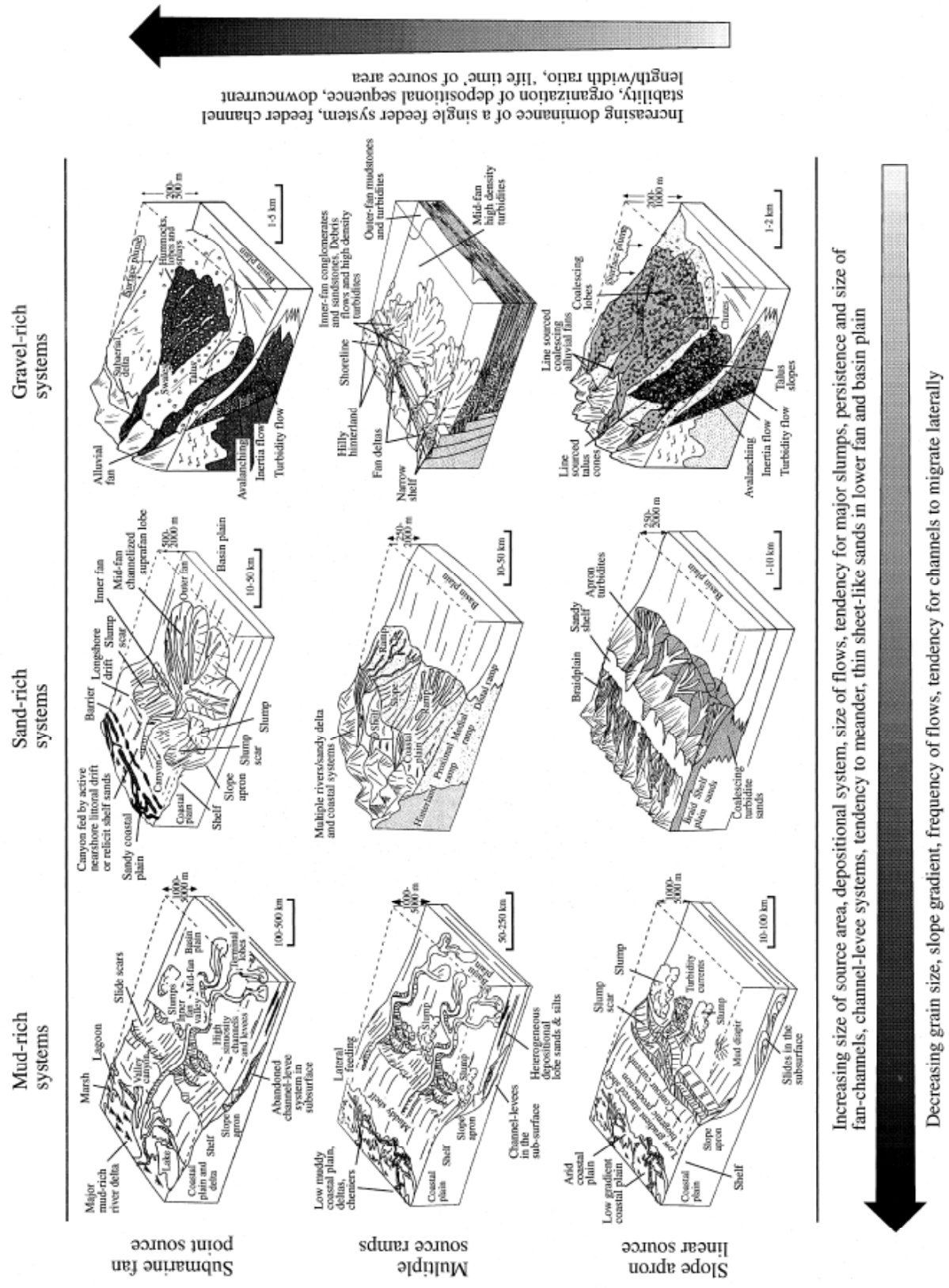

Figure I.6: Summary environmental models for submarine fans, classified on the main grain size of the supply sediments and number of input points. In Stow and Mayall (2000) after Reading and Richards (1994) and Stow et al. (1996).

2.2 DEPOSITIONAL ELEMENTS AND INVOLVED PROCESSES

Because many models of deep-water clastic systems proved to be too broad to place observed sub-environments into context, attempts were made to break systems down into their fundamental building blocks, or architectural elements (Miall, 1999).
Depositional element classification are based on a combination of seismic studies and of, when available, lithologic core information of modern deep-sea fans and outcrop studies of ancient deep-sea fans. The observations of modern and ancient fan are complementary in view of their different resolution due to the different data. The characterization of depositional elements is constantly in evolution, as new studies, particulary those based on 3-D seismic data, reveal new details. As a consequence, sub-classifications and various terminologies for architectural elements are applied (e.g. the various terminologies for a lobe: suprafan lobes, depositional lobes, fan lobes, ponded lobes, mounded lobes, sheet lobes, channel-mouth lobes, terminal lobes, distal lobes, frontal splays, crevasse splays, …) without proposing a general model for deep-sea fans.
In continuation of the depositional element classification of Mutti and Normark (1991), Posamentier and Kolla (2003) proposed the following key elements for turbiditic depositional elements: (1) turbidity-flow leveed channels, (2) channel-overbank sediment waves and levees, (3) frontal splays or distributary channel-complexes, (4) crevasse-splay complexes.
I will present in the following the principal characteristics of these depositional elements.

2.2.1 Leveed channels

Leveed channels are elongated negative features produced and maintained by turbidity currents. They represent pathways for sediment transport or deposition or both. The channel pattern is variable in width and sinuosity. Leveed channels can grow by lateral migration, down-system migration or by vertical stacking, and they can show a complex cut-and-fill architecture. Channel-fill deposition is commonly aggradational and often characterized by meander-loop migration. Leveed channels can be associated with overbank sediment waves, frontal splays or crevasse splays. In some cases levees can be absent and the flows can be completely confined by the erosional walls of the channel.

2.2.2 Levees

Levees are generally composed of fine-grained, thin-bedded turbidites coming from

overbanking processes of the channel, i.e. flow stripping. They commonly decrease in height from up- to down-fan (Skene et al., 2002). Levee height of inner bends can be lower than that of the outer bends. Some levees show sediment-waves that are best developed on outer bends (Migeon et al., 2006).

Based on earlier studies (e.g. Piper and Normark, 1983; Bowen et al., 1984; Normark and Piper, 1984; Hay, 1987; Hiscott et al., 1997), Peakall et al. (2000) differenciated two processes that lead to overbank deposits (Figure I.7):

1. **Flow stripping** (or inertial overspill), which is the process of turbidity flows escaping the confinement of the leveed channel towards outer bends due to super-elevation of turbidity flows resulting from centrifugal forces (Komar, 1973; Piper and Normark, 1983; Hay, 1987).
2. **Flow spilling** or continuous overspill, which occurs when an equilibrium is reached between entrainment of water through the upper interface of flows, loss of material on the levees, and change in channel depth or width (Hiscott et al., 1997). This equilibrium leads to long-distance overspill over significant parts of a channel.

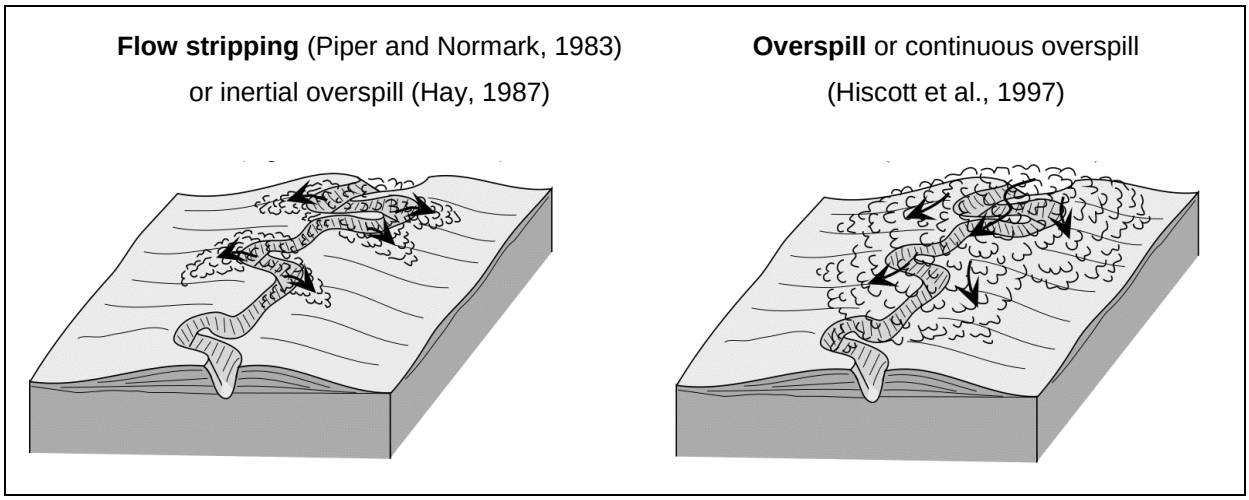

Figure I.7: Typical overbanking processes forming levees and associated features (in Babonneau, 2002).

Channel-levee systems can show different morphologies: symmetric [e.g. Petit-Rhône: Bellaiche et al. (1983), Amazon: Flood et al (1991), Zaïre: Babonneau et al. (2002)] or asymmetric [e.g. Var: Migeon, (2000)] development of the levees, aggradational [e.g. Amazon: Flood et al. (1991)] or incisional [Bengal: Hübscher et al. (1997), Zaïre: Babonneau (2002)] channel-levee systems. Beside, levees can show depositional features like sediment waves [e.g. Var: Migeon et al. (2000), Monterey: Fildani and Normark (2004), Zaïre: Migeon et al. (2004)].

2.2.3 Frontal splays or channel-mouth lobes

Some levee-confined channels are observed to feed relatively unconfined splay complexes that can display a distributary-channel pattern (Figure I.8). The term frontal-splay complex implies both a process of formation as well as a morphologic shape (Posamentier and Kolla, 2003).

These splays have been observed from mud-rich systems [e.g. Mississippi : Twitchell et al. (1995), Neofan of the Rhône: Kenyon et al. (1995b), Zaïre: Babonneau (2002), Bonnel (2005), Amazon: Jégou et al. (2008)] and sand-rich systems [e.g. Monterey Fan: Fildani and Normark (2004), Klaucke et al. (2004); Navy Fan: Normark et al. (1979), Piper and Normark (1983); Huneme and the Dume Fan: Piper et al. (1995), Normark et al. (1998), Piper et al. (1999); East-Corsica: Gervais et al. (2004); West-Corsica: Kenyon et al. (2002); Celtic Fan: Zaragosi et al. (2000); Valencia Fan: Morris et al. (1998)).

In settings characterized by relatively featureless sea-floor topography, splay complexes tend to develop a lobate planform. These splay complexes are thought to correspond to sheet sand deposits (Hackbarth and Shaw, 1994; Mahaffie, 1994) of unconfined flows. These deposits are also referred in the literature to channel-mouth lobes or channel-mouth lobe complexes, the term "complex" being used to designate several migrated or stacked lobes at the mouth stacked channel-levee systems (Jégou, 2008).

The transition zone from well-defined channel-levees to well-defined lobe deposits is called the Channel-Lobe Transition Zone (CLTZ, Mutti and Normark, 1987). The identification of this zone is based on morphologic characteristics, with frequent erosional and depositional features (scours, erosional lineations, sediment waves and mounds associated with scours) (Wynn et al., 2002).

The deposition of the frontal splays can be explained by the combination of two main topographical conditions associated to the CLTZ:

1. In this zone an abrupt decrease of slope gradient can occur and lead to a hydraulic jump (Komar, 1971; Garcia and Parker, 1989). The slope change causes a decrease of the velocity and therefore a thickening of the flows, especially the high-density basal sandy part of the flows (Posamentier, 2007) (Figure I.9).
2. In addition, because of the decreased levee height in this zone, the flows pass from laterally confined by levees to unconfined in the CLTZ, causing the basal sandy high-density part of the flow to overflow (Figure I.10).

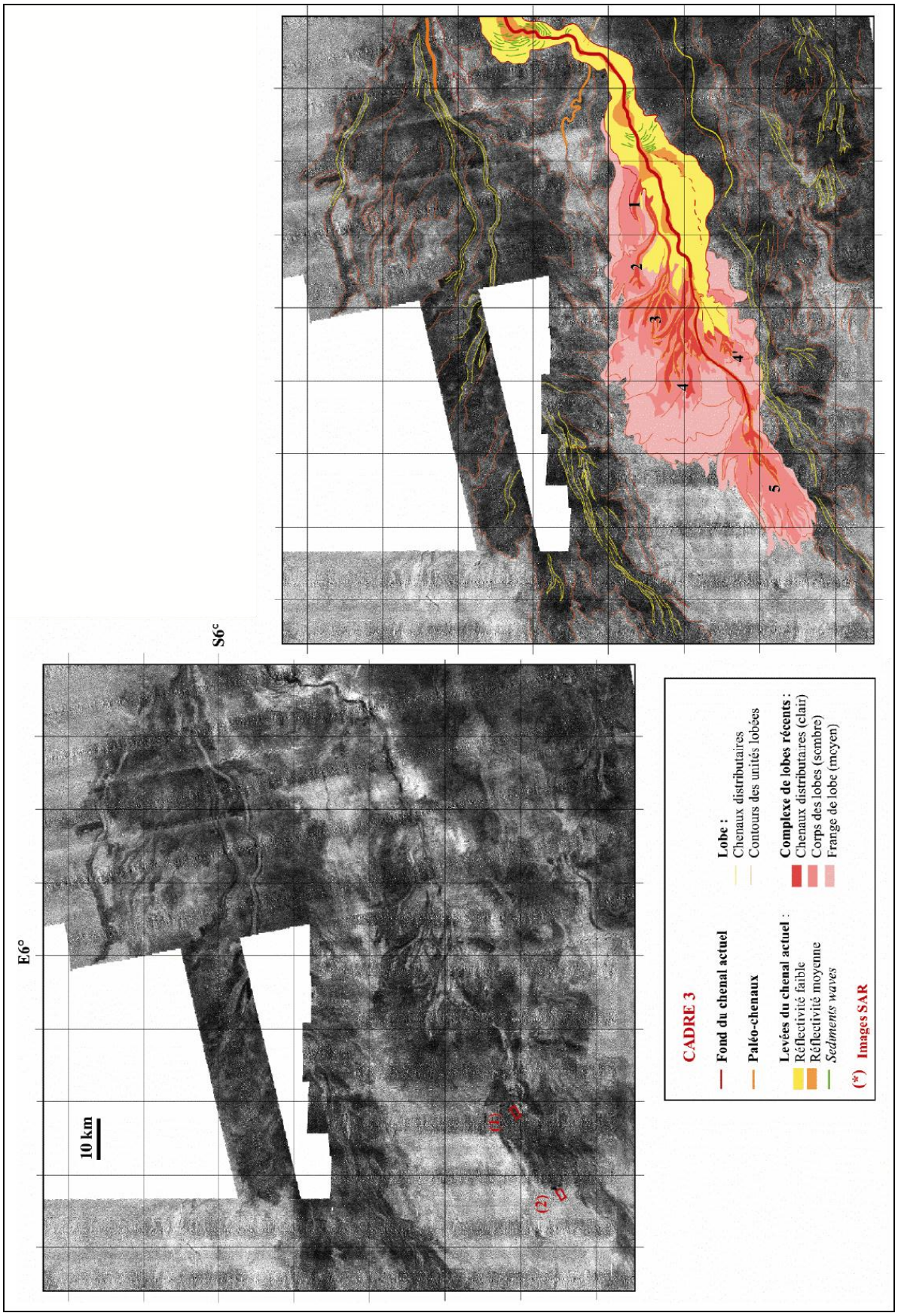

Figure I.8: Example of the lobes complex of the most recent Zaïre Channel showing a distributary channel pattern (Babonneau, 2002), suggested to be frontal-splay deposits.

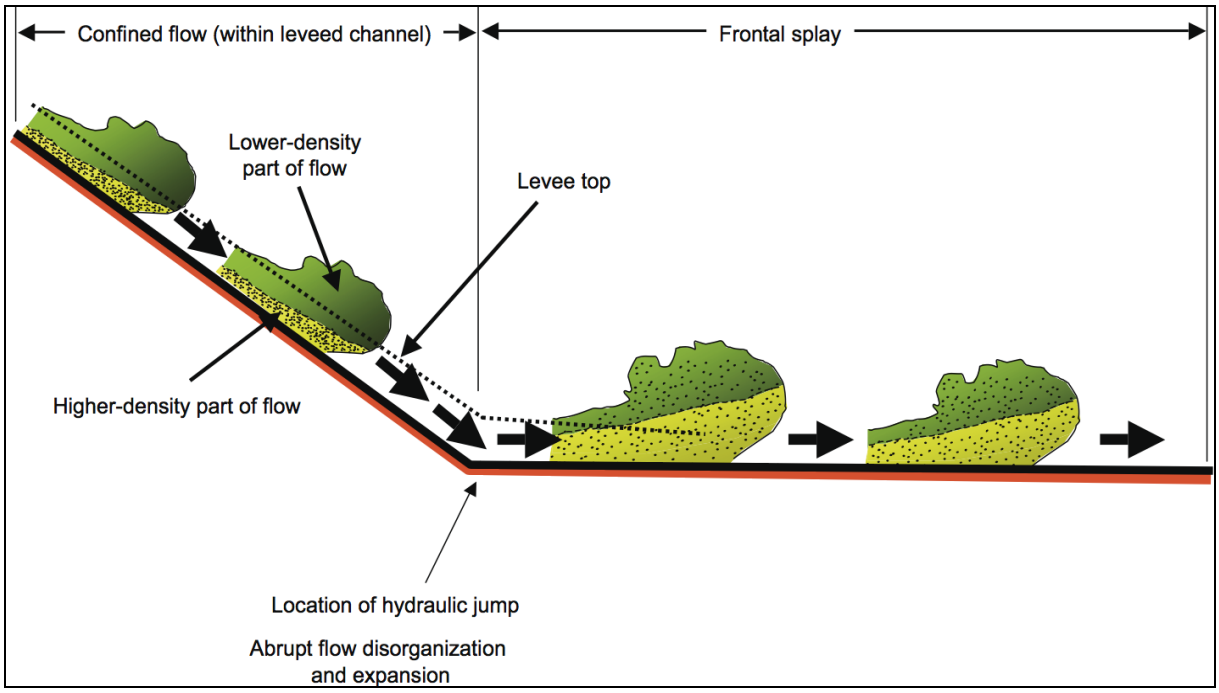

Figure I.9: Schematic view of the thickening of a turbidity current, caused by a hydraulic jump in the turbidity current due to a rapid change from high to low slope gradient. As a result the thickening of the basal high-density part can induce sandy overflows (Posamentier and Kolla, 2007).

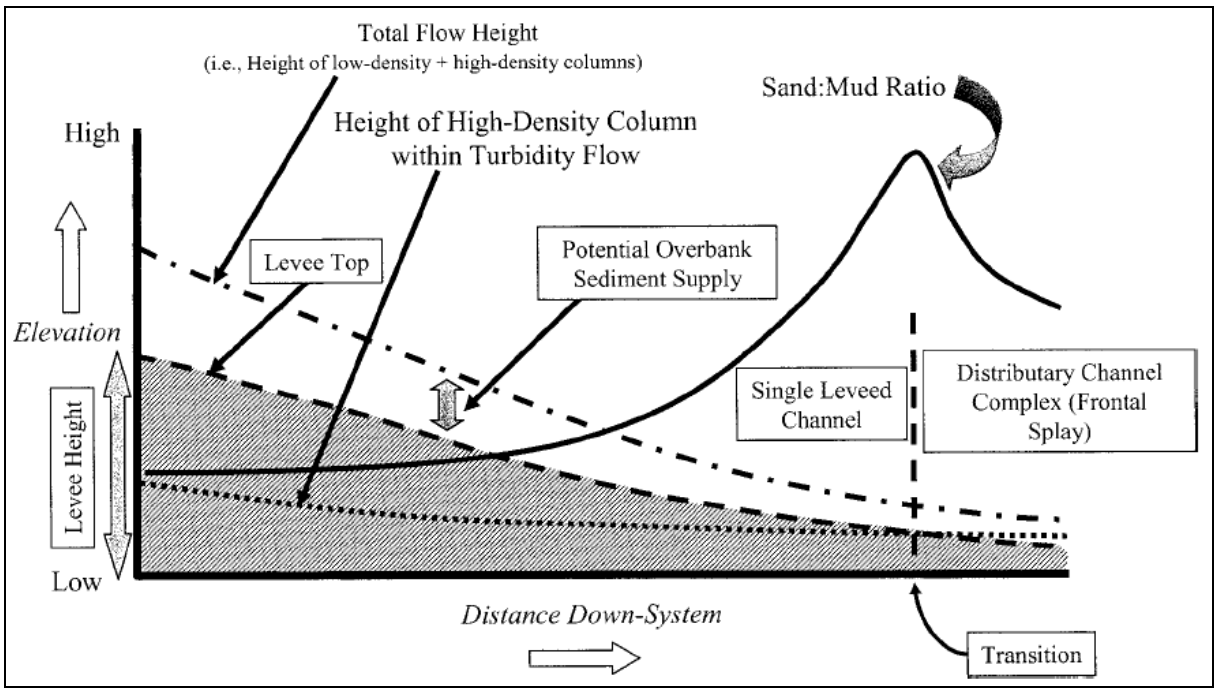

Figure I.10: Relationship between total turbidity flow height (dashed-doted curve), height of basal high-density part of the flow (doted curve), and levee height (dashed curve) (Posamentier and Kolla, 2003).

This effect can be amplified by a rapidly decreasing slope gradient (i.e. smooth but strongly concave-upward longitudinal profile) without a sharp gradient break. In this case, there is a tendency for flow vectors to be directed both downward and outward onto the channel floor

and against the levees. This increased lateral stress favors the formation of frontal splays. The greater the slope curvature, the greater the stress directed laterally against the levees and therefore the greater the likelihood of a transition from leveed channel to frontal splay. As a result, an increased slope curvature, i.e. a local or autocyclic parameter, results in a landward shift of the CLTZ (Posamentier and Kolla, 2003).

Mutti and Normark (1987) and Wynn et al. (2002) suggest that depending on the volume and sand:mud ratio of the flows, the lobes will be connected to the channel mouth (attached channel-mouth lobes deposited by sand-rich flows) or will be separated from the channel mouth by a by-pass zone (detached lobes deposited by mud-rich flows).
The CLTZ is supposed to migrate through time (Hübscher et al., 1997; Jégou, 2008) and Posamentier and Kolla (2007) propose that the CLTZ migrates in response to sea level variations that control the sand:mud ratio of the sediment supply, a basinward migration being associated to a decreasing sand:mud ratio during late lowstand of sea level (Figure I.11). The basinward shifting of the CLTZ results into a channel-levee progradation and aggradation over a former frontal splay.

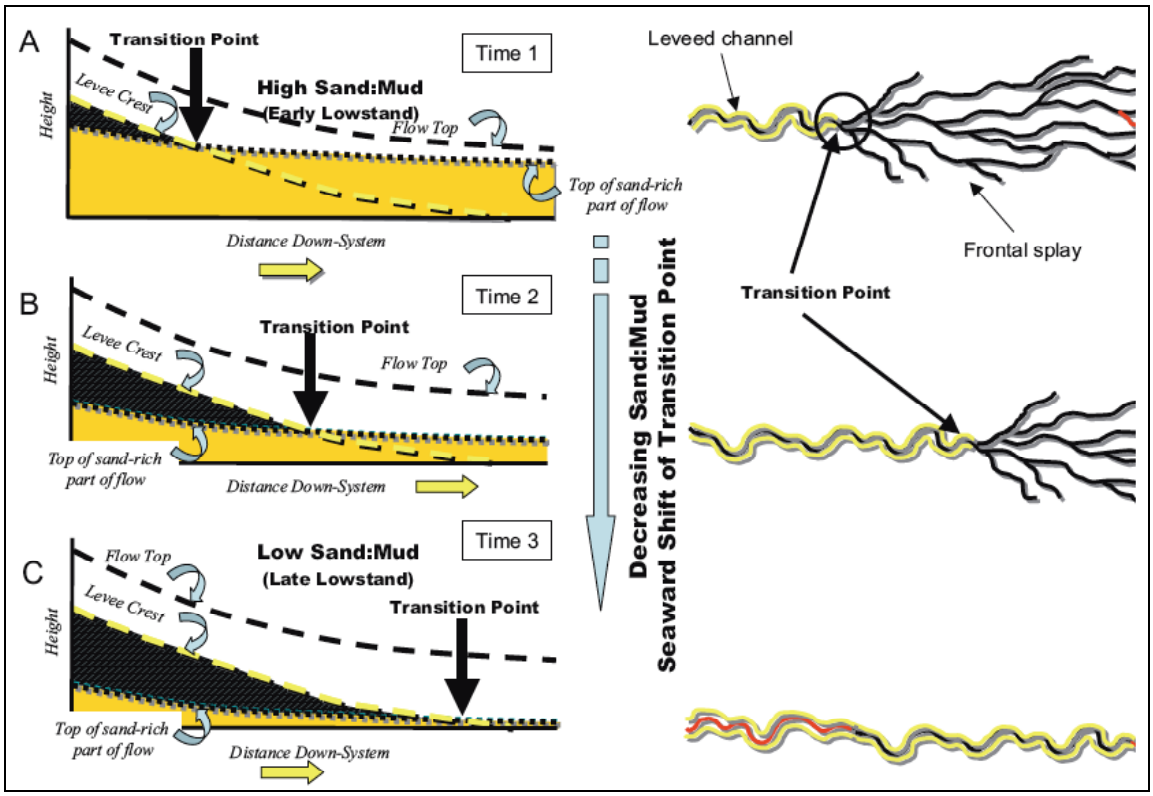

Figure I.11: Shift of the CLTZ (transition area from leveed channel to frontal splay) in response to changes in the sand:mud ratio of the flow, influenced by sea level variations (Posamentier and Kolla, 2007).

Posamentier and Kolla (2007) show an example that could be a result of such a process with a channel-levee system that overlies basal high-amplitude reflectors interpreted in that case as a frontal splay (Figure I.12).

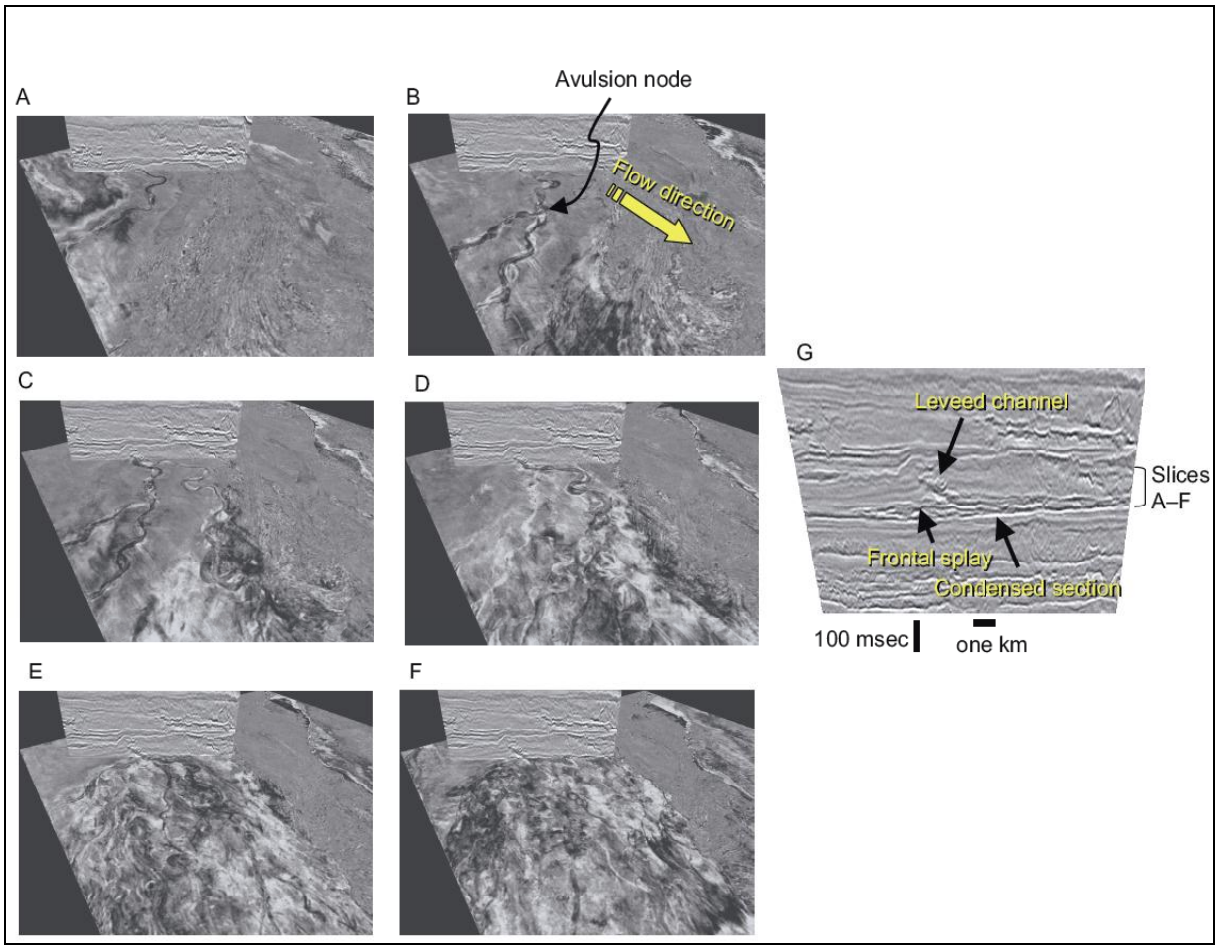

Figure I.12: Succession of horizon slices through a deep-water turbidite system, eastern Gulf of Mexico (A-F) with a cross-section view (G). A-F horizon slices illustrate the evolution of this system from an initial frontal splay (F), evolving into a channel-levee system (A).

2.2.4 Crevasse splays

Another form of overbank deposit is the crevasse splay (Figure I.12). In contrast with aggrading levees, that are associated with flows over the levee crest and on the overbank, the crevasse splay is associated with flow through the levee and into the overbank environment. Because the crevasse splay involves flow through the levee, this flow taps deeper into the main flow (i.e. with coarser-grained sediments) than simple spillover flow, which taps only into the upper part of the flow (i.e. with finer-grained sediments). As a result, flows through a breach in the levee are sourced by the sandy basal part of high-density flows (Posamentier and Kolla, 2007).

A typical crevasse splay is characterized by a short channel leading away from the main channel and feeding a smaller distributary channel system. Channels within this distributary network are associated with low-relief, probably sand-prone levees.

A crevasse splay can be considered as a failed avulsion channel (see below). The distinction is that, in the case of an avulsion channel, flow is permanently diverted through the crevasse and associated channel, whereas with the crevasse splay the flow diversion is temporary and relative short-lived. Some studies have shown that the early stage of a crevasse splay can be characterized by a levee breach that feeds a field of transverse sediment waves, and as the system becomes progressively better organized, the sediment waves are overlain by a gradually expanding distributary channel network (Posamentier and Kolla, 2007). The most distinctive sedimentary structure associated with crevasse-splay deposits are climbing current ripples. In addition, because of erosion through the levee, locally derived mud rip-up clasts can be common.

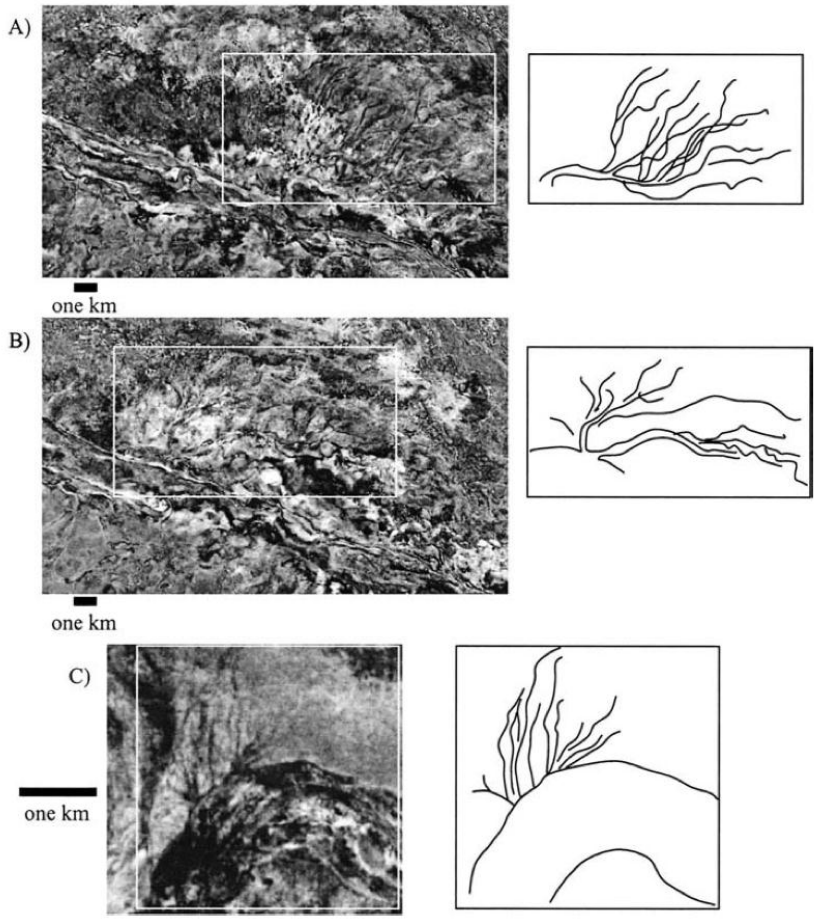

Figure I 13: A to C show examples of crevasse splays beside channels from the Pleistocene of the Gulf of Mexico. The images are amplitude extractions from seismic horizon slices (Posamentier and Kolla, 2003).

Posamentier and Kolla (2007) suggest several characteristics to distinguish crevasse splays from frontal splays:

1. Crevasse splays tend to be smaller, insofar as they involve only part of the flow discharge in contrast with the entire flow discharge involved for frontal splays deposition.
2. Crevasse splays commonly tend to be associated with levee-derived mud-rich rip-up clasts.
3. Crevasse splays lie in close proximity to channel-levees, where the flows have passed though a breach.
4. Slope instability with resulting bed convolution and slumping is more common in crevasse-splay settings, insofar as they are deposited on potentially higher slopes of the overbank deposits.

3 HARPS AND AVULSION PROCESS

The notion of HARPs (High-Amplitude Reflection Packets; Flood et al., 1991), also referred to as base-of-levee depositional lobes (Pirmez et al., 2000) was initially a seismic facies term and was later on related to a distinct sedimentary environment and process, i.e. the basal part of the channel-levee systems related to avulsion. Avulsion events imply the abandonment of parent channels in favor of the development of new channel-levee systems (Figure I.13).

Since its first recognition in the Amazon (Manley and Flood, 1988; Flood et al., 1991; Flood et al., 1995; Flood et al., 1997), it has been also identified in other mud-rich deep-sea fans [e.g. Indus Fan: Kenyon et al. (1995a); Danube Fan: Popescu et al., (2001); Zaïre Fan: Droz et al. (2003); Neofan of Rhône: Bonnel et al. (2005); Bengal: Schwenk et al. (2003)].

The top of a HARP unit constitutes a downlap surface for the overlying channel-levee system, and its base may conform to the underlying unit or truncate it (Flood et al, 1991; Droz et al., 2003). The HARPs are highly sand-prone (Pirmez et al., 1997), and are interpreted to be avulsion lobes, deposited by unchannelized sediment-gravity flows within inter-channel-levee lows, during initial stages of channel avulsion. When levees fail, sediment gravity flows move through the breach and into inter-channel lows, where lack of confinement results in sheet-like sand deposits. These characteristics are compatible with crevasse splays of Posamentier and Kolla (2003). A prograding or aggrading new channel-levee system is built over this basal HARP body.

The first conceptual model for HARP deposits related to channel avulsion has been established by Flood et al. in 1991 (Figure I.13) on the Amazon Fan. Since then this model has been refined by several authors.

Beside the vision that HARPs are related to avulsion, they have also been described as huge packets without a relationship to channel bifurcation and without an associated overlying channel-levee system (Damuth et al., 1988; Babonneau, 2002; Schwenk et al., 2005). These authors discussed that these HARPs are downfan deposits related to channel-mouth lobes (i.e. frontal splays of Posamentier and Kolla, 2003).

3.1 THE AMAZON FAN AVULSION MODELS

3.1.1 Channel-levee and basal HARPs: first avulsion model (Flood et al., 1991)

Initially, two seismic facies were identified in the Amazon Fan (Flood et al., 1991):

1. Semi-transparent channel-levee system wedges, building lens-shaped deposits,
2. High-amplitude reflection packets (HARPs) that underlie these channel-levee systems.

The relationship between a channel avulsion and the HARP unit is illustrated on Figure I.14, where the new Channel 1 bifurcates from the previous Aqua channel-levee system. The HARPs of Channel 1 appears to have been deposited immediately following the bifurcation.

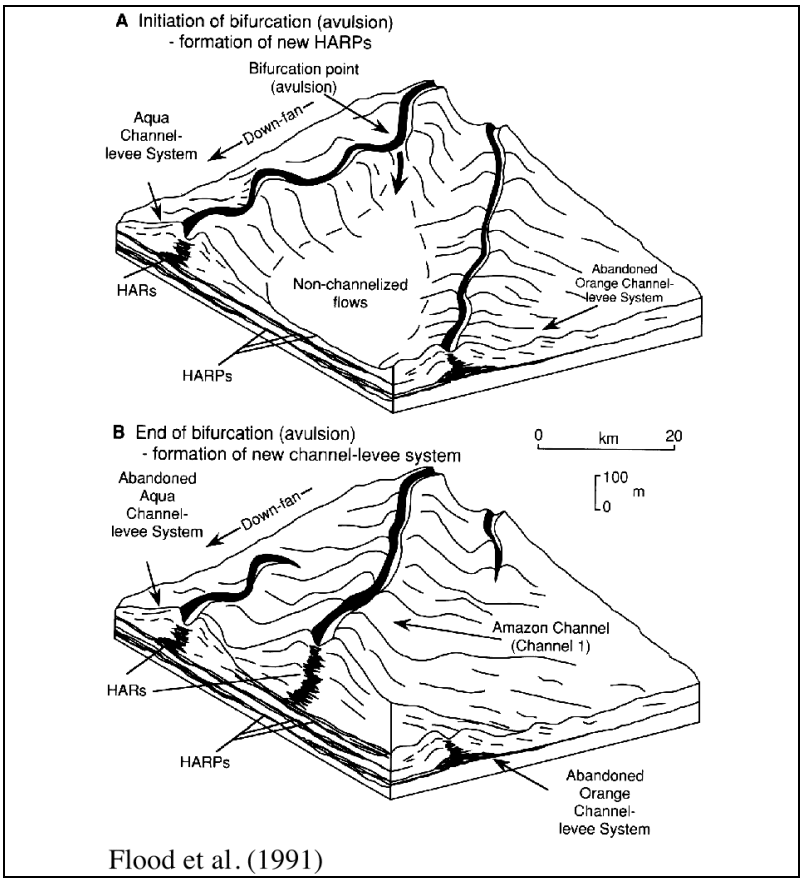

Figure I 14: Avulsion model of Flood et al. (1991) taken from a case study of the Aqua to Channel 1 avulsion.

Because of the perched nature of the channels that avulse, the inter-channel low in which the turbidity currents must flow is at least several tens of meters lower than the pre-avulsion channel floor. The gradient of the new channel is higher and causes the currents in the new channel to erode progressively upslope (Flood et al.,1991). The combination of an increased sedimentary load (due to local upstream erosion) and the lack of channel walls results in rapid deposition of unchannelized sand deposits, downfan from the bifurcation site.
Mapping of the HARP units (Figure I.15A and B) on closely spaced water-gun profiles shows that these units are extending far downslope (several 10 km) and that their lateral extent is in the order of 20 km. The lateral distribution of HARPs is controlled by pre-existing topography, i.e. by the Orange system on the west and by the Aqua system in the east (Figure I.15A).

The event that causes the avulsion of a channel is suggested by Flood et al. (1991) to be slumping of the entire levee flank or local breaching by erosion of the levee wall by large sediment gravity-flow.

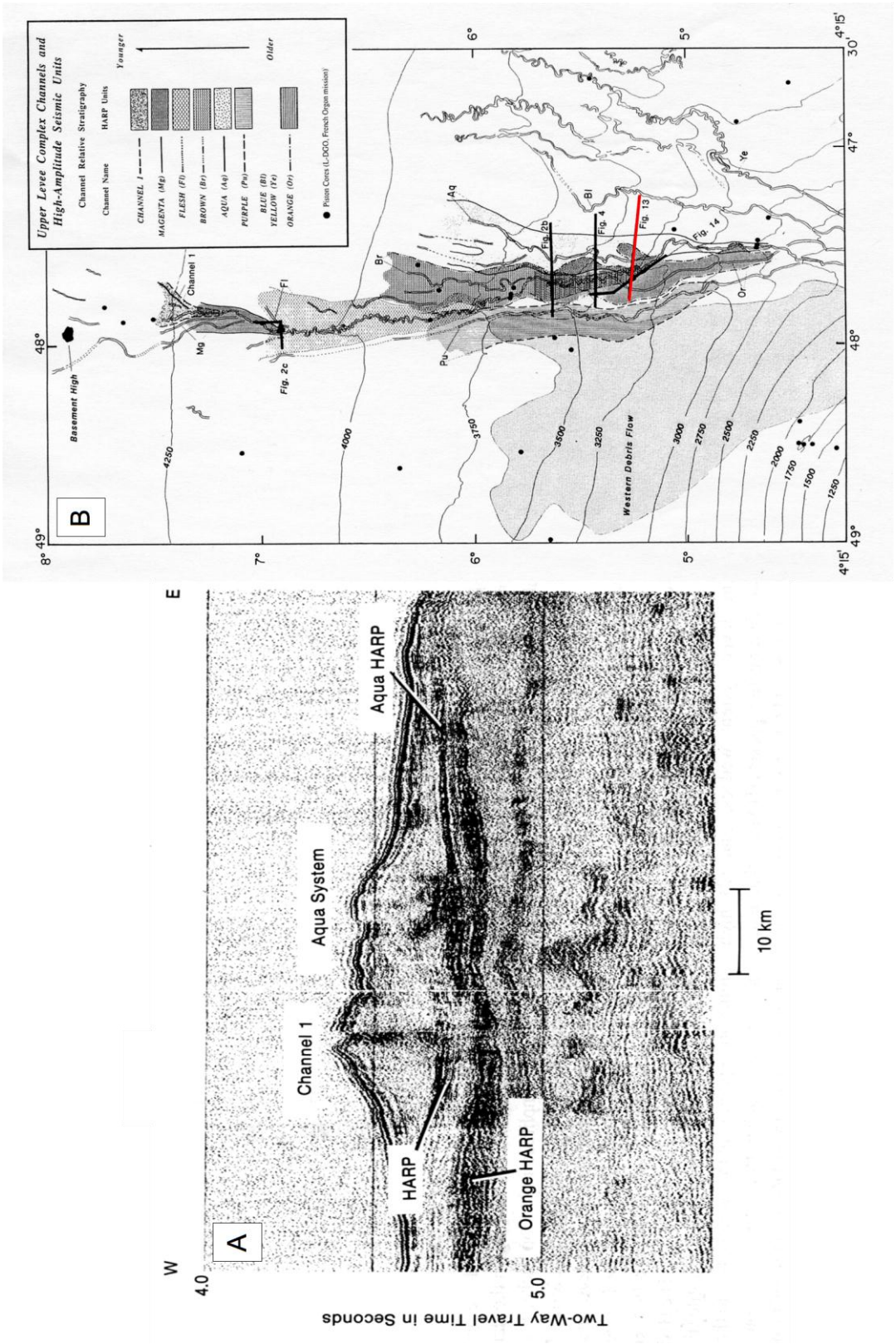

Figure I.15: HARPs at the base of channel-levee systems of the Amazon Fan. A: Watergun seismic-reflection strike profile located immediately downfan from the site of the bifurcation of Channel 1 from the Aqua system (red line in B). Interpretations show HARP units beneath channels 1, Aqua and Orange, and these units appear to be the earliest post-avulsion deposits). B: Distribution of HARP units within the Upper Levee Complex on the middle fan. Modified from Flood et al. (1991).

Flood et al. (1991) suggest from the observation of Flood and Damuth (1987) that the thalweg profile (along-channel slope) is generally nearly uniformly decreasing downfan, whatever the slope variations are in the fan. One way to maintain this regular downfan decreasing of the thalweg slope is the development of channel sinuosity when fan slope locally increases. This relationship between slope and sinuosity variations has also been observed in rivers (Schumm et al., 1972). Flood et al. (1991) observed however some local downfan changes in channel slope related to the presence of the bifurcation points.
This observation will be the cornerstone for following studies, which introduced the notion of disruption of a graded channel profile caused by avulsion.

3.1.2 Lithology of the HARPs (ODP Leg 155)

During ODP Leg 155 (Flood et al., 1995), cores penetrated the HARPs and the lithology of the Amazon HARPs were identified as mainly sandy deposits (Pirmez et al., 1997), with thick-bedded intervals of fine- or medium-grained massive to graded sand where mud clasts are common, interbedded or bounded by thin-bedded clays and silty-clays. The sandy intervals are several tens of meters thick. HARPs are thought to be the deposits of successive flows related to rapid lateral switching of the depocenters during the avulsion that produces stacked, subtly lens-shaped bedsets of sand by sheet flood and debris-flow processes (Lopez, 2001).

The published ODP results differentiate the laterally extensive HARP deposits at the bases of levee systems from lobe deposits of the lower fan. Pirmez et al. (1997) consider that, on the middle fan, HARP deposition coincides in time with the initiation of a new channel segment after channel bifurcation, whereas toward the lower fan, HARP deposition tend to stack directly on top of each other. As overbank deposits thin downfan; these HARP units probably contain deposits formed at the mouths of channels.
However, the differentiation seems not really clear concerning the lithologic content. HARPs and lower fan deposits contain medium to thick (up to 12 m) beds of disorganized structureless to chaotic sand and are associated to the same facies (Facies 2, Normark et al., 1997, see Chapter II 4.5.1.3.).

3.1.3 Equilibrium profile and nature of sediment supply (Pirmez et al., 2000)

Pirmez et al. (2000) suggest that the erosional and depositional action of turbidity currents over periods of thousands of years leads to the development of a depth profile tending to an equilibrium condition, i.e. with a local slope such that the prevailing sediment discharge is carried through the channel with minimum aggradation or degradation. Where sedimentary processes are the dominant shaping mechanism, the channel tends to acquire a concave-up thalweg profile typical of an equilibrium state. The processes through which profile concavity or sinuosity in submarine channels develop is not entirely understood. However Pirmez et al (2000) assume that relative important slope disruption (i.e. knickpoints) in the channel thalweg will influence the sedimentary flow behavior and generate erosion of the knickpoints and/or deposition in lows (space-compensation) to readjust the equilibrium of the channel profile. Steep segments across knickpoints tend to enhance erosion by accelerating turbidity currents. However, during the headward migration of knickpoints the rate of erosional downcutting at any particular location should decrease with time because sediment becomes increasingly harder to erode at depth and gradients are reduced as the knickpoint retreats.
Deposition rate gradually takes over erosion rates as gradients decrease in the downstream direction (Figure I.16).

Following an avulsion event (Figure I.17) a new channel profile is generated downdip of the avulsion point. This new profile (called the avulsion profile) corresponds to that of the backside of the levee of the parent channel, which has a higher gradient than the previous channel profile. Therefore, a knickpoint, corresponding to a disruption in the previous equilibrium profile, is created at the avulsion point, separating a rather smoothed and low gradient portion of channel upstream and a high gradient lower portion downstream. Erosion will occur at the knickpoints in order to smooth the new channel profile and acquire an equilibrium gradient.
Figure I.17 illustrates the pre- and post-avulsion profiles of the parent channel (Aqua) and new channel (Brown) respectively. The pre-avulsion profile is difficult to document because of further erosion/deposition, but Pirmez et al (2000), used the abandoned Aqua levee to estimate it. The avulsion profile is reconstructed by the Aqua levee backside and the base of the Brown HARPs. This avulsion profile shows a disruption (i.e. knickpoint) at the avulsion site, which is erased by both, headward erosion causing knickpoint retreat and deposition downdip of the knickpoint. The headward erosion finally results in the entrenchment of the new channel, which becomes deeper than the parent channel (e.g. about 75 m between the parent and the new channel in Figure I.17). This entrenchment makes it difficult for "normal"

turbidity currents to follow again the parent channel and therefore induces its abandonment.

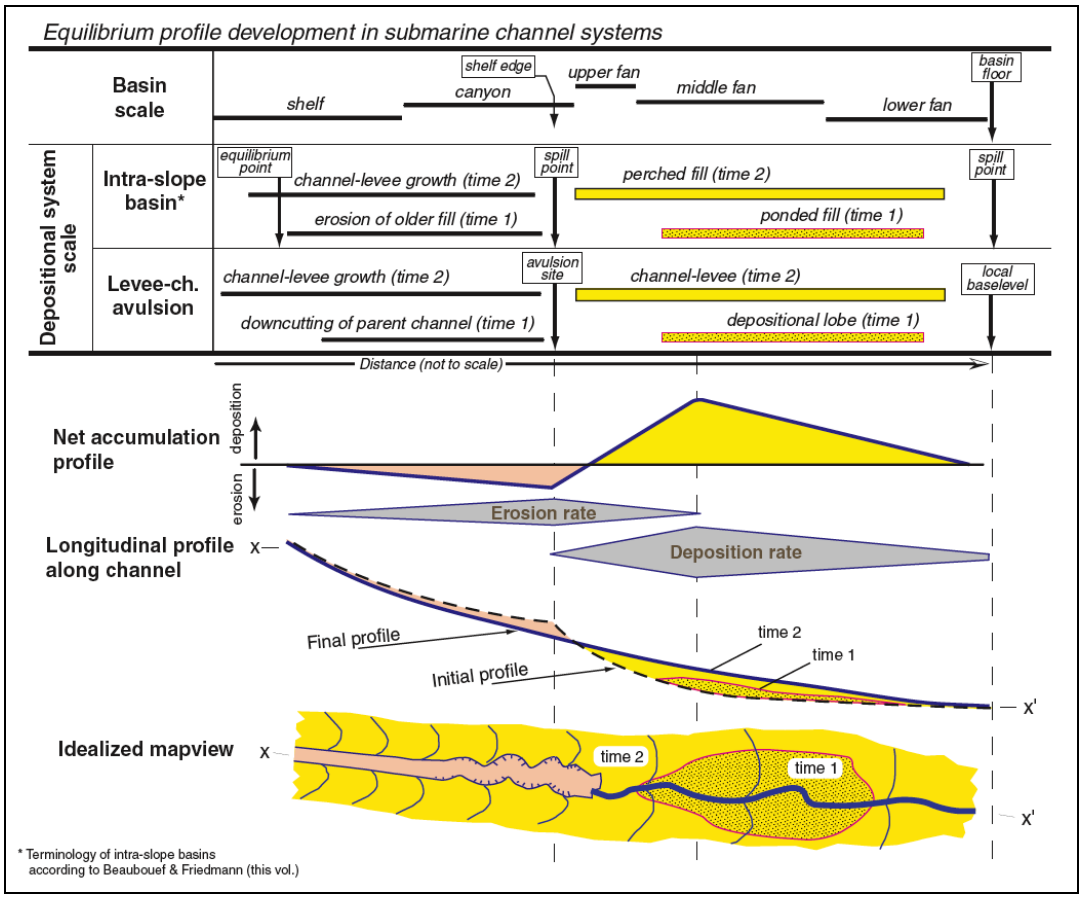

Figure I.16: Summary of depositional processes associated with the formation of equilibrium profiles along submarine channels (Pirmez et al., 2000)

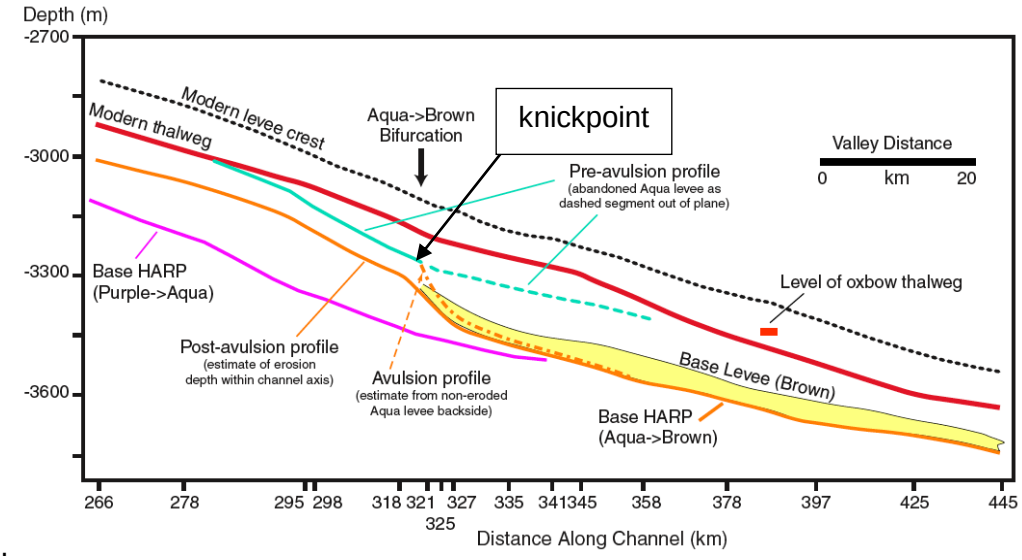

Figure I.17: Reconstruction of pre-and post-avulsion profiles for the Amazon Channel (Aqua to Brown channels) showing the evolution of the gradients following an avulsion event. In Pirmez et al. (2000) after Pirmez (1994) and Pirmez and Flood (1995).

Pirmez et al (2000) suggested that the specific shape of a thalweg profile and local gradients depend on a number of factors that are most likely dominated by the discharge of the turbidity flows, the grain size characteristics of the sediment load, and local topographic effects (such as the degree of lateral confinement which affects velocity and flow discharge). The switching from HARPs to channel-levee growth appear to be primarily controlled by the proportions of sand and mud in the turbidity current. Relatively fine grain sizes and steep gradients will lead to increased tendency of flows to channelize (Imran et al., 1998), whereas coarser grain sizes and lower gradients will induce formation of HARP lobes.

In the case of the Amazon channel, abrupt lithological changes, from mainly sandy to mainly silty clay, characterize the transition from HARP to levee. Pirmez et al. (2000) suggest that the grain size has to change rapidly to a lower sand:mud ratio when levee begins to grow.

Volume estimations from Pirmez et al. (2000) indicate that headward erosion mechanism does not significantly influence the sediment load in flows, because the volume of eroded material is only a fraction of the sediment deposited downdip of avulsions. These authors therefore suggest that the keydetermining factor for the architectural style of the deposits are the processes that impact the nature and frequency of sediment delivery to the deep-water environment, i.e. the sediment load composition delivered to the head of the system, itself controlled by sea level and climate changes.

3.1.4 Internal seismic structure and refined model related to equilibrium profile through time (Lopez, 2001)

Lopez (2001) firstly propose an internal seismic characteristic of the avulsion HARPs, which includes parallel and subtly lens-shaped internal reflections, the latter suggesting the presence of small, unleveed channels (Figure I.18).

This author details the avulsion model linked to the adjustment of an equilibrium profile. The evolution of the avulsion process through time, is characterized by 3 main steps (Figure I.19):

1. Initiation of the bifurcation caused by particularly intense turbiditic flows. Overpressure exerted by the turbiditic column on the levee walls, exceeding the limit of stability, causes inner-levee slope failure, allowing the turbidity currents to escape from the channel. The currents overflow and spread out from the bifurcation point into the adjacent lows on a disrupted equilibrium profile (stage A).
2. Construction of sheet-like sand-rich deposits, visible as HARPs on seismic, as a result from upslope erosion of the channel-floor and entrenchment of the channel during the adjustment phase of the equilibrium profile (stage B).

3. HARP deposition wanes when an equilibrium profile is reached. Levees growing down-fan confines the sand-rich basal parts of turbidity currents to a narrow channel axis (stage C).

Subsequently, the advance of a new leveed channel over the sheet-sands focuses sand transport along the channel axis, with simultaneous accumulation of muddy overbank deposits on the Levees.

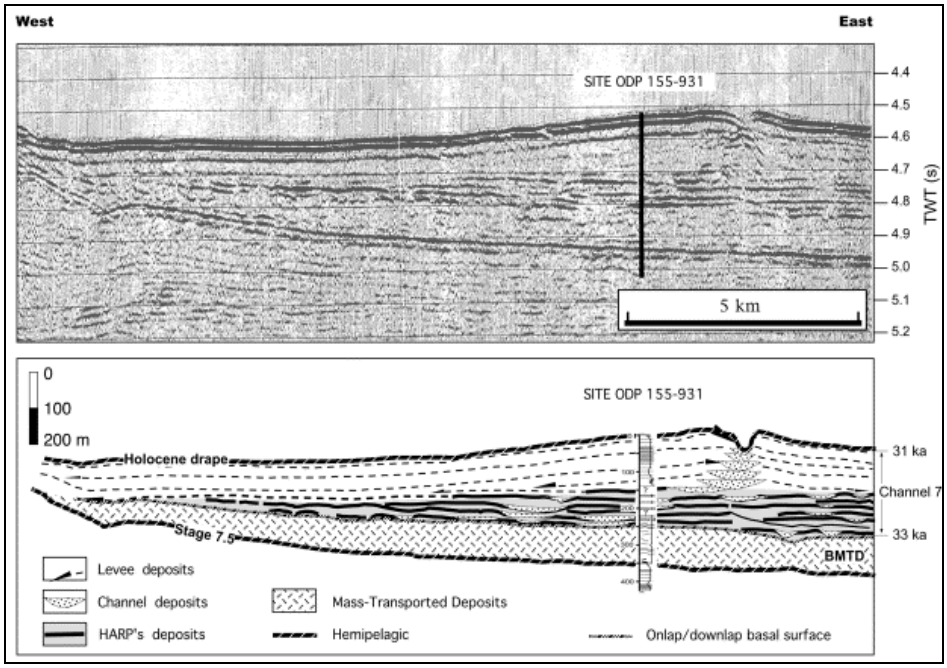

Figure I 18: Seismic line and linedrawing showing example of HARPs and associated channel-levee system of the Amazon Middle Fan (Lopez 2001).

By reviewing the chronostratigraphic works of the Amazon Fan (ODP 1995 and 1997), Lopez (2001) considers that avulsion occurs during a single glacial period by autocyclic processes and conditions both the accumulation of sand-sheets and muddy levee deposits. He suggests that sea level changes influence the frequency of avulsion, i.e. they are more frequent during lowstands of sea level. Further, he considers that the transition from HARP's construction to aggradation/progradation of a new channel-levee system is an autocyclic process depending of the equilibrium profile of the thalweg and doesn't include allocyclic factors like variation of the sediment supply at the head of the deep-water system.

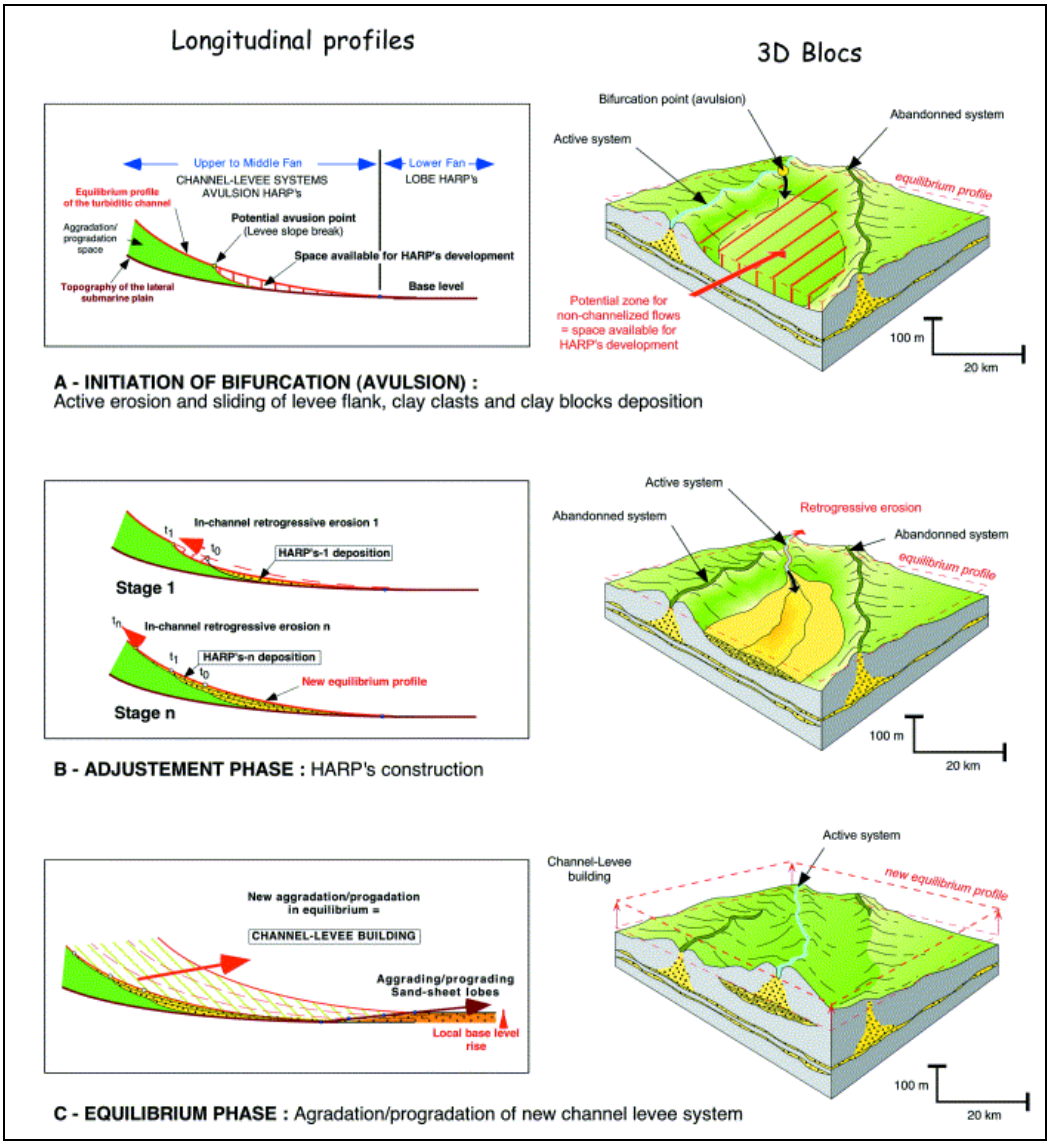

Figure I 19: Refined model for the HARP deposits related to a channel avulsion including the notion of an equilibrium profile (Lopez, 2001).

3.2 HARPS IN OTHER FANS

3.2.1 The Zaïre Fan

In the Zaïre Fan, high-amplitude reflection units are recognized as a basal sole for channel-levee systems (Babonneau, 2002; Droz et al., 2003) (Figure I.20). They are suggested to consist in high-amplitude reflection packets related to avulsion processes below the avulsion points and coarse-grained basal levees related to the initial stages of levee aggradation subsequent to the avulsion event. These deposits can be considered as HARPs deposited from processes similar to those in the Amazon Fan HARPs.

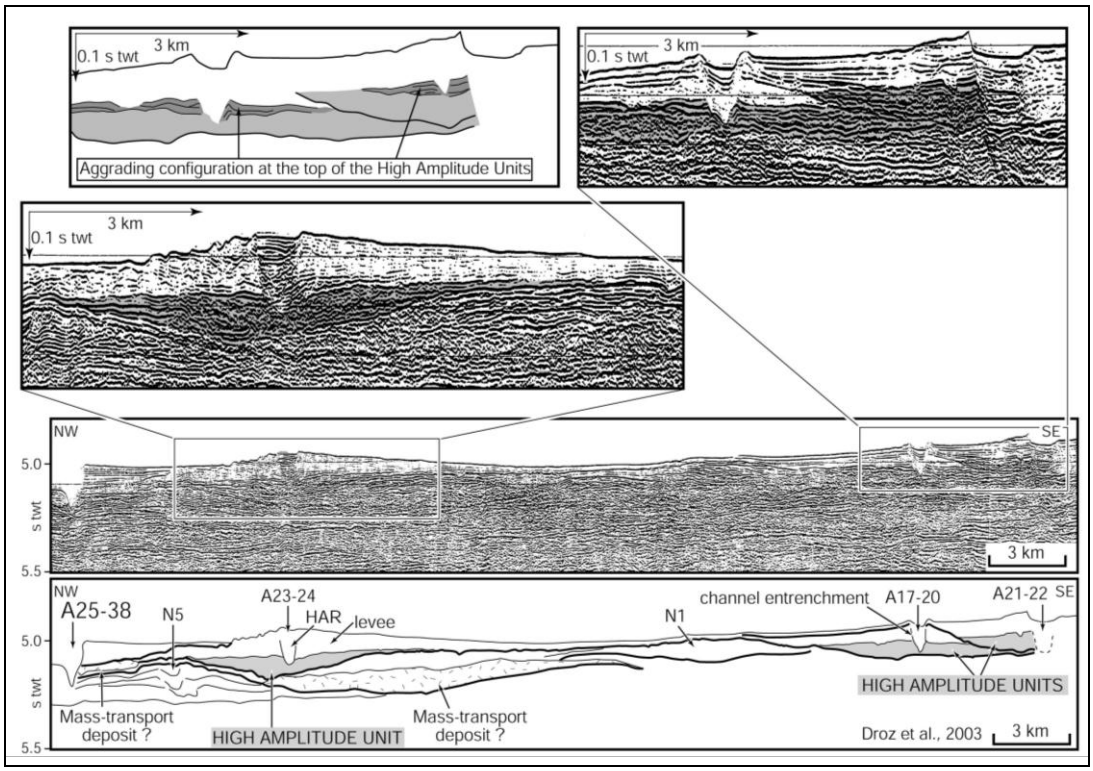

Figure I 20: Seismic section on the Zaïre Fan showing HARPs ("high-amplitude Unit") identified under channel-levee systems at the avulsion points (Droz et al., 2003).

In contrast to the Amazon, HARPs in the Zaïre Fan are emplaced generally very close (few kilometers at maximum) to the bifurcation point (Droz, pers. com.). They are observed downstream from about 70% of the bifurcation points under their corresponding new channel-levee systems, more or less symmetrically with regards to the channel axis, and extend up to 250 km downdip. Their lateral extent is of the order of 10 km (Droz et al., 2003). In one bifurcation point analysed with greater detailed, (Droz et al., 2002; Droz and Marsset, submitted) showed that the high-amplitude packet is made of several stacked elementary units 10-20 m thick, 1 to 6 km wide (in cross sections) that are laterally shifted and overlap each other.

Babonneau (2002) suggests that the transition from HARP deposits to channel-levee system is a function of space-compensation and will depend on the size of the inter-channel-levee system lows (Figure I.21). A new channel will prograde when the space has been sufficiently filled, so that HARP deposition will cease and allow a channel to erode in continuity of the channel-mouth at the avulsion point. The thickness of the HARP therefore depends on the available space at the channel mouth. The sooner the channel will be able to develop levees, the thinner the HARPs will be (see case 1, Figure I.21), and the more place is available, the more HARP lobes will compensate this place before a stable channel with aggrading levees can build (see case 2, Figure I.21). The lateral switching of HARP lobes occurs also by avulsion, but at a much more smaller scale than for the typical middle fan avulsions.

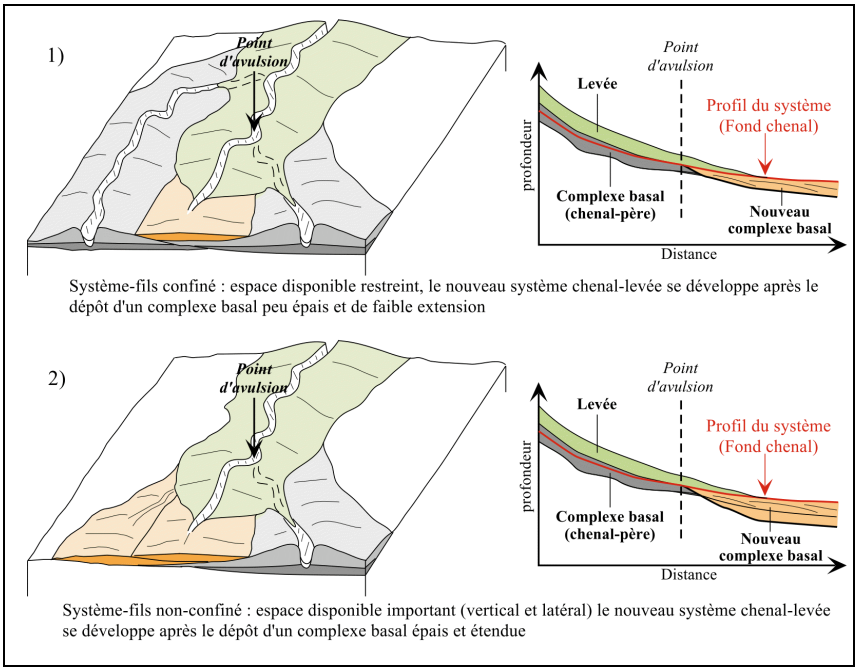

Figure I 21: Influence of the space-compensation (lateral confinement) on the dimension of the HARP deposits (Babonneau, 2002).

In the Zaïre Fan some basal high-amplitude deposition without a clear connection to an avulsion point are also observed. It seems that these deposits fill large unconfined spaces of greater dimensions than the lows where avulsion lobes are deposited. Babonneau (2002) hypothesizes that these deposits correspond to channel-mouth lobes. The channel-mouth lobes would represent basal fills over which the channel-levee system progrades (Figure I.22). This mechanism of lows infilling and channel-levee progradation would be repetitive as the channel-levee system progrades downfan and meets topographic lows, resulting in a huge basal lobe accumulation where the dimensions depend on the topographic low that has to be filled before the channel is able to erode and construct levees.

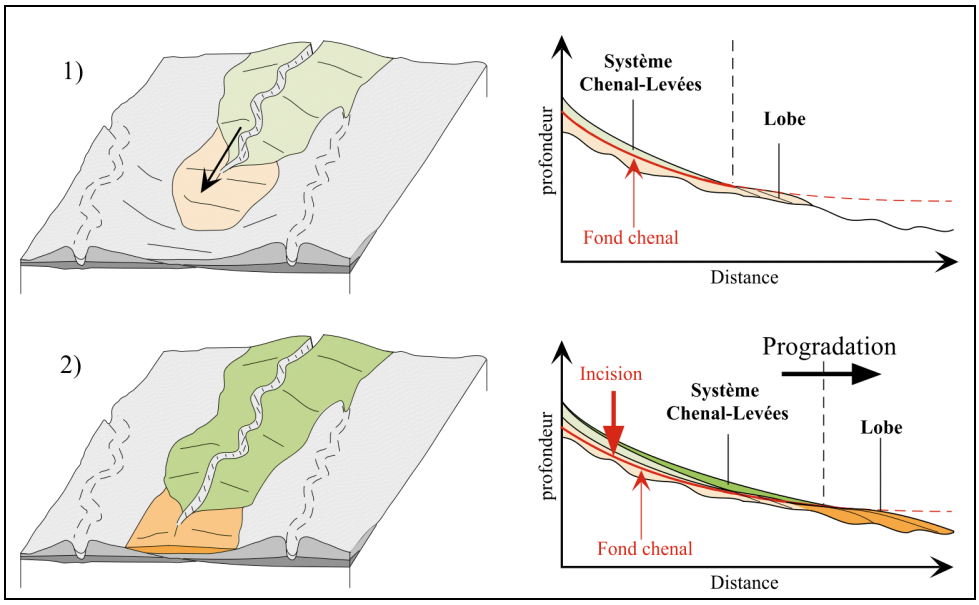

Figure I 22: Progradation of a channel-levee system over channel-mouth lobes (Babonneau, 2002).

The transition from either terminal lobes or avulsion lobes to channel-levee aggradation and progradation is controlled by space compensation which will determine the thickness of the terminal or avulsion lobes (Babonneau, 2002).

These models therefore invoke only autocyclic mechanisms. However, from the observation of the evolution through time of the position of avulsion points and of the channel lengths, Marsset et al. (in press) highlighted periodic foreward and backward movements of the depocenters. They hypothetically attribute these movements, at least partly, to allocyclic factors, i.e. environmental changes in relation to climate changes in the Zaïre River drainage basin.

3.2.2 The Danube Fan

HARPs have also been described by Popescu et al. (2001) and Popescu (2002) in the Danube Fan (Black Sea). On the middle fan, near channel bifurcations, each channel-levee system overlies high-amplitude reflection packets similar to the HARPs identified in the Amazon Fan (Figure I.23).

These authors suggest that the HARPs in the Danube Fan are related to four main channel avulsion event. Each event occurred following the same pattern as already exposed for the Amazon Fan:

- breaching of the left (northern) levee,
- deposition of HARPs,
- initiation of a new meandering channel.

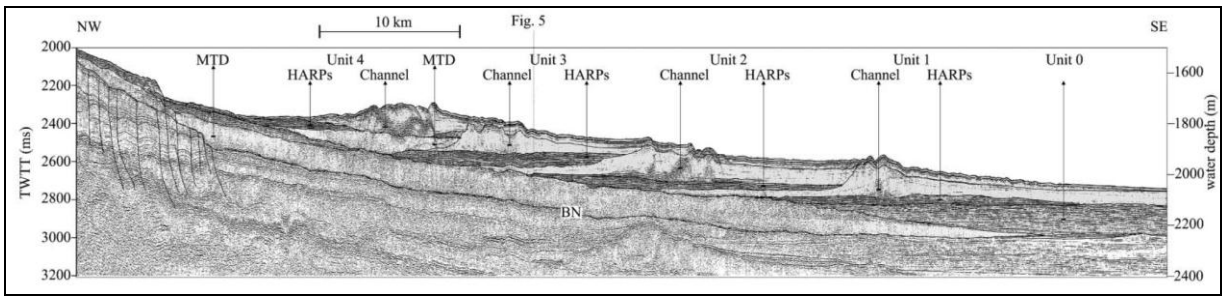

Figure I.23: Seismic section on the Danube Fan showing HARPs identified under each main channel-levee systems (Popescu et al., 2001).

The HARP units are located some km (up to 15 km) downward from the bifurcation point and extend along up to 100 km for the longest unit (Figure I.24). Popescu et al. (2002) suggest that the location of HARPs is controlled by pre-existing topography and that they were deposited during the time that the channels adjusted their equilibrium profiles. The HARPs of the most recent phase of avulsion are the most severely constrained by local topography and form an elongated feature that is half as thick as the preceding HARPs possibly indicating that the adjustment of the equilibrium profile was attained faster than in the previous HARP deposits (Popescu et al., 2001). The youngest new confined channel-levee system that developed abandoned the path of the HARPs, providing an example of HARPs that are not covered by the corresponding channel-levee system (Figure I.24d).

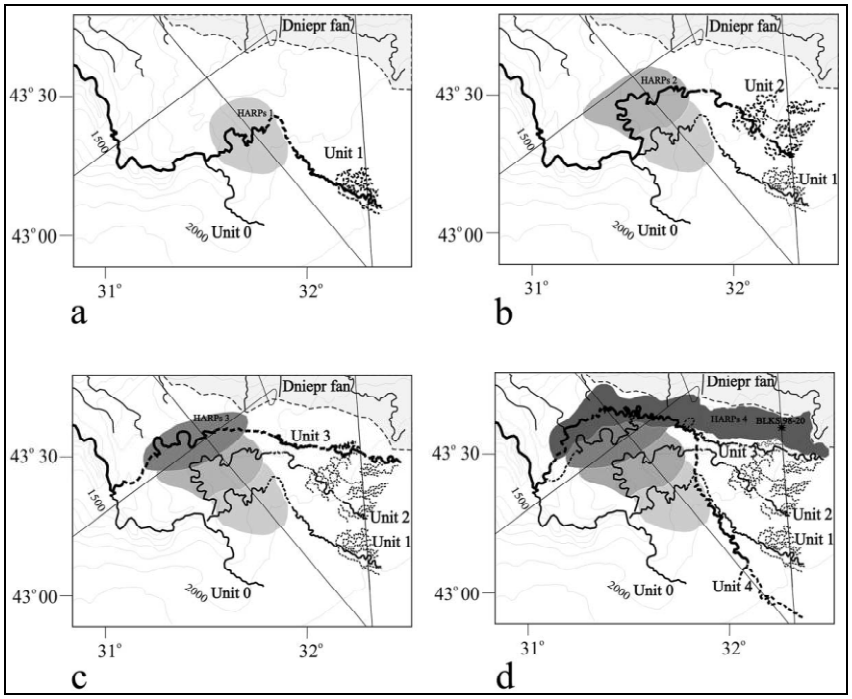

Figure I.24: Channel and HARP units of the four main avulsion phases of the Danube Fan (a to d from the oldest to the youngest avulsion event) (Popescu et al., 2001).

3.2.3 The Bengal Fan

Schwenk et al. (2003; 2005) distinguish meander cut-off and new channel building as two different processes of avulsion in the Bengal Fan, whereas only the second is interesting for our study. Avulsions leading to new channels are described in Schwenk et al. (2005) as responsible to the existence of widespread packets of mostly parallel, high-amplitude reflectors, intercalated between the channel-levee systems. These packets are identified as HARPs by comparison with the Amazon Fan (Figure I.25). Some of them extend from W to E across the entire study area indicating extensions as wide as 53 km and thicknesses up to 110 m are found (Schwenk et al., 2005).

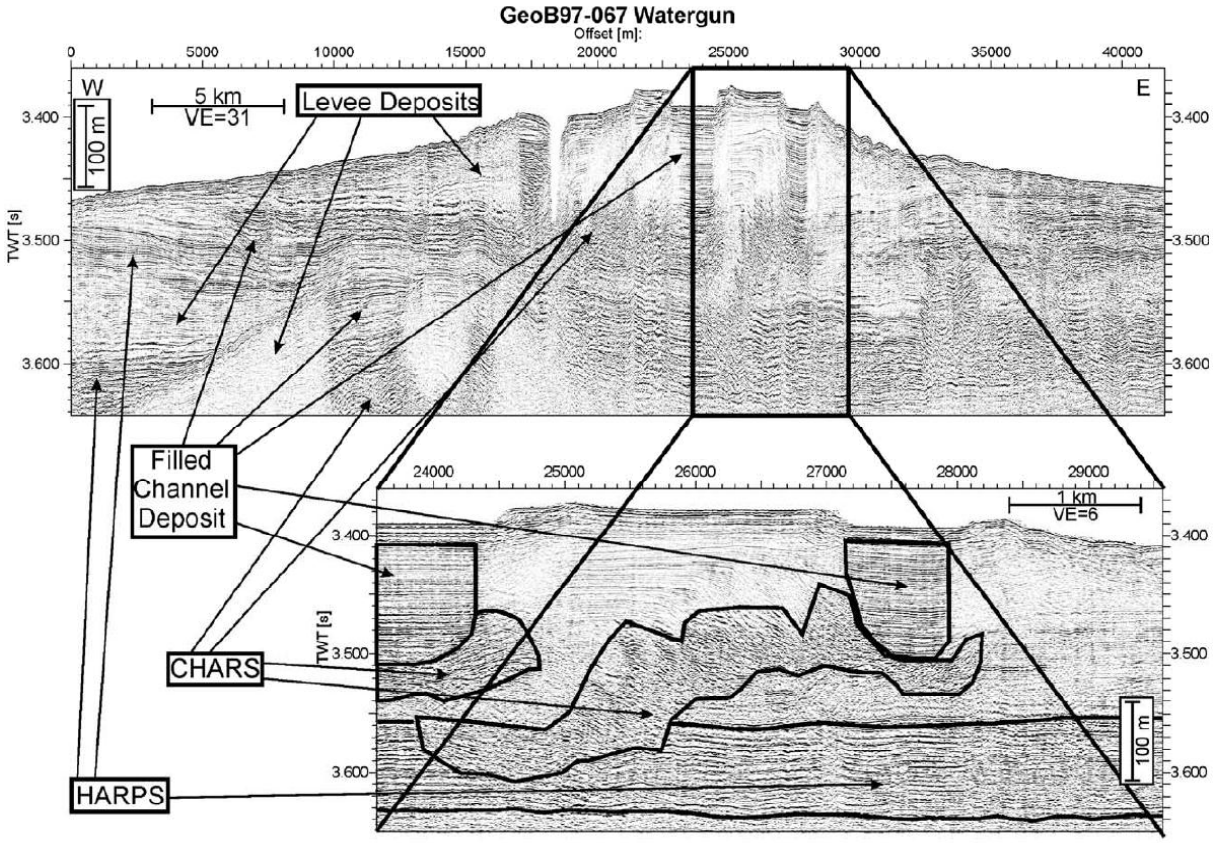

Figure I.25: High-resolution water-gun data imaging the active channel-levee system of the Bengal Fan, and showing the interpreted facies for levees, channel deposits (CHARS), filled channel deposits and HARPs (Schwenk et al., 2005).

As already proposed from the Amazon, Zaïre and Danube fans (see above), Schwenk et al. (2005) indicate that at the first step in the evolution of the active channel-levee system, turbidity currents erode a deep valley, filling with HARPs a low between two older channel-levee systems. The overlying levees are built up by overspilling. Lateral migration and vertical aggradation of the channel occur by erosion and deposition of turbidity currents.

Studies in the Bengal Fan also identified thick units of high-amplitude reflections that are not linked to bifurcation pattern of the channels but are located at the termination of a channel-levee system (Schwenk et al., 2005) in distal position. This distal position led Schwenk et al. (2005) to interpret these units as stacked channel-mouth lobes.

-Chapter II-

Geological Background of the Amazon Fan

The Amazon Fan and its terminal lobes, located in the Southern Atlantic, off the northern Brazilian margin (Figure II.1), has been the objective of a recent PhD (Jégou, 2008, Jégou et al., 2008). In her manuscript, Jégou made an extensive bibliographic report about previous works on the Amazon Turbidite System, including information on the Amazon River drainage basin, the Amazon Delta, the continental shelf, the Amazon Fan itself and the tectonic and climatic evolution of the margin.

Therefore I decided to restrain my bibliographic input to a rapid overview of the regional setting and sediment source of the fan, the main characteristics and architecture of the fan and describe the ODP drilling data that were used extensively in the framework of my study of the avulsion process.

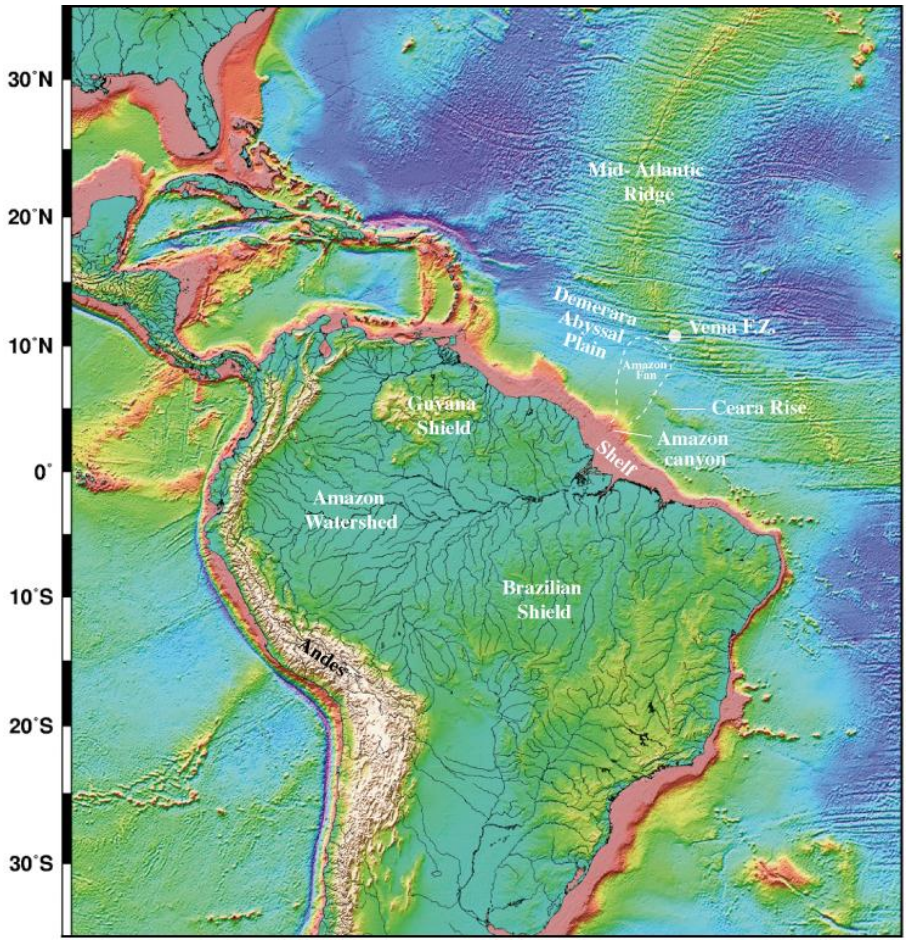

Figure II.1: Overview map of the Amazon system from source (Amazon River system) to sink (Amazon Fan system). The Amazon Fan extends from the slope of north-eastern Brazil until the Demerara abyssal plain, near to the Mid-Atlantic Ridge (Jégou (2008) after Smith and Sandwell (1997)).

1 A LONG-TERM STUDY ZONE

The initial studies of Damuth (1973), Damuth and Kumar (1975), and Damuth and Embley (1981) described the morphology and architectural elements of the Amazon Fan, based on

high-resolution seismic and piston core data.

In order to address problems such as the exact number, trends, bifurcation patterns and relative ages of the distributary channels, Damuth and others initiated a series of state-of-the-art studies in 1981, using side-scan sonar, bathymetric swath-mapping and deep coring techniques through a series of international cooperative programmes between the Lamont-Doherty Geological Observatory, PETROBRAS (the Brazilian national petroleum company) and the Instituto de Geosciencas de Universidade Federal do Rio de Janeiro (UFRJ).

In 1982, in cooperation with the Institute of Oceanographic Sciences (IOS) in the UK, the GLORIA MK II long-range side-scan sonar was used to survey most of the upper and middle portions of the fan. It was used to map the configuration of the distributary channel system on the upper and middle fan, and to determine the meandering and bifurcation patterns of channels, the relative age relationship of individual channels to each other and to other fan features, and the relationship of the distributary channel anatomy to fan sedimentation processes and growth pattern (Damuth et al., 1983a; 1983b; Damuth and Flood, 1984; 1985; Damuth et al., 1988). These studies showed that only one of the numerous distributary channels is presently connected to the Amazon Submarine Canyon. This channel was inferred to be the most recently active channel on the fan and was called the Amazon Channel.

In 1984 the Amazon channel was continuously surveyed and mapped using a Sea Beam multi-narrow-beam echo-sounder from the Amazon Canyon downslope to 4273 m water depth on the lower fan, where the channel became too small to be imaged on Sea Beam bathymetry. In addition, high-resolution watergun (<250 Hz) seismic and 3.5 kHz echograms were recorded. The watergun seismic data revealed the stratigraphic relationships of the youngest channel-levee system to older adjacent channel-levee systems. Piston-core (< 10 m penetration) transects across the youngest channel and its levees were taken at several locations along the channel's course (Appi et al., 1988; Manley and Flood, 1988; Flood et al., 1991). In 1995 deeper sampling (up to 433.8 mbsf, core 936A) of the sediments of the fan were realized during ODP leg 155 to determine stratigraphy, sedimentation processes and growth pattern (Flood et al., 1997).

2 THE FOZ DO AMAZONAS BASIN

The Amazon Fan, a wedge of clastic sediment up to 10 km in thickness (Cobbold et al., 2004), is the third largest modern deep-sea fan and is located in the Foz do Amazonas Basin (also called the Amazon Mouth Basin) that underlies the Amazon River mouth, continental

shelf, and upper Amazon Fan (Castro et al., 1978; Brandão and Feijó, 1994; Mello et al., 2001; Cobbold et al., 2004) (Figure II.2).

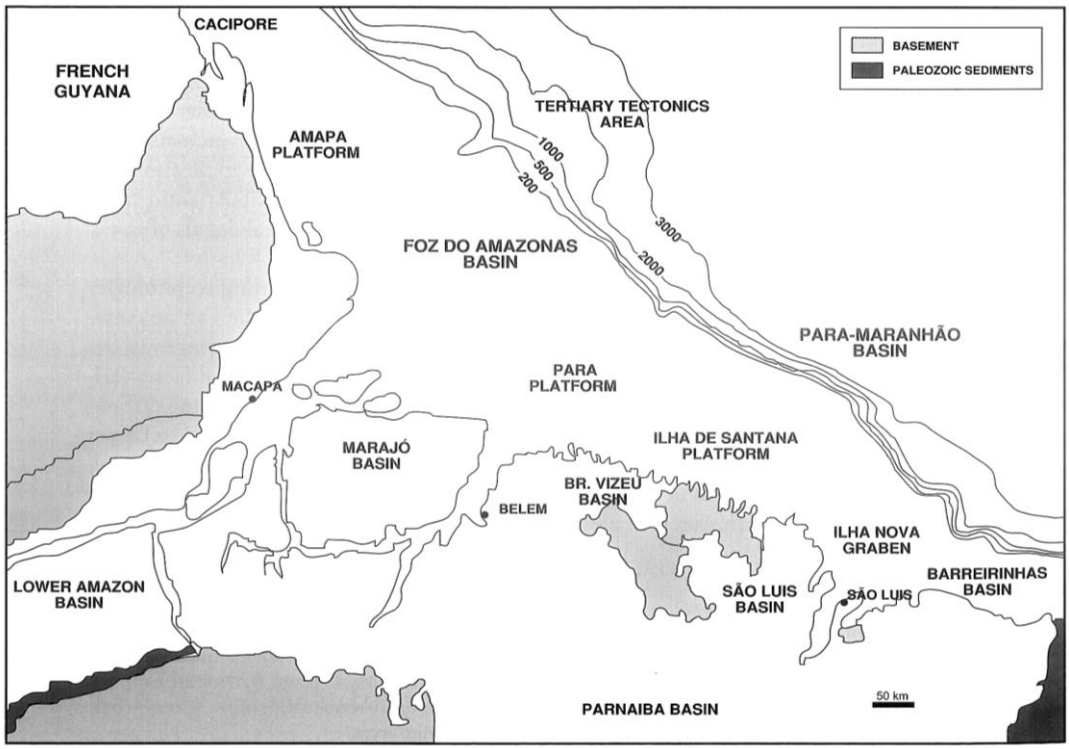

Figure II.2: Regional setting of the Foz Do Amazonas Basin (Mello et al., 2001) inside which the Amazon Fan accumulated.

The Foz do Amazonas Basin is located offshore of the states of Amapa and Para in the northern Brazil. This basin covers an area of about 268,000 km^2 (Reis, submitted) and includes the continental shelf, slope, and deep basin down to the 3000 m isobath. The Foz do Amazonas basin is a conjugate basin to offshore Liberia in West Africa and was separated from the African continent when rifting along the Atlantic margin in this area began around 120 Ma.

At the end of the rifting at ca. 100 Ma, thermal subsidence formed progressively a deep-marine basin by the end of Cenomanian time. During this deep-water basin formation, the first post-rift deposits may be shallow-marine sediments of the uppermost Albian, which have been onlapped by transgressive marine shales in the Cenomanian and Turonian.
The post-rift sedimentation (100-0 Ma) can be subdivided into two time intervals:

- The pre-Amazon Fan interval (ca 100-11 Ma), which is Cenomanian through Middle Miocene in age and represents deposition in the basin prior to the establishment of the Amazon River as a major, continental-scale drainage system.
- The Amazon Fan interval begins in Middle Miocene with the transition from a

cratonic-derived sediment regime to one dominated by Andean-derived sedimentation, resulting in the onset of the transcontinental Amazon River and the buildup of the Amazon Fan. Sediments of Andean origin have reached the Foz do Amazonas Basin between 11.8 and 11.3 Ma (Figueiredo et al., 2009). The siliciclastic sediment delivery to the Atlantic shelf and deep sea has been high enough to replace the carbonate platform sediments of the former upper pre-Amazon fan interval (Amapá Formation) by shoreline to deepwater facies (Tucunaré, Pirarucu to Orange Formation during the Tortonian and Messinian), (Brandão and Feijó). As a result, a megasequence of clastic sediments has been accumulated in the Amazon Fan and Figueiredo et al. (2009) determined three phases of the Amazon Fan interval (see 3, this chapter).

Several studies (Silva et al., 1999; Cobbold et al., 2004; Reis et al., submitted) show, based on a structural and seismic-stratigraphic analysis, that the marine sequences of the Foz Do Amazonas Basin were affected by very intense gravity tectonics caused by rapid siliciclastic sedimentation They identified contractional and thin-skinned extensional structures (folds and thrust faults), considered to root into basal weak levels. Silva et al. (1999) defined a tectonic model for the area based on gravity gliding and spreading. Cobbold et al. (2004) suggest that fluid overpressure, caused by gas generation, was probably the cause of the common basal detachment of the structures and that hydrocarbons may originate in a Cenomanian-Turonian regionally extended source interval. Reis et al. (submitted, see 4.3, this chapter) pointed out that gravity tectonics is a triggering mechanism of slope instability that has to be taken into account for the investigation of deposition processes, particulary mass wasting processes in the Amazon submarine fan.

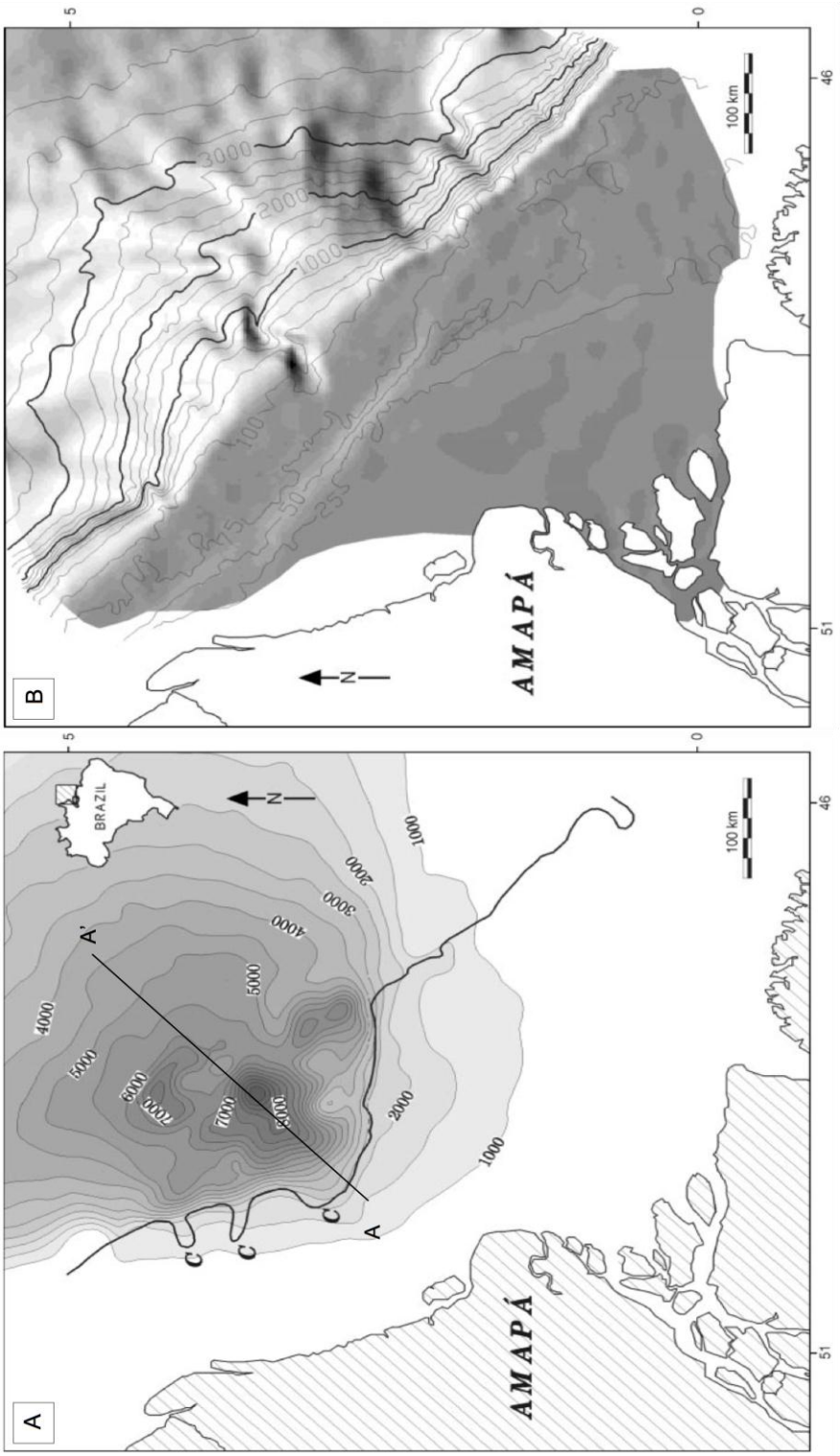

Figure II.3: The Amazon Fan interval (Silva et al., 1999). A: Isopach map of Late Miocene-Recent megasequence (10 Ma to Present). The heavy line is the shelf edge of Upper Miocene. C = canyons. B: Present-day bathymetric map.

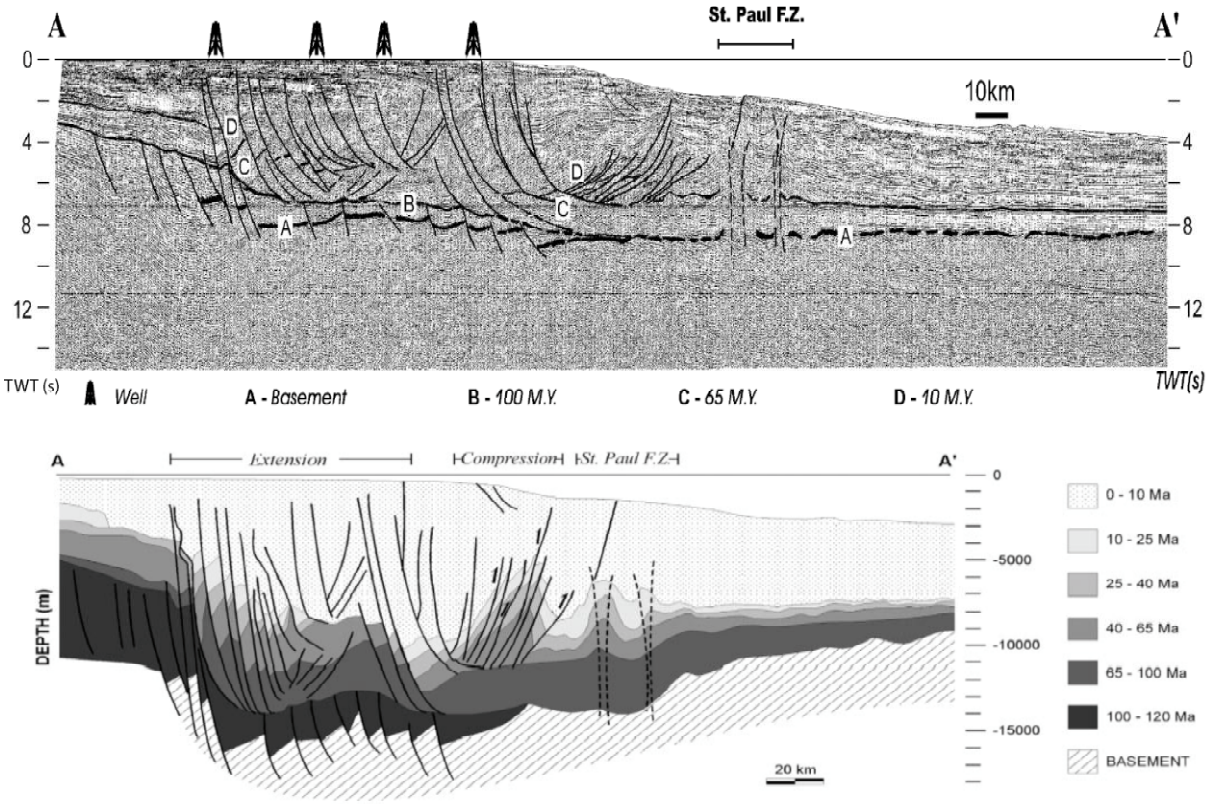

Figure II.4: Structure and stratigraphy of the Foz do Amazonas Basin (Silva et al., 1999). A: Multichannel seismic section AA' (location in Figure II.3A), showing the carbonate platform on the left side between 2 and 4 s, growth faults along the shelf margin and thrust faults on the central part. Notice that numerous faults are occurred during the Amazon Fan interval (0-10 Ma), B: Line drawing of A, in m.

The stratigraphic organization of the Amazon Fan since the Late Miocene remains unknown for most parts of the fan, and particulary for the oldest parts because of the lack of data for chronostratigraphy and facies analysis. Most of available data and studies focus on the Quaternary fan section (representing just a few hundred meters of the upper part in the Late Miocene to Recent Megasequence), involving deposition of channel-levee systems and mass transport deposits (e.g. Damuth and Kumar, 1975; Flood et al., 1997).

3 THE AMAZON RIVER AND THE CONTINENTAL SHELF

The functioning of the Quaternary Amazon Fan, i.e. "on-off" functioning, is of the same type as most of the turbidite systems that are separated from the fluvial feeding system by a large continental shelf (e.g. the Bengal, the Rhône, the Nile, the Danube or the Mississippi fans). During sea-level highstand periods, the Amazon River mouth is disconnected from the deep basin, and the fan is inactive (fan off). Detritic sediments accumulate predominantly on the continental shelf in a large subaqueous delta (Kuehl et al., 1982; Nittrouer et al., 1983, 1986;

Flood et al., 1995), whereas pelagic sediments are currently being deposited on the Amazon Fan. During glacial sea-level lowstands, the Amazon River incised into the shelf and discharged terrigeneous sediments directly into the Amazon Canyon (fan on) (Damuth and Kumar, 1975; Milliman et al., 1975) and fed the Amazon Fan.

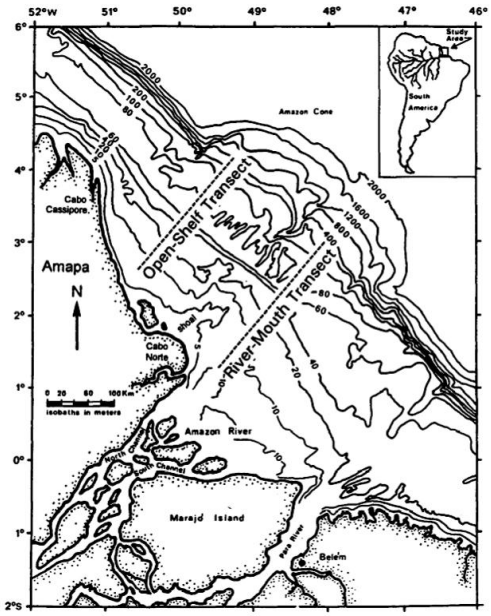

Figure II.5: Morphology of the Amazon shelf and slope. Contours are in m (Nittrouer and DeMaster, 1996).

The Amazon continental shelf stretches along the seaside border of the Amapa region and extends 1600 km northwestward from the river mouth to the Brazilian border with French Guiana. The shelf break is situated around the 100 m isobath, reached by the head of the Amazon canyon (Figure II.5). Sediment supplied primarily from the Andes has formed a muddy modern subaqueous delta with clinoform morphology, which is prograding over a relict carbonate-rich sandier substrate. Radiochemical analyses indicate that this modern delta, with its characteristic clinoform morphology and stratigraphy is a late Holocene feature (Kuehl, 1986; Sommerfield et al., 1995). However, some strata preserved beneath the modern subaqueous delta and the transgressive sand layer have been described and are associated with recurrent sea-level changes, preserved on time scales of 10^4 yr or longer. The delta is potentially around 70 m thick and 200 km wide at the river mouth (Nittrouer and Kuehl, 1995).

The present-day Amazon fluvial system has the largest in discharge volume in the world (i.e. 209,000 m3/s of water flow including any suspended solids, Molinier et al., 1993) and a length of approximately 6800 km (http://en.wikipedia.org/wiki/Amazon, accessed January 24, 2010).

Concerning the drainage history of the Amazon River, Figueiredo et al. (2009) present a study for the time interval from the onset of the Amazon Fan deposition (Upper Miocene) to the present. They determined ages and provenances of the sediments based on biostratigraphic, isotopic, and well log data from exploration wells on the outer continental shelf and propose three phases for the sediment supply history of the river to the deep-sea.(1) The onset phase (11.8-6.8 Ma) is defined by the Amazon River adjustment that results into a connection between the river and the western Amazonian wetland. This event is marked in the Foz do Amazonas Basin as a regional unconformity, a sequence boundary that marks the onset of the transcontinental river and the Amazon Fan. Sedimentation rates were low (around 0.05 m/ka). (2) The middle phase (6.8-2.4 Ma) is marked by an increase of the sedimentation rates (to 0.3 m/ka) despite a rise in global sea level. Intensive Andean erosion combined with additional supply from the craton allowed this high sediment delivery by a large entrenched Amazon River to the deep sea. (3) The Late phase (2.4 Ma ago to present) is marked by a further increase in sedimentation rates (1.22 m/ka) of Andean sediments on the Fan.

Rossetti and Valeriano (2007) combined spatial analysis with geological data available from literature in order to discuss the geological history of the lowest Amazon drainage basin (i.e. the Tocantins River, one of the largest tributaries and the Marajó Island, the largest fluvial island in the world). A preliminary model has been proposed, which shows that tectonic activity was the main factor controlling the distribution of the sedimentary units and the development of the modern morphology. The model considers that the Tocantins River had a complex evolution, changing its position according to tectonic reactivations in the Plio-Pleistocene, which might have taken place even during the Holocene. The model approaches also the mechanism that would have promoted the detachement of the Marajo Island from mainland. All in all, the model suggests that the modern Amazon drainage basin might be a relatively recent development. Many possible changes in the river positions due to tectonics might have taken place in past times.

The position of the canyon heads of the late Miocene of the Amazon Fan (Fifure II.3A) lies around 50 km northwest of the present-day canyon system, suggesting that the Amazon River may have flowed farther to the north in the past. The river diverted to its present eastward course (Figure II.3 B) probably because of tectonic reasons (Cobbold et al., 2004).

The studies concerning tectonics in the Amazon fluvial system and drainage basin show that sediment supply by the Amazon River through time has been affected by the Andean uplift and other tectonic events in the Amazon drainage basin (e.g. Figueiredo et al., 2009; Rossetti and Valeriano, 2007; Driscoll and Karner, 1994; Cobbold et al., 2004). Some tectonic events seem well constrained and have been linked to deposits and sedimentation rates in the deep-sea. Other tectonic events need to be studied in more detail, in particular

their timing, to compare them to climatic and sea-level changes, and to discuss their influence on the sediment supply and deposition in the deep-sea.

A proxy for river input through time is Fe/Ca measurements that have been performed on sediments retrieved off Brazil (core GeoB 3104-1/3912-1, for location see Figure II.6, Arz et al., 1998). Together with other measurements, they indicate a linkage between marine and continental climate signals (Arz et al., 1998; Stuiver and Grootes, 2000; Wang et al., 2004; Leduc et al., 2007), (Figure II.7).

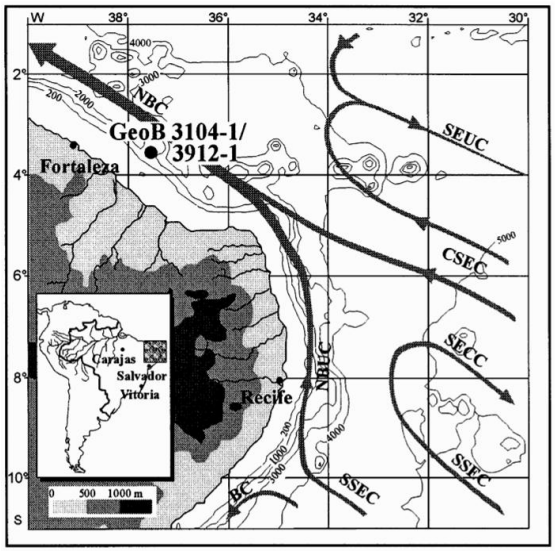

Figure II.6: Schematic view of surface circulation patterns in the Western Equatorial Atlantic. S/C-SEC, Southern/Central-South Equatorial Current; SECC, South Equatorial Counter Current; SEUC, South Equatorial Undercurrent; NBC, North-Brazil Current; NBUC, North-Brazil Undercurrent; BC, Brazil Current (Peterson and Stramme, 1991 and Da Simlveira et al., 1994 in Arz et al., 1997).

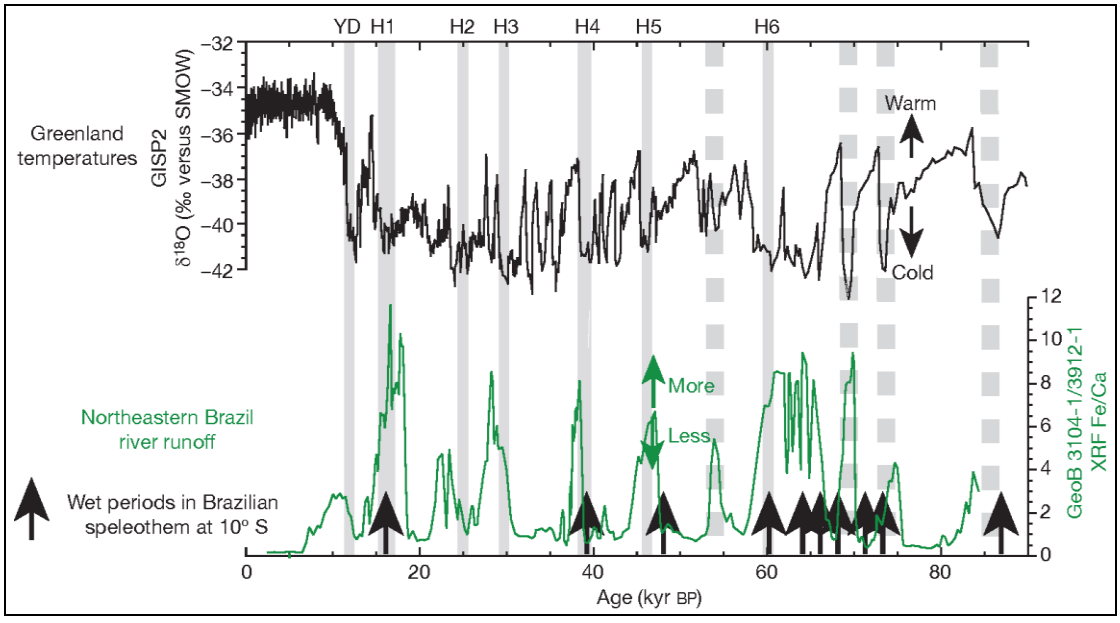

Figure II.7: River input offshore Brazil from Fe/Ca measurements (green curve, location of core is indicated in Figure II.6) compared to Greenland temperatures (black curve). Wet periods in Brazil (black arrows) are also indicated, as well as Younger Dryas and Heinrich events (grey vertical bars). Modified from Leduc et al. (2007).

4 THE QUATERNARY AMAZON FAN

Most published investigations about the Amazon Fan focused on the Quaternary upper and middle fan based on the high-resolution seismic data and sediment samples recovered by the Ocean Drilling Program, whereas older parts of the fan since its beginning in the Late Miocene remain unknown.

Prior to the Lobestory cruise (2004), the Amazon Fan was known to extend 700 km seaward of the shelf break off Brazil to abyssal depths over a fan-shape area of 375 000 km² in water depths of 1000 to 4300 m (Damuth and Flood, 1985). Jégou (2008) and Jégou et al. (2008) showed that the Amazon Fan terminal lobes are present at 4500 m water depth, extending the total length of the fan to more than 1000 km.

The upper 500-800 m of the Amazon Fan built up by aggradation, i.e. laterally and vertically through the stacking and overlapping of wedge-shaped, channel-overbank deposits. The bathymetric map shows a distributary network of meandering channels, the most recent one being the so-called Amazon (1A) channel (Figure II.8).

4.1 THE MAIN DOMAINS OF THE FAN

Damuth and Flood (1985) divided the present Amazon Fan into three morphologic and acoustic domains (Figure II.8):

1. The upper fan extends from the shelf break to about 3000 m water depth where the bathymetry shows a break in slope. Gradients range from about 25 m/1000 m (1:40 or 1.4°) near the shelf break to 10 m/1000 m (1:100 or 0.6°) near 3000 m, the average gradient is 14 m/1000 m (1:70 or 0.8°). The main feature in this area is the Amazon Canyon that appears as a deeply-incised valley up to 600 m deep.

Figure II.8: Morphology of the Amazon Fan. A: Distributary channels on upper and middle fan with channel dimensions. Numbers 1 through 6 beside major channels indicate relative ages of channels in order of increasing age (Damuth and Flood, 1985). B: EM12D backscatter image of the middle and lower fans. The channel-levee systems (Aqua, Brown, 1F, 1E, 1D, 1C, 1B, 1A and Amazon) and channel-mouth systems are shown and their local morphological characteristics are indicated (W: channel width and R: channel relief). Red doted line marks the outer limit of one lobe (A3). Thick white lines indicate the location of bathymetric cross-sections that show the downstream morphological changes of the Amazon channel-levee system (modified after Jégou et al., 2008).⇒

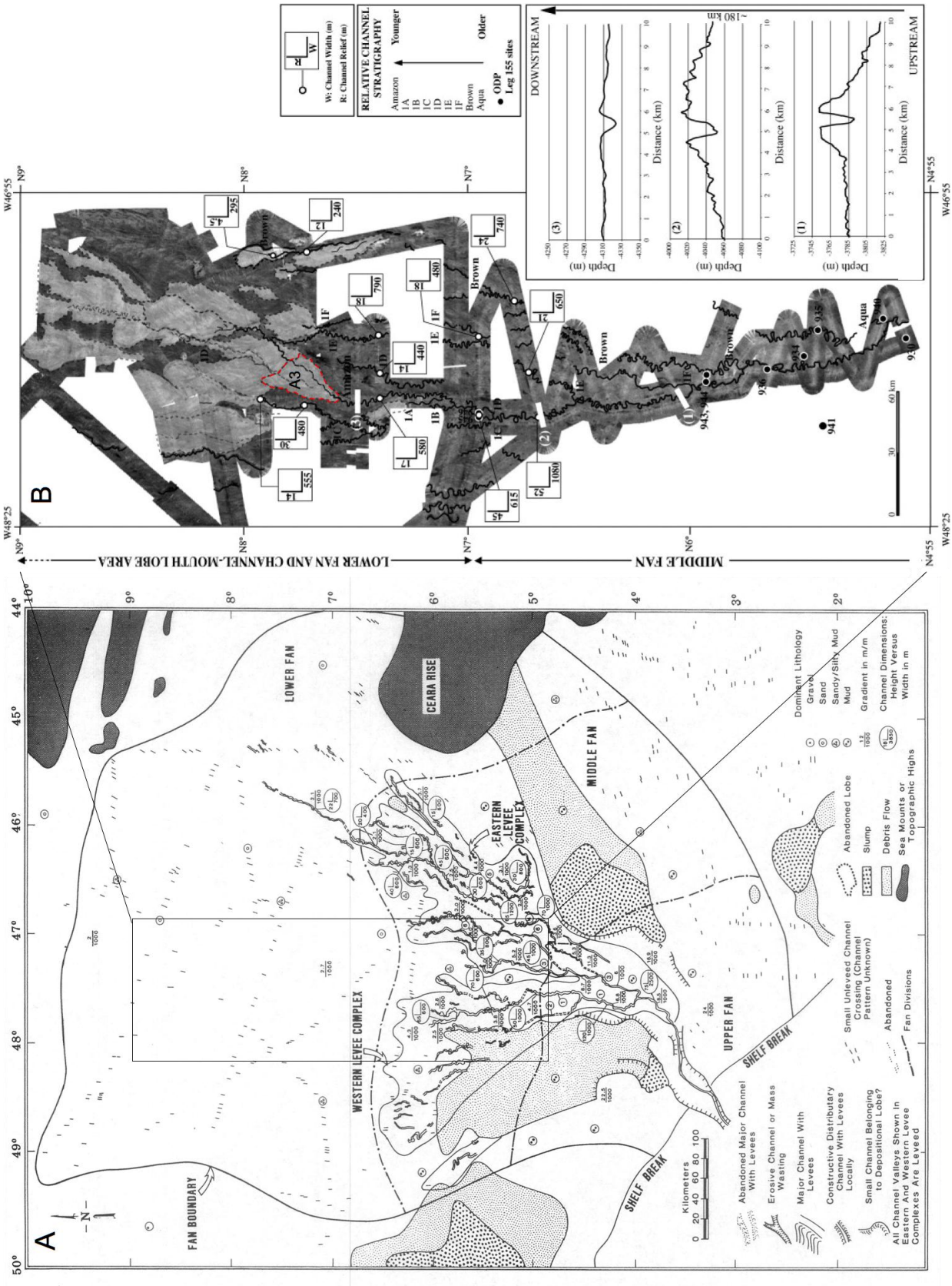
A
B
FAN BOUNDARY
LOWER FAN
CEARA RISE
MIDDLE FAN
EASTERN LEVEE COMPLEX
WESTERN LEVEE COMPLEX
UPPER FAN
SHELF BREAK
SHELF BREAK
LOWER FAN AND CHANNEL-MOUTH LOBE AREA
MIDDLE FAN
DOWNSTREAM
UPSTREAM
~180 km
RELATIVE CHANNEL STRATIGRAPHY
Amazon
Younger
Older
Brown
Aqua
ODP
Leg 155 sites
W: Channel Width (m)
R: Channel Relief (m)
Dominant Lithology
Gravel
Sand
Sandy/Silty Mud
Mud
Gradient in m/m
Channel Dimensions: Height Versus Width in m
Abandoned Lobe
Slump
Debris Flow
Sea Mounts or Topographic Highs
Small Unleveed Channel Crossing (Channel Pattern Unknown)
Abandoned
Fan Divisions
Abandoned Major Channel With Levees
Erosive Channel or Mass Wasting
Major Channel With Levees
Constructive Distributary Channel With Levees Locally
Small Channel Belonging to Depositional Lobe?
All Channel Valleys Shown In Eastern And Western Levee Complexes Are Leveed
Kilometers
0 20 40 60 80 100
Distance (km)
Depth (m)

2. The middle fan extends from about 3000 m to 4000-4200 m where a subtle change in gradient occurs. Gradients range from 10 m/1000 m to 4 m/1000 m (1/100 to 1/250 or 0.6° to 0.2°); the average gradient is about 5 m/1000 m (1:200 or 0.3°). The middle fan is characterized by numerous, large, leveed, distributary channels (Damuth and Flood, 1985). The most recent Amazon channel (1A) shows max. levee thickness (measured from thalweg to levee crest) of 300 m (Pirmez, 1994).
3. The lower fan is smooth and very gently sloping with an average gradient of 2.3 m/1000 m (1:430 or 0.1°). Numerous small distributary channels cross the lower fan, (Figure II.8A). These small channels were thought to be unleeved channels, but recently, Jégou (2008) showed that, even at more than 800 km from the canyon head, channels in the lower fan are still leveed and highly meandering. They are terminated by very flat lobate features interpreted as terminal lobes. Several lobes can be associated to a single channel. The lobes are only some meters thick (max. 25 m) and a single lobe covers an area of a few hundred km^2.

4.2 THE AMAZON CHANNEL

The Amazon channel is the most recent channel and, because of its well-preserved morphology, has been well described (Pirmez, 1994; Pirmez and Flood, 1995; Pirmez et al., 1997). The concave-up, relatively smooth longitudinal thalweg depth profile of the Amazon channel suggests that the channel tends to be in an equilibrium state, (see Chap. I, Figure II.9A).

Canyon width (max. around 13 km) decreases rapidely as the canyon gives rise to a leveed channel. The channel width decreases to < 1 km in the distal fan (Jegou, 2008). The max. thickness of the Amazon levees is 300 m and decreases to some meters in the distal fan and channel-mouth lobes, at 1100 km from the canyon head, i.e. the maximum length of the Amazon channel. The average height difference between inner and outer levee for meanders along the channel was measured as 20 to 60 m in the upper fan to as low as 2-5 m in the lower fan, with most meander bends having an outer levee less than 10 m higher than the inner levee (Pirmez 2003). The net topographic aggradation, integrating the entire erosional/depositional history of the channel, is illustrated in Figure II.9A (Pirmez and Imran, 2003). As a topographic levee begins to form in the canyon-channel transition zone, the constructional edifice rises above the surrounding fan surface, while the thalweg still sits below this surface. In the upper fan, the thalweg sits approximately at the same elevation as the surrounding fan surface, i.e. the upper fan channel represents a site of net sediment by-pass. Farther down system in the middle fan, the thalweg is perched above the surrounding

fan, implying net aggradation in the channel over the last thousand years (Pirmez, 2000; Pirmez and Imran, 2003) (Figure II.9). The overall thinning of the levee deposits has not only been observed for the Amazon channel, but also for older channel-levee systems (Pirmez and Imran, 2003).

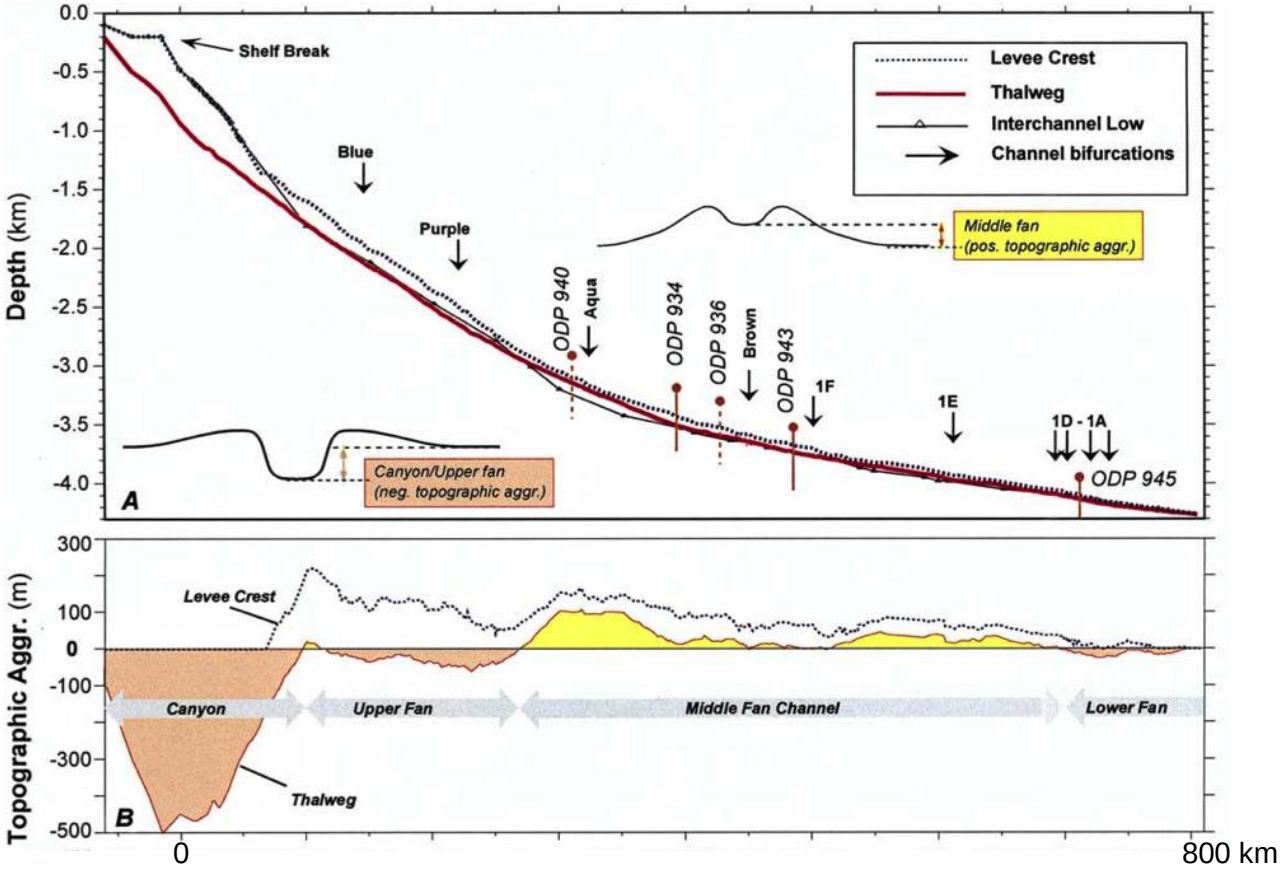

Figure II.9: Principal morphological features of the Amazon Channel (Pirmez and Imran, 2003). A:Longitudinal depth profiles (channel, levee, interchannel) with location of channel bifurcations and ODP sites (dashed are projected levee sites). Schematic cross-sections illustrate measurement of topographic aggradation. B:Topographic aggradation measurements (levee and thalweg relief with respect to inter-channel low).

4.3 ARCHITECTURE OF THE FAN

The Amazon Fan has aggraded principally by the deposition of thick channel-levee systems deposited by turbidity currents (Manley and Flood, 1988). The architecture of the fan is characterized by the stacking of these channel-levee systems. In these systems, the channels are perched on a thick acoustically transparent wedge-shaped system that appears to be constructed by overbank deposits from turbidity currents. High Amplitude Reflections (HARs) observed in the channel are interpreted as coarse-grained channel-fill deposits that accumulate on the channel floor and are buried as the channel-levee system aggrades. In addition, HARPs (High-Amplitude Reflection Packets) are observed to form the bases of

hannel-levee systems. HARPs are interpreted to consist of coarse sediments that were posited either from flows spreading laterally from a channel mouth to form a lobe deposit r from flows moving through a crevasse during an avulsion event (i.e. crevasse splays). The channel-levee systems seem to prograde over the HARPs. These lithological interpretations of seismic facies were later on confirmed and detailed thanks to the ODP Leg 155 drillings (see below).

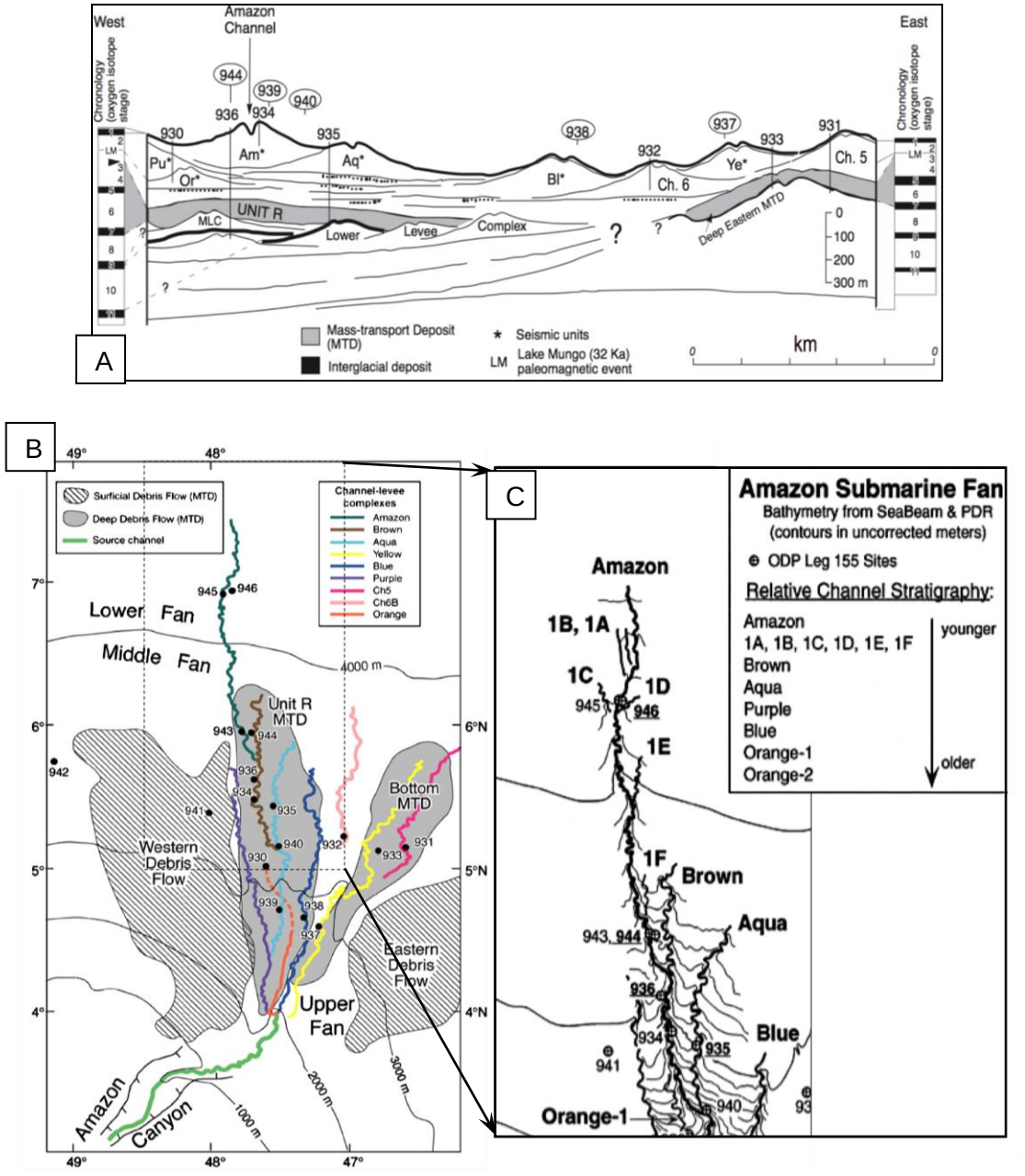

Figure II.10: Architecture of the Amazon Fan. A: Schematic cross section showing overlapping relationships between the channels the 4 main Levee Complexes (Basal, Lower, Middle and Upper Levee Complexes) and Mass-transport Deposits. Holes drilled during ODP Leg 155 are placed on this cross section. Thick lines on the complexes mark the interglacial lmud deposits (Maslin et al., 2005 after Flood et al, 1997). B:Refined stratigraphy for the channels of ULC including the position of Mass-Transport Deposits and a changed age relationship based on C14 dates (Maslin, 2006). B: The most recent channel-levee systems. The location of sites drilled during Ocean Drilling Program Leg 155 is shown as numbered black dots After Flood et al. (199)1 and Pirmez (1994),, in Pirmez et al.(1997).

Channel avulsion, i.e. the abrupt shift from an ancient channel to a new one (see Chapter I), has resulted in the deposition of a series of overlapping channel-levee deposits (Figure II.10A, Figure II.13). Previous workers on the Amazon Fan have assigned color names to all the recognized channel-levee systems (Figure II.10), with the exception of the two systems on the eastern fan, called Channel 5 and Channel 6 (Damuth et al., 1983, 1988; Manley and Flood, 1988) and the most recent channels that have been mapped by Flood et al. (1991) and Pirmez (1994) as channels 1F to Amazon (Figure II.10B).

The individual channel-levee systems of the Amazon Fan appear to be grouped into larger complexes: the Upper, Middle, Lower, and Bottom Levee Complexes (ULC, MLC, LLC and BLC respectively), from the youngest to the oldest (Figure II.10A). The number and names of the channel-levee systems constituting each group are indicated in Table II.1

Levee complexes	**Channel-levee systems**	**Mass-Transport Deposits**
		Eastern and Western Debris Flow (EDF and WDF)
Upper Levee Complex (ULC)	Amazon (Am) Brown (Br) Aqua (Aq) Purple (Pu) Blue (Bl) Yellow (Ye) Channel 5 (Ch 5)* Orange (Or)* Channel 6 (Ch 6)*	
		Unit R Mass-Transport Deposit and Bottom Mass-Transport Deposits (URMTD and BMTD)
Midle Levee Complex (MLC)	Red	
Lower Levee Complex (LLC)	Gold Green Lime Gray	
Basal Levee Complex (BLC)		

* The age relationship between Orange and Channels 5 and 6 has not been clearly delineated from seismic profiles.

Table II.1: Chronology of the architectural elements of the Amazon Fan: Levee Complexes, channel-levee systems and Mass-Transport Deposits. Table established from Damuth et al. (1983), and Manley and Flood (1988). Note that this chronology has been later confirmed by Flood et al. (1997), but discrepancies exist with results of Maslin (2006) (see 4.4, this chapter).

The ULC is separated from older levee complexes by two huge (up to 100 m thick and 70 km wide) Mass-Transport Deposits: the Unit R Mass-Transport Deposits (URMTD) and the

Bottom-Mass-Transport Deposits (BMTD) also called the Deep Eastern MTD (Figure II.10A). It is locally covered by 2 superficial MTDs, called the Western Debris Flow (WDF) and the Eastern Debris Flow (EDF).

From Maslin et al. (2005) these catastrophic failure events were climatically driven (see 4.4 below) and there were two different mechanisms operating during the glacial (gas-hydrate release for the BMTD and URMTD) and the deglacial (sediment over-burdening/shifting depocenters for the superficial MTDs) periods.
In addition to the above mentioned Mass-Transport Deposits, (Reis et al., submitted) mapped gravity-related slide complexes in the area (Figure II.11) that are geographically coincident with part of the MTDs previously mapped in the Amazon Fan, but that originate from thrust belts on both side of the Amazon canyon. While former studies considered the MTDs were triggered by climatic sea-level changes (e.g. higher sedimentation rates and/or gas hydrates dissolution), Reis et al. (submitted) pointed out that gravity tectonics have also to be taken into consideration as a triggering mechanism of slope instability.

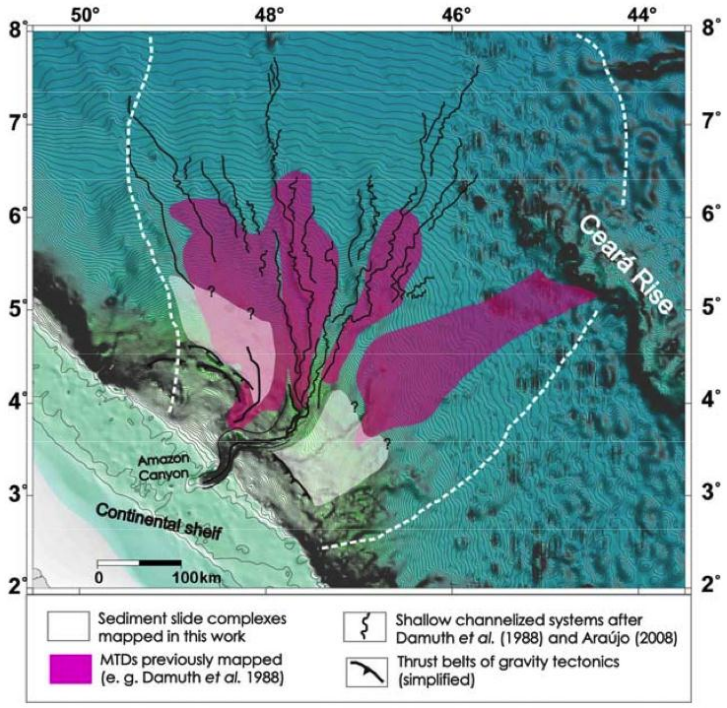

Figure II.11: Sediment slide complexes originating from thrust belts of gravity tectonics on the continental slope (Reis et al., submitted).

4.4 CHRONOSTRATIGRAPHY OF THE FAN

The age assignments of the sediments drilled during ODP Leg 155 are based on biostratigraphic analysis of calcareous nannofossils and planktonic foraminifers, combined

with paleomagnetic data (Cisowski and Hall, 1997; Mikkelsen et al., 1997).

Because foraminifer abundances were too low for extensive AMS-14C dating in the glacial age sediment, the only way to construct age-depth models was through $\delta^{18}O$ stratigraphies (ANNEX II.2), along with the biostratigraphic and paleomagnetic datums (Showers et al., 1997).

Some ^{13}C stable isotope measurements have also been done locally, essentially to date the MTDs (Vilela and Maslin, 1997).

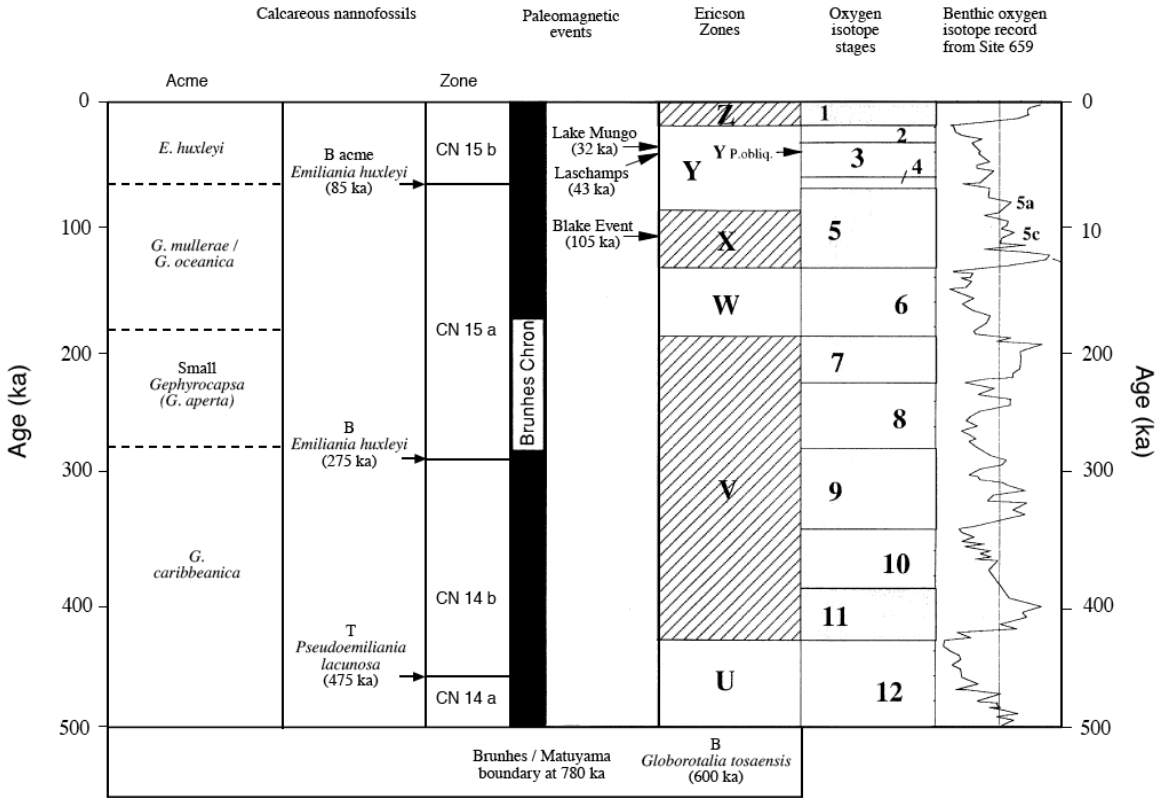

Figure II.12: Summary of proxies used in the framework of ODP Leg 155. From left to right: nannofossil acme zones of Weaver (1993) and Pujos and Giraudeau (1993); nannofossil zones of Okada and Bukry (1980); paleomagnetic events Cisowski, (1995); planktonic foraminifer stratigraphy (Ericson Zones of Ericson and Wollin (1968), Ericson (1961)); oxygen isotope stages and oxygen isotope curve at site 659. From Tiedemann et al. (1994) in Mikkelsen et al. (1997).

^{14}C measurements (Maslin et al., 1997) were rare and limited to shallow sediments or MTDs, until recently published ^{14}C dates by Maslin et al. (2006). These new dates helped us correcting the ODP age models locally.

4.4.1 $\delta^{18}O$ isotopic ages

Age models have been constructed at each core using curves from $\delta\ ^{18}O$ planktonic foraminifers. The dating of the sedimentary deposits for the Amazon Fan was first based on

the $\delta\ ^{18}O$ curves of the drilling sites. In the study of Showers et al. (1997) isotopic events were identified by comparison to the $\delta\ ^{18}O$ stacked chronologies of Imbrie et al. (1984), Prell et al. (1986), Pisias et al. (1984) and Martinson et al. (1987). In addition, the Younger Dryas Event is represented in some sites. The age for the end of this $\delta\ ^{18}O$ event was taken at 11 ka Flower and Kennett (1900).

4.4.2 Biostratigraphy

Calcareous nannofossils (only two standard nannofossil datums)

The Quaternary nannofossil biostratigraphy is based on the zonal scheme of Bukry (1973, 1975, 1978) and Okada and Bukry (1980), combined with the high-resolution Quaternary studies of Gartner (1977), Raffi et al. (1993), Weaver (1993), and Pujos and Giraudeau (1993). Abundant and well-preserved nannofossils are only found in hemipelagic deposits of the Holocene calcareous clays at the top of the Amazon Fan and in deep-carbonate layers. Well-preserved nannofossils are also present in discrete calcareous clasts within the turbidites and MTDs and provide an estimating for the maximum ages of the turbidite deposits.

The constraining calcareous nannofossils events are:

- Absence of Pseudoemiliania lacunose, indicative of sediments younger than 475 ka,
- Onset of Emiliania huxleyi which defines the base of Zone CN15a at 275 ka,
- Bottom of the acme of *E. huxleyi,* which defines the base of nannofossil Zone CN15b at 85 ka.

Planktonic foraminifer assemblages (primarily based on the sequential stratigraphy of the Ericson Climate Zones)[1]

The Pleistocene/Holocene zonal schemes based on acme episodes (Weaver, 1993; Pujos and Giraudeau, 1993) were better adapted to the disrupted nature of the recovered sequences than the classical first/last appearance datums. However, no complete succession of acme periods as reported from the deep-sea record by Weaver (1993) and Pujos and Giraudeau (1993) has been found in the Amazon Fan.

The constraining planktonic foraminifer events are:

[1] Ericson Zones do not always correlate with interglacial-glacial climate shifts (e.g. Zone V spans over several interglacial phases from oxygen isoptope stages 7 to 11).

- Presence of the *Globorotalia menardii* complex, indicative of ages covering oxygen isotope stages 7 (around 200 ka) to 11 (around 400 ka),
- Ericson Z/Y boundary or reappearance of *Globorotalia tumida* in the Atlantic Ocean, indicative of the Holocene/Pleistocene boundary at 9 ka in the Western Equatorial Atlantic.
- Disappearance of *P. obliquiloculata*. This event is diachronous, extending from 36 to 44 ka, but in the ODP study an age of 40 ka was assigned. Its reappearance is dated at 11 ka based on 14C-AMS-measurements (Jones, 1994, pers. comment in Flood et al., 1997).

4.4.3 Age model for the Amazon Fan based on $\delta^{18}O$ evolution and biostratigraphy

Detailed foraminifer study (at Site 934, adjacent to the most recently active fan channel, Scientific Shipboard Party, 1995a) shows that calcareous mud first accumulated around 9 ka, when the sea level was around 30 m below present sea level, indicating rising sea level that resulted in the end of significant cross-shelf transport of sediments from the Amazon River to the Amazon Fan. The end of activity of the Amazon Fan, which is marked by the hemipelagic drape over the ULC, has been ^{14}C dated at 9 to 7.3 ka (in Showers et al., 1997). This timing corresponds also to the reappearance of *Globorotalia tumida* and to the occurrence of an iron-rich crust dated at 9.3 ^{14}C ka (Showers and Bevis, 1988). This crust is, however, diachronous across the Amazon Fan and adjacent Western Equatorial Atlantic (McGeary and Damuth, 1973; Damuth, 1977; Damuth et al., 1983). The base of the surficial carbonate-rich mud was arbitrarily given an age of 9 ka (Piper et al., 1997). Before the complete end of activity of the fan, a $\delta^{18}O$ peak is observed and ^{14}C dating at site 934 gives an age of 11 ka corresponding to the Younger Dryas event (Showers et al. 1997).

Similar but buried carbonate-rich muds overlie the Middle, Lower, and Bottom Complexes (Figure II.10A).

Oxygen isotope stratigraphy reported in Piper et al. (1997) allowed to date the calcareous muds overlying the Middle Levee Complex as Stage 5 highstand deposits. Calcareous muds overlying the Lower Levee Complex are assigned to isotopic Sub-stage 7.3 and those overlying the Bottom Levee Complex to Sub-stage 7.5, suggesting that each complex built of a number of individual channel-levee systems, developed during a major lowstand of sea level (Figure II.12) (BLC: stade 8 (245 – 300? ka), LLC: stade 7.4 (225 ka), MLC: stade 6 (130-190 ka), ULC: stade 2-4 (70-11.5 ka) and the begining of stade 1 (beginnig of the

Holocene). These ages have been adopted in further studies (e.g. Lopez, 2000). However, Maslin et al. (2005) consider the ages for the BLC and LLC as uncertain (compare Figure II.13B).

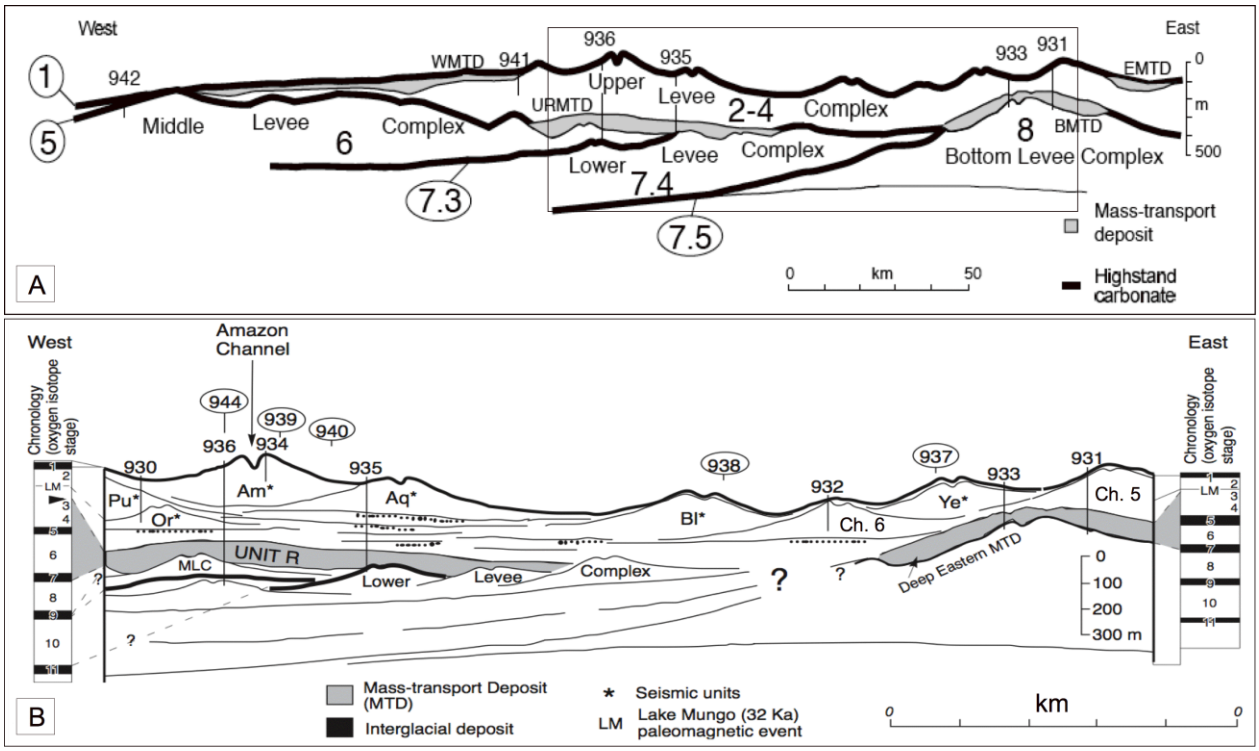

Figure II.13: Schematic cross section of the Amazon Fan. A: age assignment of the major channel-levee complexes, based on correlation with the dated (isotopic and nannofossil analysis) highstand carbonate-rich units (Piper et al., 1997). Stages and sub-stages are given in large, bold numbers.B: Individual channel-levee systems based on seismic stratigraphy, Ye = Yellow, Bl = Blue, Aq = Aqua, Am = Amazon, Pu = Purple, Or = Orange (see Table II.1). In Maslin et al. (2005), modified from Flood et al., (1997).

While the major complexes appear to be controlled by major sea-level variations, the activity of each individual channel-levee systems seems to be unrelated to major sea-level changes (Figure II.14B). Flood and Piper (1997) attributed the activity of individual channel-levee systems of the ULC to isotope stages 4 to 2. The timing for most of the channel-levee systems of the ULC is proposed in Figure II.14 and is mainly based on $\delta^{18}O$ age models (based on datations at each site, ANNEX II.2). Age models could only be constructed with isotopic data into isotopic stages 2 and 3, because isotopic signal is disturbed by sediment reworking that dominate the sedimentary record older than stage 3 (> 25 ka). The Orange to Aqua systems were active during isotopic stage 3, the Brown system was constructed during isotopic stage 2 and the activity of the Amazon system spanned from the end of stage 2 to the beginning of stage 1.

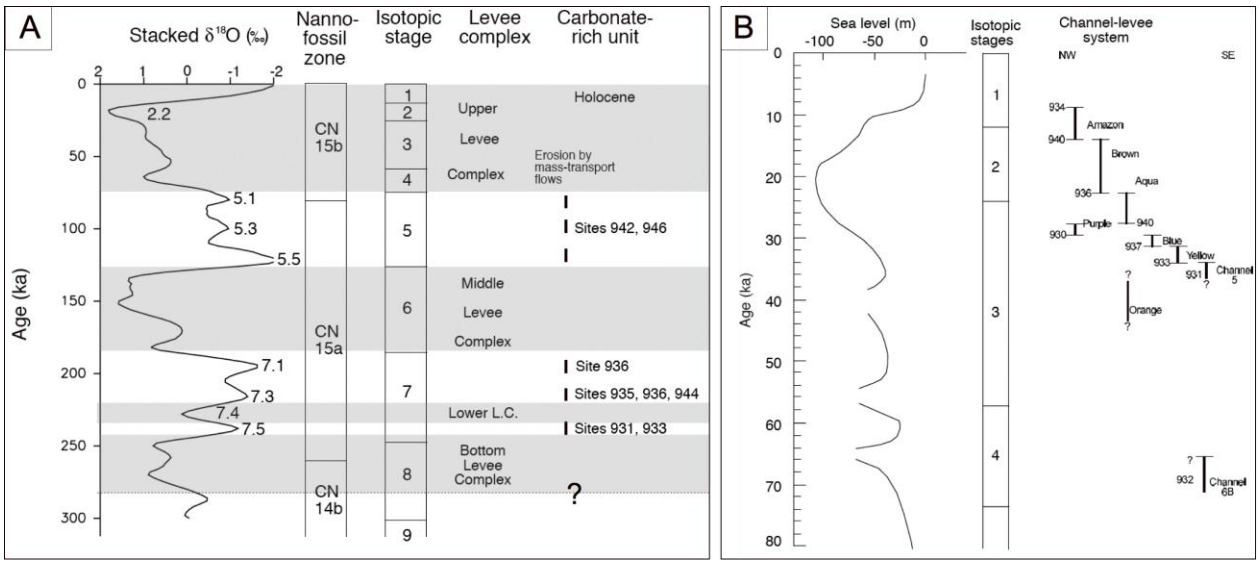

Figure II.14: Relation between the sea-level fluctuations and the building of the major architectural features of the Amazon Fan. A: Complete Amazon Fan (Piper et al., 1997). B: Timing of channel-levee systems activity during the past 50 ka (Flood and Piper, 1997, after Flood, Piper, Klaus, et al., 1995).

Concerning the MTDs, Maslin et al. (2005) propose an age of 35-37 ka cal. BP for the BMTD, of 41-45 ka cal. BP for the URMTD and of 13 ka cal. BP for the WMTD and EMTD, suggesting that the MTDs correlate with rapid, critical shifts in past sea level (Reis et al., submitted) also refer to gravity tectonics as a probable triggering mechanism of slope instability (see 4.3 above).

4.4.4 Age model based on radiocarbon dating

The radiocarbon datings have been realized on various material either foraminifers, organic matter, or mollusks (see Table III.8 for the details of measurements and resulting ages).
These measurements allowed Maslin (2006) to propose a stratigraphy (Figure II.15) that is not always in agreement with the age model based on biostratigraphy and isotopic record (compare Figures II.14 and II.15).
Taking into account that both age models are not in agreement, and in order to be able to choose one of them for our study, we had to evaluate their respective validity (see Chapter III).

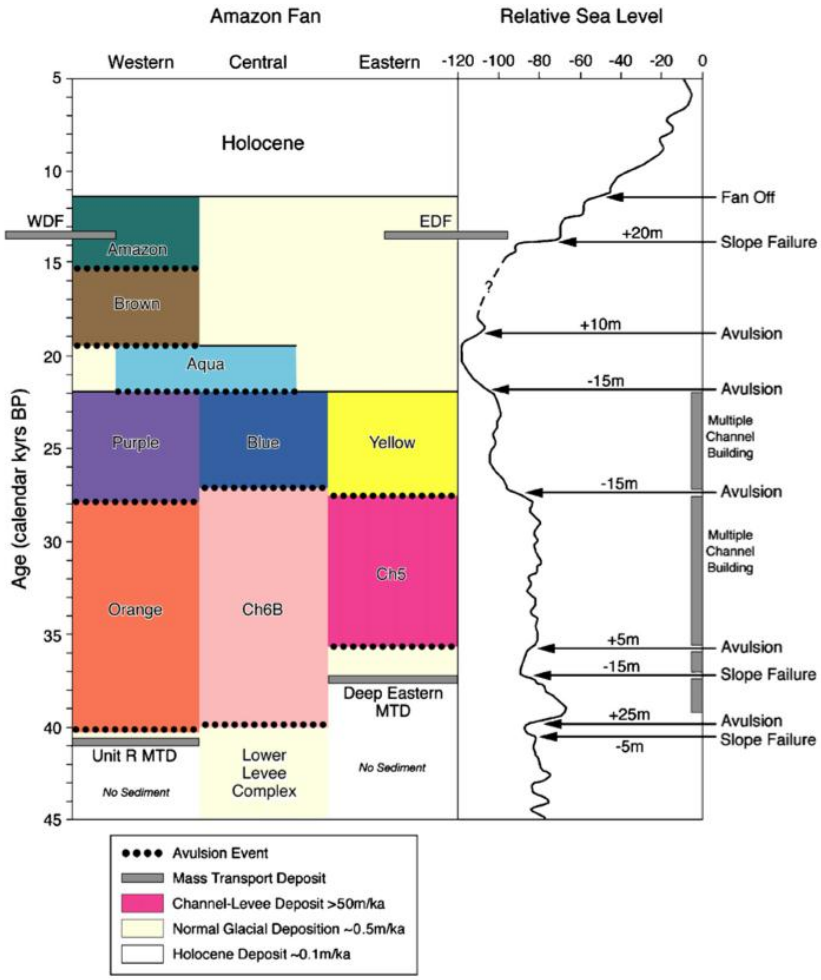

Figure II.15: Timing of the depositional events and slope failures in the different part of the Amazon Fan ULC (Maslin, 2006). The spatial distribution of the channel-levee systems is shown in Figure II.10B. Note that there exist discrepancies for the timing of some channel-levee systems (e.g. Amazon, Brown, Aqua) with the chronostratigraphy of ODP (compare with Figure II.14). WDF : Western Debris Flow, EDF : Eastern Debris Flow, Unit RMTD : unit R Mass-Transport Deposit, Deep Eastern MTD : Deep Eastern Mass Transport Deposit.

4.4.5 Deposition rates and channels duration

The age model based on $\delta^{18}O$ stratigraphy allowed to calculate for the central fan:

- An average sedimentation rate of 3 to 10 cm/ka for the Holocene, which is similar to open ocean rates and of maximal 30 m/ka for the glacial sedimentation rate, (Showers et al., 1997; Flood and Piper, 1997).
- The recurrence time of major channel shifts within the latest Pleistocene Upper Levee Complex (ULC), which occurred by avulsion in the ULC. It is maximum every 2 to 3 ka (Cha. 5 to Aqua, during sea level fall) and 5 to 10 ka (Brown to Amazon during sea level rising), Figure II.14 (Flood and Piper, 1997).
- An average occurrence of 1 flow event every 2 years at site 940. A 240 m thick levee

succession, built of silt-laminated muddy turbidites (about 2.5 cm per turbidite), is estimated to represent a 20 ka record of turbidity current activity (from ~30 to ~10 ka), (Piper et al., 1997).

4.5 SEDIMENT DISTRIBUTION

Prior to Leg 155 drillings, the distribution of sedimentary facies within the fan was inferred from the seismic facies (3.5 kHz and 100 Hz seismic-reflection profiles), GLORIA side-scan sonar records, and short (< 10 m), widely spaced piston cores.
Already these older seismic-reflection data showed that the elementary depositional feature of the fan is the aggradational channel-levee system, and that individual channel-levee systems display several seismic facies that are suggestive of turbidite depositional processes.

Results from ODP Leg 155 supported these interpretations. Leg 155 recovered long continuous cores through all of these seismic units and allowed observation of the sedimentary facies of the channel-fills (including HAR), levees, HARPs and MTDs (Figure II.16).

Recovered sediments showed that the levees are comprised of mainly mud with thin silt and sand beds typical of overbank deposits, whereas the channels contain coarser, thicker silt and sand beds. Additional piston cores from the lower Amazon Fan contain the coarsest and thickest beds of sand, and cores from surficial debris flows showed disturbed, contorted sediments.

ODP drilling resulted in the identification of lithofacies that were classified into 15 sedimentary facies (Normark et al., 1997). In addition to this general classification of lithofacies, at a smaller scale, 12 fine-grained turbidite facies have been distinguished from visual core description, X-radiography, and grain-size (Piper and Deptuck, 1997). These fine-grained facies will not be described here because they were not used in my study.

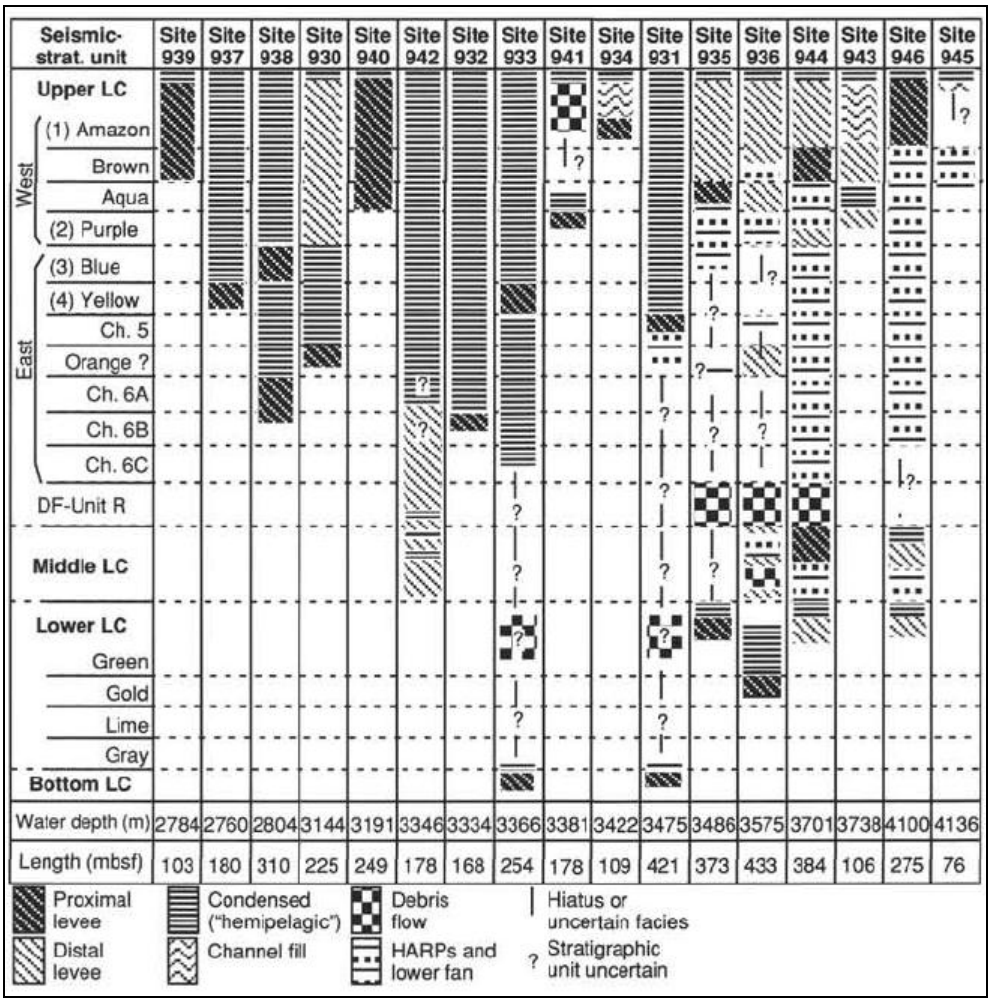

Figure II.16: Architectural element drilled at each ODP Leg 155 site (Flood et al., 1995). The location of the sites is given in Figure II.10.

4.5.1 Sedimentary facies observed during ODP Leg 155

Fifteen sedimentary facies have been recognized by Normark et al. (1997) in the 4 km of sediment cored by the 17 ODP sites on the Amazon Fan (Table II.2). Twelve of these facies are terrigeneous sediments and correspond to the 4 architectural elements of deep sea fans (levees, channel-fill deposits, HARPs and MTDs).

The following facies descriptions refer to the shipboard distinctions for bed thickness where “thick bedded” refers to sedimentary units thicker than 30 cm, “medium bedded” to 10 to 30 cm thick units, and “thin bedded” to units less than 10 cm thick.

	Facies (Normark et al., 1997)	**Environments**
1	Medium- to thick-bedded disorganized gravel and sand gravel	Lobes
2	Medium- to thick-bedded disorganized sand: massive or structureless to chaotic with deformation and clasts	Lobes
		Channel fill
		MTDs
3	Thin- to thick-bedded organized sand beds (includes grading, parallel stratification, and cross stratification)	Lobes
		Levees
		Channel fill
4	Laminated to medium-bedded disorganized or structureless silt	Levees
5	Laminated to thin-bedded organized silt (includes grading, parallel stratification, and cross stratification)	Levees
6	Very thin (~1 mm), regular silt and mud laminae	Levees
7	Irregular or discontinuous silt laminae	Levees
8	Color-banded and/or color-mottled silt and mud laminae and thin beds	Levees
9	Color-mottled and/or color-banded mud and clay	Levees
		(Hemi-) Pelagic
10	Homogeneous, structureless mud and clay	Levees
11	Disorganized pebbly or gravelly mud and sandy mud	Levees
12	Deformed or chaotic mud (including mud clasts and/or dipping, folded, contorted, faulted and/or truncated strata	Levees
		Channel fill
13	Biogenic mud	(Hemi-) Pelagic
14	Biogenic sand	(Hemi-) Pelagic
15	Chemiogenic sediment	(Hemi-) Pelagic

Table II.2: Sedimentary facies identified during ODP Leg 155, in the Amazon Fan, based on megascopic description of cores (facies description is from Normark et al., 1997)

The architectural elements of the fan are composed of these sedimentary facies, as summerized in Figure II.17 (Normark et al., 1997).

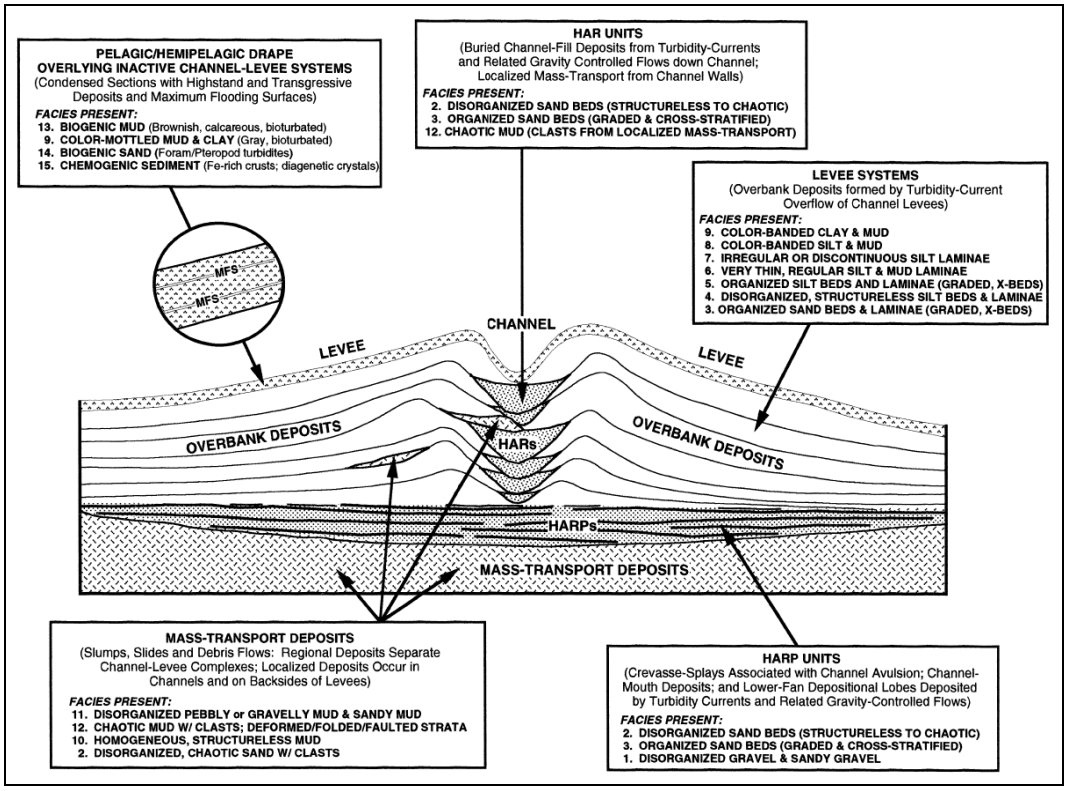

Figure II.17: Schematic diagram showing the distribution of sedimentary facies within acoustic units (e.g. HAR, HARPs, and levees) and mass-transport deposits (MTDs) of the Amazon Fan (Normark et al., 1997). The diagram shows a transverse cross-section of a typical channel-levee system, which is the elementary architectural unit of the fan, a basal HARP unit and an underlying regional-scale MTD.

4.5.1.1 Levees

The levee deposits consist in 7 interbedded facies:

- The color-banded mud and clay Facies 9 (Figure II.18A) is the most common facies in these deposits. Interbeds of coarser sediment are rare to extremely abundant and are mainly composed of silt-size particles, occurring in laminae and thin beds. Beds of medium thickness are rare to common, and thick beds are very rare.
- The most common granular facies is organized in silt laminae and thin beds (Facies 5, Figure II.18B), which is usually present as parallel- and cross-laminated laminae and thin beds, rarely with normal grading or with climbing ripples.
- Less common are disorganized or structureless silt laminae and beds (Facies 4, Figure II.19A), color-banded silt and mud (Facies 8, Figure II.19B), and irregular or discontinuous silt laminae (Facies 7, Figure II.20A). Very thin, regular silt and mud laminae (Facies 6, Figure II.20B) are rare.
- Organized beds and laminae of fine sand, which commonly show normal grading, parallel- and/or cross-lamination locally (Facies 3, Figure II.21).
- Deformed or chaotic mud with contorted, folded, and discordant, truncated beds

(Facies 12, Figure II.22) are also present in levees. They are interpreted as thin, localized MTDs that occur on the backsides of levees as a result of local sediment failure.

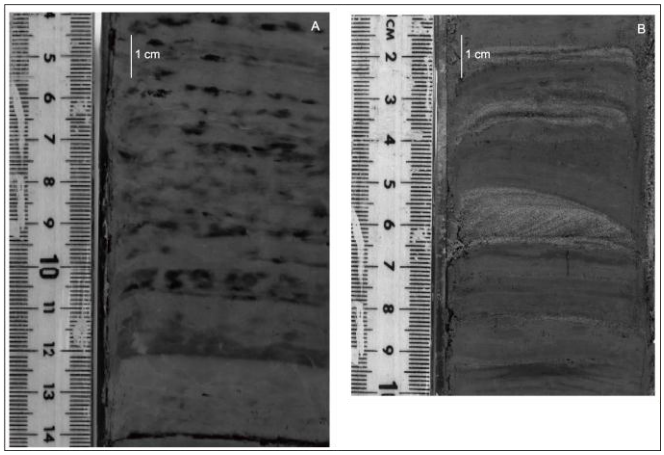

Figure II.18: Levee facies (Normark et al., 1997). A: Facies 9, color-banding in dark gray mud of overbank deposits from the Amazon channel that fill the channel in a cutoff meander at Site 934 (interval 155-934-1H-3). B: Facies 5, parallel- to cross-laminated silt laminae and thin beds from the distal portion of the Purple levee.

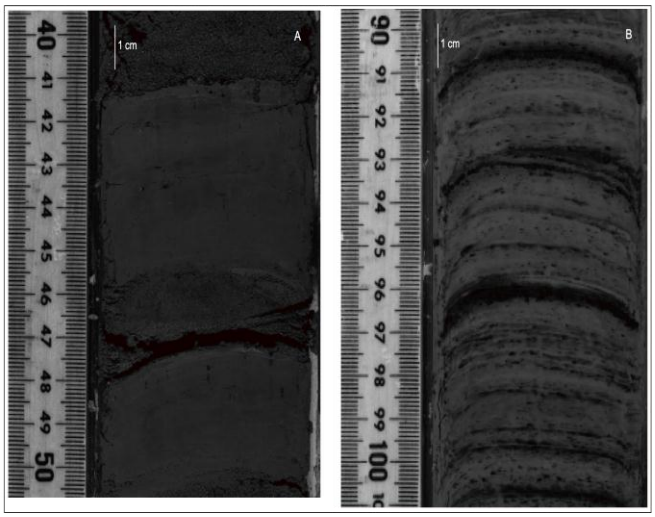

Figure II.19: Levee facies (Normark et al., 1997). A: Facies 4, structureless, closely spaced, thin coarse silt beds from levee deposits of the Yellow system (interval 155-937C-6H-3). B: Facies 8, color-banded silt laminae in levee deposits of the Amazon channel-levee system (interval 155-940A-3H-4).

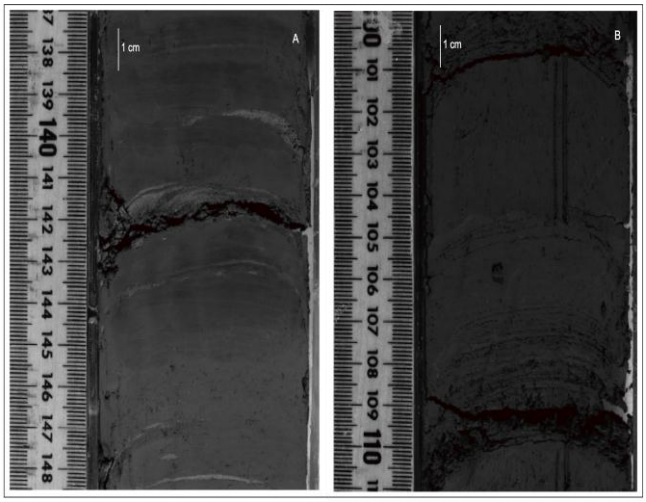

Figure II.20: Levee facies (Normark et al., 1997). A: Facies 7, thin and discontinuous silt laminae and thin beds from levee deposits of the Aqua system (interval 155-935A-8H-6). B: Facies 6, consisting in very thin, regular silt and mud laminae, Channel 5 levees (interval 155-931A-4H-3).

Figure II.21: Levee facies (Normark et al., 1997). Facies 3, thin- to –thick bedded organized sand, including cross-stratified, wavy and normally graded beds (interval 155-942A-6H-5). Note burrow truncation at 90-92 cm.

Figure II.22: Facies 12 (Normark et al., 1997). Deformed, contorted, and folded color-banded mud in a local slump deposit in the Amazon levee (interval 155-940-3H-5).

4.5.1.2 Channel-fill deposits

- The most common facies is Facies 2 (Figure II.23A), made of thick-bedded, disorganized structureless to chaotic, poorly sorted fine to coarse sand that contains abundant large mud clasts.
- Medium- to thick-bedded organized sands, commonly fine to medium sand, (Facies 3, Figure II.23B) are also common to abundant in the HARs Many sand beds grade upward to silt to clay at the top.
- Deformed or chaotic mud with abundant mud clasts and deformations (Facies 12, Figure II.24) are also observed in channel-fill. They are suggested to be localized MTDs, slumped from the channel walls towards the channel floor.

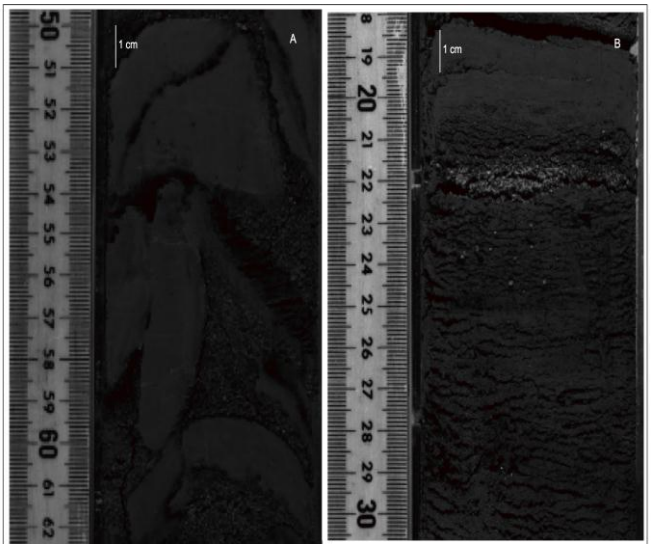

Figure II.23: Channel-fill facies (Normark et al., 1997). A: Facies 2, consisting in fine to medium sand with irregular, rounded mud clasts from the Amazon channel on the lower fan (interval 155-945A-1H-4). B: Facies 3, normally graded medium sand to coarse silt from channel-fill deposits in cutoff meander of the Amazon channel (interval 155-934A-10H-6).

Figure II.24: Facies 12 (Normark et al., 1997). Deformed and truncated clay laminae, probably corresponding to local MTD in channel-infill deposits (interval 155-934A-1H-1).

4.5.1.3 HARPs deposits

- HARP deposits are made principally of Facies 2, (structureless, poorly sorted and thick beds of medium to coarse sand with common large mud clasts, Figure II.25A) and Facies 3 (organized medium to thick sand beds of mainly fine to medium sand, Figure II.25B).
- Some intervals of little core recovery appear to contain thick beds of disorganized gravel or sandy gravel (Facies 1, Figure II.26).
- Facies 5 and Facies 11 (normally indicative of debris flow, Figure II.27) can be present although very rare.

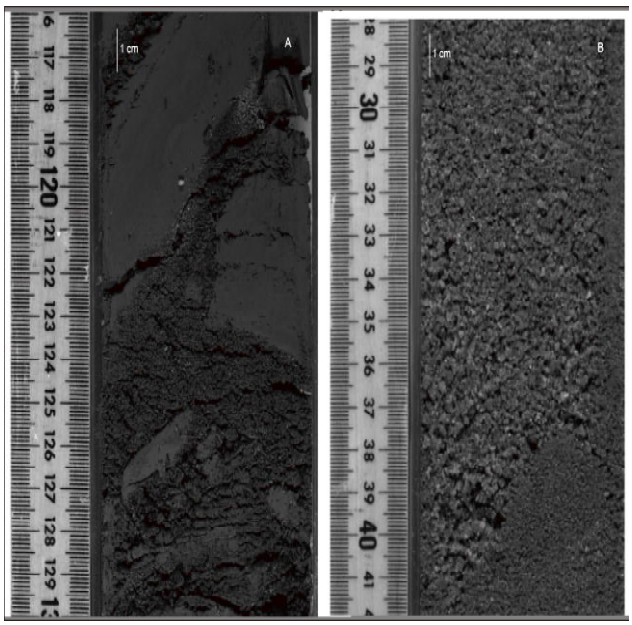

Figure II.25: HARPs facies (Normark et al., 1997). A: Facies 2, consisting in poorly sorted, thick, medium to coarse sand with large mud clasts from HARP units of the Brown system (interval 155-936A-10H-1). B: Facies 3, consisting in normally graded medium to coarse sand beds from Brown HARPs (interval 155-936A-10H-1).

Figure II.26: HARPs Facies 1 (Normark et al., 1997), showing lithic pebbles recovered from deposits interpreted to be HARPs of the Red system. Core recovery was very poor, however, these pebbles suggest a gravel or sandy gravel facies (A: interval 155-936A-36X-CC, B: interval 155-936A-38X-CC).

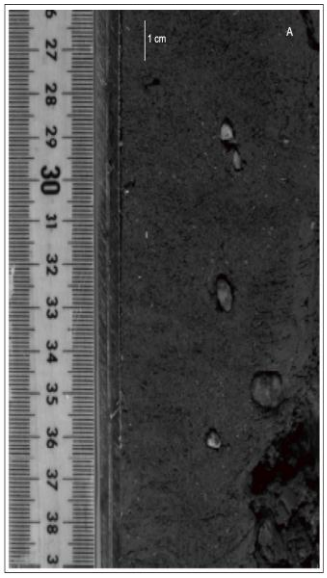

Figure II.27: HARPs facies (Normark et al., 1997). Facies 11, consisting in quartz and rock granules and pebbles scattered through the mud of a MTD in a HARP unit (interval 155-936A-9H-2).

4.5.1.4 Regional Mass Transport Deposits

- Extensive MTDs consist in thick intervals (tens of meters) of deformed or chaotic mud with mud clasts and blocks, or discordant, contorted, folded, faulted, or truncated beds (Facies 12, Figure II.28A).
- Thick intervals of disorganized pebbly or gravelly mud and sandy mud (Facies 11, Figure II.28B). Intervals of homogeneous, structureless mud (Facies 10) that may

represent large undeformed displaced blocks are commonly interbedded with Facies 12.

Figure II.28: MTDs facies 12 (Normark et al., 1997). Facies 12 composed of discordant, truncated, and contorted mud in the URMTD (interval 155-944A-25X-5).

The analysis of facies distribution and vertical evolution within the architectural elements led ODP Scientists to conclude that:

- Thin-to-thick-bedded organized sand (Facies 3) is the only facies common to levee, channel (HAR), and HARP deposits. However, sand beds in channels are thicker and coarser than in the levee deposits.
- Where the core recovery is relatively complete, silty facies (facies 3 to 8) common in the levee sequences abruptly overlie coarse-grained facies of HARPs. This abrupt upward change in facies in the sediment column indicates that the levees rapidly prograde over the HARPs.
- The angular shapes of the mud clasts within sand beds of Facies 2 inside the channels are indicative of limited transport distance and suggest that erosion and failure of the inner walls of the meandering channels are common.
- The coarsest and thickest beds (Facies 1 and 2) are found in the HARP deposits. This suggests that the Amazon Fan should not necessarily be considered a “mud-

rich" turbidite system.

- The lack of thick-bedded coarse facies in the levee sections, compared to the channel-fill and lobe deposits, indicates that the sand clasts carried through the Amazon channel-levee systems remained confined within the channel until reaching the active depositional lobe area at the channel mouth, unless an avulsion occurs. The dense lower parts of the turbidity currents and related gravity flows stay confined within the channel, even when the levee-crest to channel-relief is as little as 35 m (at sites 945 and 946).

4.5.2 Sediment distribution in the Lower fan and terminal lobes from Lobestory cores

Sand deposits have been observed in cores of the distal lobes (Figure II.29), e.g. at the channel-mouth of the Amazon channel at 1100 km from the canyon head (Jégou, 2008). This observation highlights that the turbidity currents and related gravity flows moving throughout the Amazon Fan channel-levee systems are "highly efficient" in transporting sand and gravel for hundred of kilometers.

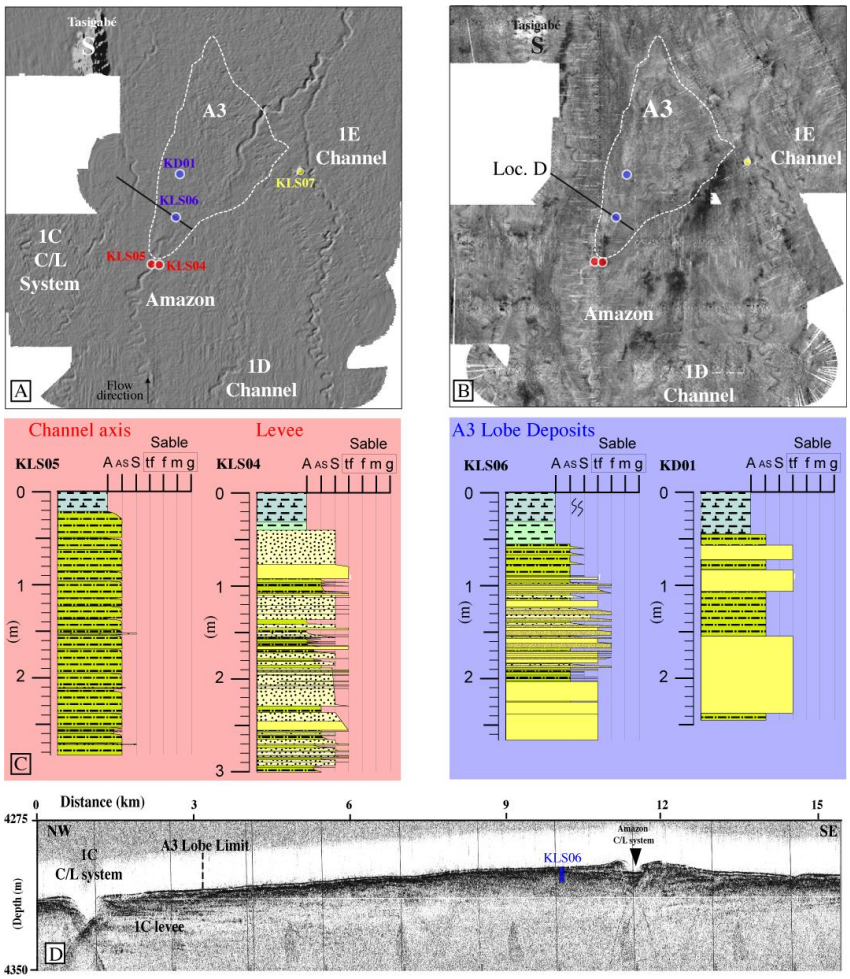

Figure II.29: Zoom of the lobe A3, one of the three Amazon channel lobes, in the distal fan area (Jégou, 2008) (location of A3 in Figure II.8B). A:bathymetric map. B: EM12D backscatter image. C: Lithology of sediments at the entrance of the lobe, i.e. in the channel axis (KLS05) and levees (KLS04). D: Lithology of sediments inside the lobes (KLSO6 and KD01). D: 3.5 kHz seismic line of the lobe (position marked by black line in A and B).

4.5.3 Electrical and sedimentary facies

The Formation MicroScanner (FMS) allows measurement of vertical and lateral variations of formation resistivity (which depends on the resistivity of the formation fluid, the pore space, and mineralogy) and images the borehole walls.

The sediments of the Amazon Fan are unconsolidated and the pixel tone of the images can be correlated with grain size, silt and sand showing lighter tones and muddy sediments showing darker tones. Bed boundaries and structures have also been interpreted (Pirmez et al.,1997).

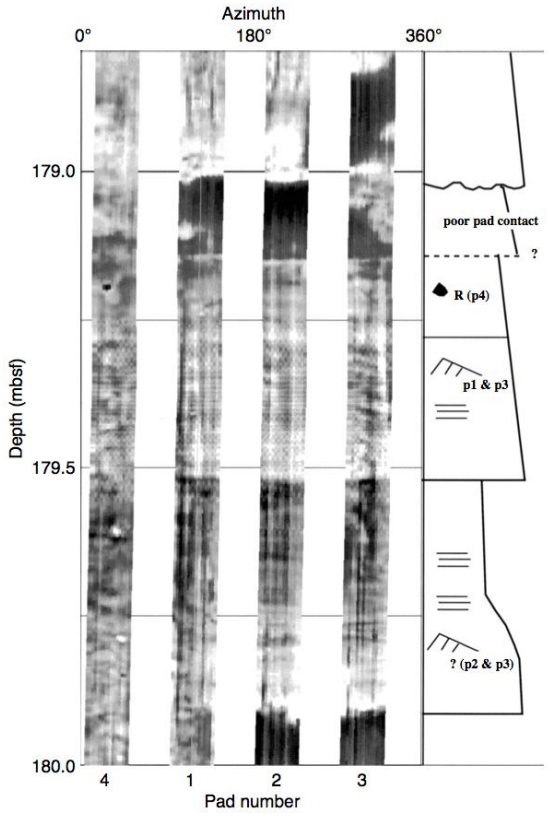

Figure II.30: FMS image of hole 944A (179-180 mbsf) and interpretation of the images showing medium beds of silt and sand with sharp basal contacts (Pirmez et al., 1997).

Pirmez et. al. (1997) defined the following main facies based on correlation with lithologic logs that are also characterized by a wireline log signature :

- color banded mud,
- thin laminae and beds of silt and silty clays,
- thin to medium beds of silt and sand,
- medium to thick beds of silt and sand,
- very thick sand beds with or without clasts,
- gravel and scattered clasts.

This author produced log-based bed-by-bed sections for poor recovery parts of cores, by using these FMS facies (Figure II.31).

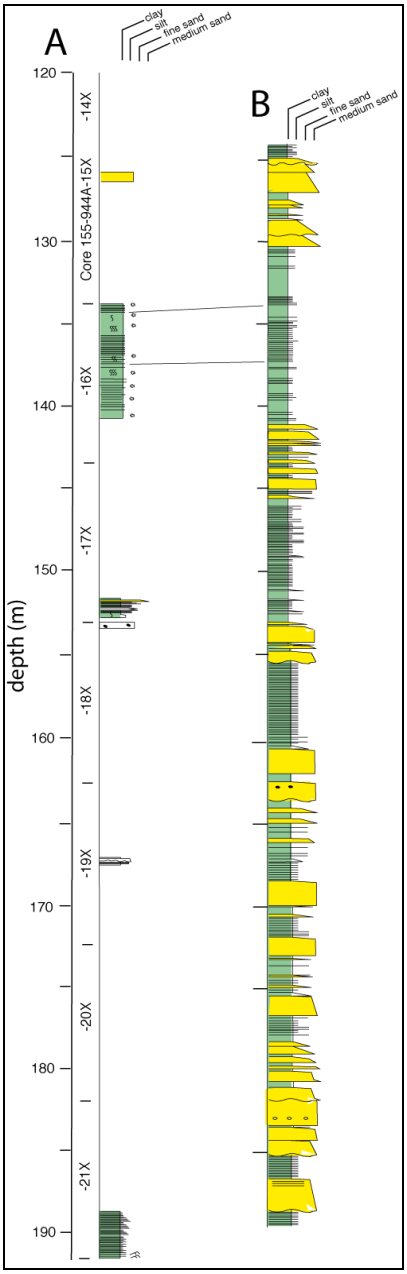

Figure II.31: Lithological logs at site 944 (Pirmez, pers. comm.). A: incomplete log obtained from the recovered sediments. B: log established from FMS and gamma-ray interpretation.

4.6 CHARACTERISTICS OF THE TURBIDITY CURRENTS IN THE AMAZON FAN

Hiscott et al. (1997) suggest that the overspill process (see Chapter II) best explains both the muddy levees and sandy lobes of the Amazon Fan. They concluded, based on samples taken from the coarsest spillover turbidites in the upper 10-50 m of the Amazon Channel levees, that flows that transported sand as bedload along the channel thalweg were also responsible for levee construction and emplacement of graded coarse silt and very fine

sands on the backsides of the levees. The overspill was probably episodic, and concentrated at low points in the levee crests along the Amazon Channel. The hypothesis that levee height is a control on grain size of spillover turbidites is supported by the fining upward trends observed in the levee successions cored during Leg 155.

Pirmez and Imran (2003) describe the turbidity flows responsible for the formation of the most recent Amazon channel, based on observations of channel-cross-section morphology, meander dimensions, flow modeling and grain size of deposits. They suggest that turbidity currents were probably relatively thin in the canyon and must have increased in thickness, due to water entrainment, dramatically in the initial 100 km in the lower fan. Once the flow thickness exceeded the channel relief, overspill of flows began to deposit sediments and construct levees. The currents carried a mixed sediment load, dominated by a large silt fraction (around 90 to 95 %). Flows occurred frequently, probably once every 1-2 years and each individual flow probably lasted for days, indicating long duration. Initial mean flow concentration was of the order of 1%. They estimated turbidity current velocities of 2-4 m/s in the canyon decreasing to 0.5-1 m/s in the lower fan. Both the concentration and average grain size of the suspended load decrease from the base to the top of a turbidity current. Inferred from the grain size data on the Amazon channel, sand is interpreted to be limited to < 2 km from the axis of the channel and at levels no higher that 20-30 m above the base of the flow.

Most of the Amazon channel currents were in a subcritical state, probably a necessary condition for long-distance sediment transport and formation of long sinuous channels (Pirmez et al., 2003). Successive flows had probably similar values of velocity, density and thickness. The regularity with which flow events occurred indicates that the amount of sediment available for each flow also was approximately constant. Unusually large turbidity currents may have occurred less frequently, and were not in equilibrium with the channel morphology developed previously. Pirmez and Imran (2003) suggest that such large turbidity currents probably resulted in channel avulsion.

-Chapter III-

The Amazon Data and Methods

This study is based on geophysical data (bathymetry, imagery and seismic data) and geological data (ODP drillings) acquired in 1995 by ODP (Flood et al., 1995) and 2004 by Ifremer on the Amazon Fan (Figure III.1).

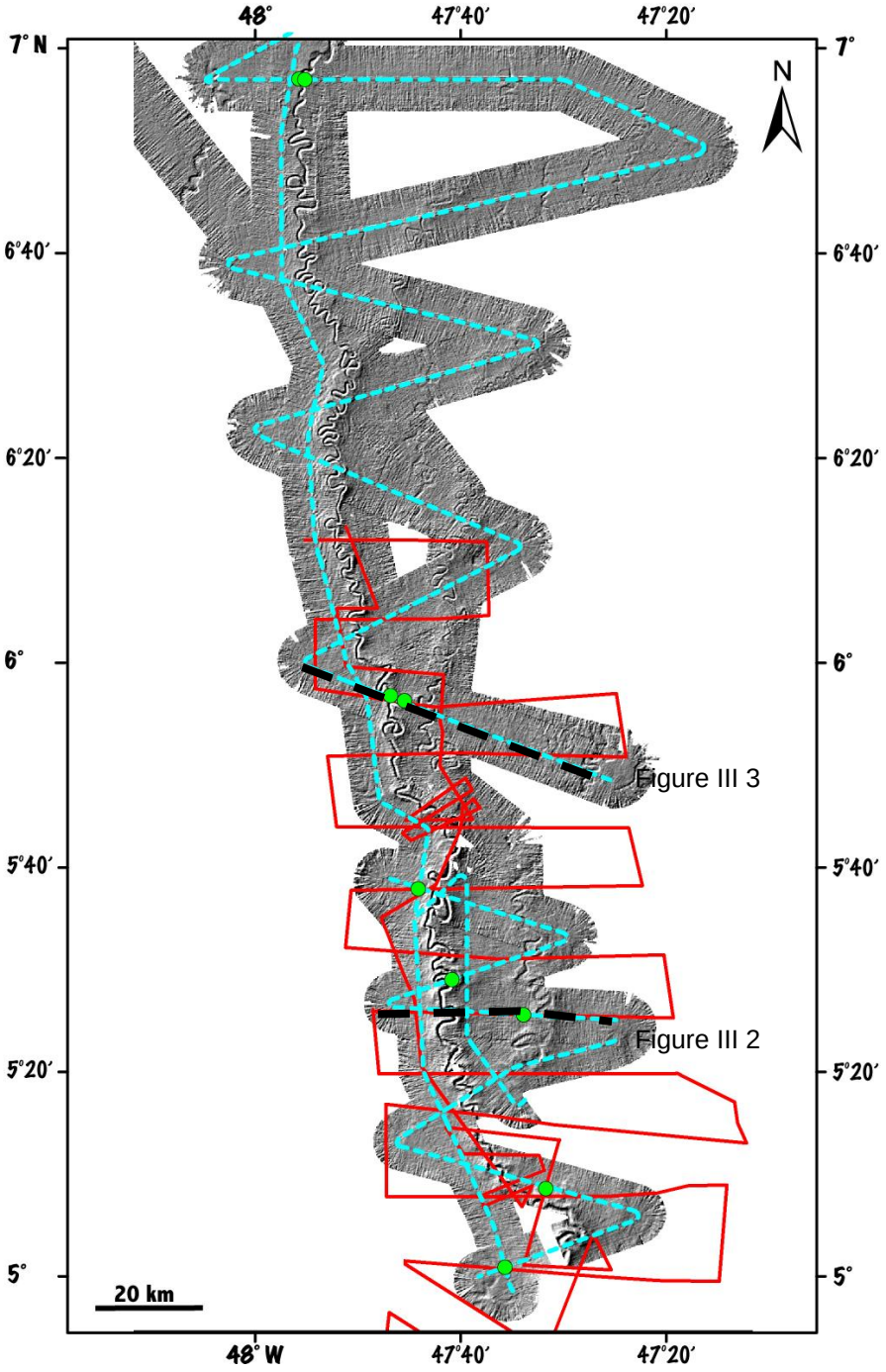

Figure III.1: Data available from Ifremer and Lamont on the middle Amazon Fan: Blue lines: Lobestory seismic and EM12 bathymetric data. Red lines: older seismic lines of cruise RC25-14 of the Lamont Doherty Geological Observatory (courtesy ExxonMobil). Green dots: ODP Leg 155 drilled sites. Yellow lines indicate the location of 2 transect lines shown in Figure III.2 and Figure III.3.

Most of the geophysical data that I used are high-resolution data (EM12 multibeam bathymetry and imagery, multi-channel seismic and 3.5 kHz profiles) acquired in 2004 during

the Lobestory cruise on board the R/V L'Atalante of Ifremer (22 February to 16 March 2004) and concern the upper/middle part of the fan (data acquired at the termination of the channels have been studied by Jégou (2008) during her PhD).
Thanks to ExxonMobil I also had the opportunity to use some older seismic lines (cruise RC25-14 of the Lamont Doherty Geological Observatory, Pirmez, 1994), which have a much lower resolution. These lines were however useful in areas where Lobestory data were missing. The bathymetric and seismic data I used are mainly located in the central part of the fan, and image mostly the morphology, architecture and facies of the recent channel-levees systems of the upper and middle fan parts of the Upper Levee Complex.

Geological data consist mostly of drilling results acquired during the Leg 155 of the Ocean Drilling Program, in 1995 (Flood et al., 1995). All the sites drilled during ODP Leg 155 and used in the framework of this study (Sites 930, 934, 935, 936, 940, 943, 944, 945 and 946) are positioned on a Lobestory profile (Figure III.1).

1 THE DATA SET

1.1 GEOPHYSICAL DATA

1.1.1 2D high-resolution seismic data

During Lobestory cruise digital, high-resolution 2D, 72-channel seismic data were acquired at great water depth, from 3,500 to 4,700 m.
The source was composed of 2 arrays of 3 mini-GI-guns positioned at 1 m below sea level in calm sea conditions and at 1.5 m below sea level when waves height was up to 2 m.
A total of 31 profiles were acquired at a velocity of 5 knots (see location on Figure III.1) mostly as strike lines crossing the channel-levees systems of the Upper Levee Complex from Aqua to Amazon (see Chapter II). In addition, a long dip line runs parallel to the Amazon channel, on its left (western) levee.

The lines have been migrated with a constant velocity of 1500 m/s. They show good resolutions (vertical resolution is 5-10 ms twt and horizontal resolution is 12.5 m) for penetration reaching up to 1000 ms twt, but just the first 500ms twt, and a much higher quality of images than those acquired previously in this type of environment (Figure III.1).

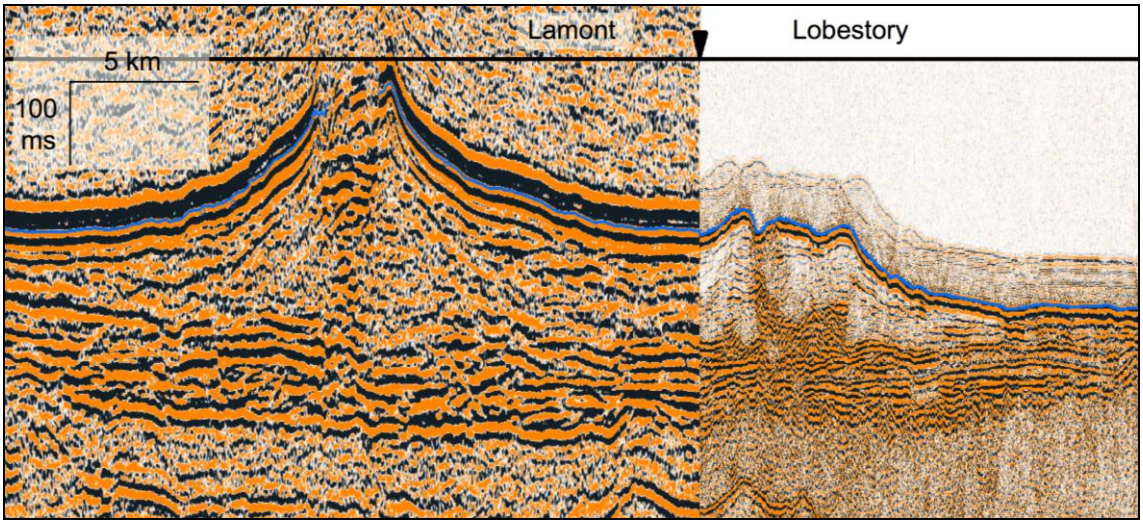

Figure III.2: Comparison between Lobestory seismic data (right) and older RC25-14 data (left). The lines are at the same scale and are crossing. (for location see Figure III.1).

1.1.2 3.5 kHz seismic data

A total of 59 very high-resolution 3.5 kHz profiles (Figure III.1) have been acquired continuously during Lobestory cruise, either at 5 or 8 knots, depending on the simultaneous or not acquisition of multi-channel seismic profiles. The resolution of these lines is on the meter scale and the penetration is generally in the order of 30 ms, but can reach locally 70 ms.

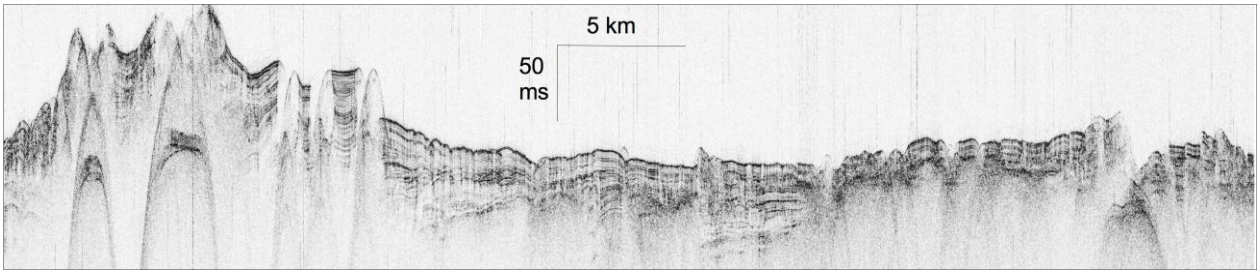

Figure III.3: Example of a Lobestory 3.5 kHz profile (for location see Figure III.1).

1.1.3 EM12Dual bathymetric and acoustic data

Bathymetric and acoustic imagery data were acquired with the EM12 Dual multibeam system that operates at a frequency of 13 kHz.

The EM12 D data were acquired continuously during the Lobestory cruise, at a speed of 5 or 8 knots, depending on the simultaneous acquisition of multi-channel seismic data.

In order to limit the acquisition artifacts, the EM12 was operated at an opening angle of 114°.

A total area of around 130,000 km^2 of the Upper Levee Complex of the Amazon Fan has been mapped with a resolution of 100 m.

1.2 GEOLOGICAL DATA: LITHOLOGY AND WIRELINE DATA FROM ODP LEG 155

Core and wireline log data were acquired within the Ocean Drilling Program (ODP) during Leg 155 (Flood et al., 1995b), on the drillship Joides Resolution (JOIDES = Joint Oceanographic Institutions for Deep Earth Sampling) in 1995.

1.2.1 Drilling system

Cores were cut by the Joides Resolution using Advanced Piston Corer (APC) and then the Extended Core Barrel (XCB), which are dedicated to studies with sedimentological, climate, and paleoceanographic objectives.
The APC is a hydraulic piston corer designed to recover relatively undisturbed continuous 9.5 m long oriented core samples from very soft to firm sediments that cannot be recovered well by rotary coring. The XCB is used for soft to moderately hard formations.

ODP procedure to describe cores consists in:

- A megascopic description of each core, section by section, on visual core description sheets,
- The creation of summary sheets of visual core descriptions computer-generated using the ODP “VCD” program,
- A sediment classification along a core using these summaries,
- Graphic sedimentological logs were made where sediments are classified in lithologic units by ODP (Flood et al., 1995).

1.2.2 Wireline log data

Well logging is classically used for geological interpretations to avoid low core recovery.
The well log types (geophysical recordings of various rock properties in boreholes) are those routinely employed for facies analyses (lithology, porosity, fluid evaluation) and stratigraphic correlations (gamma ray, neutron porosity, bulk density, photo-electric effect, borehole

diameter, resitivity, and sound velocity). I mainly used the total gamma ray curve for the intervals that I discussed in this study (Chapter IV.2).

2 INTERPRETATION METHODS

In this study, I analyzed both seismic and lithologic data.
Seismic facies associated in seismic units have been identified on seismic profiles and have been compared to synthetic lithologic logs of the sites described in Flood et al. (1995) and to redrawn lithologic logs from FMS interpretation of Pirmez (pers. comm.) and Pirmez et al. (1997).
For specific intervals, e.g. HARPs and limits between different depositonal bodies (HARPs/levees, HARPs/HARPs, levees/levees), I used the visual core description of the sites (available on http://www-odp.tamu.edu/).

2.1 SEISMIC DATA ANALYSIS

The seismic data has been analyzed following the seismic stratigraphy method (e.g. Payton, 1977; Sangree and Widmier, 1977; Vail et al., 1977). This method is based on the identification of 2 major types of surfaces:

- The diachronous unconformities, either erosional or non-depositional, evidenced by the reflection terminations (onlaps, downlaps, truncations),
- The chronostratigraphic depositional surfaces (seismic reflections), that are stacked to form seismic units. The characteristics (amplitude, continuity, frequence) of the reflectors and their vertical and lateral evolution determine different types of seismic facies that are associated to form the seismic units.

The stratigraphic relationships that link the seismic units are revealed by overlapping geometries.

Seismic facies and geometry of seismic units can give some clues to the depositional setting, i.e. they can be associated to typical architectural elements in my study (levees, HARs, HARPs and debris flows; see Chapter I) of distinct depositional systems (individual channel-levee systems or mass-transport deposits).

2.1.1 Criteria for seismic facies classification

The classification of the seismic facies in this study is based on the description of both the internal reflection character and the external form.

1. Internal reflection character (Figure III.4)

The internal reflection character can be described by three parameters:

The **reflection configuration**, i.e. the relationship of individual reflections to one another within the seismic facies, can be parallel, sub-parallel, divergent (or convergent), discordant or reflection free (i.e. transparent).

The **reflection continuity**, i.e. the general continuity of individual reflections throughout the seismic facies, can be continuous, discontinuous or variable.

The **reflection amplitude**, i.e. the general range of amplitudes predominantly exhibited by the reflections throughout the seismic facies, varies between high and low, both laterally and vertically.

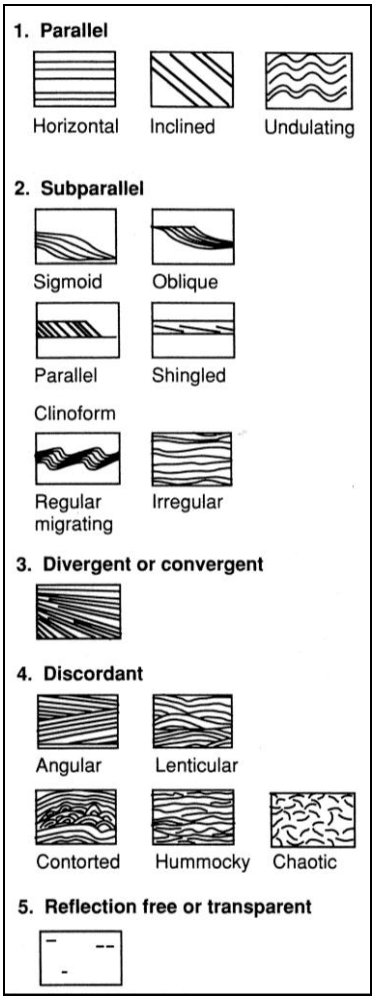

Figure III.4: The main refection configurations (Flood et al., 1995a).

2. External Form (Figure III.5)

The external form describes the external geometry or shape of the upper and lower boundaries of a seismic facies: a two-dimensional external form is termed a seismic facies shape and a three-dimensional external form is termed a seismic facies unit.

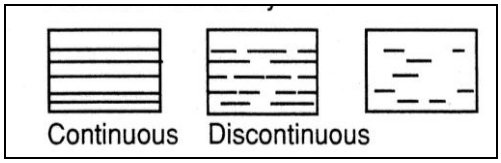

Figure III.5: Reflection continuity of seismic facies (Flood et al., 1995a).

2.1.2 Interpolation of depositional systems

The seismic data have been interpreted using Kingdom 8.2 software. Interpolation of the channel-levee systems and mass-transport deposits between the seismic lines allow the creation of isochron maps (in s twt) of the base and the top of the individual depositional systems.

I digitized the amplitude peak signal of the interpreted seismic reflector marking the base of the individual depositional systems and created interpolated maps of these base reflectors for each system by using the Kingdom software.

I decided that the inverse distance-weighting algorithm is the best-adapted gridding method in view of my sparse seismic line distribution. The calculator tools of the Kingdom software allowed creation of thickness maps of the depositonal systems.

2.2 LITHOSTRATIGRAPHY

In the framework of my study, the lithological information of ODP drillings is needed to bring out evidences about the internal structure of the architectural elements on a small scale.

In that objective, I correlated my seismic units, interpreted from the more recent Lobestory data, with the lithologic units defined by ODP.

In some cases, when I considered that it would be important for a more detailed correlation with seismic, I refined ODP units in sub-units. I refined also some graphic sedimentological logs and completed them when possible by the interpretation of the gamma ray logs.

Lithologic units of ODP are lithologic intervals based on macroscopic description from visual core description and sediment classification (Flood et al., 1995a). Lithologic units have been

established by the Shipboard Scientific Party of ODP Leg 155 for each site and are illustrated by synthetic graphic lithologic logs (Flood et al., 1995b). The colored and modified version (Pirmez, pers. comm.) of these graphic lithologic logs has been used in this study (see chapter IV.2). The logs show grain-size variation, sedimentary structures and bed thickness, where beds with a minimum thickness of 10 cm, were thick enough to be shown at the represented scale. The symbols and colors used for the graphic sedimentological logs from Pirmez (pers. comm.; modified from Flood et al., 1995) are summarized in Figure III.6.

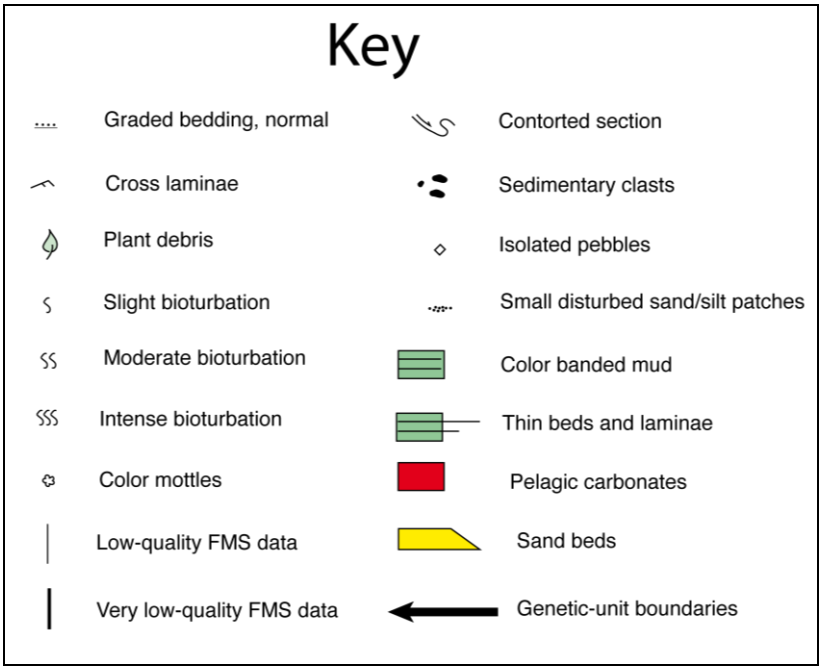

Figure III.6: Key to the symbols and colors used in the synthetic graphic sedimentologic logs of Pirmez (pers. comm.; modified from Flood et al., 1995).

2.2.1 Correlation of seismic units interpreted in this study with ODP lithologic units

As a first step, I applied a time-depth conversion using the time-depth spreadsheets for each site prepared by Pirmez (pers. comm.) from the time-depth correlation defined by (Flood et al., 1997) (Table III.1). The interpreted seismic units of this study, converted in depth are shown in ANNEX III.1a.

In a second step I correlated the seismic units from my interpretation with the synthetic logs and lithologic units defined by the Shipboard Scientific Party of ODP leg 155 (Flood et al., 1995). Differences in depth for the correlated HARP intervals are mostly less than 10 m (ANNEX III.1b) and, considering that the thickness of the seismic signal is about 5 m, I considered this a good tie.

Considering that HARPs were well tied to lithologic logs using the existing time-depth chart, I did not try to go further in the search for other time-depth conversion.

Traveltime (ms)	Site depth (mbsf)																
	930	931	932	933	934	935	936	937	938	939	940	941	942	943	944	945	946
0	0.0	0.0	0.0	0.0	0.0	0.0	0.0	0.0	0.0	0.0	0.0	0.0	0.0	0.0	0.0	0.0	0.0
10	7.2	7.2	7.2	7.2	7.3	7.2	7.2	7.2	7.3	7.3	7.2	7.2	7.2	7.3	7.3	7.3	7.3
20	14.5	14.4	14.5	14.4	14.6	14.6	14.5	14.5	14.5	14.7	14.6	14.6	14.4	14.8	14.7	14.6	14.7
30	21.8	21.8	21.8	21.8	22.1	22.0	22.0	21.9	21.8	22.1	22.0	22.1	21.7	22.3	22.1	22.1	22.1
40	29.3	29.2	29.3	29.3	29.7	29.4	29.5	29.4	29.3	29.6	29.6	29.8	29.0	29.8	29.7	29.5	29.6
50	36.7	36.7	36.8	36.8	37.3	37.0	37.1	36.9	36.8	37.2	37.1	37.5	36.5	37.4	37.4	37.3	37.3
60	44.2	44.4	44.3	44.4	44.9	44.6	44.7	44.6	44.3	44.9	44.8	45.4	44.1	45.2	45.0	45.4	45.0
70	51.7	52.1	52.0	52.0	52.7	52.3	52.4	52.2	51.9	52.6	52.5	53.2	51.7	53.0	52.6	53.9	52.7
80	59.3	59.8	59.7	59.7	60.6	60.1	60.2	60.0	59.6	60.3	60.2	61.2	59.5	60.8	60.4	62.0	60.4
90	67.1	67.6	67.4	67.4	68.5	67.8	68.0	67.8	67.3	68.1	68.0	69.4	67.1	68.7	68.2	70.3	68.3
100	74.9	75.4	75.3	75.2	76.5	75.7	76.0	75.7	75.0	75.9	75.7	77.7	74.8	76.7	76.0		76.4
110	82.8	83.4	83.2	83.0	84.4	83.6	84.2	83.6	82.8	83.8	83.6	85.9	82.7	84.8	83.9		84.5
120	90.7	91.3	91.1	90.9	92.4	91.6	92.3	91.6	90.7	91.7	91.5	94.2	90.7	92.7	91.9		92.7
130	98.7	99.4	99.1	98.9	100.5	99.7	100.4	99.6	98.6		99.6	102.4	98.7	100.8	99.9		100.9
140	106.7	107.5	107.1	107.4		107.8	108.5	107.7	106.6		107.6	110.6	106.8		107.9		109.2
150	114.7	115.7	115.3	116.0		116.0	116.5	115.7	114.5		115.7	118.9	114.8		115.9		117.4
160	122.8	123.9	123.4	124.7		124.3	124.5	123.8	122.5		123.8	127.2	122.9		123.9		125.5
170	131.0	132.1	131.6	133.3		132.7	132.6	132.0	130.5		132.1	135.4	130.9		132.0		133.7
180	139.0	140.4	139.9	142.2		141.3	140.6	140.3	138.5		140.4	143.6	139.0		140.1		141.9
190	147.1	148.8	148.2	151.2		149.9	148.7	148.7	146.7		148.7	151.9	147.1		148.3		150.2
200	155.3	157.1	156.6	160.0		158.3	157.2	157.1	154.9		157.1	160.2	155.3		156.7		158.6
210	163.5	165.5	165.2	168.5		166.7	165.8	165.5	163.1		165.5	168.6	163.5		165.1		167.3
220	171.8	174.0		176.8		175.0	174.4	174.0	171.4		173.8				173.5		175.9
230	180.2	182.6		185.2		183.6	183.1		179.6		182.1				181.9		184.5
240	188.6	191.4		193.7		192.4	192.0		187.9		190.5				190.5		193.2
250	197.7	200.2		202.3		201.3	200.9		196.2		199.1				199.2		202.1
260	207.2	209.0		210.9		210.1	209.8		204.6		207.7				208.1		210.9
270	216.9	217.7		219.5		219.0	218.7		213.0		216.3				217.2		219.6
280	226.5	226.6		228.2		228.0	227.7		221.5		225.0				226.5		228.4
290	235.9	235.9		237.0		237.1	236.9		230.0		233.6				235.8		237.2
300		245.4		246.0		246.1	246.2		238.5		242.4				245.1		246.0
310		255.2				255.3	255.4		247.1						254.5		254.9
320		264.9				264.5	264.7		255.8						263.5		263.7
330		274.5				273.7	274.2		264.4						272.4		272.8
340		284.1				282.2	283.7		273.1						281.2		
350		293.6				291.0	293.2		281.7						289.9		
360		303.3				300.0	302.0		290.3						298.7		
370		313.1				308.8	310.6		299.0						307.5		
380		322.9				317.6	319.1								316.2		
390		332.7				326.3	327.7								325.0		
400		342.4				335.1	336.4								333.8		
410		351.6				343.9	345.0								342.6		
420		360.4				352.9	353.6								351.3		
430		369.7				361.9	362.3								360.1		
440		378.9					370.9								369.0		
450		388.2					379.7										
460		397.5					389.2										
470		406.9					399.1										
480		416.5					409.0										
490							418.3										

Table III.1: Depth at each site as a function of traveltime (Flood et al., 1997).

2.2.2 Refined lithologic description of specific intervals

I essentially used visual core descriptions that were more detailed than the synthetic lithologic logs of ODP to redraw some intervals of the HARP deposits used in this study (Figure III.7) (see Chap. IV.2).

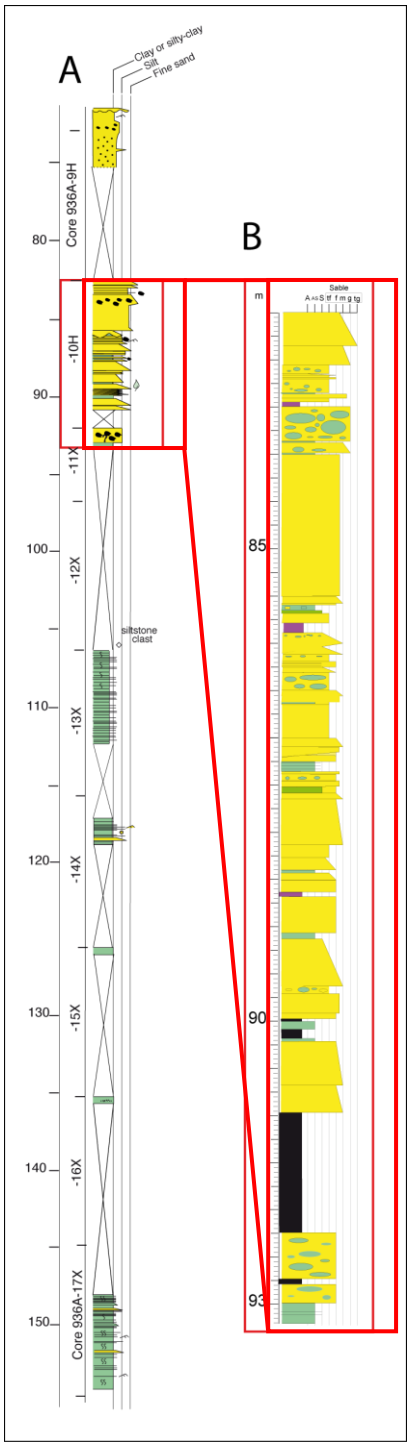

Figure III.7: Example of lithologic logs of Brown HARPs unit at site 936. A: Lithologic log of ODP (Pirmez, pers. com. after (Flood et al., 1995b). B: Redrawn log of a sandy interval (this study).

2.2.3 Interpretation of diagraphic logs to fill gaps at specific intervals

Low core recovery or gaps are associated to very sandy intervals (Flood et al., 1995b), often corresponding to the HARPs on seismic, and therefore important for my study.

Based on gamma ray well log records at Site 935, 936 and 944, that penetrated

corresponding HARP deposits, I was able to interpret gaps of the cores in view of their silty clay or sand content (Figure III.8).

This method was used to interpret the gamma ray curve in this study and to get a maximum, a minimum, and an average value of the SGR gamma ray data based on recovered silty clay and sandy intervals. These values have been compared to the SGR data recorded in the gap intervals and allowed me to propose a lithologic interpretation (Tables III.2 to III.7).

Note that resolution with these tools is much less than that of visual core description and than the reconstructed high-resolution logs from FMS interpretation by Pirmez et al. (2007).

Seismic correlation	ODP core 935 A		SGR	
	Lithology	Depth (mbsf)	SGR Value	Depth (mbsf)
HARPs top (Aqua)	Sand	98.5	50.22	100.74
HARPs base (Aqua)		101.5 or 103 mbsf	68.51	103.94
Levee top (Aqua)	Silty clay with silt laminae	5.94 (top of overflow deposits, including deposits younger than Aqua)	76.11	63.09 (depth of first available good data), already into the Aqua deposits
Levee base (Aqua)		97.3 (just above the sand bed deposit at the base of the Aqua levee deposits)	97.84	91.19

Table III.2: Site 935A. Reference intervals for silty clay and sand deposits, corresponding seismic units and corresponding SGR interval that can be different in depth.

Lithology 935 A	SGR Average value	SGR min		SGR max	
		Value	Depth (mbsf)	Value	Depth (mbsf)
Sandy	61.32	50.22	100.74	72.92	103.33
Silty clay	91.74	68.90	65.38	107.21	82.30

Table III.3: Average, minimum and maximum values for the SGR data taken from the intervals proposed in Table III.2.

Seismic correlation	Litho core ODP 936		SGR	
	Lithology	Depth (mbsf)	Value	Depth (mbsf)
HARPs top (Brown)	Sandy	72.10	71.75[1]	63.55[2]
HARPs base (Brown)		106.30	63.89	96.77
Levee top (Brown)	Silty clay	0.96	Not available[3]	
Levee base (Brown)		72.10		
Clay top (Orange-1B)	clay	106.3	112.74	106.38
Clay base (Orange-1B)	clay	112.3	115.99	112.17

[1] For the calculation of the SGR values of the Brown HARPs I excluded the data from 75.13 to 82.19 mbsf because they are thought to correspond to a wash-out interval after the caliper data.

[2] The top of the gamma ray signal corresponding to the Brown HARPs doesn't show a clear limit to the upper laying levee deposits, either because the limit is into the not available data or because the limit is transitional.

[3] Log response is highly attenuated where the tool was in the drill pipe (until 63.55 mbsf).

Table III.4: Site 936A. Reference intervals for clay and sand deposits, with corresponding seismic units and SGR interval that can be different in depth. SGR data for the silty-clay interval are not available.

Lithology 936 A	SGR Average value	SGR min		SGR max	
		Value	Depth (mbsf)	Value	Depth (mbsf)
Sandy	71.30	46.32	83.82	85.95	67.06
Clay	109.46	100.81	111.71	115.99	112.17

Table III.5: Average, minimum and maximum values for the SGR data taken from the intervals proposed in Table III.4.

Seismic correlation	Litho core 944 A		SGR	
	Lithology	Depth (mbsf)	Value	Depth (mbsf)
HARPs (Brown)	Sandy	Not available, very low to no recovery		
Levee[1]	Silty clay	[1]	82.63	76.05[2]
Levee base (Brown)		124	102.75	114.45

[1] Limit between the top of the Brown levees and the overlying levee deposits has not been determined because of similar lithology.
[2] *Values between 0 and 76.05 mbsf are not valid*

Table III.6: Site 944A. Reference interval for silty clay deposits correlated to Brown levee on seismic, with corresponding SGR interval that can be different in depth.

Lithology 944 A	SGR Average value	SGR min		SGR max	
		Value	Depth (mbsf)	Value	Depth (mbsf)
Silty clay	92.31	82.63	76.05	114.45	102.75

Table III.7: Average, minimum and maximum values for the SGR data taken from the interval proposed in Table III.6

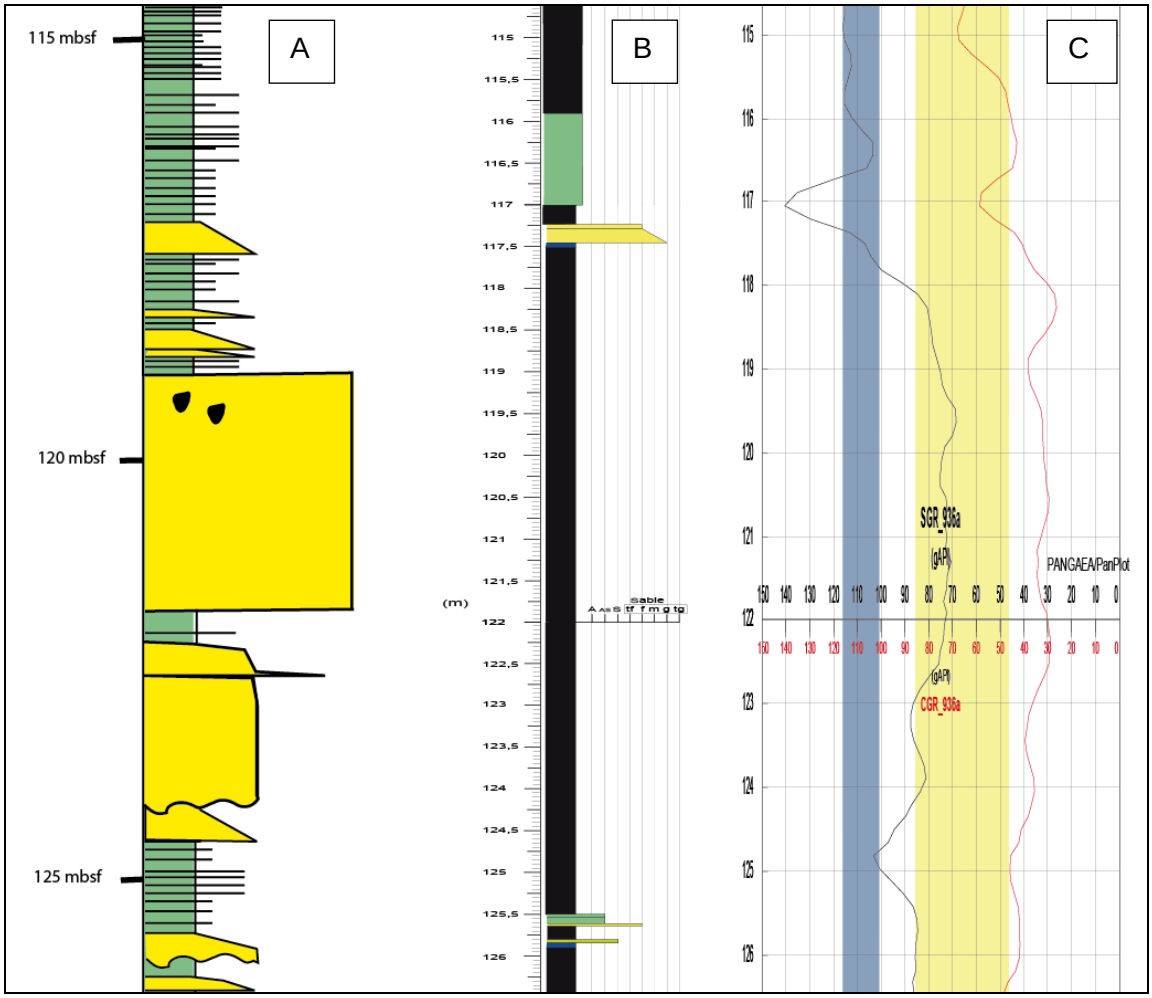

Figure III.8: Example of an interpreted section of core 936 A.A: Lithologic section from FMS interpretation (Pirmez, pers. com., Pirmez et al., 1997). B: Redrawn section after visual core description, showing large intervals of gaps (in black), (this study). C: gamma ray curves, where the yellow and blue colors show the intervals of SGR values for sand and clay respectively (this study) (see Table III.5 for values).

2.2.4 Validity of the age models

A synthesis of available $\delta\ ^{18}O$ data interpreted for ages (Showers et al., 1997) and the ^{14}C dates (Maslin et al., 2006) is given in Table III.8.

I can notice that these ages are not always consistent (see red and green cells in Table III.8). Therefore, in order to be able to choose one of them for my study, I had to evaluate their respective validity. This evaluation was not realized systematically for all sites, but was restrained to sites and stratigraphic levels where ^{14}C dates with depth indications were available (i.e. at sites 936, 940 and 944, Table III.8).

Dating methods and accuracy:

- ^{14}C dates were obtained from biologic material (foraminifers or mollusks) or from

organic matter. When the measurement is conducted on hemipelagic intervals, this dating method is generally accurate. A problem inherent to turbiditic environments is that they consist of reworked materials. Therefore the biologic content can be older than the age of turbidite deposition, because the method dates the death of the animal and not the time of deposition (of reworking). This is a possible cause for age's incoherency.

- $\delta\ ^{18}O$ method is based on the comparison of a local curve with a global curve, and the recognition of dated peaks of the global curve. This method is therefore highly dependant on the foraminifer content and on the continuity of the curve. When the foraminifer content and/or core recovery are low as it was frequently the case during ODP Leg 155, some peaks correlations proposed by Showers et al. (1997) can be questioned.

In the case I observed inversions of ages provided by $\delta\ ^{18}O$ and ^{14}C (i.e. at site 936: 61.16 to 72.64 mbsf and site 944, interval 58.83 to 112.22 mbsf, Table III.8) and by $\delta\ ^{18}O$ and paleomagnetism (i.e. at site 930, interval 85.2 to 124.92 mbsf, Table III.8), I preferentially favored the ages provided by ^{14}C and paleomagnetism.

I used the time-depth chart (Flood et al., 1997; see above) to convert limits between seismic units into depth (mbsf) in order to get an approach for the position of dated intervals where sediments have not been clearly correlated to depositional elements (levees, channels or HARPs), in particular for the stacked levee deposits of different systems.
The dates within the levees are sometimes difficult to correlate to the respective seismic unit, because the stacking pattern in levees failed to give clear indication of the limit between different channel systems. This was particularly the case for levees located upfan of the avulsion points (i.e. no pattern has been correlated to downfan avulsions). It was also the case for overlapping levees of different channels where seismic limits were not clearly correlated to changes in sedimentation pattern of the lithological cores (e.g. frequency of silt laminations can fluctuate and be similar for top of levees and distal levee deposits). For this later case, the conversion of seismic limits into depth helped determine the limits on cores where the variances between limits on seismic converted in meters and limits on lithology are mostly in the range below 10 m. However, a maximum variance of 24 m was observed. Consequently, the dates of the levees to the seismic units converted in meters, and defined an uncertainty interval of 12 meters below and above the depositional limits.
Sedimentation rates have been calculated for the dated intervals and correlated from my core-seismic tie in this study to the different depositional elements (Table III.9).

Sites	Depths (mbsf) of top interval	$\delta^{18}O$ (ka)	Paleo-mag. (ka)	^{14}C (ka)	^{14}C cal (ka)	Material dated or control point	References	Correlated seismic units (this study)
930	0	2.32				1.1	Showers et al., 1997	(Calcareous clay) Aqua or recent levee
	8.42	9				G. tumida	Showers et al., 1997	Aqua or recent levee
	15.35	11				YD	Showers et al., 1997	Aqua or recent levee
	28.42	17.85				2.2	Showers et al., 1997	Aqua or recent levee
	37.5	19.22				2.21	Showers et al., 1997	Purple, Aqua or recent levee
	85.2 (to 87.5)		32			Lake Mungo excursion	Cisowski et al., 1997	Orange-1A or Purple levee
	100.6	23.17				2.23	Showers et al., 1997	Orange-1A levee
	124.92	24.11				3	Showers et al., 1997	Orange-1A levee
940	2.12	9				G. tumida	Showers et al., 1997	Brown or recent levee
	58.55	11				YD	Showers et al., 1997	Brown or recent levee
	59.9			13.31 +/- 0.21	15.15 +/- 0.80	Foraminifer	Maslin, pers. com.	Brown or recent levee
	167.48	17.85				2.2	Showers et al., 1997	Aqua levee or Nouveau levee
935	0.53	9				G. tumida	Showers et al., 1997	(Calcareous clay) Aqua or Brown levee
	28.2	17.85				2.2	Showers et al., 1997	Aqua or Brown levee
	35.2	19.22				2.21	Showers et al., 1997	Aqua or Brown levee

	93.47	23.17				2.23	Showers et al., 1997	Aqua levee
	104.03	24.11				3	Showers et al., 1997	Aqua HARPs
	173.4 (to 178.87)	40				P. obliq. datum	Scientific Shipboard Party, 1995	Hemipelagic drape over Orange-1 B levees
	200.4	50.21				3.3	Showers et al., 1997	URMTD
934	0.9	9				G. tumida	Showers et al., 1997	(Calcareous clay) Brown to recent levee
	8.61	11				YD	Showers et al., 1997	Brown or recent channel infill
	89.7	17.85				2.2	Showers et al., 1997	Brown or recent channel infill
936	2.7	9				G. tumida	Showers et al., 1997	Brown to recent levee
	28.02	11				YD	Showers et al., 1997	Brown or recent levee
	61.16	17.85				2.2	Showers et al., 1997	Brown or recent levee
	72.64			16.25 +/- 0.090	19.075 +/- 0.195	Mollusk	Maslin, pers. com.	Brown HARPs
	72.64			17.78 +/- 0.100	20.575 +/- 0.375	Foraminifer	Maslin, pers. com.	Brown HARPs
	154.7			34.62 +/- 0.100	40.28 +/- 0.2120	Organic matter	Maslin, pers. com.	Orange-1B HARPs base or URMTD top
943	1.64	9				YD	Showers et al., 1997	1D or recent channel infill
	2.26	17.85				2.2	Showers et al., 1997	1D or recent channel infill
944	0.5	9				G. tumida	Showers et al., 1997	1D levee or recent

	0.54			10.51 +/- 0.070	11.65 +/- 0.618	Foraminifer	Maslin, pers. com.	1D levee or recent
	2.2	11				YD	Showers et al., 1997	1D levee or recent
	58.83	17.85				2.2	Showers et al., 1997	1D levee or Brown levee
	65.35	19.22				2.21	Showers et al., 1997	1D levee or Brown levee
	112.22			13.73 +/- 0.100	15.825 +/- 0.563	Foraminifer	Maslin, pers. com.	Brown levee
	143.74			22.74 +/- 0.100	27.62 +/- 0.220	Organic matter	Maslin, pers. com.	Brown HARPs or HARPs X
	144.12			23.22 +/- 0.110	28.11 +/- 0.220	Organic matter	Maslin, pers. com.	Brown HARPs Or HARPs X
945	1.23	9				G. tumida	Showers et al., 1997	Hemipelagic
946	0.24	9				G. tumida	Showers et al., 1997	(Calcareous clay) 1B levee
	22.6	17.85				2.2	Showers et al., 1997	1D, 1C or 1B levee

Table III.8: Compilation of available dates (Cisowski et al., 1997; Showers et al., 1997; Maslin, pers. com.) and corresponding seismic units (this study). Age inversions occur for some sites and the data interpreted as invalid in my study are marked in gray. G. tumida and P. obliq. datum: biostratigraphic events (see Chapter II.4.4.2); YD: Younger Dryas

Sites	***Ages of top (ka)***	***Correlated depositional elements***	***Depth (mbsf) of dated top***	***Depth base (mbsf) (= top of next underlying dated intreval)***	***Time interval (ka)***	***Sedimentation rate (m/ka)***
930	2.32	Levees	0	8.42	6.68	1.26
	9		8.42	15.35	2	3.47
	11		15.35	28.42	6.85	1.91
	17.85		28.42	37.5	1.37	6.63
	19.22		37.5	85.2	12.78	3.73
	32		85.2			
940	9	Levees	2.12	58.55	2	28.22

	11		58.55	59.9	4.15	0.33
	15.15		59.9	167.48	2.7	39.84
	17.85		167.48			
935	9	Levees	0.53	28.2	8.85	3.13
	17.85		28.2	35.2	1.37	5.11
	19.22		35.2	93.47	3.95	14.75
	23.17	HARPs, levees, hemipelagic and part of URMTD	93.47	104.03	0.94	11.23
	24.11		104.03	173.4	15.89	4.37
	40		173.4	200.4	10.21	2.64
	50.21		200.4			
934	9	Channel infill	0.9	8.61	2	3.86
	11		8.61	89.7	6.85	11.84
	17.85					
936	9	Levees	2.7	28.02	2	12.66
	11		28.02	61.16	6.85	4.84
	17.85		61.16	72.64	2.725	4.21
	20.575	HARPs and levees	72.64	154.7	19.705	4.16
	40.28		154.7			
943	9	Channel infill	1.64	2.26	8.85	0.07
	17.85		2.26			
944	9	Levees	0.5	0.54	2.65	0.02
	11.65		0.54	112.22	4.175	26.75
	15.825	Levees and HARPs	112.22	143.74	11.795	2.67
	27.62		143.74	144.12	0.49	0.78
	28.11		144.12			
945	9	Hemipelagic	1.23	0.24		
946	9	Levees	0.24	22.6	8.85	2.53
	17.85		22.6			

Table III.9: Average sedimentation rates calculated for intervals where available dates (Cisowski et al., 1997; Showers et al., 1997; Maslin, pers. comm.) are interpreted as valid (this study, see Chapter III).

-Chapter IV-

The Quaternary Amazon Fan revisited

1 SEISMIC ANALYSIS: ARCHITECTURE OF THE FAN

1.1 SEISMIC FACIES ANALYSIS

The analysis of multichannel high-resolution Lobestory seismic data allowed me to distinguish 4 main facies that I grouped into 3 classes of facies (A to C) based on the observation of the reflection amplitudes.

1.1.1 High-amplitude facies (A)

A1 HAR (High-Amplitude Reflection)

Internal reflection character: contorted, short, low frequency and high-amplitude reflections. Internal unconformities are frequent.

External form: in most cases, the HAR facies comprise laterally restricted bodies (maximum width 6 km due to a channel meander, see Aqua HARs LS 50, IV.1.3, Figure 15b) limited by concave-shaped basal limits, which are generally erosional unconformities (Figure IV.1). The exact form of the basal unconformities can be sometimes hard to identify when the HARs are truncating into a depositional body of facies A2, corresponding to HARP deposits (see below). The top surface is generally flat but can be mounded in some cases. The HAR facies can generate an attenuation of the underlying reflections, indicating that the sediments imaged by this facies are making acoustic masks (Figure IV.2).

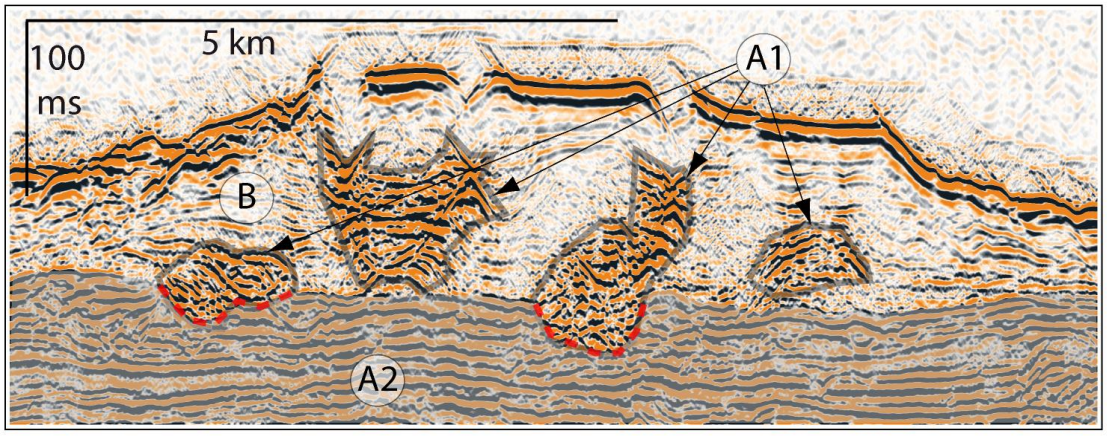

Figure IV.1: Facies A1 (HAR) with probably an erosive basal contact (doted red line) into the underlying deposits of facies A2 (HARPs). B refers to levee facies described in text (see below). Line LS 42, see Figure IV.15a (IV.1.3).

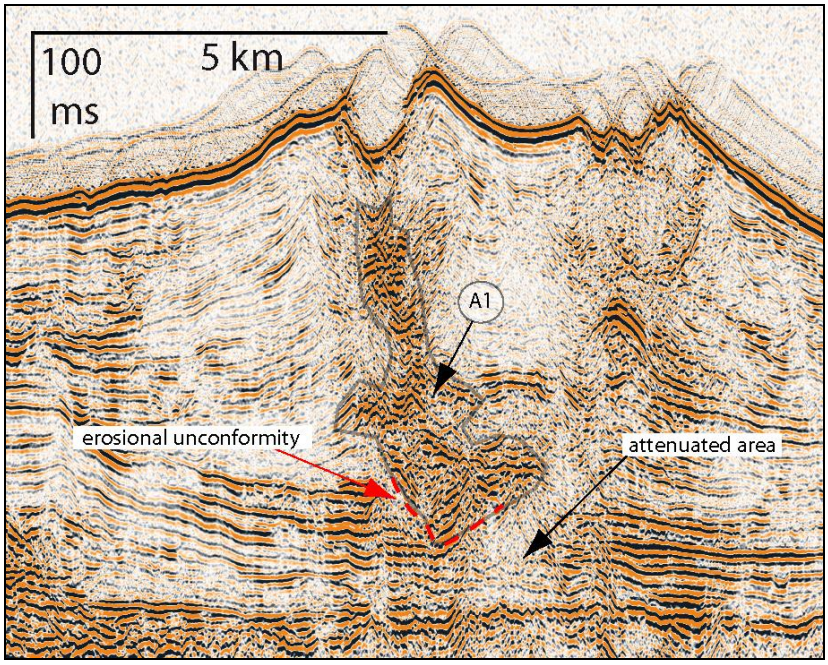

Figure IV.2: Facies A1 (HAR) eroding into underlying deposits and creating acoustic masks. Line LS 52, see Figure IV.15b (IV.1.3).

A2 HARPs (High-Amplitude Reflection Packets)

Internal reflection character: mainly flat-lying or mounded, continuous to discontinuous, low frequency and high-amplitude reflectors. Numerous internal angular and/or erosional, either U-shaped or V-shaped unconformities contribute to the discontinuous aspect of this facies (Figure IV.3b). Patches of low amplitude, low to high frequency reflections also interrupt the flat-lying high amplitude reflections.

External form: the HARPs constitute lens-shaped or isopach bodies (Figure IV.14). Their basal limits are erosional unconformities, and their top limits are frequently angular unconformities defined by the down-lapping or on-lapping of the overlying reflections (Figure IV.3a).

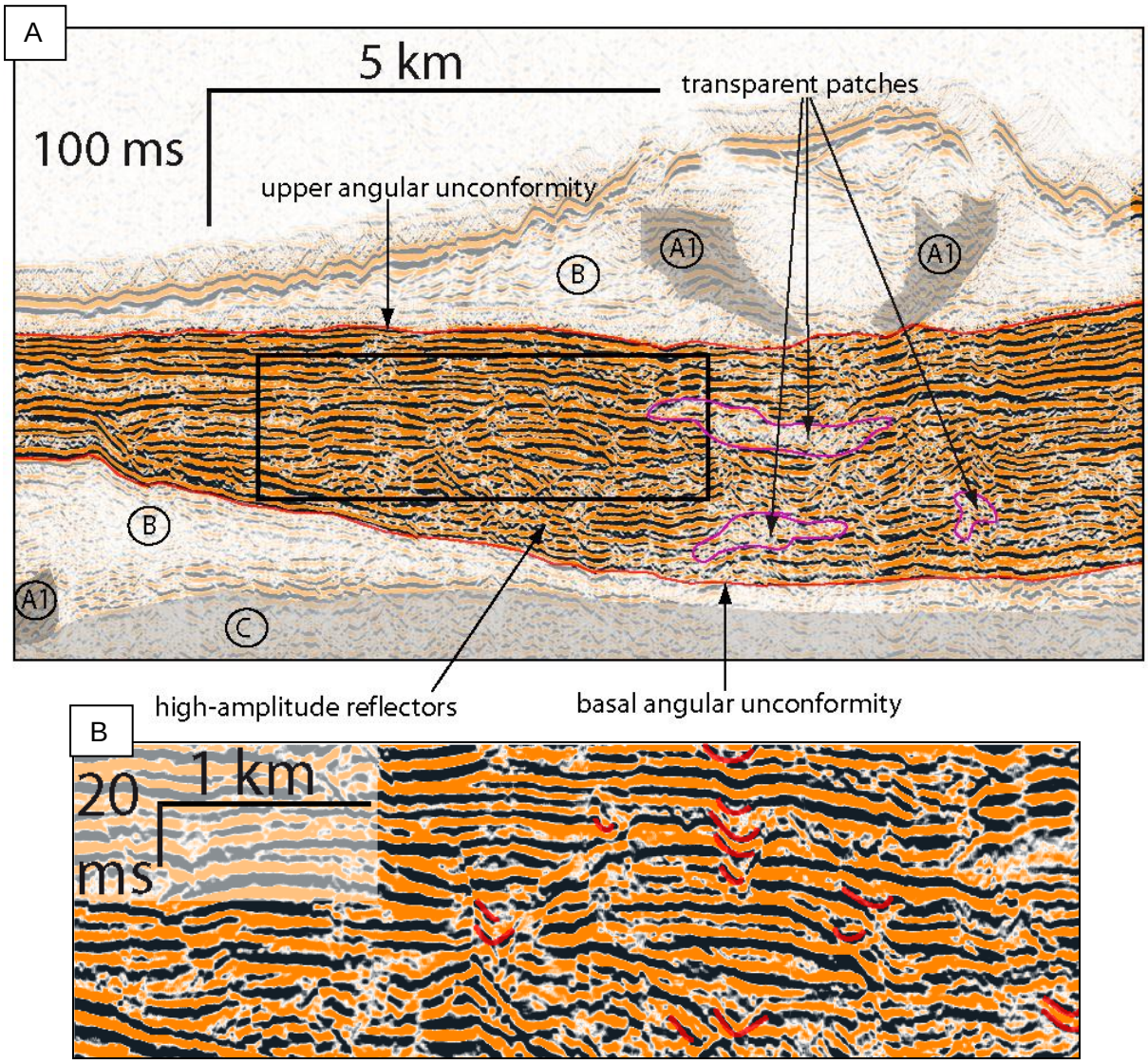

Figure IV.3: Facies A2 (HARPs) and adjacent deposits of other facies. A: The HARPs shows high-amplitude reflectors characterized by numerous internal angular contacts and some transparent patches. B: Close-up of (A) highlighting V-shaped erosional features (in red) within the HARPs. Line LS 43, see Figure IV.15a (IV.1.3).

1.1.2 Medium to low amplitude facies (B)

Internal reflection character: convergent, continuous, mostly medium to low-amplitude reflections to transparent. Some high-amplitude reflectors can also occur (Figure IV.4). The amplitude variations occur both vertically and horizontally. The reflections are mostly flat lying, but undulated reflectors are frequent (Figure IV.4).

External form: mostly wedge-shaped bodies on profiles transverse to the channel axis. Thickness remains approximately constant on profiles parallel to the channel axis.

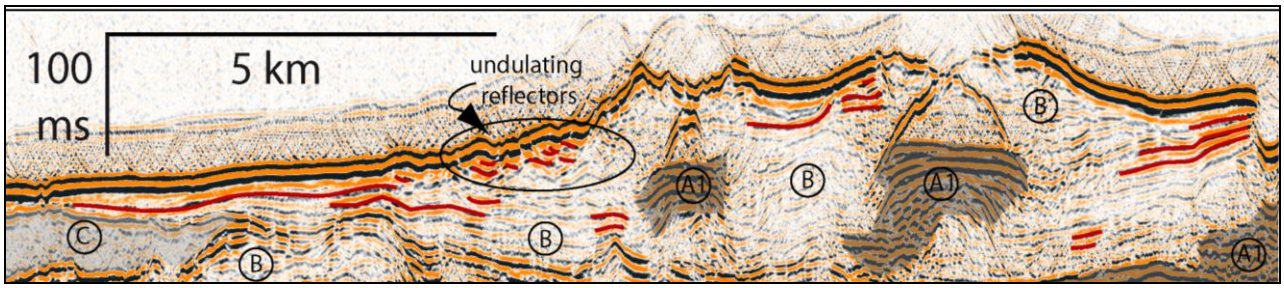

Figure IV.4: Facies B (levees) showing mainly low to medium amplitude reflectors organized in wedge-shaped bodies. Note the vertical and lateral variation reflectors amplitudes (higher amplitudes are highlighted in red). Line LS 45, see Figure IV.15a (IV.1.3).

1.1.3 Low amplitude facies (C)

Internal reflection character: chaotic, low amplitude reflectors, almost transparent, with some hyperbolic echos at the top surface.

External form: laterally extended, more or less isopach packages. Lateral limits are not visible on my data set and maximum thickness is up to 275 ms twt (see thickness map of a depositional body of this facies, Figure IV.27). The base limits of these packages are erosional unconformities as indicated by the erosional truncation of underlying reflectors (Figure IV.5).

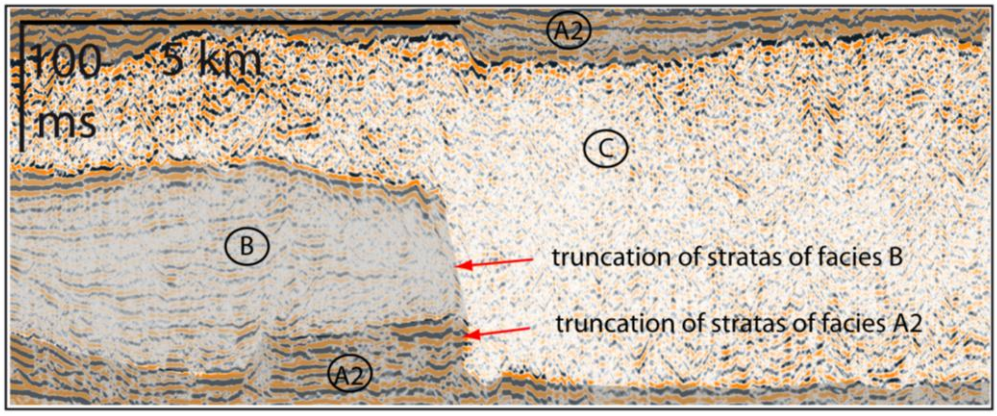

Figure IV.5: Transparent facies C1 (Mass-Transport Deposits). Line LS 45, see Figure IV.15a (IV.1.3) for location.

1.2 INTERNAL STRUCTURE OF THE TURBIDITIC ELEMENTS

The seismic facies described above (IV.1.1) are organized into distinct facies associations and represent, in agreement with previous works, the typical depositional elements (i.e. channel, levees and HARPs and debris flows) of deep-sea fans.

- The facies A1 and B are associated to form channel-levee systems.

- The HARPs of facies A2, already known from other studies (see Chap. I), are found as lenticular depositional bodies at the base of channel-levee systems, or as isopach bodies at the base of several channel-levee systems or outcropping at the basin floor.
- Facies C represents debris flows lying between the turbiditic elements (i.e. channel-levees and HARPs).

I will describe in the followings the internal structure of the HARPs and the levees.

1.2.1 Internal architecture of the HARPs

As illustrated in Figure IV.6, although globally of high-amplitude character, the HARPs consist of a variety of superposed and amalgamated seismic facies including transparent patches, mounded to flat-lying bodies, high-amplitude reflectors, U-or V-shaped erosional surfaces, etc., that contribute to giving a discontinuous and even sometimes chaotic aspect to the facies.

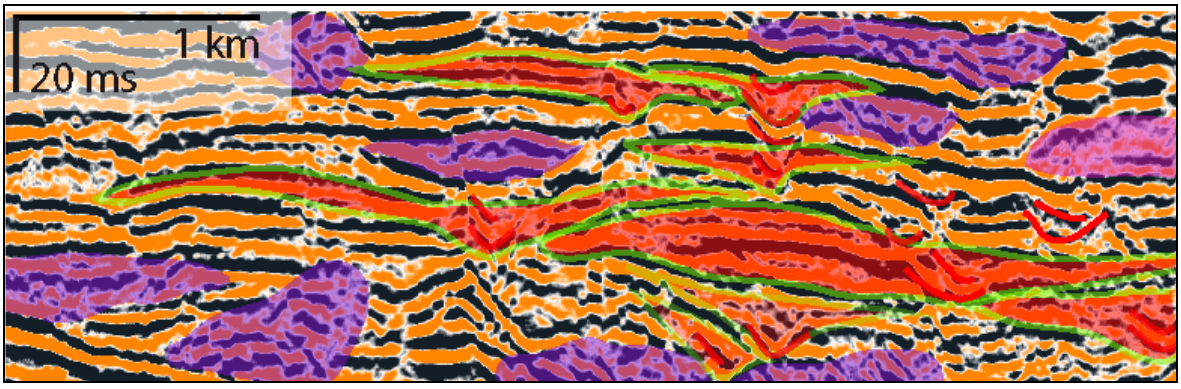

Figure IV.6: Details of the internal structure of the HARPs showing mainly mounded to flat-lying high-amplitude reflectors. These reflectors can be interrupted by erosional features (V- or U-shaped reflectors highlighted in red) The erosional features can be associated with adjacent reflectors to form eventually small channel-levee units (colored in red and limited in in green). Patches of chaotic reflectors (colored in purple) are also frequent.

These various sub-facies appear to be organized into four main types of seismic sub-units:

a Flat-laying reflections without V-shaped surfaces representing small unchannelized sub-units (lobes ?).

b V-shaped surfaces that are associated laterally with flat-lying or wedge-shaped high-amplitude reflectors. This geometry and the facies association suggest the presence of very small erosive channels (represented by stacked U- or V-shaped features up to max 30 ms thick) and eventually very small channel-levee sub-units (max 20 ms twt thick and several hundred of m or some km wide). While they are very frequent on cross sections (i.e. transverse to the inferred current directions), the erosional V- or U-shaped features are

generally lacking in dip seismic sections, indicating that these features are elongated longitudinally and arguing for their interpretation as small channels.

c Transparent patches eventually fill the V-shaped erosional features (Figure IV.7A) and possibly represent the abandonment of the small channels. The transparent patches are most frequently narrow in cross sections (e.g. some hundreds of m wide in Figure IV.7A. When cut on a dip section (Figure IV.7B), the longitudinal extension of the transparent patches can be several km, giving a minimum length for these small erosional features up to 4 km.

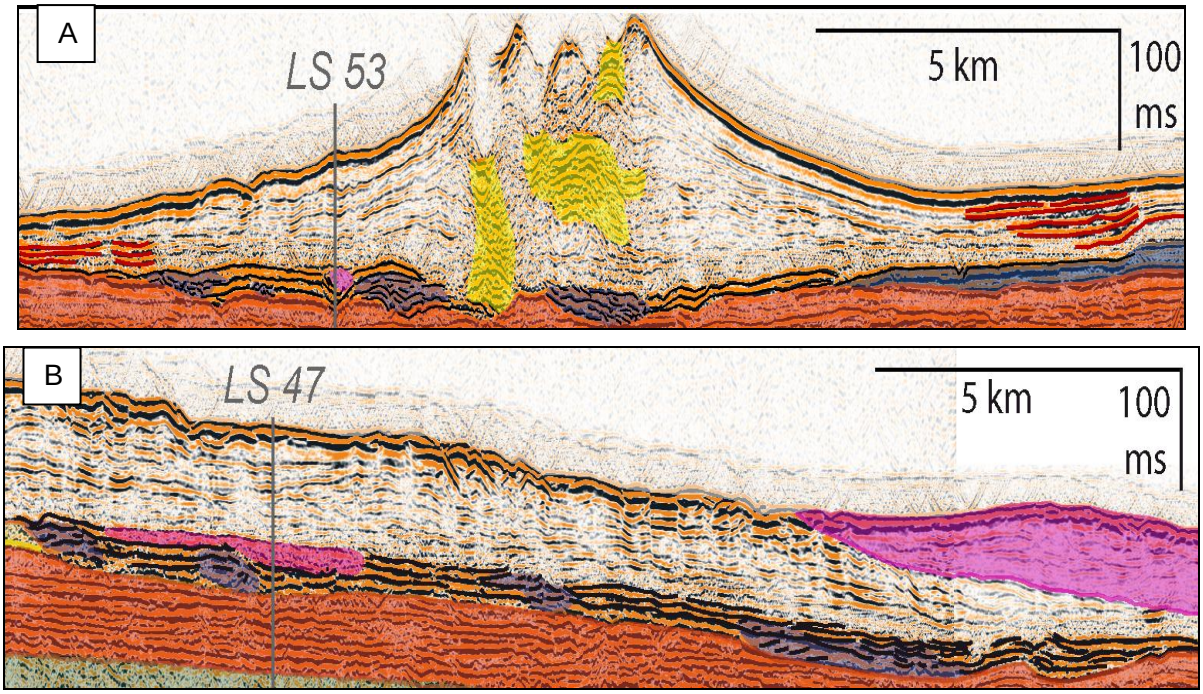

Figure IV.7: U-shaped erosional features within the HARPs (high-amplitude reflectors are highlighted in black, chaotic patches are colored in purple) A: Cross section showing the infill of the erosional channel by a transparent patch (colored in pink). B: Dip section, showing the longitudinal extension of the transparent fill, over several km. HARs of the overlying channel-levee system are in yellow, the high-amplitude reflectors in the levees are highlighted in red). Other colors represent channel-levee-Harps systems Orange-1 in orange and 1D in dark pink (see IV.3). Lines LS 47 (A) and LS 53 (B), see Figure IV.15a, b (IV.1.3.) for localization.

d Patches of mounded and chaotic reflectors are also present. Their signification remains unclear. They can rarely represent the main part of the depositional body of the HARPs (Figure IV.8), but more often they occur as small patches (Figure IV.6). Their resemblance to HAR facies suggests they could be channel fills. Since I did not observed any downfan continuity of these patches, I suspect that they could be short and frequently shifting channels. On an other hand, these patches could also be lobes of a different type than the above mentioned flat-lying lobes (see a), either micro-channelized lobes or a succession of numerous small lobes stacked up through rapid shifts on short distance, possibly because of topographic constrain. The limit between HARPs and overlying HARs is sometimes diffcult to define due to the resemblance of the two facies, the main criteria being

then the greater lateral extension of the HARPs (Figure IV.8).

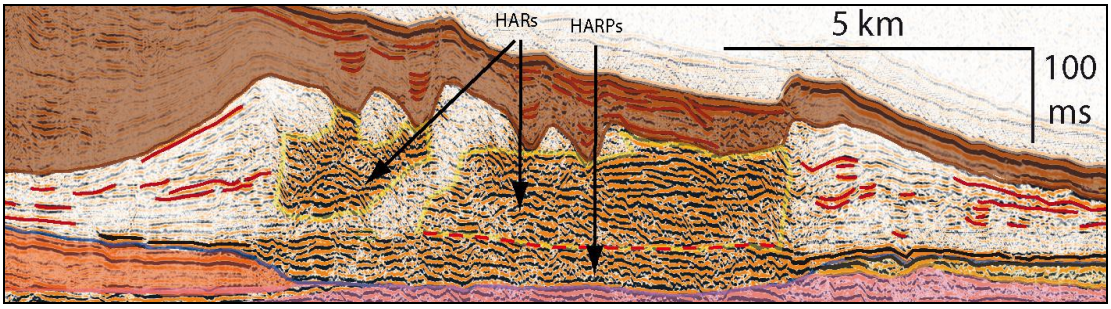

Figure IV.8: Wide HAR facies (external limit is colored in yellow) superposed on HARPs facies (some continuous reflectors at the base of the levees are highlighted by black lines). The limit (marked by the red doted line) between the two facies is not clear because of the strong resemblance of the two facies in this case. Line LS 51, see Figure IV.15b (IV.1.3) for localization. Other colors represent high-amplitude reflectors in levees (highlighted in red), adjacent channel-levee systems (colored in brown, orange, yellow or pink, see IV.1.3).

In transect sections each sub-facies is present whereas in longitudinal sections (IV.1.3, Figure IV.18) the erosional V- or U-shaped features are generally lacking, indicating that these features are elongated longitudinally and arguing for their interpretation as small channels.

	Total HARPs	Flat-lying unchannelized sub-units (yellow)	U- or V-shaped features	Small channel-levee systems (red)	Chaotic patches (purple)	Transparent patches (pink)
Max. thickness (ms twt)	85	30	30	20	Several tens	20
Max. lateral extension (km)	25	< 5	< 1	< 5	< 5	< 5 km

Table IV.1: Dimension of the constitutive elementary sub-units within the HARPs.

No special organization of these sub-units has been evidenced on either strike or dip sections, the stacking pattern appearing quite random, with an irregular vertical and lateral alternation of channelized and unchannelized sub-units. However, It must be emphasized that the small number of profiles available for each HARP body of the fan restrains the possibility to highlight a specific organization, if any.

The maximum thickness and lateral extension of the constitutive elements of Harps observed

in the studied area are provided in Table IV.1.

1.2.2 Internal architecture of the levees

The levees of the Amazon ULC channel-levee systems are generally represented by facies B and made of continuous, parallel to convergent, low to medium amplitude, on- or down-lapping reflectors, accumulated in wedge-shaped bodies, laterally away from the HAR facies of channel fills. In association with the HAR, they form lens-shaped bodies corresponding to channel-levee systems. The lenticular form can be modified by channel migration when the channel partly erodes the levee of the side against which it is shifting. On profiles parallel to the channel axis, the lenticular form is not expressed, and the levee consists of parallel reflectors.

Detailed analysis of levees of most of the channel-levee systems highlights vertical and lateral facies variations, such as sets of high-amplitude and/or discontinuous reflectors, unconformities and transparent patches. These variations attest to a complex architecture that probably reflects the complexity of the process that build the levees.

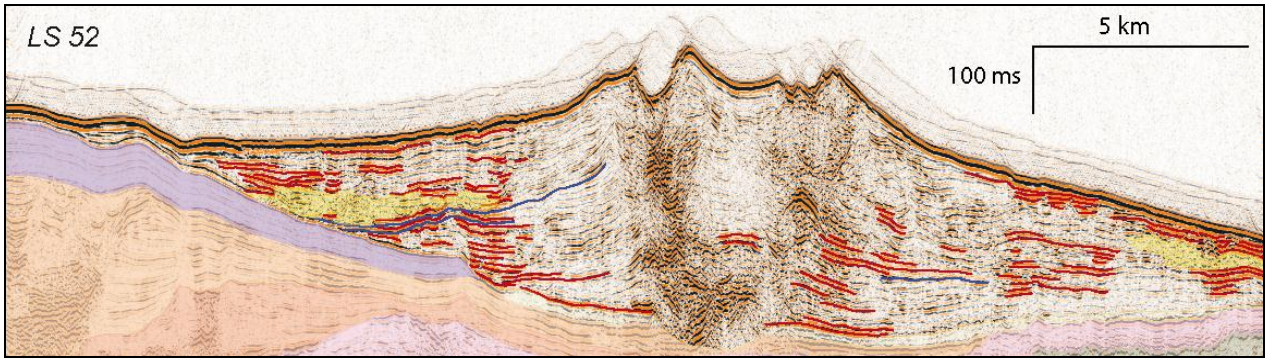

Figure IV.9: Internal structure of the levees. Main facies variations observed are:high-amplitude reflectors (highlighted in red), discordances (marked as blue lines), transparent wedge-shaped units (colored in yellow). Line LS52, see Figure IV.15b (IV.1.3) for localization.

In more details I observed in cross sections of the levees:

1. Internal unconformities, (blue reflectors, Figure IV.9). These unconformities attest of the occurrence of abrupt changes in the sedimentary processes that contribute to levee deposition.

2. Variable amplitudes of reflectors both laterally and vertically: the amplitudes are generally low to medium, but high amplitudes (red reflectors, Figure IV.9) are seen at specific locations. High-amplitudes reflections are more frequent in the outer levee and near the unconformities. They can be associated laterally to low to medium amplitude "normal" facies of the levee and constitute small channel-levee systems

inside the levee (Figure IV.10). High-amplitude reflections are also observed in local lows in the levee that are channel-axis lows of former systems (Figure IV.11, LS50). Variations in amplitude of the reflectors generally are related to variations in grain size of the sediments, high-amplitudes being generally imaging coarse-grained sediments in siliciclasitc environments. Therefore, it can be concluded that high-amplitude facies inside the levees reflect events of sandy overflow of turbidity currents on the levees. The cause of such coarse grained overflow could possibly be related to an increase of the currents volume or a local lowering of the levee crest (because of local breaching ?) both allowing coarser sediments, normally confined at the basal part of the current, to escape from the channel.

3. Variable stacking pattern of reflections, either aggrading (parallel reflectors) or aggrading/laterally prograding (convergent reflectors). Some parts of the levee can also show wedge-shaped unconformable sub-units made of low amplitude to transparent facies (yellow patches in Figure IV.9) or even chaotic facies (Figure IV.10) intercalated between aggrading or aggrading/prograding "normal" levee.

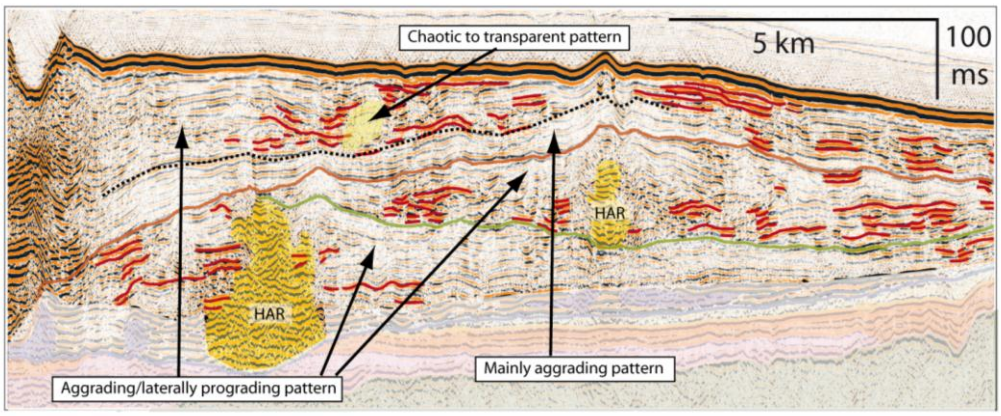

Figure IV.10: Variability of the stacking pattern of the levees at Line LS51, see Figure IV.15b (IV.1.3) for localization.

The downfan evolution of the levees does not show drastic changes in their internal structure (Figure IV.11), except a relatively more frequent variability of the reflections amplitudes and stacking pattern in the upfan area (LS52, 51, 50). In any case, I did not observed significant changes of these characteristics from upstream to downstream the avulsion points (e.g. LS52 to LS51, Figure IV.11).

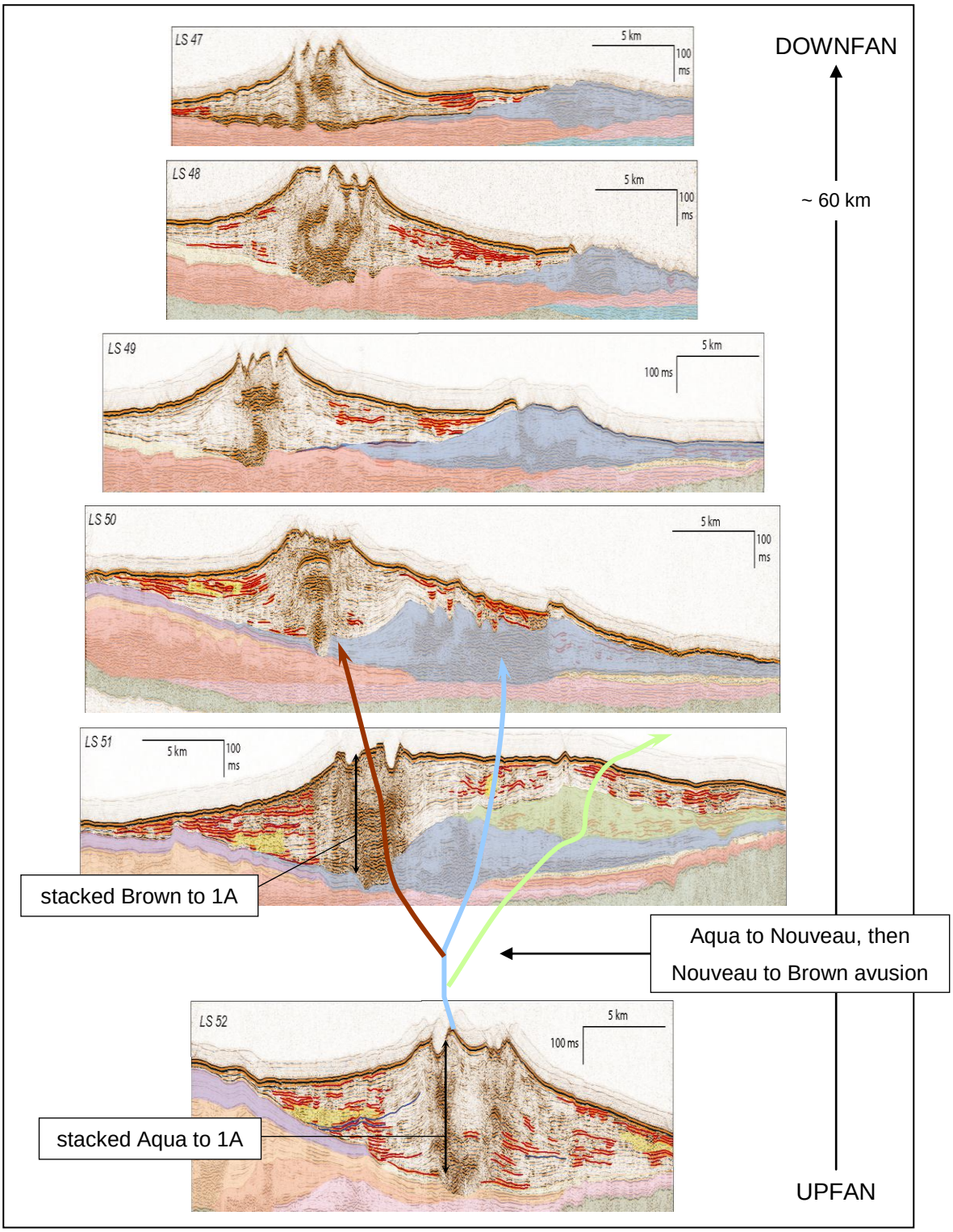

Figure IV.11: Downfan evolution of the architecture and seismic facies of the levees a channel-levee from up to downstream an avulsion point. Main facies variations observed are:high-amplitude reflectors (highlighted in red), discordances (marked as blue lines), transparent wedge-shaped units (colored in yellow

1.2.3 CONCLUSIONS

The seismic facies analysis identified 4 seismic facies (HARs, HARPs, Levees and Mass-Transport Deposits). HARs and Levee facies are associated to form channel-levee systems that are some times underlain by a basal sole of HARPs.

In my objective to study the avulsion process, I conducted a detailed analysis of the internal architecture of both the HARPs (the "avulsion lobe") and the levees (which should have somehow recorded the avulsion event).

Both the HARPs and the levees revealed themselves to have a complex internal architecture.

1.2.3.1 The avulsion lobe

The HARPs are made of 4 sub-facies that we interpreted in term of elementary seismic bodies related to specific depositional processes. These elementary units, schematized in Figure IV.12 are:

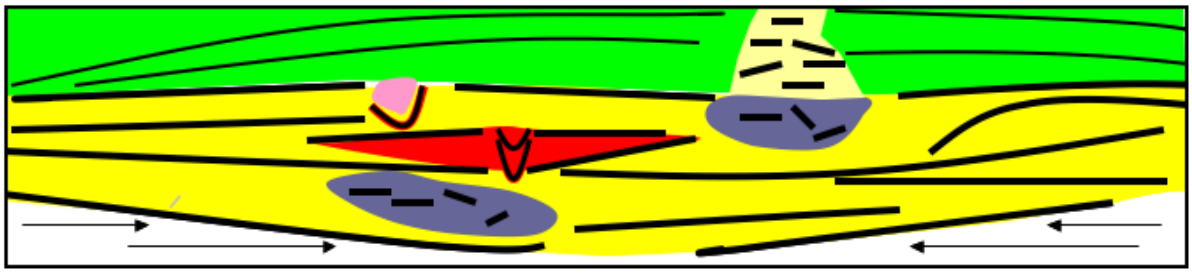

Figure IV.12: Schematic view of the internal architecture of the HARPs, with overlying channel (light yellow)-levee (green) system. The HARPs consist in 4 elementary seismic sub-units, the channelized sub-units (red), the chaotic patches (purple), the transparent patches (pink) and the flat-laying or mounded unchannelized sub-units (yellow). The basal surface is an erosional unconformity marked by truncation of underlying deposits, and the top surface is an angular unconformity marked by down laps of the overlying levee.

- The unchannelized lobes, deposited by unconfined flows,
- The small erosional channels and channel-levee units, when associated with aggradational structures, this units are progressively formed by confinement between lobes.
- The transparent channel infills representing the abandonment phase of the small incised channels, and probably consisting of fine-grained sediments.
- The possibly micro-channelized lobes or cut and fill features similar to those attributed to channel fill during the active phase of channels (similar to HAR).

These elementary units alternate without any specific rhythm (or I was not able to evidence such a rhythm).

The erosional channels, channel-levee units and cut-and-fill features are the first signs of a perpetuation of the channelization that will end up in the development of the channel-levee system above it.

1.2.3.2 The levees

The levees consist mainly of convergent reflections of variable amplitude, with frequent areas of isolated or stacked high-amplitude reflections, unconformities and transparent patches. They are schematized in Figure IV.13.

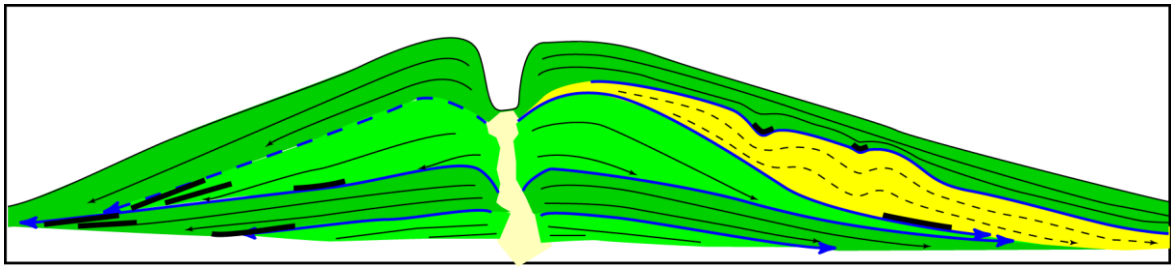

Figure IV.13: Schematic view of the internal architecture of the Amazon levees. Light green: aggrading/laterally prograding pattern; dark green: aggrading pattern; light yellow: unconformable bodies (product of levee failure and/or levee channelization); thin black lines: low to medium amplitude reflections; thick black lines: high-amplitude reflections; blue lines: unconformities.

- The strong variability of the internal reflection pattern probably reflects frequent variation of the characteristics of the overflows through time, probably due to changing sediment concentration and/or flow height of the turbidity current in the channel axis.
- Transparent wedges in association with unconformities could correspond to levee failures and high-amplitude reflectors to crevasse splays.
- Some high-amplitude reflectors in the levees follow paleomorphologies of abandoned channels and could represent overflow deposits that are caught into these paleochannels. The overflows could eventually also be guided further downfan along these paleo-confined areas and spread out and depositing flat-lying deposits where paleochannels are lost.

Unfortunately, data on levees failed to clearly evidence the impact of channel avulsion in levee deposition. However, I suspect that variations in sediment concentration and/or in flow volume of the turbidity currents are responsible for amplitude variations and unconformities that are recorded in the levees are possibly a cause for channel avulsion.

1.3 REFINED CHANNEL MAP AND HARPS DISTRIBUTION

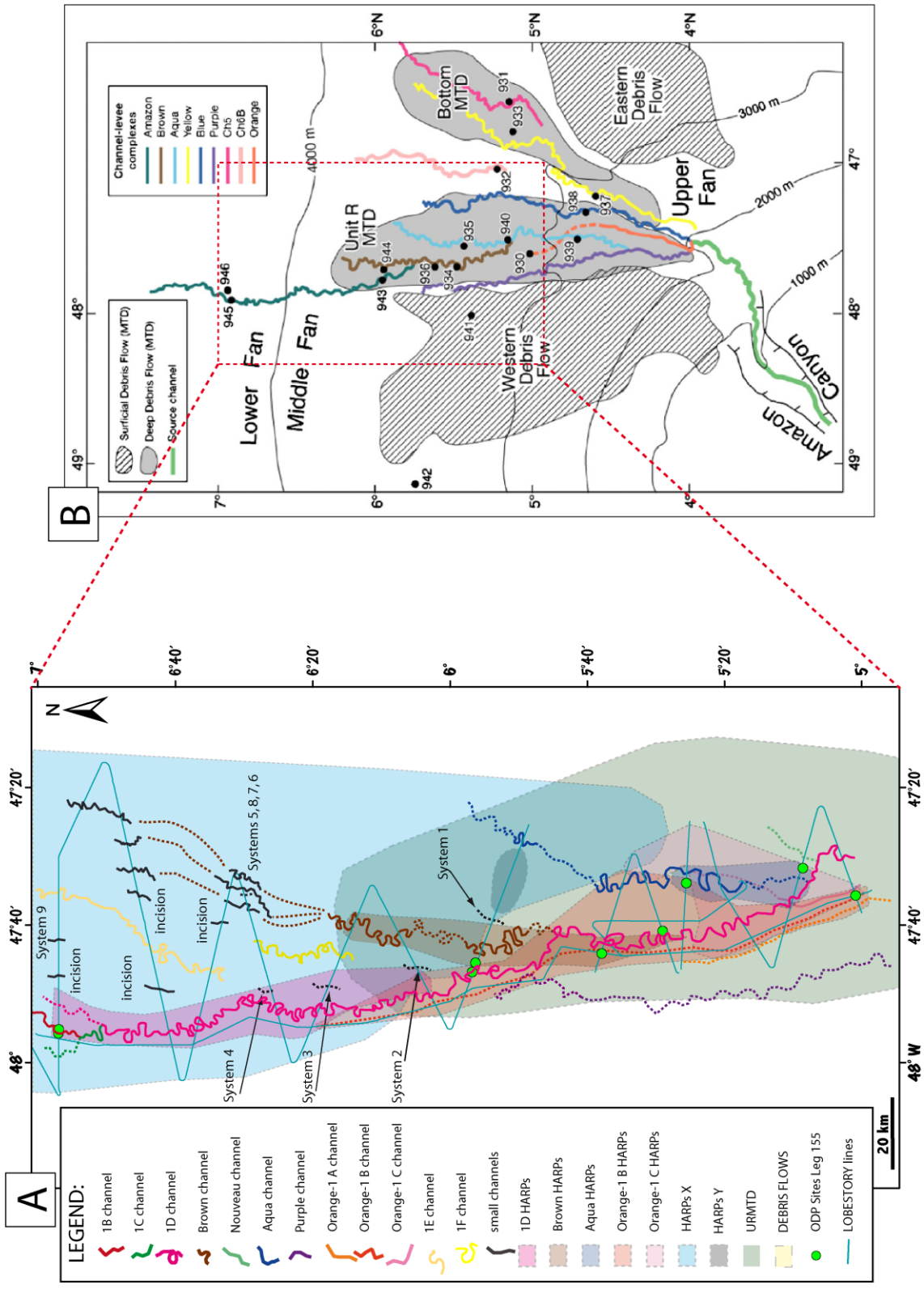

Figure IV.14: Refined channel map and chronology based on our study of the Lobestory data. (A): map of the channels, corresponding HARPs and Mass-Transport Deposit URMTD. Doted lines indicate buried channels or channel courses taken from previous work (Damuth et al., 1983a; 1983b; Damuth and Flood, 1984; 1985; Flood and Damuth, 1987; 1988; Manley and Flood, 1988; Flood et al., 1991a; Pirmez, 1994; Flood et al., 1997). (B): Previous channel map from Maslin et al. (2006).

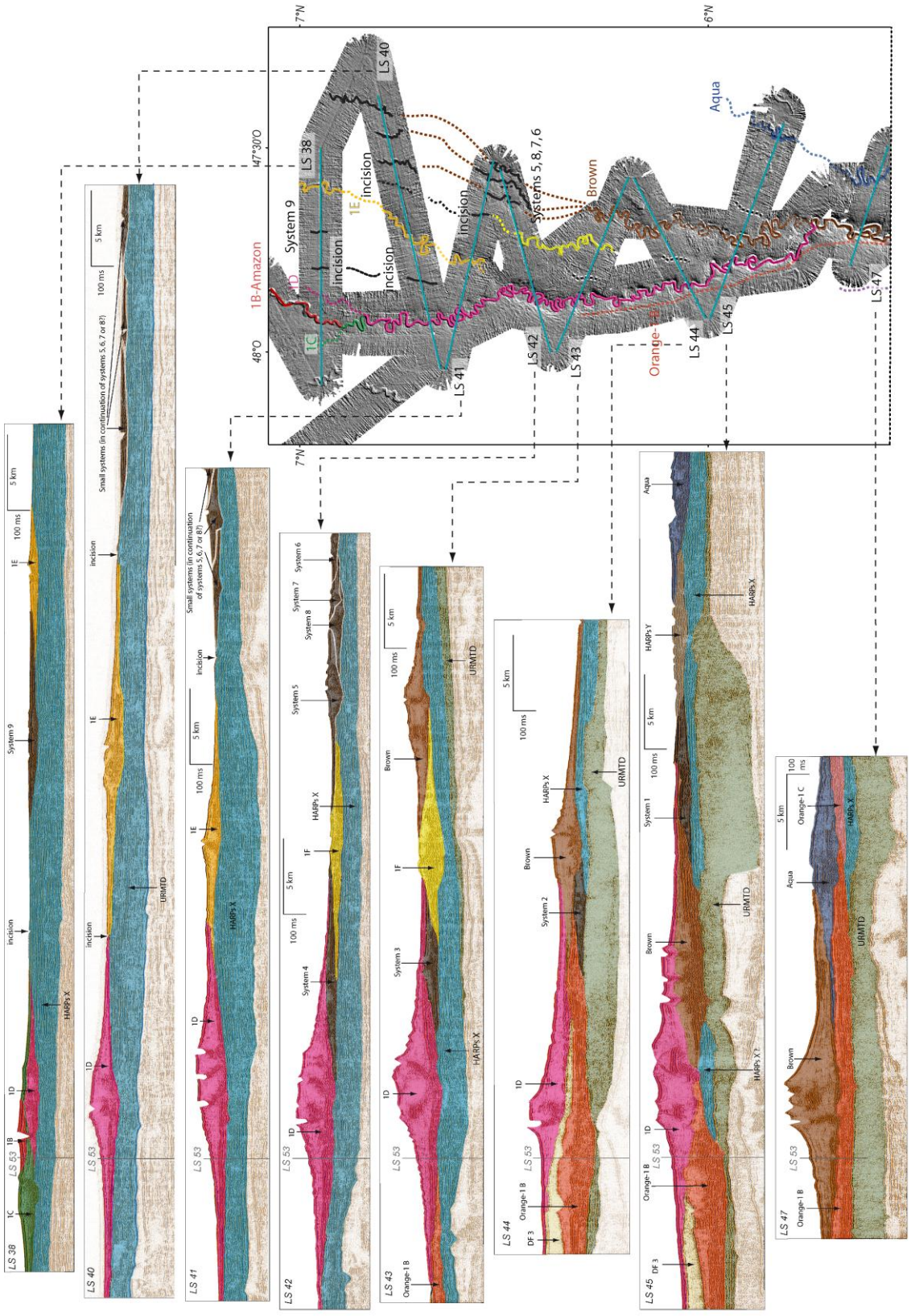

Figure IV.15a: Overview of interpreted seismic lines (LS 47 to LS 38), see also ANNEX IV.a.

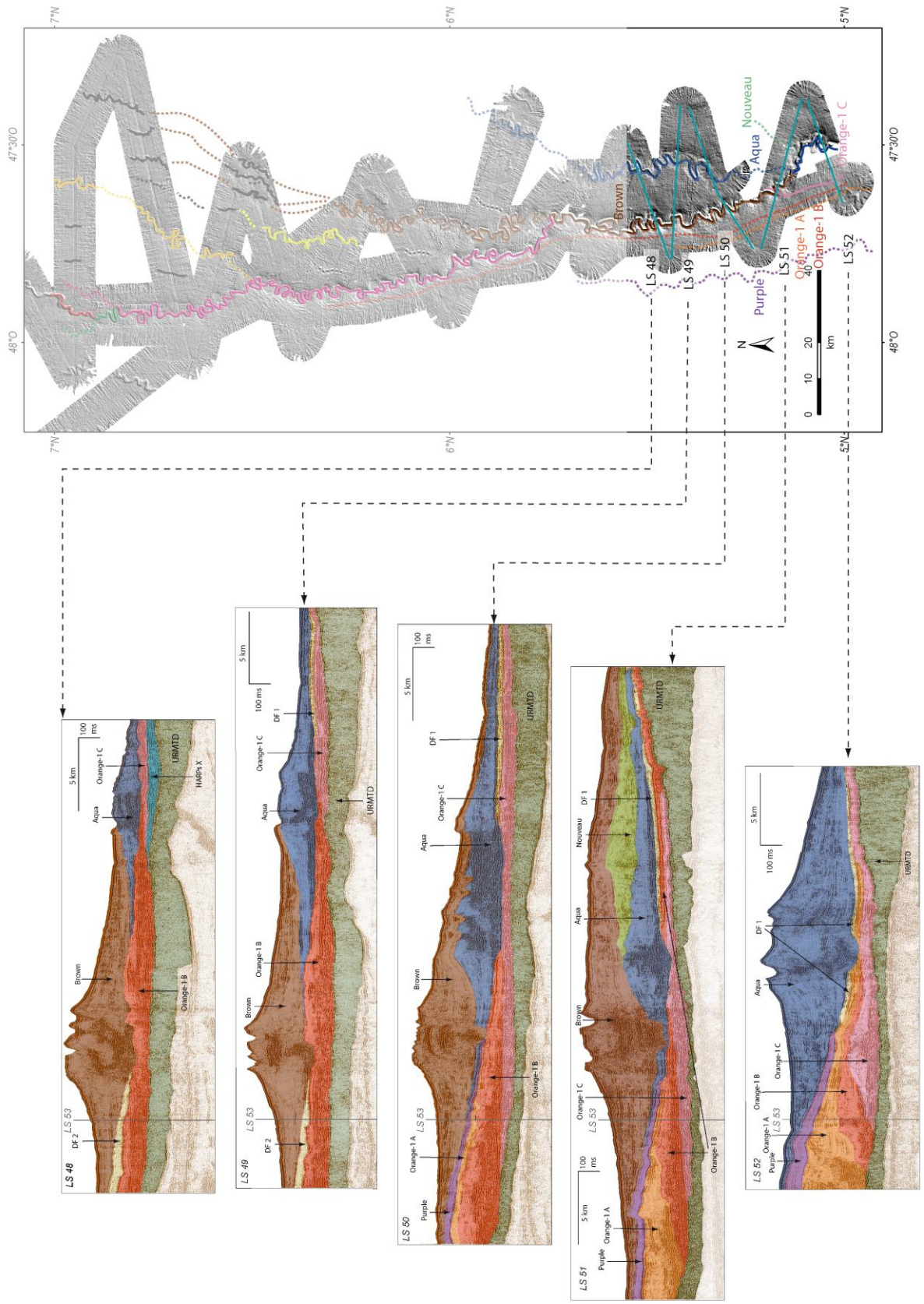

Figure IV.15b: Overview of interpreted seismic lines (LS 52 to LS 48), see also ANNEX IV.b.

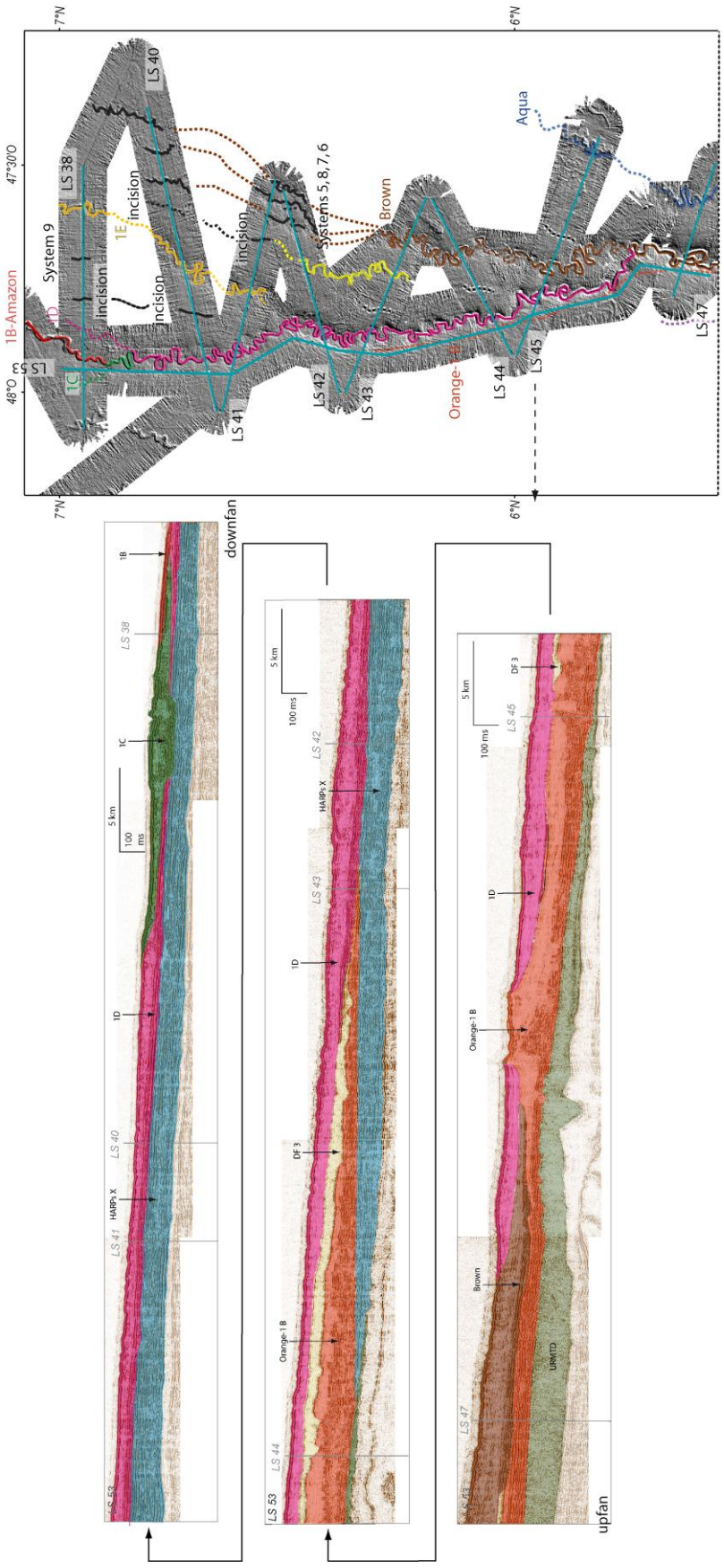

Figure IV.15c: Overview of downdip seismic line LS 53 that cross LS 47 to LS 38.

My study concerned the channel-levee systems and HARPs visible in the Lobestory area, including the channel-levee-HARPs systems between the URMTD and the top of the fan, i.e. from system Orange-1 to system 1B essentially.
In order to identify "channel-levee-HARPs" bodies on my data, i.e. to link the right HARPS to the right channel-levee system, I based my work on the previously proposed associations (Flood et al., 1991a; Flood et al., 1997) and eventually refined the associations or chronology when necessary.

1.3.1 Refined architecture

Based on my seismic stratigraphy analysis of high-resolution Lobestory data, I established a refined chronology and channel map of the Quaternary Amazon Fan (Figure IV.14) that will be described in the followings. In this map, the HARPs located at the base of a channel-levee system and corresponding to the avulsion deposits of this channel, are assigned the same color names as the overlying channel-levee deposits.

The main channel-levee systems of this part of the fan, i.e. Aqua, Brown and 1D systems are recognized and their relative stratigraphic orders are in agreement with previous work. However, I observed some discrepancies with previous mapping, including the stratigraphic order of some of the systems.
Main differences from previous work are (Figures IV.14 and IV.15):

- The Orange-1 system was observed to consist of at least 3 sub-systems (C, B, A from the oldest to the youngest) (line LS52, Figure IV.15b).
- A previously unknown system, that I called "Nouveau" system, is evidenced between the Aqua and the Brown systems (line LS51, Figure IV.15b).
- The 1F system, previously thought to be younger than the Brown system, has been clearly seen to be older than this system. However, the data do not allow a better definition of the precise stratigraphic order of 1F, that lies between HARPs X (see below) and Brown (e.g. line LS43, Figure IV.15a).
- The stratigraphic relationships of the 1E system in not clear with regard to Brown and 1F,
- Several small channel-levee systems (2 to 9 without chronological order), previously not mentioned, have also been identified on my data (Figures IV.16 and IV.24). Stratigraphic information are not sufficient to propose a precise relative chronology: System 2 is older than Orange-1B and younger than HARPs X (LS44), Systems 3 to 8 are younger than 1F and systems 3 and 4 are older than 1D and System 9 is

younger than 1E (Figure IV.15). When considering their geographical and stratigraphic positions and their sizes, Systems 5 to 8 could be downfan prolongations of the Brown system and result from successive avulsions of this system. This hypothesis is in agreement with that of Jégou (2008) and Jégou et al. (2008). Systems 3 and 4 could correlate together, and correspond to an upfan prolongation of 1E. System 2 is in good position to be the upfan prolongation of 1F, but data are not sufficient to strongly argument this possibility.

- Two Harp units (called Harps X and Harps Y) have been observed without any genetic link to channel-levee systems visible in the studied area (lines LS45 to LS38, Figure IV.15a).
- Three mass-transport deposits (called DF1 to DF3) have been identified based on facies interpretation. They are located at the bases of channel-levee-Harp bodies, but their stratigraphic position is badly constrained: DF 1 is thin (25 ms twt) and is at least younger than Orange-1A system and older than Aqua system, the overlying eroding channel (LS52, Figure IV.15b). The DF 2 appears thicker (50 ms twt) and is at least younger than Orange-1B system and older than Brown system (LS49, Figure IV.15b). The DF 3 is the thickest (75 ms twt) and is at least younger than Orange-1B system and older than 1D system (LS 45, Figure IV.15a).

1.3.1.1 The HARPs X and Orange-1 systems

A. Orange-1 systems

Analysis of Lobestory data allowed me divide the Orange-1 systems of Flood et al (1991) into 3 stacked channel-levee systems, i.e. C, B and A in chronological order. These systems appear on the southern half of the study area where they are the first systems that lay on the URMTD (Unit R Mass Transport Deposit) deposits (Figures IV.16 and IV.17). However, as argued by Flood et al (1991, 1997) (see chapter II) other channel-levee systems are probably intercalated between the Orange systems and the URMTD in other sectors.

On the most upfan seismic line (Figure IV.17) the 3 Orange-1 systems are stacked very close to each others, the channels being separated by only about 4-5 km. The associated *levees* are 100 ms twt thick in systems C and B and up to 200 ms twt thick in system A. Only the Orange-1 B channel can be followed downfan on my data (Figure IV.16), where it is truncated under the basal surface of the 1D HARPs indicating that the Orange-1B channel-levee system has been removed by erosion (Figure IV.18) and explaining its abrupt

disappearance.

The Orange systems are caped by the transparent facies of the outer levees of the Purple channel-levee system that separates it from the Aqua to 1A channel-levee system, up to 400 ms twt thick in this area (Figure IV.17).

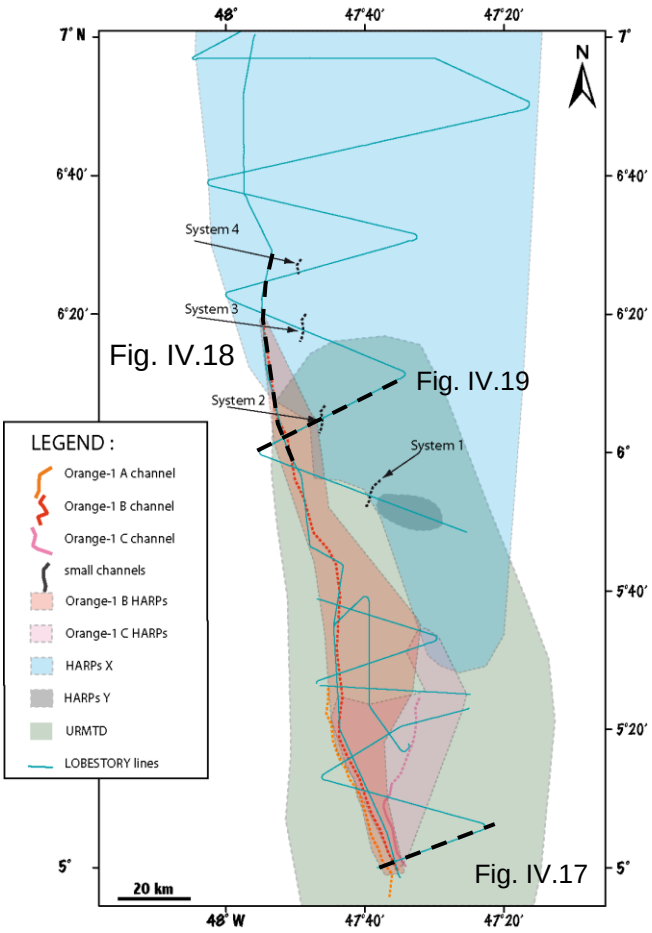

Figure IV.16: Distribution of the Orange channels (from the oldest to the youngest: C, B and A), HARPS deposits (B, C and X) and URMTD. The black dashed lines indicate the localization of profiles shown in Figures IV.17, IV.18 and IV.19.

On the seismic line of Figure IV.17, two HARPs units are visible as the basal part of the Orange-1C and Orange-1B systems respectively, whereas HARPs are lacking under the A system. The HARPs extend laterally more or less symmetrical to the channel axis on this cross section.

Mapping of the Orange-1B and 1C HARPs and channels (Figure IV.16) indicates that the HARPs are elongated lobe-shaped bodies, relatively limited in lateral extent (5 to 25 km). Only the Orange B channel and HARPs are followed downfan with available data, where it has been eroded during deposition of further channel-levee-HARPs, giving a minimum HARPS length of about 50 km. The Orange-1B channel is located approximately at the center of its HARP body.

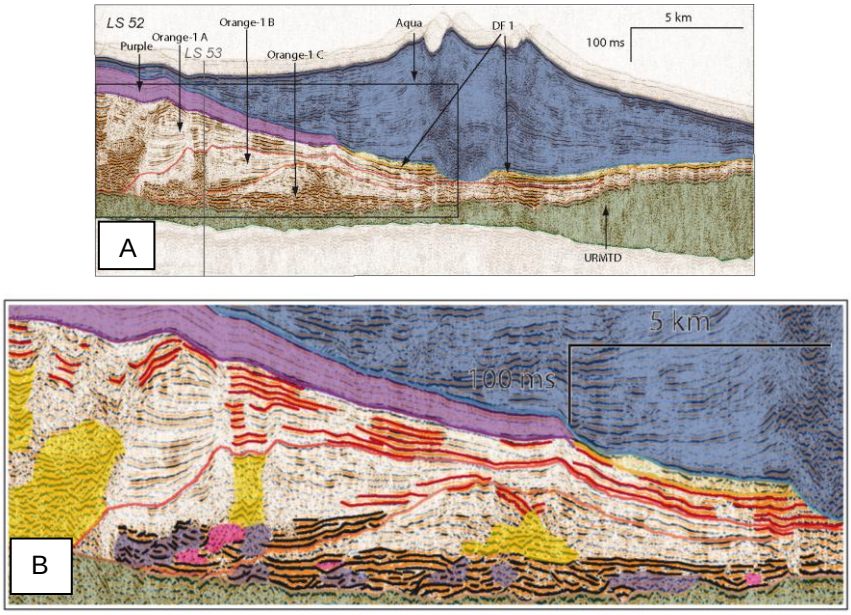

Figure IV.17: A: The Orange systems, composed of 3 stacked channel-levee systems (C, B, A in chronological order from the oldest to the youngest) with HARPs at the base of C and B (line LS 52, for localization see Figures IV.15b and IV.16. B: In HARPs, continuous reflectors are highlighted in black, chaotic areas are in purple and transparent patches are in pink; HARs are in yellow; high amplitude reflectors in levees are highlighted in red.

B. HARPs X

On the dip seismic line, which is parallel to the Orange-1B channel axis and approximately located along the channel axis (Figure IV.18), the Orange-1B channel-levee-HARPs body seems to pass downfan to a thick (up to 190 ms twt, see below) seismic unit consisting in high-amplitude reflections (called HARPs X). The cross line of Figure IV.19, upstream the disappearance of Orange-1B, shows that the HARP X unit is clearly separated from Orange-1B by a small previously unknown system (system 2) at the top of the HARPs X, indicating that the HARPs X and Orange-1B HARPS are distinctive seismic units. Due to a vertical continuity of facies characteristics, the limit between the two units on the dip line (red dashed line on Figure IV.18) is difficult to be accurately defined. The origin of the HARPs X unit will be discussed later (see conclusions, this chapter).

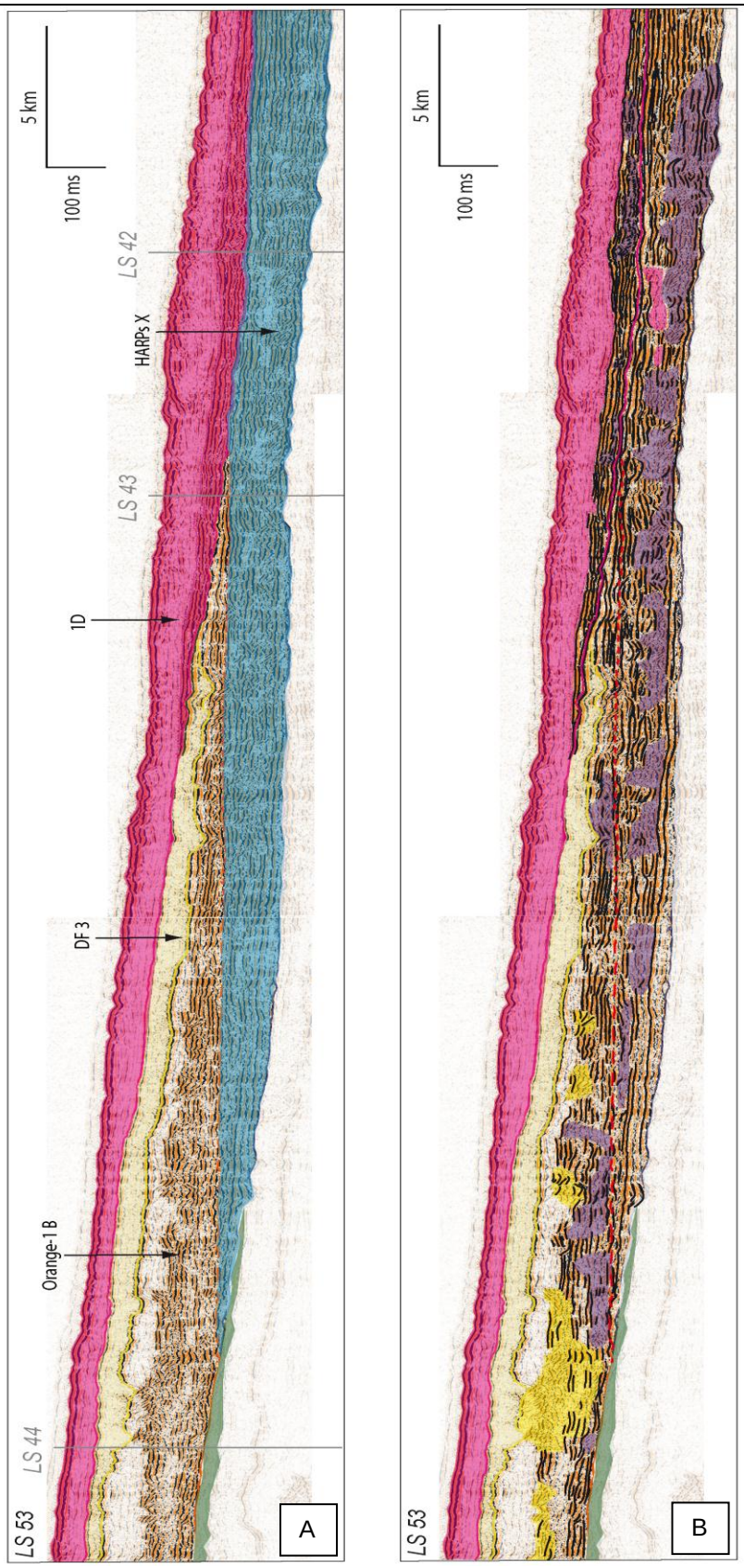

Figure IV.18: A: Dip seismic line LS 53 (for localion, see Figures IV.15a and IV.16) showing the pinch out of Orange-1B system under the 1D HARPs and the thick HARPS X under both systems. The limit between the Orange-1B system and HARPS X (red dashed line) is badly defined. B: HARP seismic facies, continuous reflectors are highlighted in black, chaotic areas are in purple and transparent patches are in pink; HARs are in yellow.

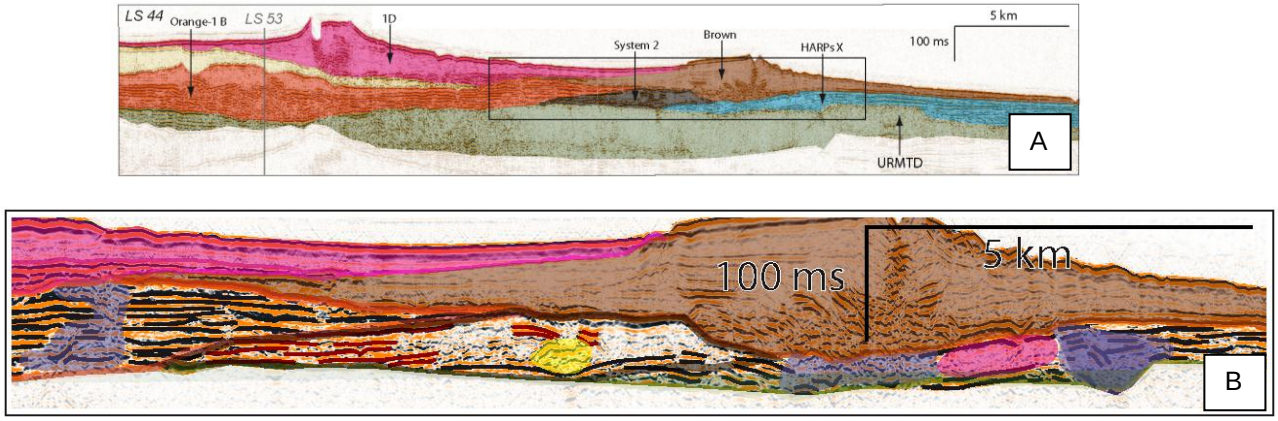

Figure IV.19: Transverse line LS 44 (for location see Figures IV.15a and IV.16) showing the Orange-1B system separated from the HARPs X deposits by a small system (System 2). In HARPs, continuous reflectors are highlighted in black, chaotic areas are in purple and transparent patches are in pink; HARs are in yellow; high amplitude reflectors in levees are highlighted in red.

1.3.1.2 The Aqua-Nouveau-Brown groups of channel-levee systems

Following the deposition of the Orange-1 systems, the depocenter shifted to the west, mainly outside my data set where the Purple channel and its HARPs deposited (Figure IV.20). Only the right levee of the Purple channel-levee system is visible, draping the Orange-1 systems on my data. Following the Purple system, the depocenters shifted again and the Aqua system deposited under the Brown system at the eastern part of the Lobestory area (Figures IV.20 and IV.21).

The deposition of the Aqua system appears more complex than previously thought because the data clearly show two successive systems under the Brown right levee, suggesting a new system that was not reported earlier and which I called the “Nouveau” channel-levee system (Figure IV.22). ODP previously interpreted these deposits as resulting from a simultaneous activity of Brown and Aqua systems (Shipboard-Scientific-Party, 1995).

I hypothesize that the Nouveau channel avulsed from the Aqua channel and therefore that the Nouveau channel is the true parent channel of the Brown channel.

The upfan courses of the Aqua and Nouveau channels are not well constrained because they are close to the Brown to 1A system and buried under long lasting levee deposition, and I are not able to localize precisely the avulsion points. However, due to this stratigraphic order (Aqua, Nouveau, Brown from the oldest to the youngest) clearly visible on line LS 51 (Figure IV.21), and considering that on the line just upfan (LS 52, see Figure IV.17) the systems from Aqua to Brown are stacked up in one thick system, I have to conclude that the avulsions took place in a small area between LS52 and LS51. The exact geometry remains uncertain.

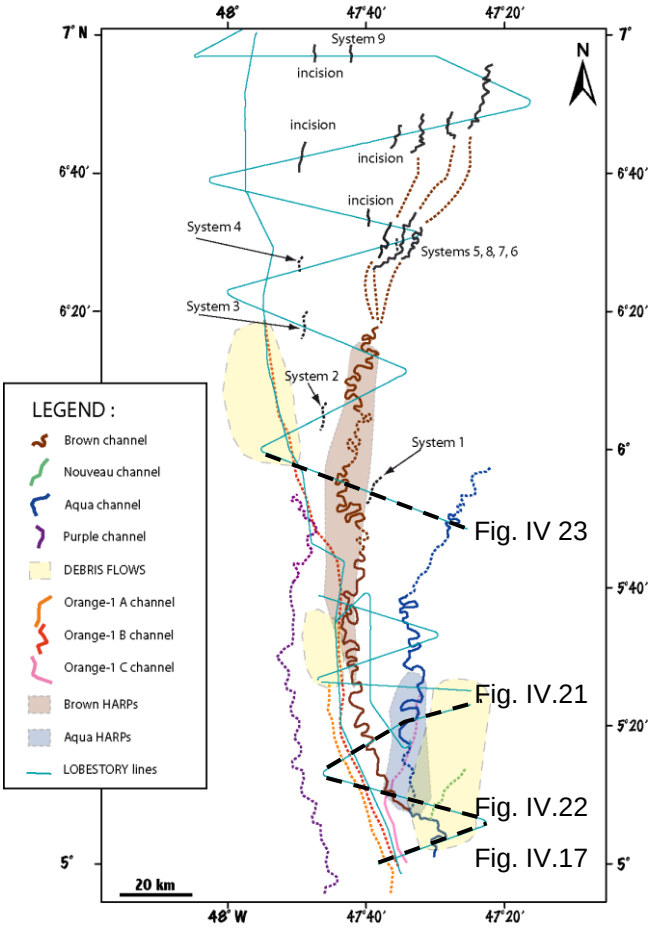

Figure IV.20: Map of the Aqua, Nouveau and Brown HARPs and channels. The Orange and Purple systems and the DF1 to DF3 mass-transport deposits are also shown.

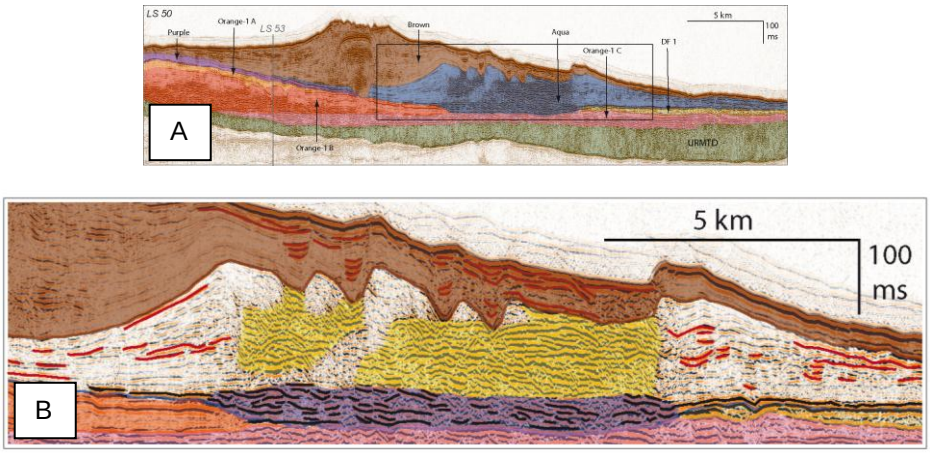

Figure IV.21: The Aqua system and HARPs (LS 50, for location of line see Figures IV.15b and IV.20. In HARPs, continuous reflectors are highlighted in black, chaotic areas are in purple and transparent patches are in pink; HARs are in yellow; high amplitude reflectors in levees are highlighted in red.

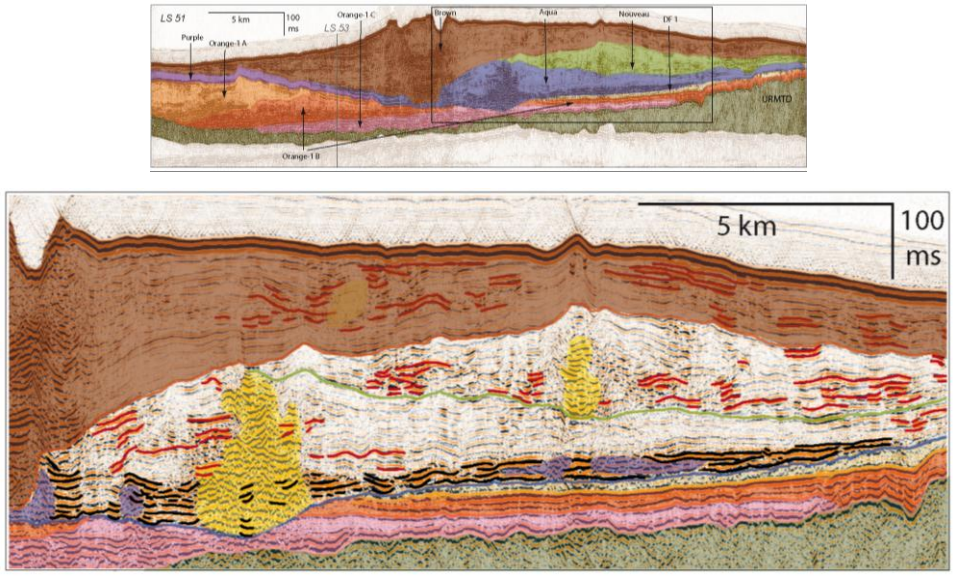

Figure IV.22: Aqua and Nouveau systems, showing the HARPs at the base of the Aqua system and the lack of HARPs at the base of the Nouveau system. In HARPs, continuous reflectors are highlighted in black, chaotic areas are in purple and transparent patches are in pink; HARs are in yellow; high amplitude reflectors in levees are highlighted in red. (LS51, for localization see Figures IV.15b and IV.20.

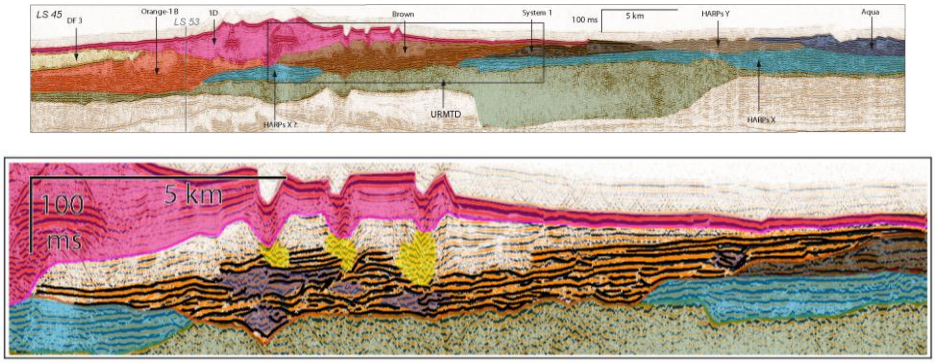

Figure IV.23: Brown HARPs at line LS 45 with a maximum thickness of around 80 ms (for localization of line, see Figures IV.15a and IV.20.

Mapping of the HARPs (Figure IV.20) shows that the HARPs of the Aqua System are identified along about 40 km and they extend laterally on up to 10 km (e.g. Figures IV.21 and IV.22), the Aqua channel is located at the center of the HARP body. No HARPs have been recognized in association with the Nouveau channel-levee system, but this system is only imaged on one line, which, moreover, is close to the inferred avulsion point (Figures IV.20 and IV.22).

The Brown HARPs (Figure IV.23) are observed at about 40 km from the Nouveau/Brown avulsion point, along a minimum of 84 km and show a lateral extension of approximately 10 km. The course of the overlying Brown channel is more or less centered over its HARP body, except in the medium part where the channel is located at the eastern limit of the HARP body.

1.3.1.3 The 1F, 1E and 1D to 1A groups of channel-levee systems

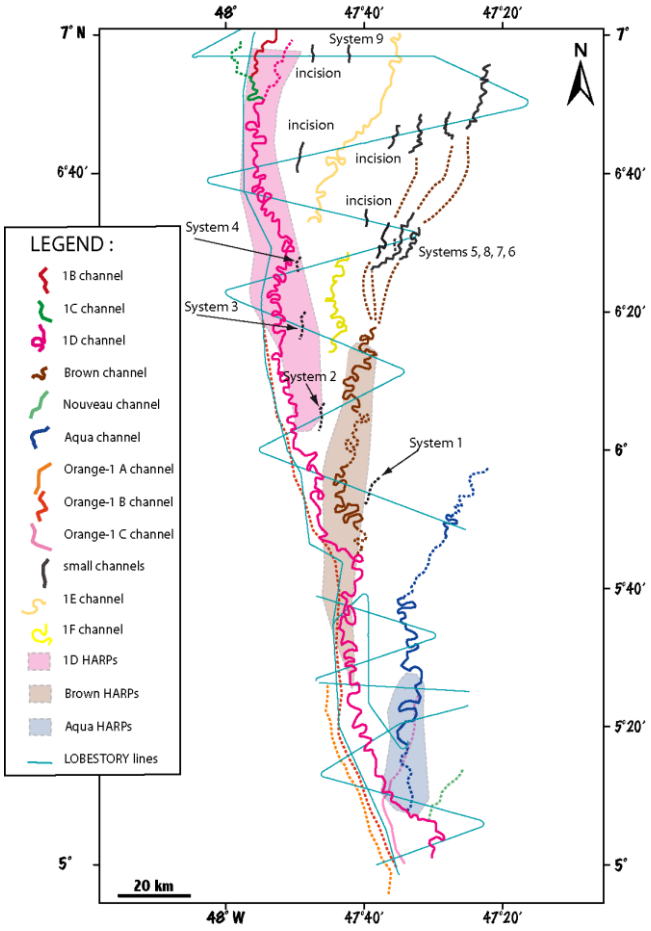

Figure IV.24: Map of Aqua, Brown, 1F, 1E and small channels (1 to 8), and Aqua, Brown and 1D HARPs. The Orange-1, Nouveau, 1C and 1D channels are also shown.

Previous work indicate that channels 1F, 1E then 1D were emplaced by successive avulsions following the deposition of the Brown system, i.e. that these channels are younger than the Brown channel (Figure IV.25)

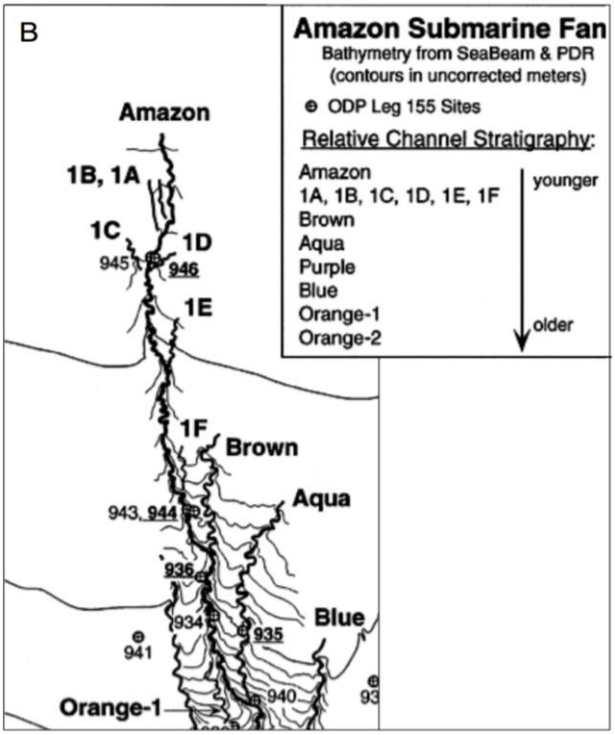

Figure IV.25: Former stratigraphy, showing the emplacement of the channels 1E and 1F younger than the Brown channel. After Flood et al. (1991) and Pirmez (1994), in Pirmez et al.(1997).

My interpretation (Figure IV.24) is not fully in agreement with this previous stratigraphic order as 1F at least appears older than Brown (Figures IV.15a, LS43 and LS42). Unfortunately, no overlapping relationship allows ordering 1F with regard to Orange-1B system. The stratigraphic position of 1E remains unclear because of the lack of overlapping relationships with other channels except with 1D, which is younger as expected from previous work.

Considering the above mentioned stratigraphic relationships two main hypothesis on the origin of 1E and 1F channels can be proposed (Figure IV.26):

(1) They are older than Brown, the 1F channel (LS 43) is a parent channel of the Brown channel, and an avulsion point is located somewhere upfan from line LS43. In the same way, 1E and its probable upfan prolongation (System 3 and System 4) could be an ancestor of the Brown or 1F channel (Figure IV.26A).

(2) The 1F and 1E channels could be linked to the Orange-1 channel (ancestors or childs) (Figure IV.26B). Moreover, if System 2, which is older than Orange-1B system, is truly the upfan prolongation of 1F, the 1F (and 1E) channel can be a parent channel of the Orange-1 channel.

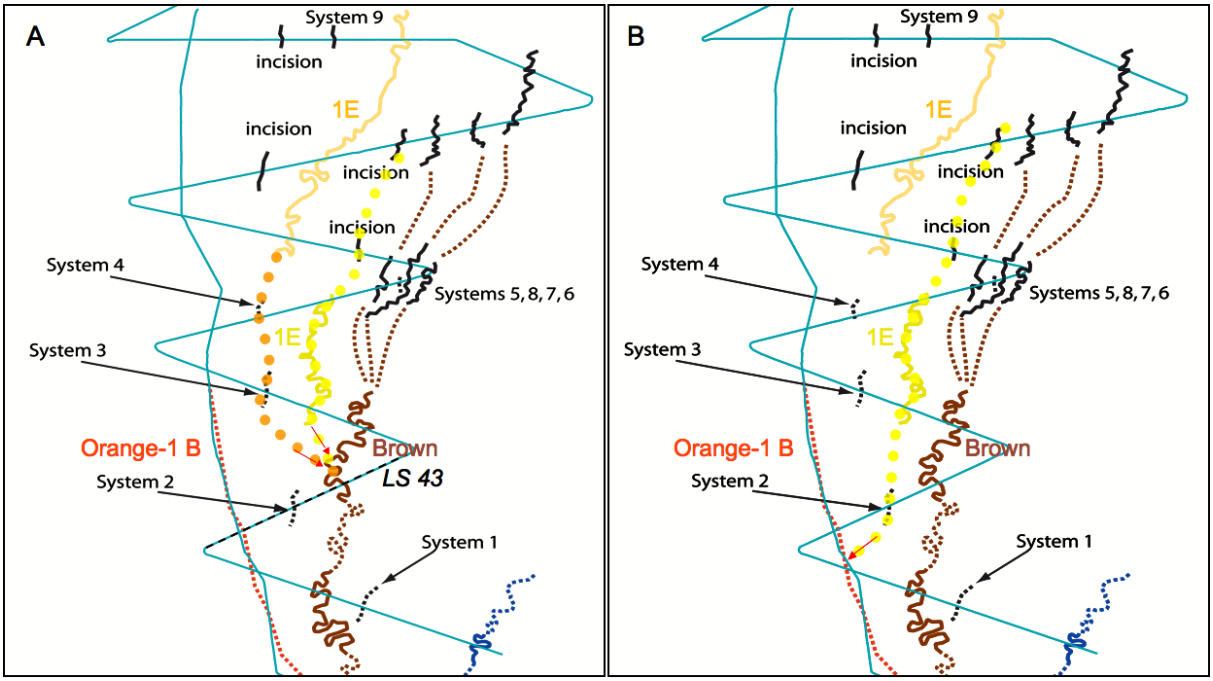

Figure IV.26: Hypothesis on the origin of 1E and 1F channels. A: 1F (and 1E ?) is a parent channel of Brown. B: 1F (and 1E ?) channel is related to Orange-1B. Blue lines show trace of Lobestory Seismic lines.

1E and 1F channel-levee systems do not show basal HARP body, except on the distal most line imaging 1F (LS42, Figure IV.15a). In contrast, 1D channel-levee system overlies a elongated lobe shaped HARP body, at least 80 km long and about 16 km wide. The upfan limit of the 1F HARP body is located at about 40 km from the Brown/1D avulsion point. The course of the overlying 1D channel is first shifted to the western limit of the HARPs and becomes more centered downfan.

1.3.2 3 D characteristics of the Harps

In order to reveal potential topographic influence on the HARPs deposition, I established the isochron maps of the basal depositional surface of the HARPs. Isopach maps were also made to describe the HARPs thickness downfan evolution.

These maps were constructed in Kingdom software (see Chapter III) for each channel-levee-HARPs bodies, but in the followings, I choose to restrict the presentation and description to the most characteristic of them.

1.3.2.1 The paleomorphology at the beginning of ULC channel-levee deposition in the Lobestory area

The base of the channel-levee systems (Figure IV.27A) that developed in the studiy area is

the URMTD in the southern part and older channel-levee systems than the HARPs X deposits in the northern part (Figure IV.15). The western and eastern limits of the URMTD being outside from my data set they were mapped based on previous works (Flood et al., 1997). Its northern limit is visible on lines LS 43 and LS 53 (Figure IV.15a).

The URMTD shows its thickest part (up to around 260 ms twt) at the eastern side of the area, where basal erosion created local lows (Figure IV.27B).

The isochron map of the top of the URMTD (or older units) (Figure IV.28A) images the morphology on which the ULC began to accumulate. It shows a rather regular topography, decreasing from 4.5 s to 5.67 s twt, from South to North.

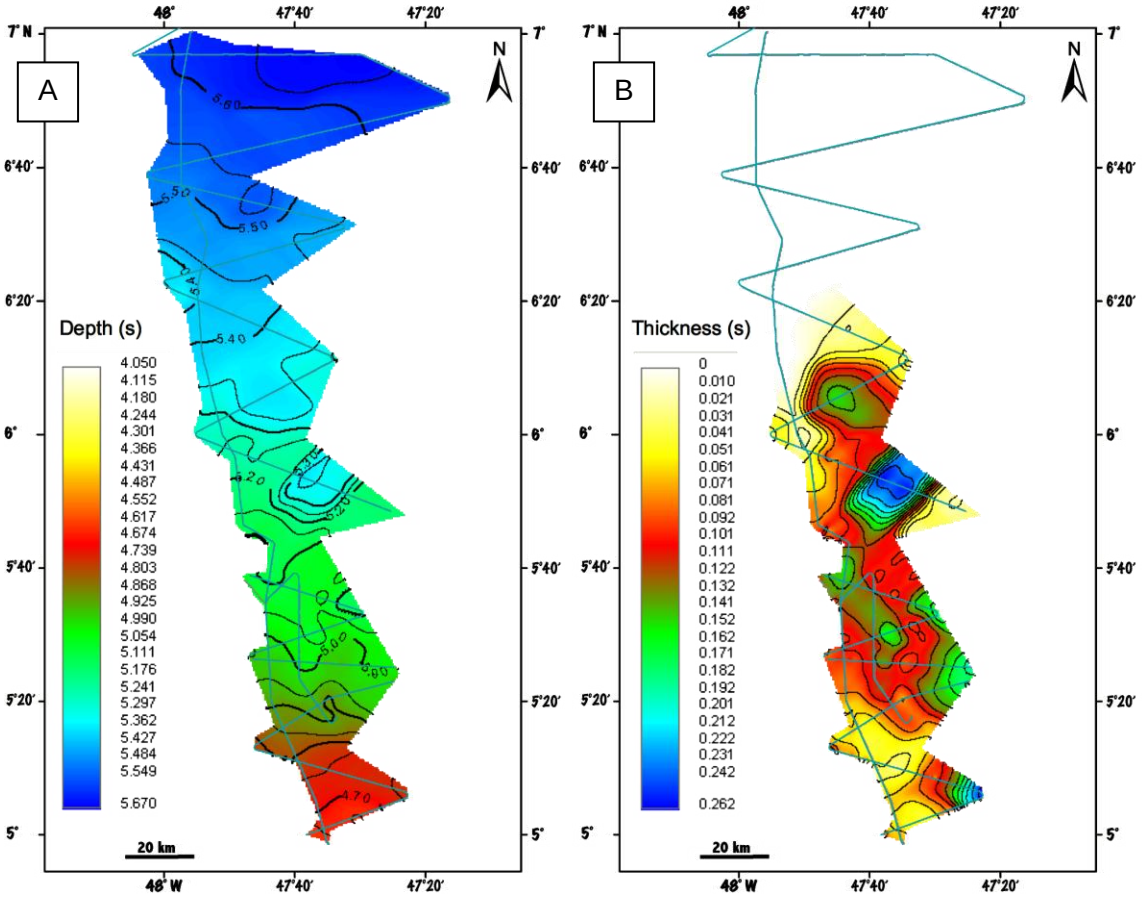

Figure IV.27: URMTD. A: Isochron map of the base of the URMTD body; B: thickness map of the URMTD body. Maps are in s twt.

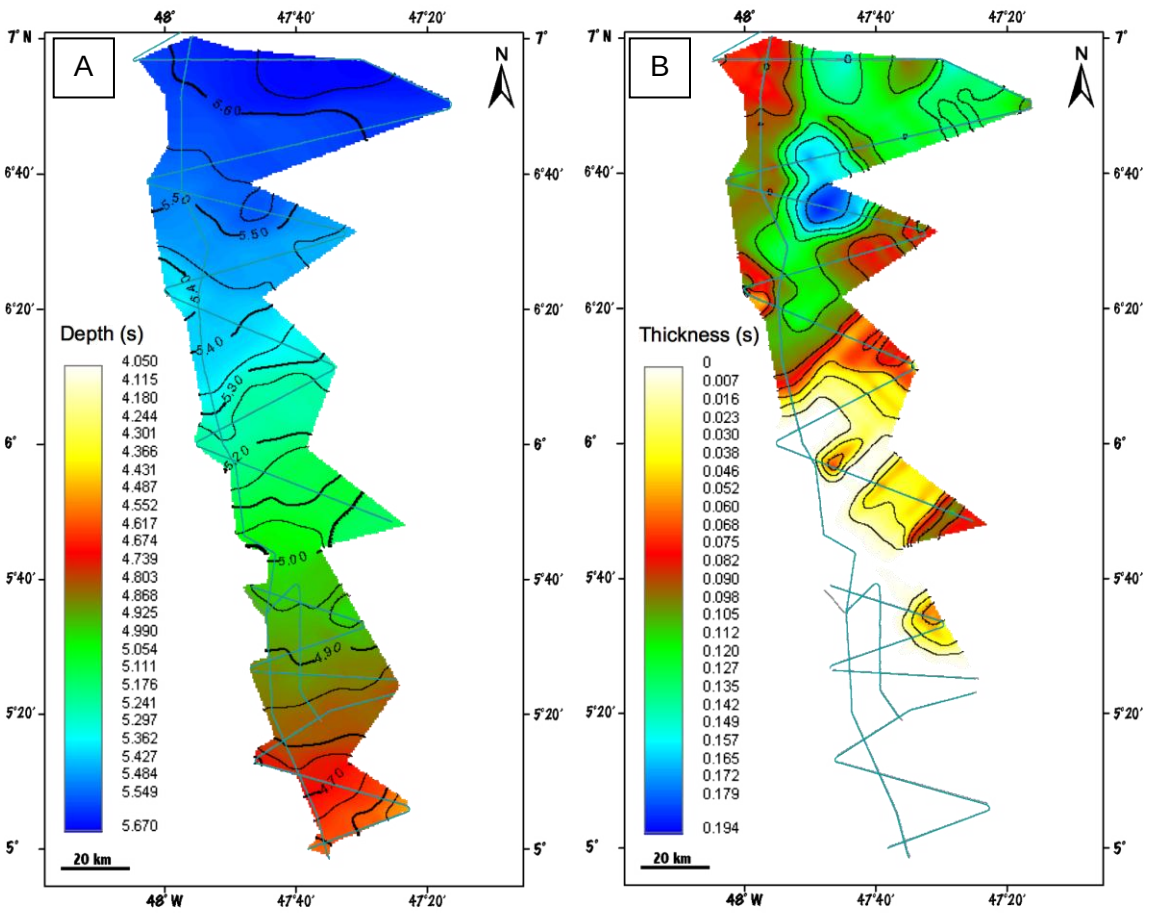

Figure IV.28: HARPs X. A: isochron map of the base of the HARPs X (i.e. top of the URMTD), B: thickness map of the HARPs X; C: isochron map of the top ofthe HARPs X. Maps are in s twt

1.3.2.2 The Harps X

The HARPs X, the lateral and distal limits of which are unknown because they are outside the Lobestory data set, seems to invade the northern half of the study area in a lobe-shaped body, SE-NW oriented, i.e., slightly oblique to the Orange-1B channel axis (Figure IV.14 and IV.16). They show a minimum longitudinal extent of 180 km and a minimum lateral extent of about 100 km.

3D mapping of this huge HARPs body (Figure IV.28B) shows that, besides its SE-NW general orientation, the HARP X maximum thicknesses (up to 0.194 s twt) follow a SW-NE axis, still oblique to the channel-levee systems known in the area. These two transverse orientations suggest a mixed origin from both the SW and the SE.

1.3.2.3 The Orange-1C and Orange-1B HARPs

An isochron map of the base of the Orange-1 systems corresponding to the base of the Orange-1C was made (Figure IV.29A). Note that because of the uncertainty of the stratigraphy of systems 1F, 1E, and small systems 1 to 4, I choose to arbitrarily include these systems under the Orange-1 systems. Therefore, the "base" horizon mapped for the Orange-1 system probably does not reflect the true topography at the time the Orange-1 systems began to develop.

This map represents the paleotopography on which the HARPs C then B were deposited following their avulsions. This topography was characterized by northwards regularly decreasing depths, from 4.55 to 5.50 stwt, with a slightly steeper slope in the upfan area (from 4.55 to 4.8 stwt). The western part of the map shows the presence of a subduded low axis. Beware however that this low axis could result from the existence of 1F, 1E and small systems that are not for sure at the base of Orange-1 systems.

In order to simplify, and because Orange-1C is very local and had small impact on topographic change except on the very upfan part of the area, I only present here the isopach maps of the Orange-1C and Orange-1B HARPs (Figure IV.29B and C).

The Orange-1C HARPs (Figure IV.29B) were deposited in the South-East area, which is characterized by a regular decreasing paleotopography from 4.5 to 4.9 s twt. Maximum thickness is around 50 mstwt.

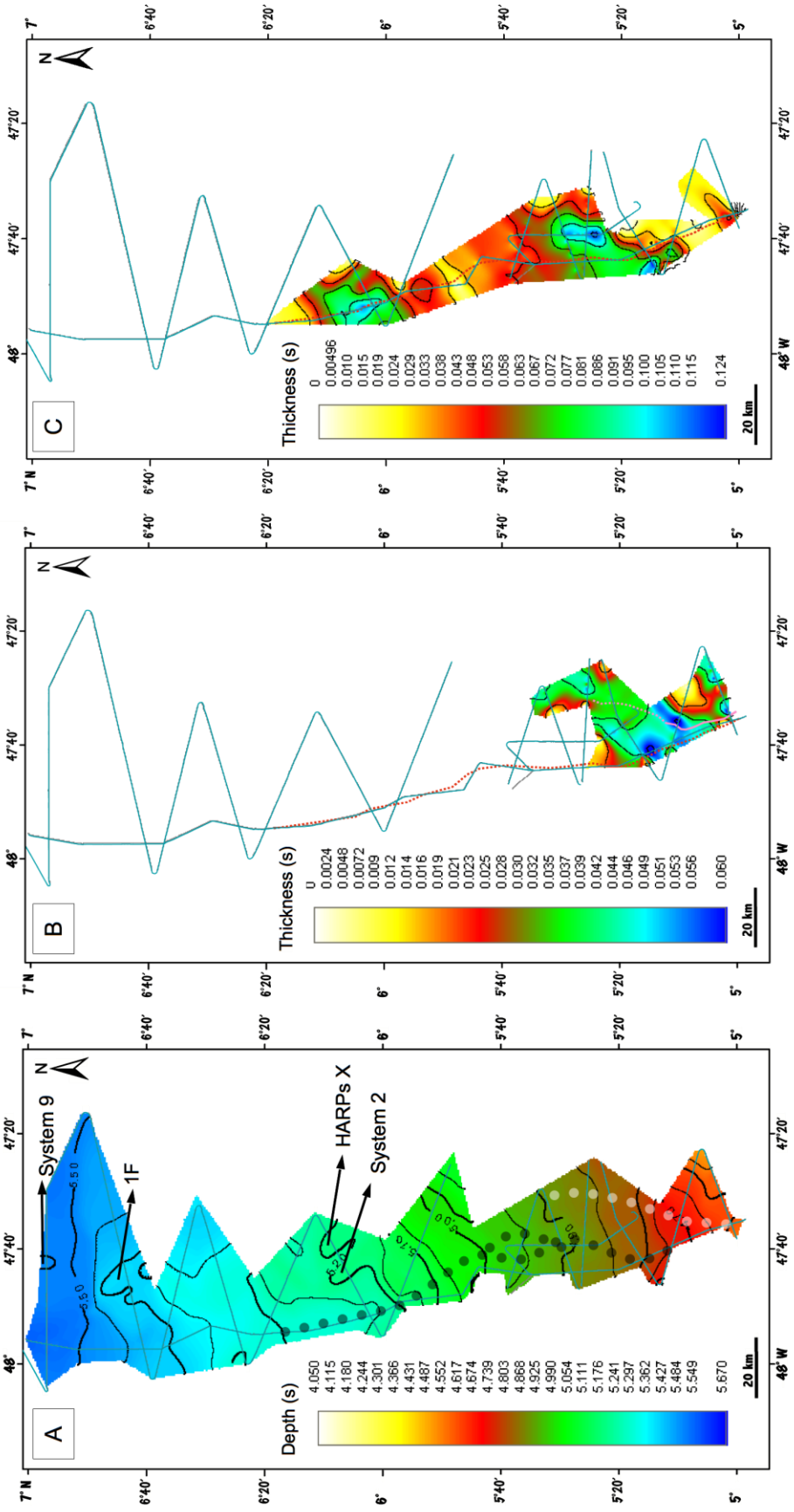

Figure IV.29: Orange-1 System. A: isochron map of the base of the Orange-1C system (i.e. top of 1F, 1E, System 1 to System 4, and System 9, see text); B: thickness map of the Orange-1C HARPs; C: thickness map of the Orange -1B HARPs. Maps are in s twt.

Concerning the Orange-1B system (Figure IV.29C), the paleotopography of the area was characterized by a more irregular upfan surface created by the deposition of the Orange-1C HARPs and channel-levee system. The slope was abrupt upfan and progressively decreasing downfan and the longitudinal depression at the western side of the area was still present. Orange-1B HARPs deposited inside this low axis. with thicknesses ranging from a minimum of 50 ms twt to a maximum of 124 ms twt. Two main areas are thicker, upfan and downfan, and are separated by a zone of minimum thickness. These thicker depocenters correspond to regions where the low axis at the basal surface was locally more expressed. The Orange-1 B HARPs have a maximum length of about 140 km.

1.3.2.4 The Aqua HARPs

The isochron map of the base of the Aqua system (i.e. the top of Purple system and debris flows DF1 to DF3) shows a steep upfan area which is affected by 2 parallel and subdued longitudinal depressions (Figure IV.30A). The eastern low axis, in which the Aqua channel-levee-HARPs system accumulated, results locally from erosion (in the order of 5 to 10 ms twt) from the Aqua HARPs and channel. The isopach map of the Aqua HARPs shows thicknesses around 50 ms twt maximum (Figure IV.30B). The Aqua HARPs reach a maximum length of 32 km.

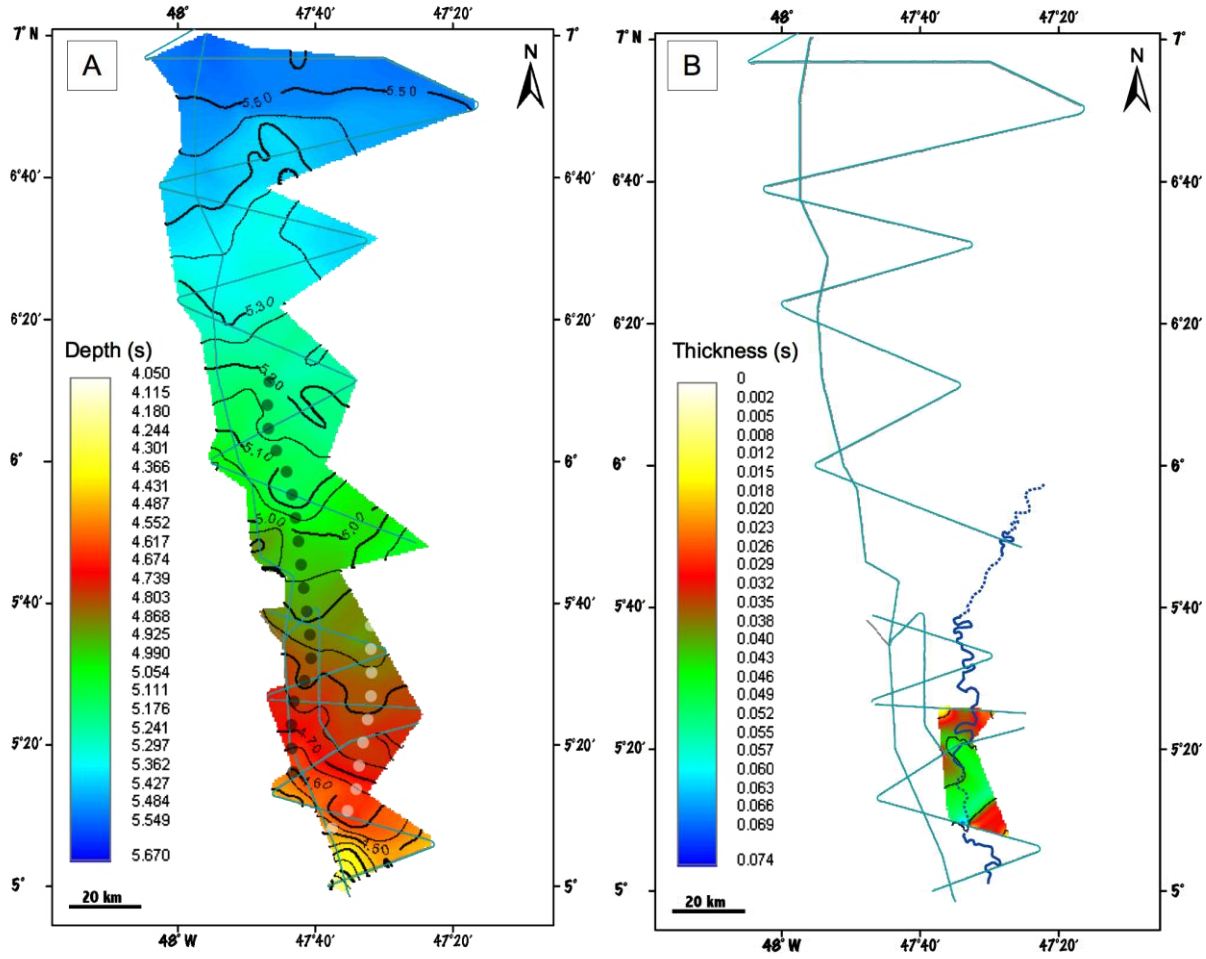

Figure IV.30: Aqua system. A: isochron map of the base of the Aqua system; B: thickness map of the Aqua HARPs. Maps are in s twt.

1.3.2.5 The Brown HARPs

The isochron map of the base of the Brown HARPs (Figure IV.31A) shows a well-expressed longitudinal depression located to the left to the levee of the previous Aqua. The upfan part of the map is characterized by steeply sloping topography, which corresponds to the upper part of the Aqua left levee. The Nouveau system, which is the true parent system of Brown is located too much to the east to have significantly imprinted the topography.

The isopach map of Brown HARPs (Figure IV.31B) indicates that the HARPs were emplaced in the longitudinal low. Their thickness ranges from 10 to 40 ms twt, with very local maximum of 80 ms twt corresponding to basal erosion by the HARPs (Figure IV.15a, LS45). The Brown HARPs reach a maximum length of 83 km.

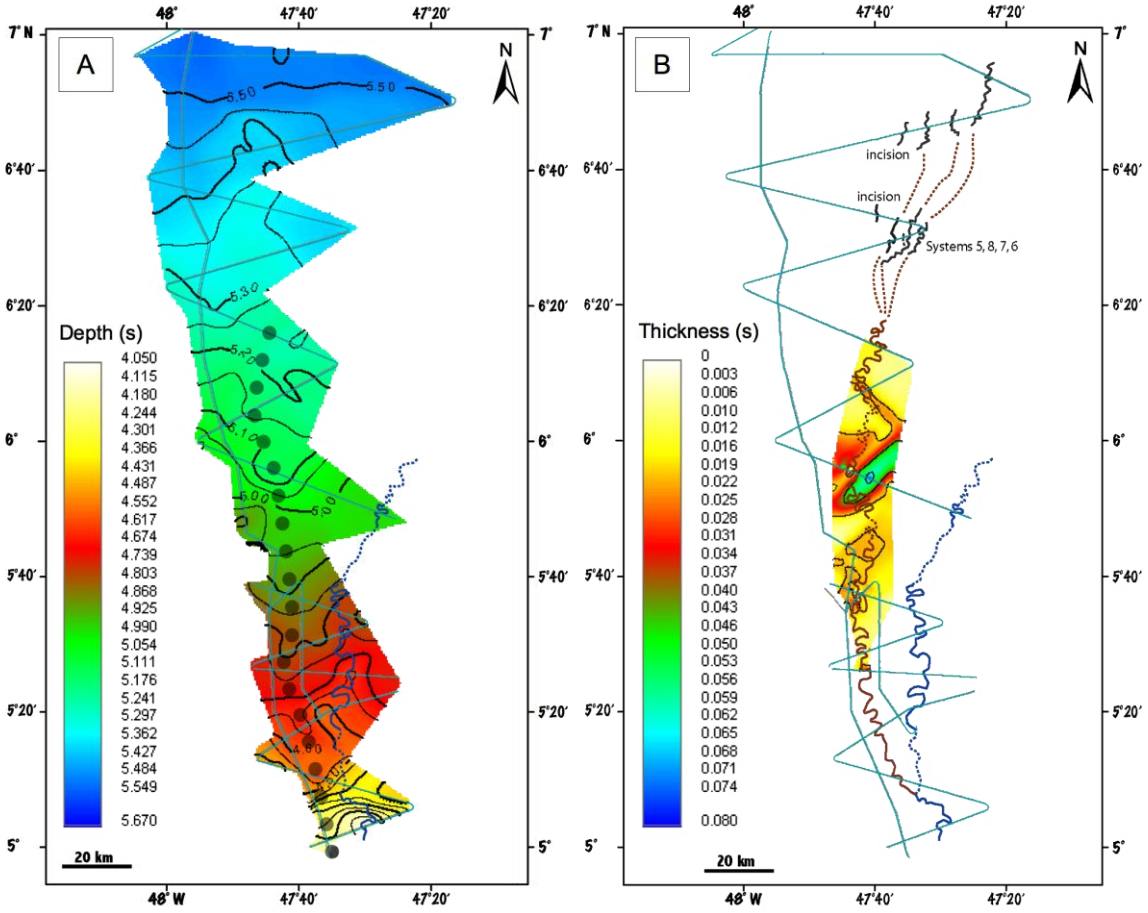

Figure IV.31: Brown system. A: isochron map of the top of the Brown system; B: thickness map of the Brown HARPs. Maps are in s twt.

1.3.2.6 The 1D HARPs

The topography preceding the deposition of 1D HARPs (Figure IV.32A) is marked by an elevation in the upfan area which corresponds to the Brown channel-levee system. The elevation becomes more subdued around the depth of 4.8 s twt. To the west of the Brown channel, the topography is irregularly sloping northwards with no well-expressed low axis except.

The 1D HARPs accumulated on this irregular topography at the western flank of the Brown system and limited to the east by the Orange-1B system (Figure IV.15a, LS44). Their maximum thickness is 40 ms (Figure IV.32B) and their maximum length is about 100 km.

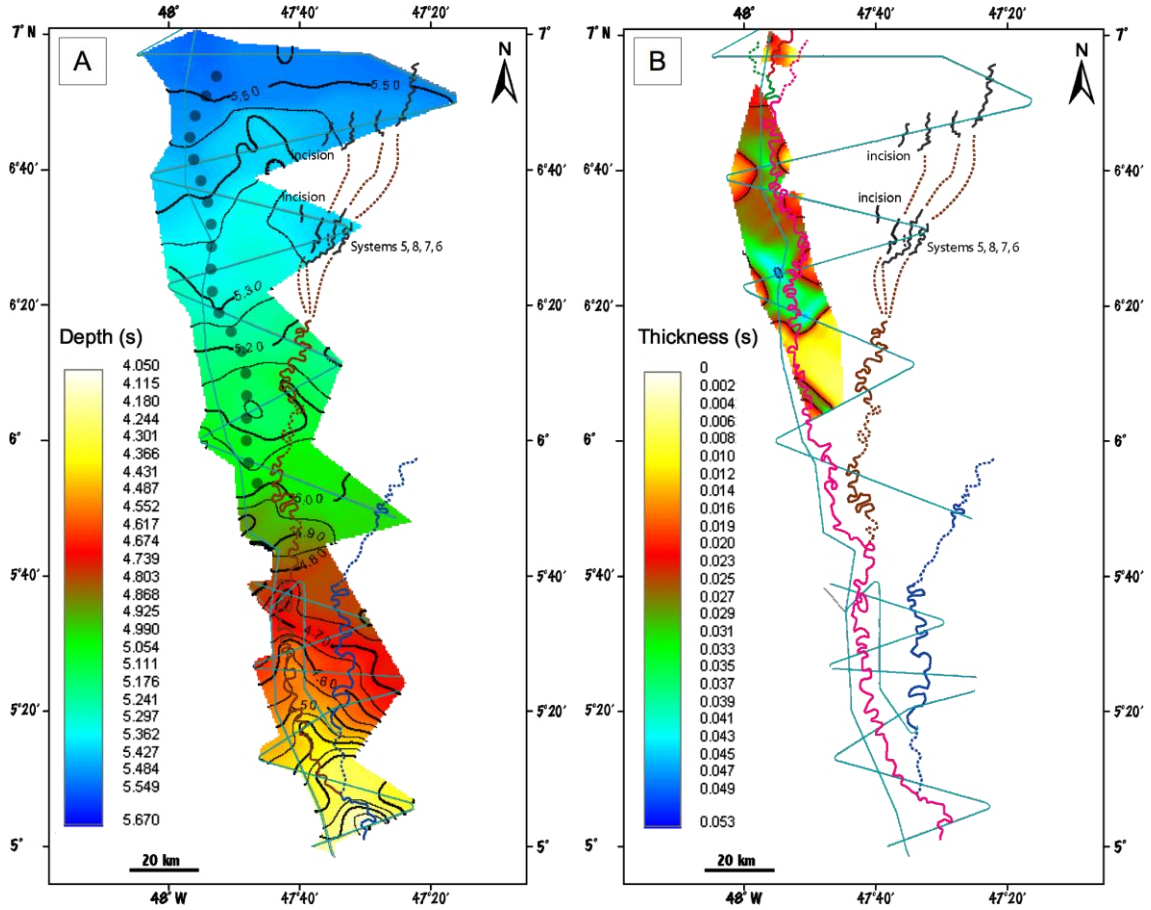

Figure IV.32: 1D system. A: isochron map of the base of 1D system; B: thickness map of the 1D HARPs. Maps are in s twt.

1.3.3 CONCLUSIONS AND DISCUSSION

Based on my seismic stratigraphy analysis of high-resolution Lobestory data, I established a refined chronology and channel map of the Quaternary Amazon Fan (Figure IV.15). Some refinements appear minor (e.g. the discovery of a new channel-levee system, called "Nouveau" channel-levee system, the identification of several small channels intercalated between the big ones, the identification of mass-transport deposits) but some are important for the sedimentary evolution of the fan:

- The refined chronostratigraphic position of 1F and probably 1E systems that are older than previously thought,
- The distinction of 3 channel-levee systems in the former Orange 1 and the prolongation of one of these farther downfan than previously mapped, and
- The identification of a thick HARP X deposits at the basal part of the ULC (Upper Levee Complex). These HARPs are suggested to be different from an avulsion lobe.

Two main type of HARPs have been identified, mainly by their size and position with regards to the channel-levee systems: those that constitute the base of channel-levee systems and can be attributed to the avulsion process (i.e. the avulsion lobes) and those that are not genetically linked to the avulsion process (of the type of HARP X and HARP Y).

(1) The HARPs that can be attributed to the avulsion process are identified as basal section of the Orange 1C and 1B systems, and under the Aqua, the Brown, and the 1D systems. The distribution maps and isopach maps have shown that these HARPs are generally organized in elongated lobate bodies, (up to 140 km long for the Orange-1 B HARPs), under the channel axis of the associated channel-levee system. The channels are often located symmetrically on their HARPs (i.e. at the middle part), but can be shifted up to their external limit. The HARPs revealed thicknesses ranging from up to 80 ms twt (i.e. about 60 m). When the avulsion point was observed, the HARPs are located at great distance from this point, ranging about 40 km for the Brown and 1D HARPs.
This great distance, already previously shown (Figure I.15) (Flood et al., 1991b) between the avulsion point and the HARPs is not observed in other fans, such as the Zaïre Fan (see below Chapter V; Droz et al., 2002) and the Danube Fan (see Chapter I.2.4.2; Popescu et al., 2001), and make this characteristic a specificity of the Amazon Fan.
The isochron maps of the bases of these avulsion lobes generally show that the HARPs were emplaced in lows axes, even faint, laterally confined by previous channel-levee systems. However, the Lobestory area is narrow and data are relatively few, introducing uncertainties in these maps. The badly constrained stratigraphic order of some of the channel-levee-Harps bodies also probably introduced errors.

(2) The Harp X has been shown to be an exceptionally huge and widespread unit that has invaded the northern (downfan) half of the study area after the URMTD instability period and prior to the deposition of the studied channel-levee systems.
This great size argues for the hypothesis that Harp X unit cannot be considered as an avulsion lobe of any of the channel-levee system known in the study area.
By comparison of facies in multichannel seismic sections of this HARP X and of the terminal lobes that characterize the distal part of the channels Brown to Amazon (Jégou et al., 2008) it is suggested that this "HARP" unit could represent

- An undistinguishable succession of small channels and sandy lobes typical of distal environments at the termination of channels. The NW-SE oriented elongation of the HARP X body argues for a feeding of these inferred terminal lobes from the SE. However, the NE-SW oriented axis of maximum thickness suggests also an origin from the SW. Because of the great thickness of this HARP body, which is about 190

m that have to be compared to the metric thickness of the terminal lobes known at the distal end of Brown to Amazon channels (Jégou, 2008), I suggest that the HARPs X were deposited by several successive channel-levee systems, or during a long lasting period.

- An undistinguishable succession of small channels and sandy lobes corresponding to the first deposits of a following turbidity cycle. In the present case this turbidity cycle may corresponds to the channel-levee systems of the Upper Levee Complex (compare Table II.1), representing the Quaternary Amazon Fan systems (this chapter). This phenomenon has been observed in the Pliocene Zaïre Fan, where a seismic unit -similar to the HARPs X in the Amazon Fan - has been interpreted as a basal unit of compensation (UBC, pages 252 and 285 in Turakiewicz, 2002).

2 LITHOLOGICAL INPUT TO HARPS AND LEVEE SEDIMENT CONTENT FROM ODP DRILLINGS

2.1 LITHOLOGY OF THE HARPS

As a general observation, lithologal units from the ODP cores that correlate to HARPs units are sandy. Two lithological facies have been identified:

- Facies 1, which consists of silty or sandy clay with silt or sand laminae or thin beds (in the range of tens of cm or thinner), often normally graded (tens of cm to m thick).
- Facies 2, which consists in thick sand beds (in the range of 10 of cm or thicker) or succession of sand beds, often normally graded, that can contain cm-size mud clasts. Mud clasts are generally considered as evidence for erosional process, and correspond probably to the erosion of older muddy levees.

The two facies are mainly observed interbedded, i.e. in an alteration of cm- to m-thick graded and massive sand beds (facies 2), and of some cm-thick beds of silty clay (facies 1).
Sands in facies 1 are mainly fine grained. Sands in facies 2 are fine- and medium-grained, sometimes coarse-grained. Sand beds can be up to several meters thick, the thickest beds having been cored at site 946 in HARPs X.

HARPs have been cored from upfan to downfan at ODP Sites 935 (Aqua and Orange-1B systems), 936 (Brown and Orange-1B system), 944 (Brown and the older HARPs X), 945 and 946 (1D system and HARPs X).

2.1.1 The Orange-1B HARPs

The HARPs at the base of the Orange-1B channel-levee system have been cored at sites 935 and 936 (Figure IV.33). Site 935 cored the Orange-1 B HARPs in a laterally distal position with respect to the channel axis, and in a more upfan position (i.e. closer to the avulsion point) than site 936.
The Orange-1 B HARPs are situated above the URMTD debris flow and are covered by the distal levees of the Orange-1B system.

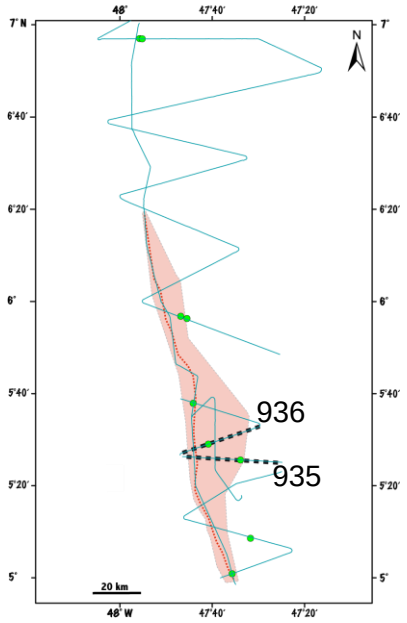

Figure IV.33: Location of sites 935 and 936 with respect to Orange-1B Harps.

At site 935, the Orange-1 B HARPs have a thickness of 40 ms and consist of flat-lying high-amplitude reflectors (Figure IV.34D). At site 936 the Orange-1 B HARPs have a thickness of 60 ms and show a chaotic patch with a flat-lying reflector, respectively at the base and at the top (Figure IV.35).

Site 935

The Orange-1B HARP deposits correlate with the ODP lithological unit IIIB that I divided into 4 sub-units after the lithologic description of ODP (IIIBd to IIIBa from the base to the top, Figure IV.34). More exactly, the HARPs of Orange-1B correspond to the recovered part at the top of subunit IIIBd to IIIBb2.

Subunits IIIBd and c show low recovery and gammaray data were not available to fill the gaps, so the basal part of unit IIIBd doesn't provide information of the true base limit of the HARPs. At the top of IIIBd (from 190.69 to 189.6 mbsf) silty clay with silt laminae and a bed of fine sand have been cored, and form the most basal sediments sampled for the Orange-1 B HARPs at site 935.

Subunit IIIBc shows at its recovered part from the base to the top (185.65 to 180 mbsf) 58 cm of silty clay with silt laminae covered by a 5 m-thick massive, medium to coarse sand, which contains 1- to 3- cm-diameter mud clasts and one 3-cm-diameter well-rounded sandstone clast. I correlate subunit IIIBc with the chaotic patch seismic facies (marked in purple on Figure IV.34D).

In subunit IIIBb2 (178.87 to 173.40 mbsf) bioturbated silty clay is present.

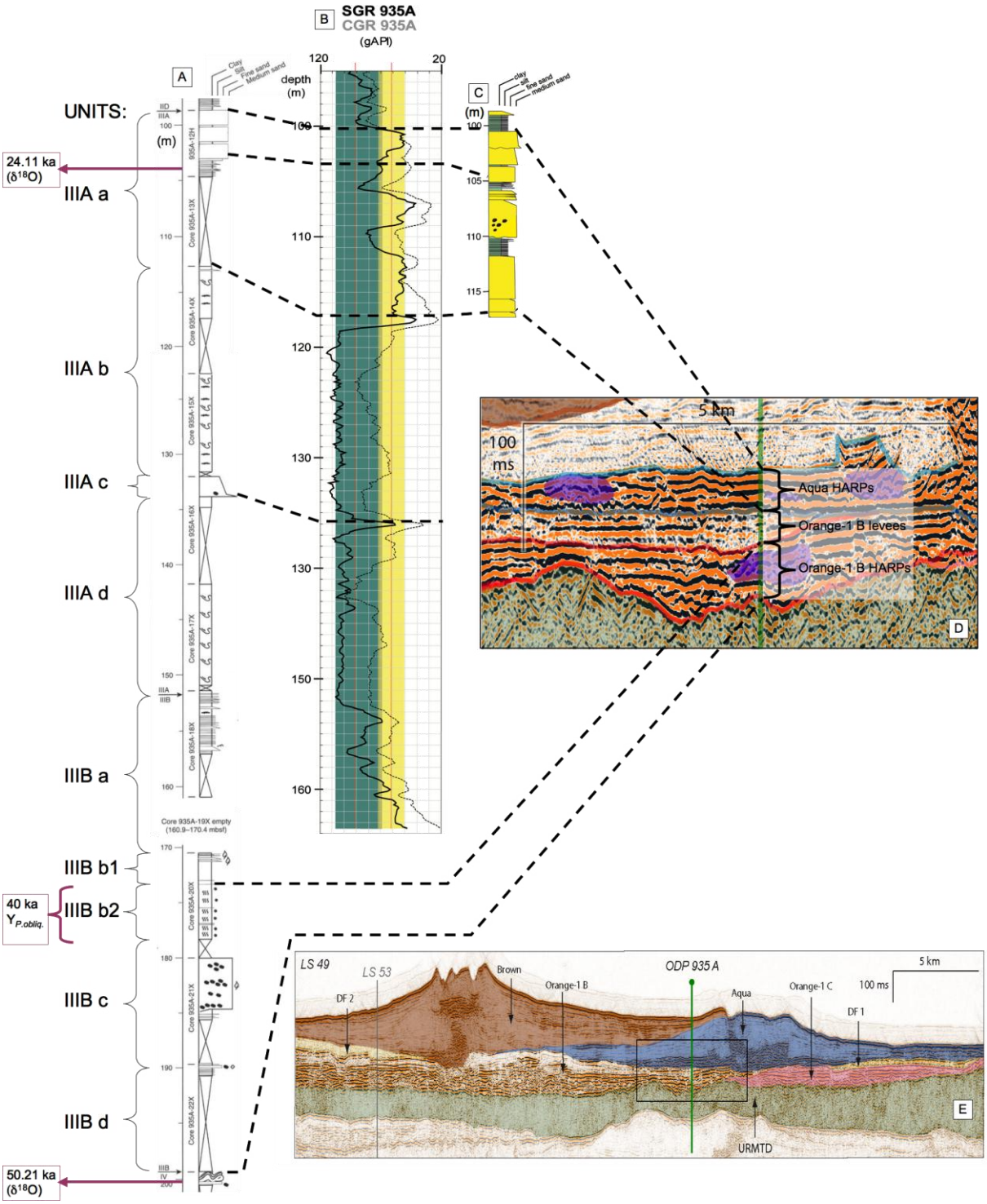

Figure IV.34: Orange-1B HARP and Aqua HARP deposits at site 935. Location of seismic line and site in Figure IV.33. A: Lithologic data with units defined by ODP (in Roman numbers and capital letters), modified from Scientific Party (1995b) and sub-units defined in this study (small letters and Arabic numbers). Datations are marked by purple arrows. B: Diagraphic gammaray log where data were available. C: Log drawn from FMS interpretation by Pirmez (pers. comm.) and Pirmez et al. (1997). D: Zoom of seismic line on the sampled seismic facies from base to top: the Orange-1 B HARPs consist of a chaotic patch (marked in purple) with a flat-lying reflector, respectively at the base and the top; Orange-1B levees consist of the B facies (Chapter IV.1.1); the Aqua HARPs consist of flat-lying reflectors. D: Position of site 935 on interpreted seismic line LS49 (see part 1, this chapter for key to colors).

As a summary, the sediments corresponding to the Orange-1 B HARPs at site 935 consist of silty clay with laminations and thin beds of silt and fine sand with a thick (around 5 m) medium to coarse sand bed.

Site 936

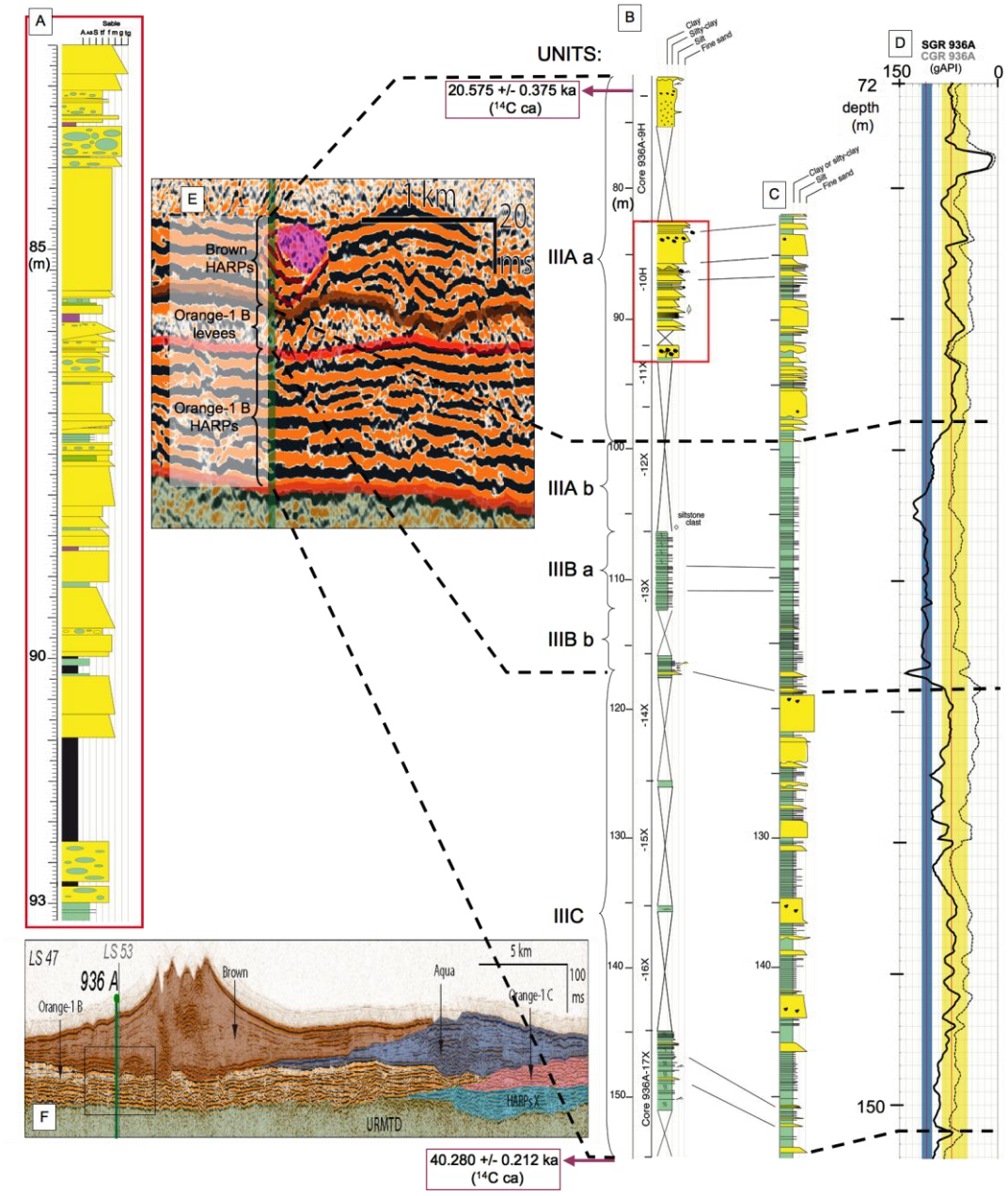

Figure IV.35: Orange-1B HARP, Orange-1B levee and Brown HARP deposits at site 936. A: Zoom on a lithologic log redrawn in this study from visual core description of recovered sediments, location in (B) marked by red square. B: Lithologic data with units defined by ODP (in Roman numbers and capital letters), modified from Scientific Party (1995c), and sub-units defined in this study (small letters and Arabic numbers). Datations marked by purple arrows. C: interpretation of FMS data (Pirmez, pers. comm.; Pirmez et al., 1997). D: Diagraphic gammaray log where data were available. E: Zoom of seismic line on the sampled seismic facies from base to top: flat-lying reflectors for the Orange-1B HARPs; Orange-1B levees consist of the B facies (Chapter IV.1.1; stacked U-shaped reflectors forming an erosional feature (highlighted in red) and a flat-lying reflector at the top for the Brown HARPs. F: Position of site 936 on seismic line LS 47 (see part 1, this chapter for key to colors).

At site 936 (Figure IV.35), the Orange-1B HARPs correlate with the lithological unit IIIC from the Shipboard Scientific Party, consisting in a series of thin to medium turbidite beds of graded silt to fine sand interbedded with silty clay. From the interpretation of FMS (Pirmez, pers. comm.; Pirmez et al., 1997) and gamma-ray data (this study), the sand beds inside this unit can be up to 2.5 m thick (see bed at 119 mbsf on Figure IV.35D).
Although the recovery was poor for this interval, the wireline logs and recovered sediments indicate that this unit is sandier with thicker sand beds than IIIBa and IIIBb (that correlates to the overlying Orange-1B levees).

2.1.2 The Aqua HARPs

The most distal part of the HARPs at the base of the Aqua channel-levee system was cored at Site 935 (Figure IV.36).

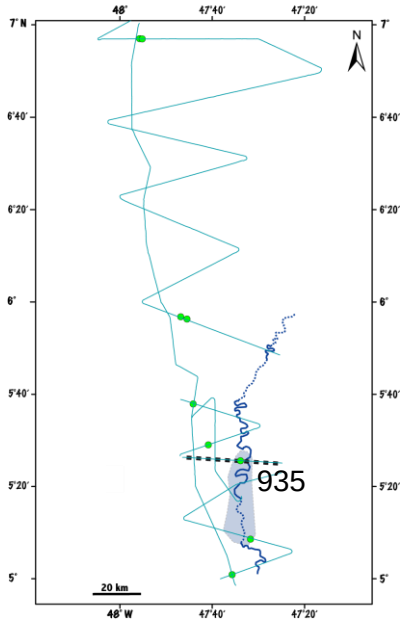

Figure IV.36: Location of site 935 with respect to Aqua Harps.

At this site, the Aqua HARPs have a thickness of 35 ms twt and are made exclusively of flat-lying high-amplitude reflectors (Figure IV.34). It is intercalated between the base of the Aqua levees and the top of the Orange-1B levees.
In contrast to the interpretation of the ODP Scientific Party (1995a) that attributes the complete unit III (i.e. IIIA to C) to HARPs deposits, my interpretation correlates the Aqua HARPs to part of the ODP lithological unit IIIA, more precisely to my sub-unit IIIAa (from probably 113.08 to 98.5 mbsf). Because of poor recovery in the basal part of this unit, FMS data and gamma ray data have been used to determine the sediments corresponding to the interval of the void (Figure IV.34D), Pirmez, pers. comm.; Pirmez et al., 1997).

The sediment of sub-unit IIIAa consists in mud with interbedded thick beds (up to 4 m) of medium sand and thin beds of fine sand and silt (Figure IV.34A and C). Some mud clasts have been determined by FMS interpretation (Pirmez, pers. comm.; Pirmez et al., 1997) at around 109 mbsf.

2.1.3 The Brown HARPs

The HARPs at the base of the Brown channel-levee system were cored at ODP sites 936 and 944. Site 936 is located more upfan and in a more central position than site 944 (Figure IV.37).

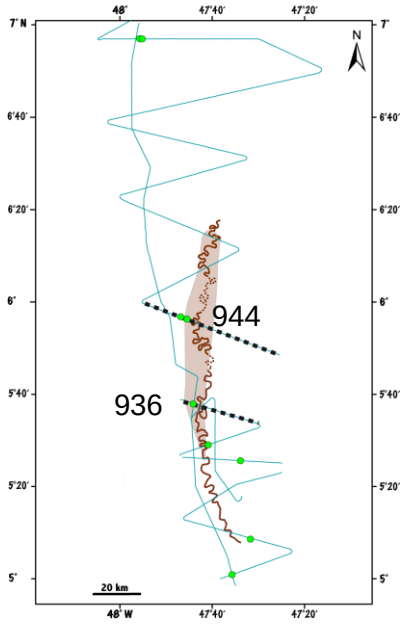

Figure IV.37: Location of sites 936 and 944 with respect to Brown Harps.

At site 936, upfan, the Brown HARPs are relatively thin (25 ms twt) and intercalated between the Orange-1B levees (below) and the Brown levees (above) (Figure IV.35E). The hole drilled successively, from bottom to top, the outer limit of stacked U-shaped reflectors, forming an erosional feature, the outer limit of the transparent infill of the erosional feature and a flat-lying reflector (Figure IV.35E).

At site 944, downfan, the Brown HARPs are 45 ms twt thick and are situated above the HARPs X and below the levees of the Brown system (Figure IV.38A). They are made exclusively of flat-lying high-amplitude reflections.

Site 936

At site 936, the Brown HARPs correspond to part of the ODP lithological unit IIIA of the Shipboard Scientific Party, in particular to unit IIIAa, determined in this study (Figure IV.35B). This unit is predominantly made of a series of thick beds of sand (the thickest has been cored at 84 mbsf with a thickness of 1.5 m, Figure IV.35A). The beds are in general tens of centimeters thick and have irregular, dipping contacts, suggesting that this interval may be a series of separate deposits.

When tied to the seismic line (LS47), the erosional U-shaped feature could correspond to basal lithological interval of graded fine to medium sand beds with more rare coarser sands and mud clasts. The transparent infill of the U-shaped feature could correlate to an overlying interval of massive sandy-silty clay (72.1 to at least 75.35 mbsf). The interval between 75.35 to 82.5 mbsf has not been cored (Figure IV.35B) and the gammaray signal seems to be an artefact. It was interpreted by the Scientific Party (1995b) as washout of probably sand (in correlation to the over- and underlying lithologies).

Site 944

At site 944, the Brown HARPs correspond to the lower part of the ODP lithological unit IIC (Scientific Shipboard Party, 1995c).

Direct lithologic information from the IIC interval are very sparse (Figure IV.38B). However, by combining cores, log data and FMS data (Pirmez et al., 1997, Figure IV.38C), the interval can be described as consisting of silty clay containing silt laminae and 5 cm to around 1 m-thick beds of silt and massive to normally graded very fine to medium sand. The occurrence of coarser-grained sand is rare and fluctuates throughout IIC.

Based on the occurrence of sand beds determined on the lithologic log of Pirmez (pers. comm.) and Pirmez et al. (1997) from FMS interpretation and in correlation to the gammaray signal (Figure IV.40 C and D), I subdivided the ODP unit IIC into 4 sub-units (IICd to IICa), where the sandier intervals are the basal part of IICd (base around 160 mbsf), the top of IICd (145 mbsf to 141 mbsf) and the IICb unit. The two predominantly silty clay with silt laminae intervals (around 8 and 11 m thick) correspond to an interval in the upper half of IICd (155 to 145 m) and the IICc interval.

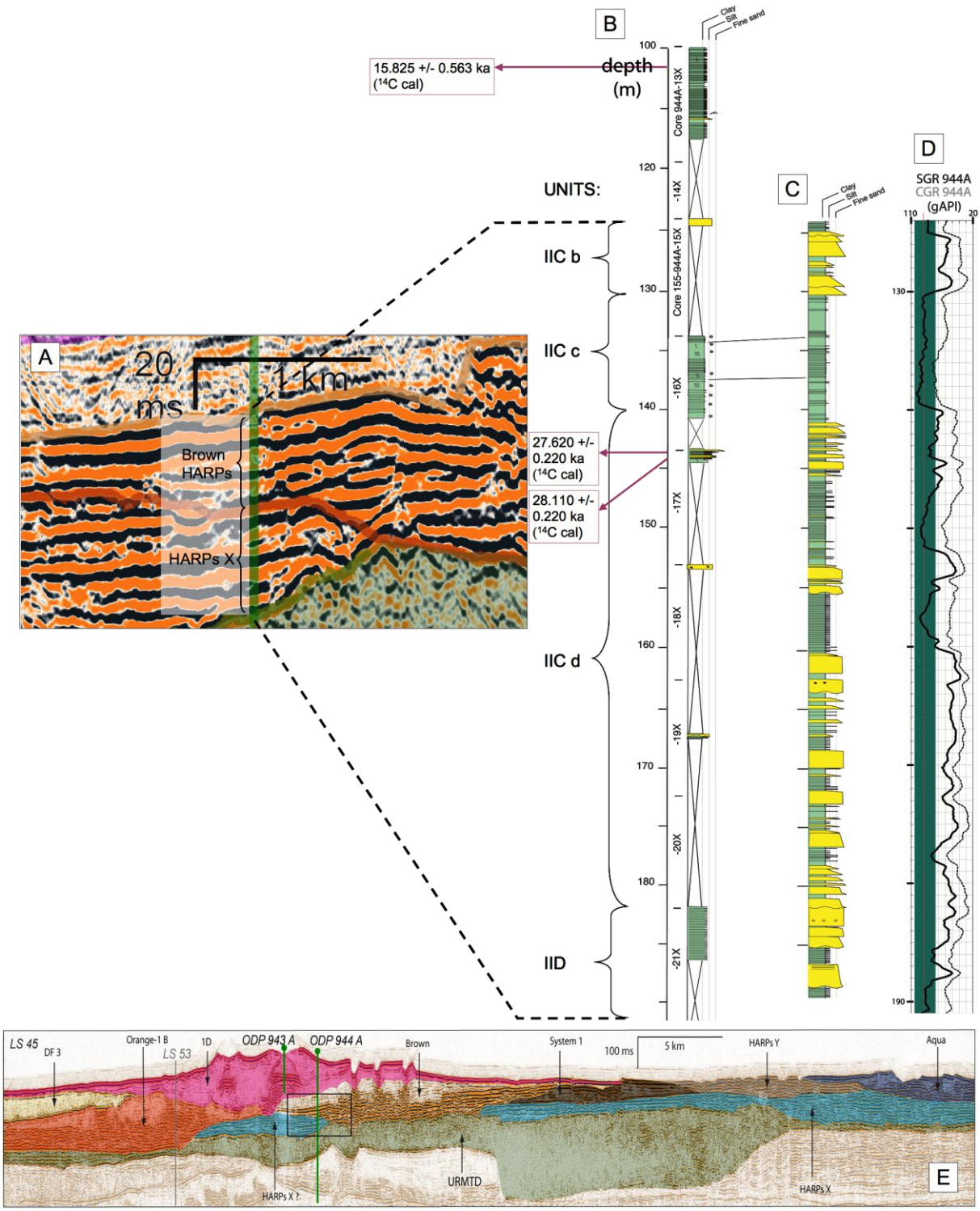

Figure IV.38: HARPs X and Brown HARP deposits at site 944. A: Zoom of seismic line on the sampled seismic facies from base to top: flat-lying reflectors of HARPs X and Brown HARPs. B: Lithologic data with units defined by ODP (in Roman numbers and capital letters), modified from Scientific Party (1995d), and sub-units defined in this study (small letters and Arabic numbers). C: interpretation of FMS data (Pirmez, pers. comm.; Pirmez et al., 1997). D: Diagraphic gammaray log. E: Position of site 944 on interpreted seismic line LS 45 (see part 1, this chapter for key to colors).

The similar seismic facies of the Brown HARPs and the underlying facies (HARPs X) consist of flat-lying reflectors, showing a homogeneous internal seismic pattern, and don't reflect the

changes from more sandy intervals to more silty clay intervals of the IIC units.
Because of similar seismic facies, it is not clear where I can define the base limit between the Brown HARPs and underlying HARPs X, and I could eventually consider the silty clay interval (IICc or 155 to 145 mbsf of IICd) as distal overflow deposits that either represent the onset of levees, or as a constitutive part of the HARPs as shown in numerous lithological succession of HARPs (e.g. Orange-1B HARPs at site 936, Figure IV.35), that marks a local abandonment of sandy deposits.

2.1.4 The 1D HARPs

The distal parts of 1D Harps have been sampled at sites 945 and 946, which are close to each other (Figure IV.39).

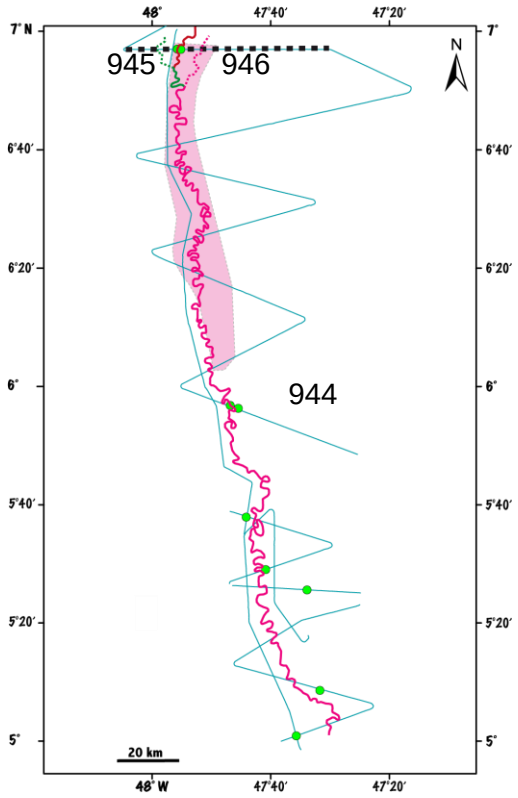

Figure IV.39: Location of sites 945 and 946 with respect to the 1D HARPs.

At site 945 (Figure IV.40), the 1D HARPs are situated below the HARs of the 1B to 1A system that have eroded the 1D levee. This means that a hiatus exists at this site. Site 945 is positioned at the western outer limit of the HARPs, where the seismic facies consists in high-amplitude, flat-lying reflectors.
At site 946, the 1D HARPS mostly consist in high-amplitude, flat-lying reflectors.

Site 945

The 1D HARP deposits at site 935 correspond to part of unit III of the Shipboard Scientific - Party (1995d). Unit III consists predominantly of thick-bedded fine-to medium sand (1 to 9 m thick), interbedded by silty clay intervals (< 5 m thick) with abundant silt laminations and thin beds of fine to medium sand. Many of the thicker beds contain mud clasts. Plant debris are also common throughout the unit.

The top limit is probably marked by the base of 8-m-thick sand bed (that is correlated to the 1B to Amazon channel infills and in agreement with the interpretation of the Shipboard Scientific Party, 1995d) at the top of unit III. I was not able to define an interval in the sediments corresponding to the base limit of the 1D HARPs, because the underlying deposits (HARPs X) seem to consist of the same type of lithology, whereas they show a trend to thicker sand bed deposits.

Site 946

In my study, I correlate the 1D HARPs at site 946 to part of the unit IIIC from the Shipboard Scientific Party, (1995e), that I devided in two sub-units, IIICb and IIICa from the base to the top. Unit IIICb (45 to 128.75 mbsf) consists of graded sand beds and some very thick (up to 10 m) massive sand deposits interbedded with some intervals of mud with numerous silt laminae.

I correlate the 1D HARPs with the upper part of sub-unit IIICb (45 to 67 mbsf). This interval is build predominantly of three massive sand deposits including respectively one interval of some to moderately mud clasts abundance, interbedded with two intervals of mud with silt and a few thin fine sand beds. The base is marked by one of the thick massive sand beds.

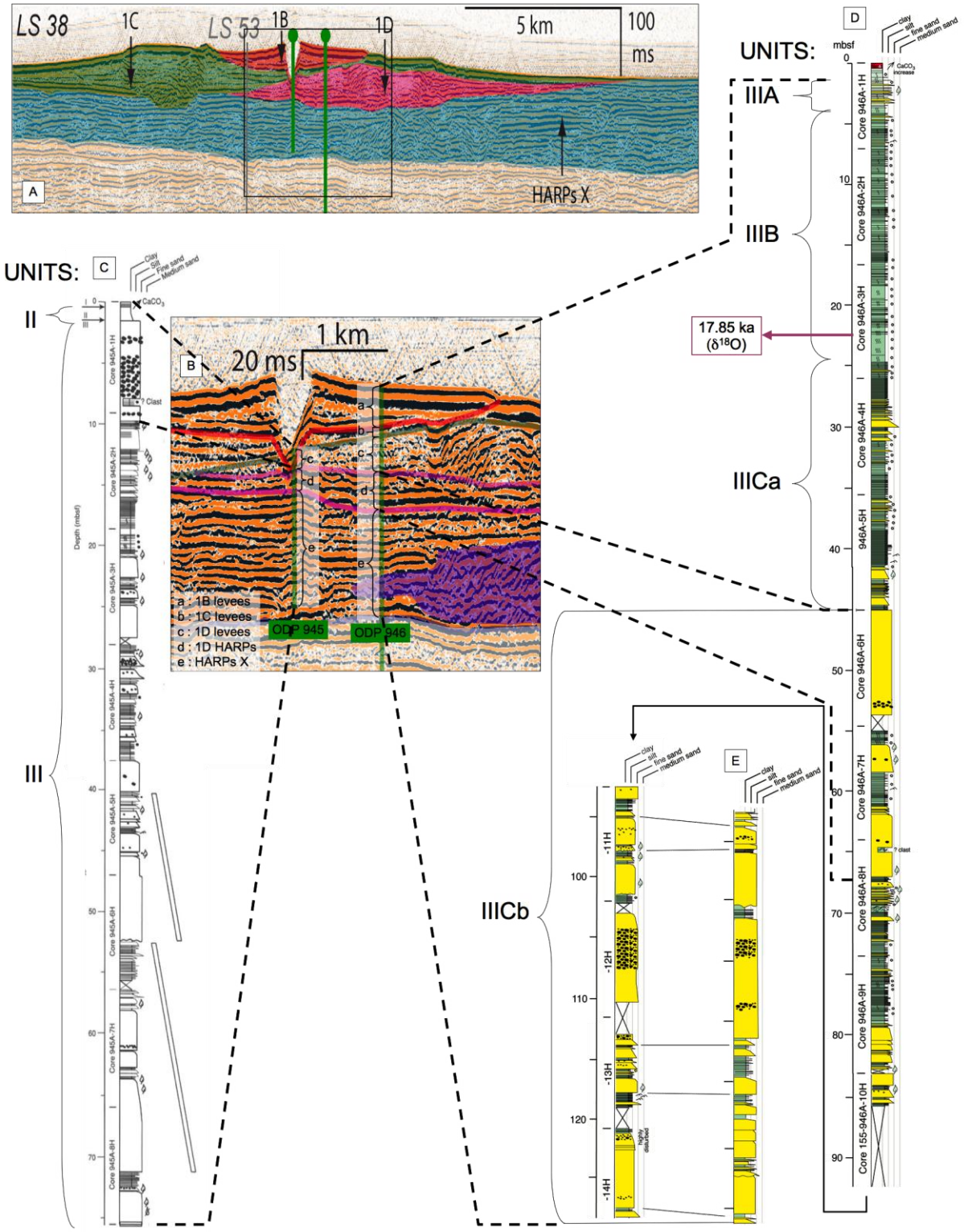

Figure IV.40: 1D HARPs and HARPs X at site 945 and site 946, 1B levee and 1D levee deposits at site 946. A: Position of site 944 on interpreted seismic line LS 45 (see part 1, this chapter for key to colors). B: Zoom of seismic line on the sampled seismic facies from base to top: flat-lying reflectors of the HARPs X and 1D HARPs at both sites, with eroded channel of 1B at site 945, and 1D levee deposits and 1B levee deposits at site 946. C: Lithologic data at site 945 with units defined by Shipboard Scientific Party (1995e) (in Roman numbers). D: Lithologic data at site 946 with units defined by ODP (in Roman numbers and capital letters), from Scientific Party (1995f) and sub-units defined in this study (small letters and Arabic numbers).

2.1.5 HARPs X

HARP X deposits have been sampled at site 944 in a proximal position, under the Brown HARPs (Figures IV.37 and IV.38), and at sites 945 and 946 in a more distal position, under the 1D HARPs (Figures IV.39 and IV.40). All cored HARPs X facies consist of flat-lying reflectors and only one thin interval of a part of a chaotic patch has been sampled at site 946, whereas the HARPs X shows on other locations also incisional features, transparent patches and thick chaotic patches.

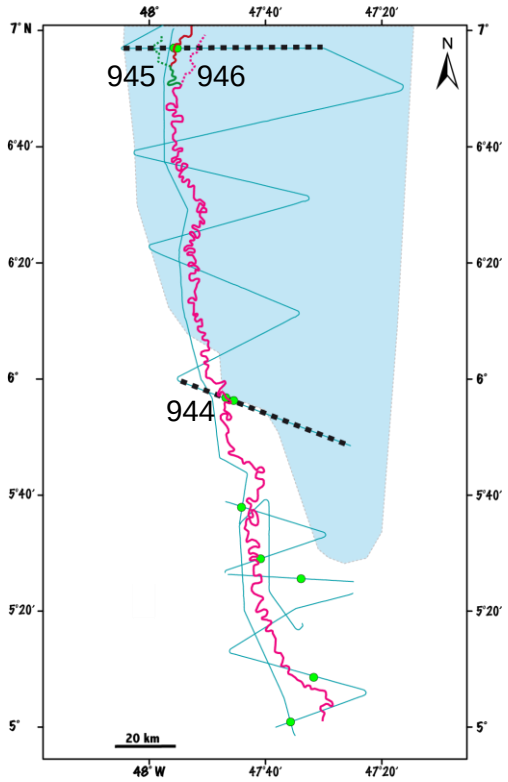

Figure IV.41: Location of sites 944, 945 and 946 with respect to the location of the HARPs X.

Site 944

The HARPs X at site 944 (Figure IV.38) correspond to the part of the IICd unit, whereas the upper limit to the overlying deposits (Brown HARPs, see above) is not clear. The basal half of unit IICd is sandier than the upper half because the silty clay intervals with silt laminae (interbedded with sand beds) become thicker to the top. I correlate the HARPs X with the basal sandier part of IICd, whereas the top could be represented by the 8-m-thick silty clay interval in the upper part of IICd or the IICc interval, marking an abandonment of local sandy deposits.

Site 945

From the tie of site 945 to my seismic interpretation, the HARPs X are recovered directly under the 1D HARPs.

When compared to the lithology of the overlying 1D HARPs, the HARPs X seems to show a clear trend to thicker sand beds (up to 9 m thick) at the lower part of unit III, the sand beds appear to be organized into two thinning-upward sequences, from 42 to 53 mbsf and from 53 to 76 mbsf. However, I was not able to define a clear top limit of the HARPs X in the cored sediments.

Site 946

At this site again, from the tie to my seismic interpretation, the HARPs X are recovered directly under the 1D HARPs.

I correlated the HARPs X at Site 946 in my study with the basal part of my subunit IIICb (67 to 128.72 mbsf). This interval consists like the upper part of IIICb (correlated to the 1D HARPs, see above) of very thick (up to 10 m) massive sand beds including intervals of abundant mud clasts, interbedded with generally less than 2-m-thick intervals of silty clay with silt laminae and thin beds of fine to medium sand. Plant debris are common in the silty-clay interval. One of the silty clay intervals is around 15 m thick and built from my interpretation the top (at 67 mbsf) of the mostly sandy sediments correlated to the HARPs X, i.e. the silty clay interval at the top has been interpreted in my study as the local abandonment of sandy depositional events.

The chaotic patch sampled at site 946 could correspond to a 7-m thick sand bed including abundant mud-clast over an interval of 3.5 m (103.3 to 106.8 mbsf).

2.2 LITHOLOGY OF HIGH-AMPLITUDE PARTS IN THE LEVEES

My objective was to see if the different seismic sub-units identified in the levees were marked by different lithologies and if the unconformities were recorded by lithological changes. In particular, I wanted to see changes that could be used as criteria for identifying avulsion time in the levee upstream from the avulsion point.

Unfortunately, the core locations are generally not in good position to document such facies changes or the facies changes are too tight (only one high-amplitude reflector within an otherwise medium amplitude facies) to be firmly identified in the lithologic log.

Levee deposits consist generally in the cored sites of silty clay deposits with variable

frequency of silt laminations throughout the levee height. Coarser grained laminations and beds of fine sand have been mainly observed (Flood et al., 1995) at the base of the levees with a generally trend to finer sediments at the top of the levees.

I observe in this study that fine sand laminations and the occurrence of silt and fine sand beds are relatively rare in the middle part of a levee deposit, but can be eventually correlated to high-amplitude intervals in the seismic images of the corresponding levees. Such very silty deposits of silt clay (up to 30%) with numerous laminations and a few beds (1- to 3-cm thick) of silt to fine sand and an interbedded slump deposit have been associated in my study to high-amplitude reflectors in the Nouveau levee deposits at site 940 (e.g. at 142 to 142.6 mbsf, from visual core description). However, the coarsest sediments in levees at this site have been observed at the base of the Aqua levee (corresponding to unit IIH), showing silty clay with silt laminations and less than 10-cm-thick beds of very fine and fine sand. The top limit is placed at the first occurrence of sand at 210.57 mbsf. Silt laminations decrease in frequency down the unit and are absent below 216 mbsf. Sand beds increase in abundance from 216 mbsf to the bottom. The interval 220 to 236 mbsf contains approximately 12 thin beds of fine sand per meter. These beds form around 50% of the unit and are in general cross laminated.

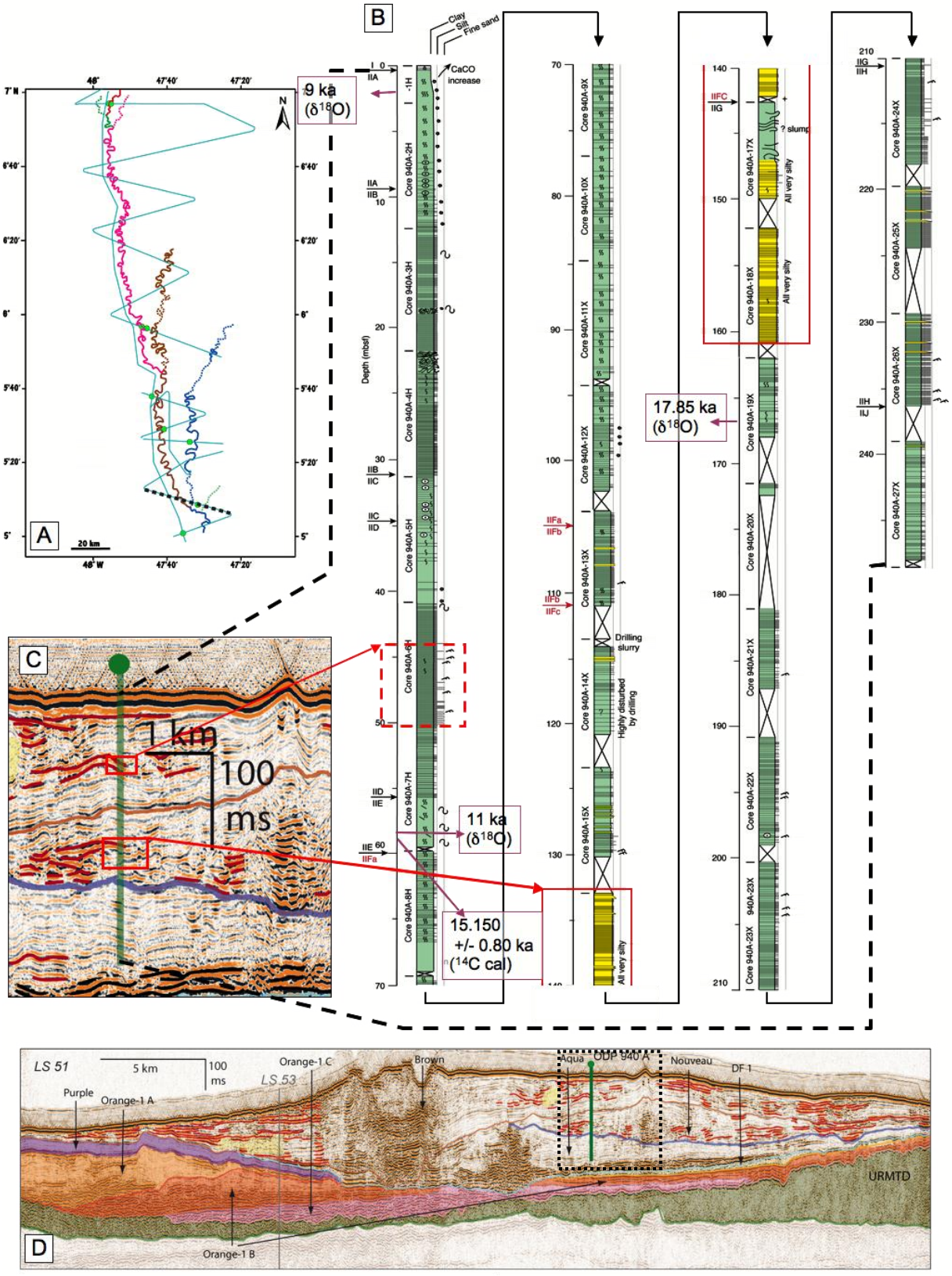

Figure IV.42: Levee deposits of Aqua, Nouveau and Brown to Amazon at site 940. A: Schematic map showing thalwegs of Aqua, Nouveau, Brown and 1D channels. B: Lithologic data (Shipboard Scientific Party, 1995g). C: Zoom of seismic line on sampled seismic facies of levees where intervals of high-amplitude reflectors are highlighted in red. D: Position of site 940 on interpreted seismic line LS 51.

2.3 CONCLUSION

2.3.1 Lithology of the elementary units of the channel-levee basal HARPs

The holes drilled during ODP leg 155 did not document the lithology of each of the four elementary sub-units identified in the HARPs. Moreover, because of their locations, they sampled only one chaotic patch and the transparent infill of a U-shaped erosional feature just on its outer limit, and therefore the results should be considered with caution for these sub-units.
However, the flat-lying unchannelized sub-units have been well documented at several sites.

- *The flat-lying unchannelized units* have been documented at each of the considered sites, i.e. sites 935 (Orange-1B and Aqua HARPs), 936 (Orange-1B and Brown HARPs), 944 (Brown HARPs), 945 and 946 (1D HARPs).

At these sites, lithological characteristics of the unchannelized sub-units are very similar and made of interbbeded coarse-grained (silt to sand beds) and finer-grained (silty clay with silt to fine sand laminations) sediments. The coarse-grained intervals are thicker than the silty-clay intervals and include beds of variable thickness, but generally in the order of tens of cm and 1- to 3- m, whereas some very thick sand beds have been sampled at site 945 and 946 (respectively up to 8 and 10 m thick)
An up to downfan evolution of the lithology was observed for the Orange-1B HARPs. It shows a downfan decrease in both grain-size of the sands (from coarse to medium sands upfan to fine sands downfan) and mud clasts frequency, possibly indicative of a decrease of the erosion with increasing distance from the Orange-1C/Orange-1B avulsion point.

- *The transparent infill and part of the associated underlying U-shaped reflectors* have been documented at a single site, i.e. site 936 (Brown HARPs). The lithology of the transparent sub-unit consists in massive sandy clay, and that of the U-shaped reflectors corresponds to a succession of cm to m- thick sand beds where some intervals of mud-clasts occur.

-*The chaotic patch has been sampled at site 935* and is correlated to a deposit of massive sand with abundant mud clasts.

2.3.2 Lithology of the HARPs X

The HARPs X facies have been cored mostly for the flat-lying reflector sub-unit facies (sites 944, 945 and 946). Only one thin interval of a chaotic patch have been sampled (at site 946), whereas the U- and V-shaped features, transparent patches and abundant chaotic patches are present in the overall HARPs X seismic facies.

The lithology of the flat-lying reflectors of the HARPs X are similar to the lithology of the flat-lying reflectors sampled for the channel-levee basal HARPs (see above), i.e. intervals of successive sandy beds (cm- to m- thick) interbedded with silty clay intervals with silt to fine sand laminae. However, the deposits at the downfan sites 945 and 946 show a clear trend to thicker sand beds for the HARPs X (up to 10 m at site 946).
The chaotic patch sampled at site 946 could correspond to a mud-clast-rich sand bed, a similar lithology that has been sampled for the chaotic patch of the Orange-1B HARPs at site 935.

3 NEW STRATIGRAPHY AND CONSEQUENCES

3.1 AGES OF THE STUDIED CHANNEL-LEVEE SYSTEMS

A compilation of available dates (Cisowski et al., 1997; Showers et al., 1997; Maslin, pers. comm.) and corresponding seismic units (this study) is provided in Table III.8 (Chapter III). The ages of the HARP intervals for all sites (sites 940, 935, 936, 944 and 946) and levees for site 940 are shown on synthetic logs presented in Chapter IV.2, and dating for levees and HARs for all sites are presented on synthetic logs in ANNEX III.2a to e. Some dates are considered invalid (see Chapter III, 2.2.4.) and were not presented on logs.

These dates, from 40.28 cal ka up to 15.1 cal ka, and the correlated seismic units have been placed on the sea-level curve of Sidall (2003) (Figure IV.43). Note that dates that I considered as invalid (i.e. age inversions, see Chapter III) or poorly constrained (i.e. ages in HAR fill of channels) are not mentioned in Figure IV.43. Note also that uncertain dates (i.e. dates that are not consistant with my seismic stratigraphy) are marked in gray and that date of 11 and 9 ka ($\delta^{18}O$) have not been indicated because they concern the most recent systems 1D to Amazon and Holocene deposits for which my study did not bring out new results. I added also the dates for the most recent channel-mouth lobe identified by Jégou (2008) indicating an activity of the system 1A at least until 10.39 ka that marks the abandonment of the Amazon Fan in this distal area.

My seismic interpretation led us to modify the ages attributed to several of the channel-levee systems (Figures IV.43 and IV.44):

- The HARPs and levees of the Aqua system have been dated at the same site (site 935) giving very close ages, that taking into account the measurement uncertainties, probably correspond to the onset of the levees and the abandonment of the HARPs at 23.6 ka. The beginning of Aqua HARPs deposition and the end of activity of the Aqua channel-levee system are not dated.
- I attribute the ages of 19.22 ka and 17.85 ka, at sites 935 and 940 respectively, to the Nouveau channel-levee system that follows the Aqua system in my interpretation. The onset of the Nouveau system is not dated.
- The Browns HARPs stopped accumulating around 20.58 cal ka at site 936 and levees was actively deposited at least untill 15.83 cal ka. The end of Brown levee aggradation is not dated.

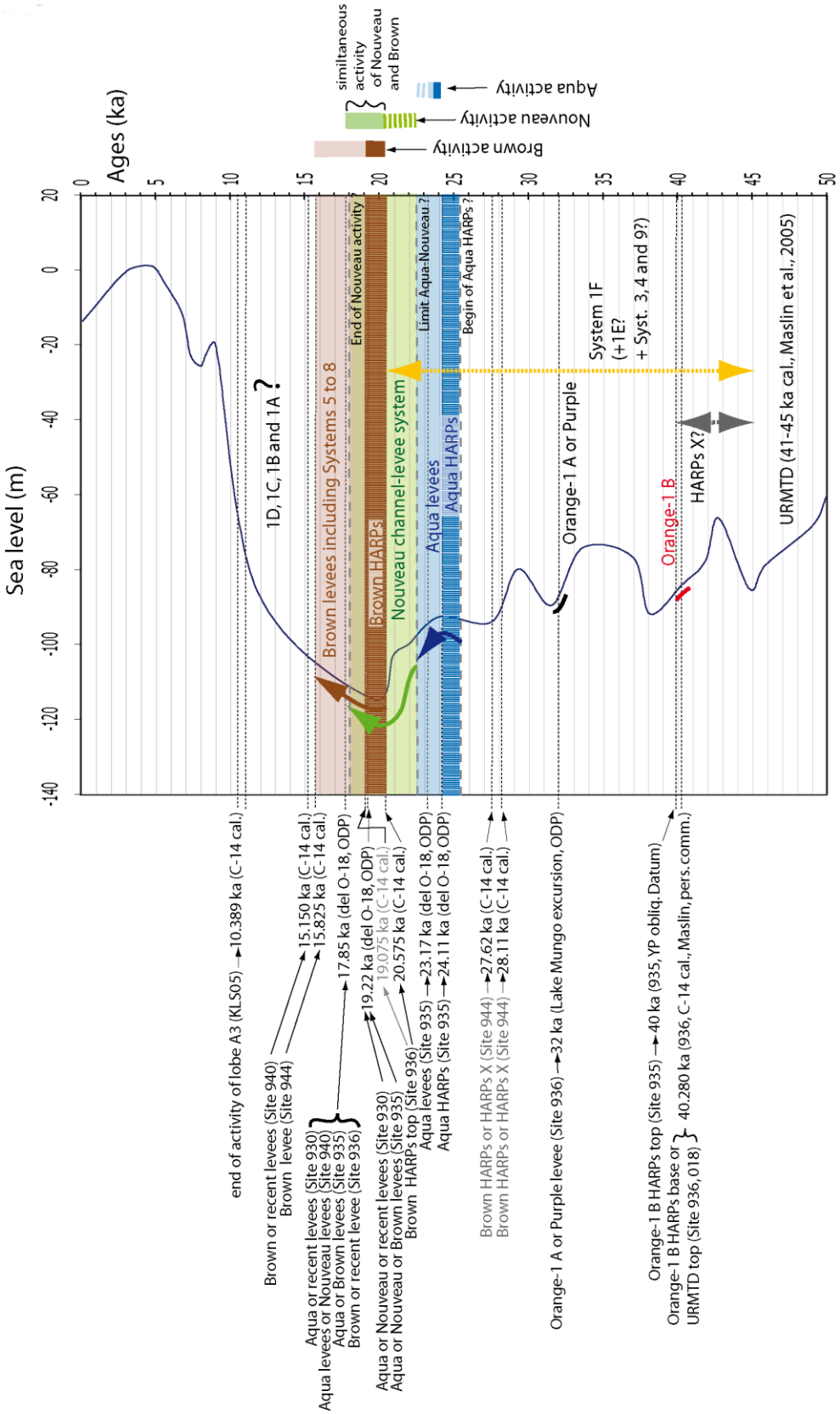

Figure VI.43: A: Available datations (Shower et al., 1997; Maslin, pers. comm.) with correlated systems (this study) ploted on a sea-level cure of Sidall (2003). The age of the end of activity of lobe A3 in the distal fan area is from Jégou (2008).

If this age attribution is correct, it indicates a time of synchronous deposition of levees of Nouveau and Brown systems. The mainly aggading structure of the base of the Brown levee and top of Nouveau system in Figure IV.5 (see also Figure IV.22) could correspond to this interval of synchronous activity of both channels.

My results also led me to place the building of 1F (and possibly 1E) after the URMTD and prior to the Brown system, i.e. somewhere between 40 ka and 20.7 ka. No more precise timing is available because this system has never been dated.

This is a main disagreement with previous works (e.g. Figure IV.25, Flood et al., 1997) that placed the 1F and 1E as channels issued from an avulsion of Brown channel and therefore younger than it.

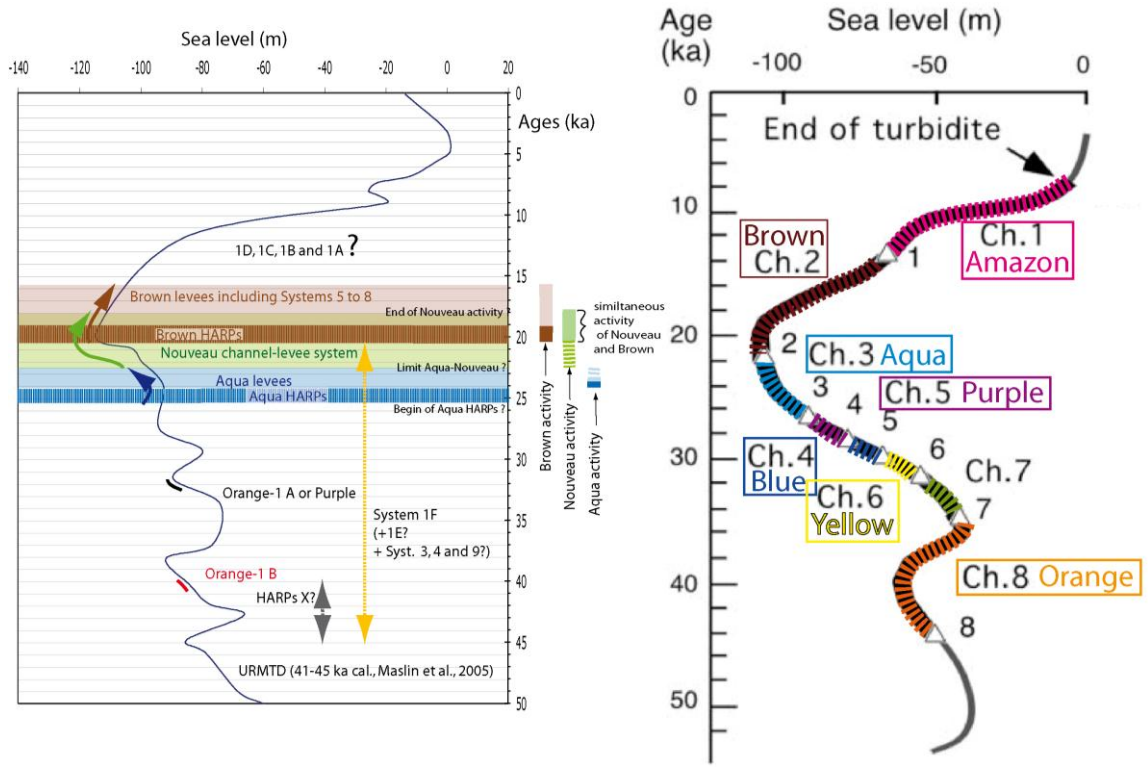

Figure IV.44: Comparison of my refined stratigrapy (A) and previous results (modified from Lopez, 2001, for channel names after Flood et al., 1997) on timing of channel-levee deposition (B). Triangles associated to numbers in (B) indicate avulsion points (i.e. starting time of channel-levee systems).

3.2 LONGITUDINAL EVOLUTION OF THE BROWN CHANNEL-LEVEES-HARPS SYSTEM: PURE AGGRADATION OR AGGRADATION/PROGRADATION ?

Although the longitudinal growth pattern of the levees of channel-levee systems over their HARPs has not been observed on seismic data, the analysis of the dates obtained for the Brown system can provide some clues to propose a growth pattern.

Sites 936 (upfan) and 944 (downfan), separated by a straight distance of 34 km (see Figure IV.37), have provided ages for the Brown HARPs and left levee deposits as schematized in Figure IV. 3. Note that the present-day along channel distance between the sites is 34 km, i.e. much longer because the Brown channel is highly sinuous. However, I opted for the straight distance between the sites because I hypothesized that the initial channel that deposited the levees shortly after the avulsion was straighter than the present channel thalweg visible on bathymetry (present thalweg length between sites: 76.4 km). Straightness of young channels is observed for example for the Rhône Neofan (Jégou, 2008).

The base of the Brown levee/top of the HARPs has been dated at 20.6 cal ka BP. at site 936. About 11.5 m above, an age of 17.7 ka has been provided ($\delta^{18}O$ peak) which from my interpretation belongs to the Brown levee. These two ages allow calculating a sedimentation rate of 4.21 m/ka.
At site 944, the only age available within the Brown system is 15.8 cal ka at about 12 m above the HARPs/levee limit. Considering the sedimentation rate calculated at site 936 (4.21 m/ka), the 12 m of thickness to the base of the levee should represent 2.8 ka of duration and therefore the base of the levee should have an age of 18.6 ka.

Considering that site 944 is closer to the channel axis than site 936, I suspect that the levee deposition rate should be higher at site 944 than at site 936. Using a higher deposition rate would give a younger age at the Brown levee base at site 944.
However, the distance difference (about 350 m) is not so high and its influence is possibly not so significant. Also, the more distal position of site 944 with regards to site 936 could lead to a lower deposition rate.
Therefore, combining the opposite influence of these two parameters on the deposition rates (distance to the channel axis and distance to the sediment source) I suspect that the deposition rate calculated at site 936 is a good approximation of that at site 944, and I

propose that the base of the levee at this site is 18.6 ka.

The only way to explain this difference in age (i.e. 2 ka) from both sites is to infer a prograding structure of the levee as shown in Figure IV.45E.

If this hypothesis is correct, I can calculate a progradation rate. The Brown channel-levee system advanced on 34 km in 2 ka, i.e. with a progradation rate of about 17 km/ka.
This value should be considered as an attempt to quantify the growth pattern of a levee following an avulsion, but it should be taken with great caution, because of numerous uncertainties related to age control and sedimentation rate. However, it should be noticed that this value is lower as the 30 km/ka obtained by Jégou (2008) in the channel-mouth lobe area.

Note that a minimum progradation rate could be calculated by giving an age of 15.8 ka at the levee base (similar to the 15.8 ka age at 12 m above the levee base, considering an instantaneous deposition of the 12 m of levee !). This minimum value is 7.1 km/ka. Maximum deposition rates of 40 m/ka has been calculated on the levee of the Amazon fan (see Table III.9, site 940, Aqua to Brown levees) that do not modify significantly the minimum progradation rate (about 17 m/ka).
Note also that, using a sedimentation rate of 2.5 m/ka (which is in the range of the deposition rates in the Amazon Fan,Table III.9), the onset of the Brown levee at site 944 would be at 20.6 ka, i.e. at the same time the levee began to grow at site 936. This would exclude a prograding growth pattern and favour a purely longitudinally aggrading pattern.

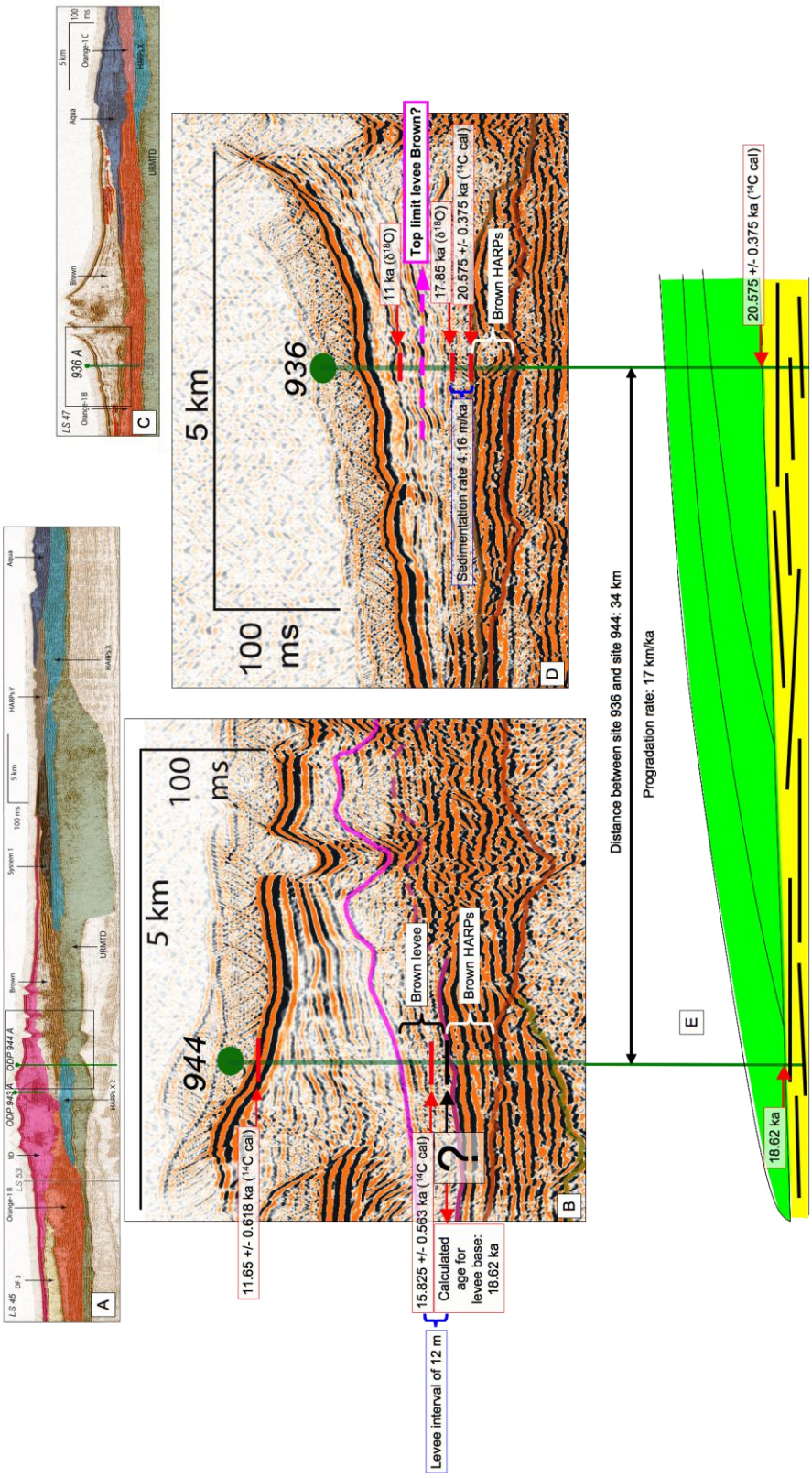

Figure IV.45: Figure showing the Brown levee at site 936 (upfan) and site 944 (downfan) on seismic lines (A and B) and zooms on seismic lines (B and D). In (E) I show a schematic view of the possible progradational pattern of the Brown levees (green) over the HARPs (yellow) with the significant dates of site 936 and 944 in the Brown levee and HARPs.

4 CONCLUSIONS

The Amazon HARPs related to avulsion are characterized on seismic data by high-amplitude reflector packets, that appear as lobate elongated features at the base of the channel-levee systems. They typically are up to 25 km wide, several tens of km long and several tens of ms twt thick.

They are composed of 4 main sub-units more or less randomly stacked showing different facies that are associated to different types of deposits within the HARPs:

- The flat-lying reflectors are made of up to 11 m-thick sandy bed successions interbedded with silty-clay intervals (cm to -m thick),
- The chaotic patches correspond to sand beds with abundant mud clasts,
- The U-shaped features are composed of similar lithological facies than the flat-lying reflectors,
- The transparent facies correspond to massive sandy clay

The most common of these sub-deposits are the flat-lying reflectors, and in view of their associated sediments, each reflector is interpreted as a flat-lying depocenter built up from intervals of sandy bed (cm- to m-thick) successions interbedded with generally thinner silty-clay intervals. The occurrence of angular contacts between the stacked flat-lying reflectors, is also observed at the base of some sand beds in the lithologic records, and reveals a highly chaotic stacking pattern of laterally switiching depocenters. I suggest that the shifts of depocenters are controled by autogenic processes due to the permanently modified topography.

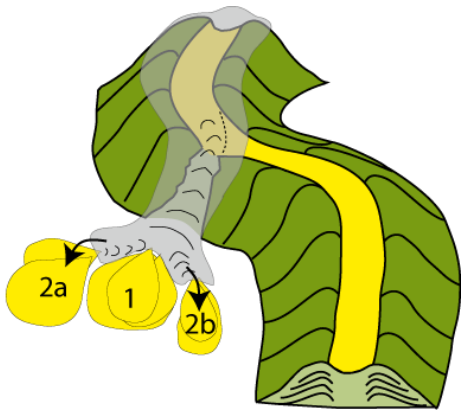

Figure IV.46: Scheme of the topographic control on the switching of the depocenters of the HARPs in front of the pathway of turbidity currents (e.g. breached levee). The yellow lobes figure the stacked flat-lying reflectors representing sandy depocenters. The gray color figures the turbidity flows that are diverted by the initial depocenter (1). This depocenter constitutes a morphological obstacle in front of the main pathway, which leads to the shifting of former depocenters (2a and 2b).

The U- or V-shaped features are either isolated or in association with adjacent reflectors.
The chaotic patches revealed similar lithologic facies than the HARs (abundant mud-clasts in a thick massive sand deposit).
I suggest that these two sub-units correspond to micro-channelizations, the U and V-shaped features being mostly erosional or by-pass features and the chaotic patches being cut-and-fill features similar to HARs (analogs to the braided systems observed in lobate deposits at channel mouths or in crevasse splays, Posamentier and Kolla, 2007).
The difference between these two erosional features can be explained by the the effects of waxing and waning flows within individual events described by Kneller (1995) . Waxing flows, commonly at or near the head of a turbulent flow, erode the substrate over which they pass. Significant amounts of sediment can bypass the system during this time (U- and V-shaped features). As the flow wanes, coarser sediments tend to come out of suspension and be deposited in the area formerly characterized as a zone of bypass (chaotic patches).

The stratigraphy of the Fan has been refined with new channel-levee systems implying new timing of deposition. Among the important modifications of the stratigraphy is the timing of 1F and possibly 1E which has been shown to be older than Brown in contrast to previous works.
The main result of age dating analysis is the possible synchronous activity of Nouveau and Brown systems between 20.8 cal ka and 17.9 ka ($\delta^{18}O$). I also was able to propose a progradational growth pattern of the levee, even if it was not observed on seismic data. I calculated a possible longitudinal progradation rate of about 17 km/ka. This value is very approximate and has to be considered as an attempt to quantify the growth pattern of the levee following an avulsion. It should be considered with caution due to the numerous hypotheses that I had to consider to obtain this value.

-Chapter V-

First and last steps of the avulsion:

Inputs from the Zaïre Fan

1 INTRODUCTION TO THE ZAÏRE FAN STUDY

The Zaïre Fan is one of the largest mud-rich fans in the world still affected by presently active turbidity currents (Heezen et al., 1964; Van Weering and Van Iperen, 1984).
Despite its continuous activity during the present high sea-level stand, the seismic facies and architecture have been shown (Droz et al., 2003) to be quite similar of those of other mud-rich fans of similar size (i.e. Amazon Fan : Flood et al., 1991 ; Mississippi Fan : Weimer, 1990 ; Indus Fan : Droz and Bellaiche, 1991). The main characteristics of these other fans are also recognizable in the Zaïre Fan, either facies associations (high-amplitude reflection channel facies and stratified to transparent levee facies) and shape of channel-levee systems, or architectural style (stacked channel-levee systems originating from avulsion processes, organized into individual fans genetically related to a common point source, the canyon and fluvial system), (Droz et al., 2003).

Because of the similarities of the Zaïre Fan with other mud-rich fans, I think that studies of local levee breaches still observable on the seafloor or of an avulsion points that has been surveyed with a dense grid of high-resolution single channel seismic data, could serve to complete the knowledge about the avulsion architectural pattern obtained from my study on of the Amazon Fan (Chapter IV)

2 PREVIOUS WORK: ARCHITECTURE OF THE ZAÏRE FAN

The Zaïre Fan extends in an approximate east-west direction from the base of slope at about 2000 m water depth to the Angola Abyssal Plain at a water depth of at least 5200 m, representing a minimum length of about 800 km. It spreads laterally from as far as the Gabon margin to the north to the Angolan margin to the south, representing a total width of more than 400 km (Figure V.1).

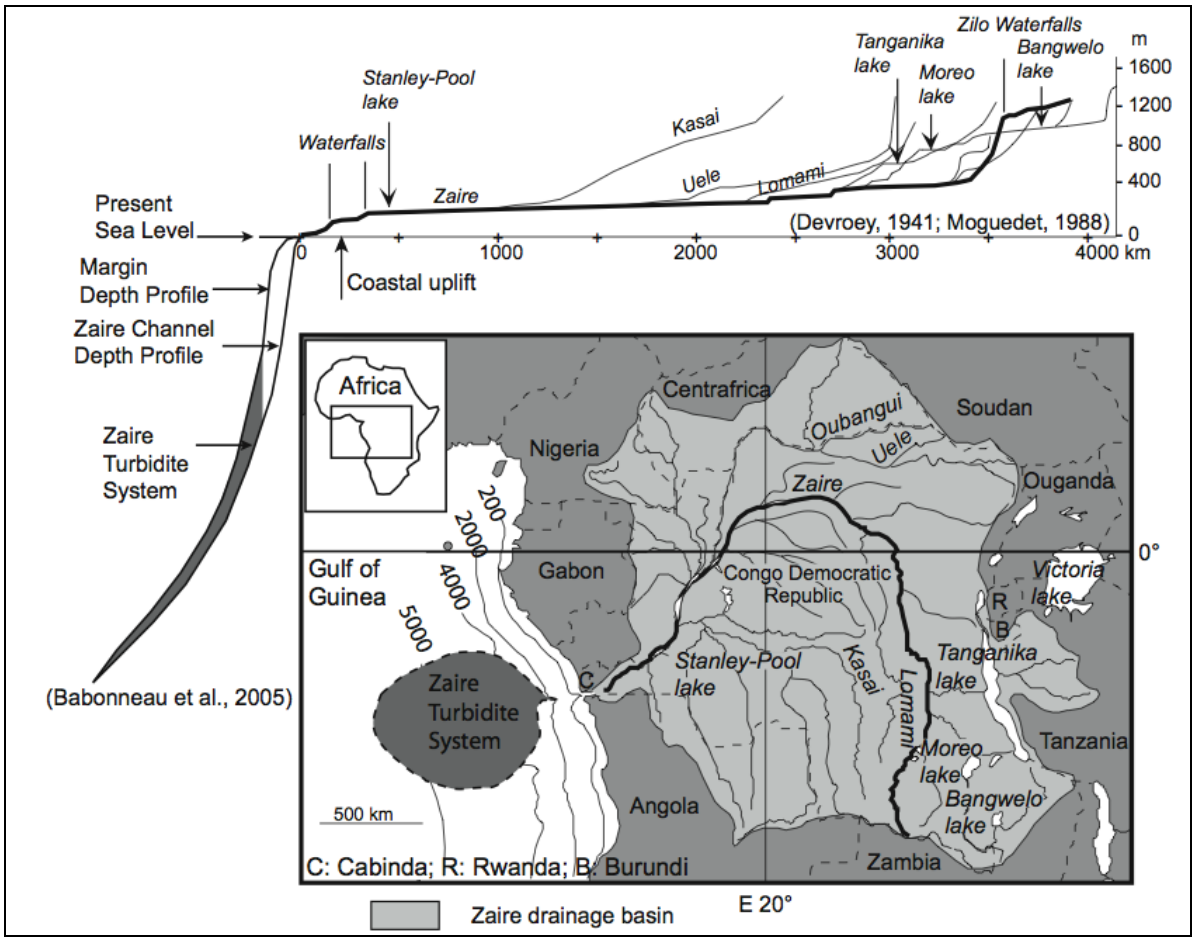

Figure V.1: Location of the Zaïre system (drainage basin, river, and turbidite system) and the longitudinal source-to-sink (Marsset et al., submitted, modified from Devroey, 1941, Moguedet, 1988, and Babonneau et al., 2005).

The Zaïre Canyon is presently connected to the so-called Zaïre Channel that is the fan's most recent channel. This active channel is characterized by extensively and variable sinuosity and cutoff meanders all along its length, until relatively close to its termination, where the channel straightens and widens significantly (Savoye et al., 2000; Babonneau, 2002). At the channel end a complex of several (at least three) partly stacked distal lobes appear (Babonneau, 2002; Bonnel, 2005) and are dated at 7 ka (Babonneau, 2002; Bonnel et al., 2005; Dennielou and Jouanneau, submitted) (see Figure I.8).

2.1 CHANNEL-LEVEE COMPLEXES

The fan surface is characterized by numerous sinuous morphological features representing meandering channels having an excellent bathymetric expression. Except for the most recent Zaïre Channel, all other channels are fossil channels. At least 80 channels, still visible on the seafloor, have been chronologically referenced and numbered (Droz et al., 2003; Marsset et

al., in press). Seismic analysis has resulted in the grouping of these channels into three main successive channel-levee complexes, the individual fans, named Northern, Southern, and Axial Fans, from the oldest to the youngest (Droz et al., 2003) (Figure V.2). The Axial Fan, the best-surveyed fan, shows the apparent progradation of the canyon that terminates more basinwards than the inferred connection points of the older Northern and Southern Fans.

ODP Leg 175 drillings (Wefer et al., 1998; Wefer et al., 2002) on the Congo continental slope provided age constraints for the main construction episodes of the Zaïre Fan (Droz et al., 2003). The Northern Fan is thought to have begun deposition at about 780 ka. Its activity halted around 540 ka, when the turbidite depocenter suddenly shifted to the Southern Fan. The Southern Fan was abandoned at possibly 210 ka, and the Axial Fan began to develop and is still currently active.

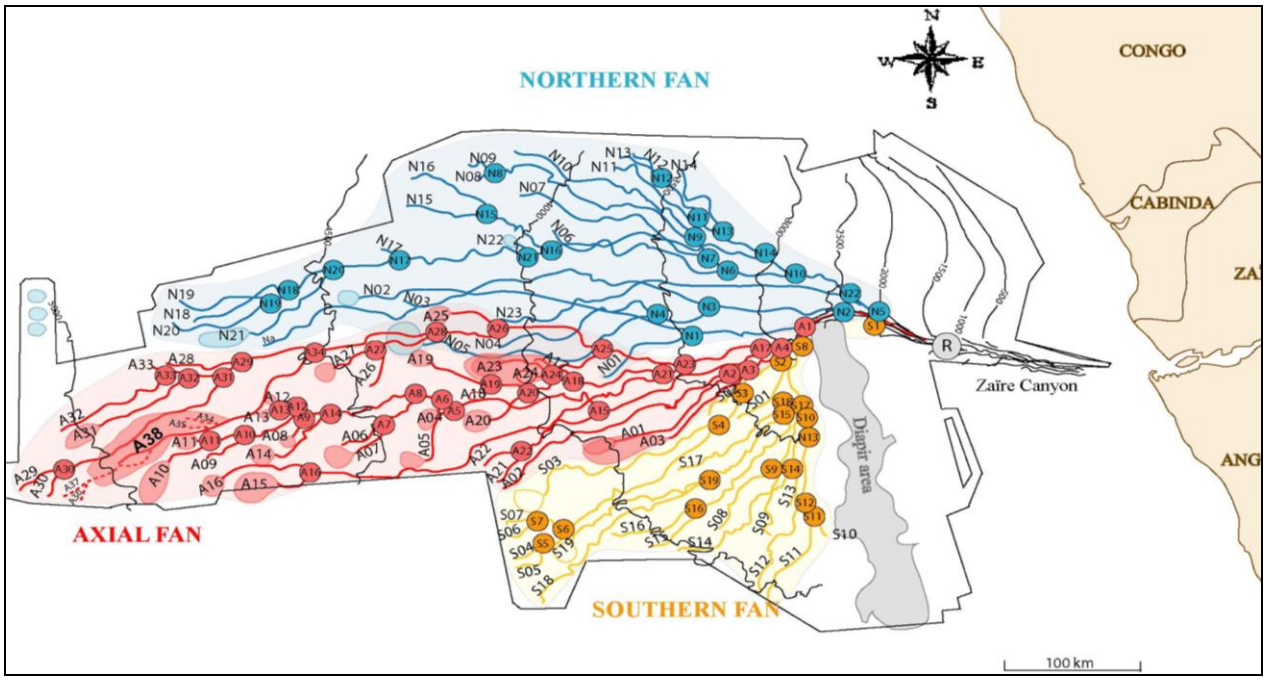

Figure V.2: Channels of the Northern, Southern and Axial Fans have been traced and chronologically numbered N1 to N23, S1 to S19, and A1 to A38, from the oldest (N1) to the youngest (A38) (Marsset et al., in press). The lobate features at the termination of the channels are channel-mouth lobes. Circled numbers figure the location and n° of the avulsion points (after Droz et al., 2003).

2.2 INDIVIDUAL CHANNEL-LEVEE SYSTEMS

The channel-levee systems of the Zaïre Fan are similar to the typical channel-levees described as architectural elements in other studies (Chapter I). They are commonly associated with underlying high-amplitude reflection units and transparent units (see Figure I.20 and 2.1, this Chapter).

The basal transparent units that truncate the levee of the ancient channel is interpreted as

mass-transparent deposits of restricted extent composed of remobilized sediments originating from levee breaching that, in some cases, initiates an avulsion (Droz et al., 2003).
About 70% of the channel-levee systems of the Zaïre Fan show a basal unit of high-amplitude, low-frequency, and relatively continuous reflectors that, in the most typical cases, infills intersystems lows, and that shows numerous similarities with the high-amplitude reflection packets described from the Amazon Fan (Pirmez et al., 1997). The top surfaces of these basal units are generally flat, but can also be convex-upward with aggradational internal configuration at the top, suggesting the contribution of aggradation processes at the units' tops.
The top surfaces are commonly eroded by small troughs and constitute a downlap surface for the overlying channel-levee system. Their basal surface can either be in conformity with, or truncate, underlying seismic units. They can extend longitudinally over several hundred kilometers (as much as 250 km), and their lateral extent is generally similar to the overlying channel-levee system. Maximum thicknesses up to several hundred milliseconds twt have been measured on seismic sections, but tabular units of 10-20 ms twt can also be observed (Droz et al., 2003).
Terminal lobes are common (Babonneau, 2002; Bonnel, 2005).

The channels are commonly several hundreds of kilometers long with a meandering course. They are laterally confined by levee deposits that show large sediment waves (Migeon et al., 2004) and are composed of fine-grained turbidite sequences (silts and muds), (Gervais et al., 2001). Channel axis accumulations are coarse-grained deposits (sand and gravels). Levees extend on 30-40 km and maximum levee height (measured from the basal to the top surface at the levee crest) is about 250 ms twt (Babonneau, 2002; Savoye et al., 2002; Droz et al, 2003). The size of the channel-levee systems decreases downslope to the distal area, where the channels disappear and feed distal lobes (Savoye et al., in press) In response to the channel morphology, turbidity currents are best-confined upfan.
Channel entrenchment of either older or more recent channels is a common feature and is suggested to be partly caused by regressive erosion inside the parent channel in response to an avulsion. The entrenchment of the channel below the regional sea floor along its whole path may be linked to the incision of the Zaïre Canyon back across the shelf during last sea-level rise (Babonneau, 2002). The entrenchment limits the overflow of turbidity currents and the turbidite sedimentation over levees, and prevents avulsion along the upper part of the Zaïre channel.

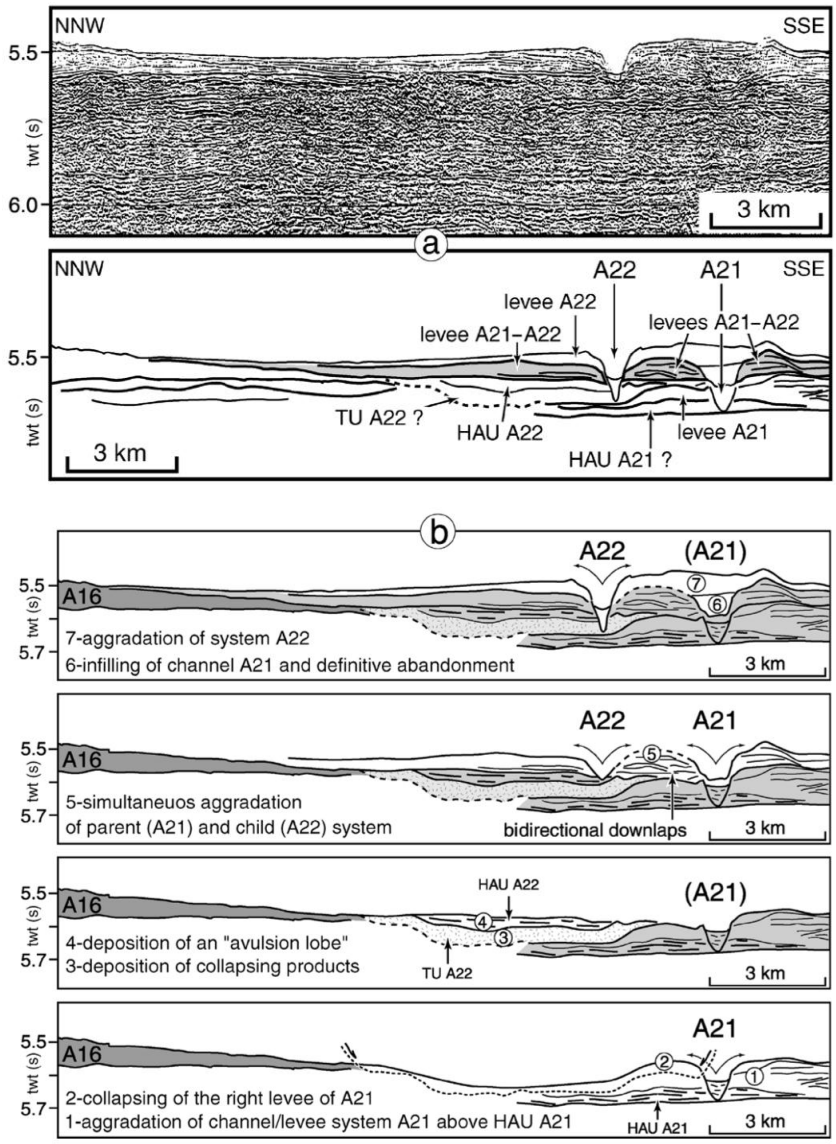

Figure V.3: Avulsion point A21/A22 (Droz et al., 2003). a: Seismic section and line drawing downfan of the avulsion point A21/A22, where A21 is the parent channel and A22 is the new channel. b: Successive sketches (in chronologic order from the bottom to the top) showing the evolution through time of the avulsion A21/A22, deduced from the interpretation of section in a. TU = transparent unit, HAU = high-amplitude unit

2.3 CHANNEL AVULSION AND HIGH-AMPLITUDE UNITS

The architecture of the fan is defined by the stacking of the channel-levees systems in response to lateral shifts of the channels due to channel avulsions. Available space is thought to dominantly control the distribution of channel-levees, although a control by the climate and sea-level changes has also been suggested (Kolla, 2007; Marsset et al., submitted).

From the literature (Chapter I), the avulsion process implies that only one channel is active at any point in time. This has been observed for most channels on the Zaïre Fan at the scale of the HR multichannel seismic data. However, and as observed on the Amazon Fan (Party, 1995; Piper et al., 1997), the study of the avulsion point A21/A22 in the Zaïre Fan (see Fig. 2 for location) highlighted, a seismic unit made of bidirectional downlaps of levee reflectors originating from both the parent A21 and new (A22) channels, attesting to inputs originating from both channels, and indicating that ancient channels can maintains a temporary activity synchronous with the new ones. The definitive abandonment of the parent channel is marked by its infill with transparent deposits (Droz et al., 2003) Figure V.4).

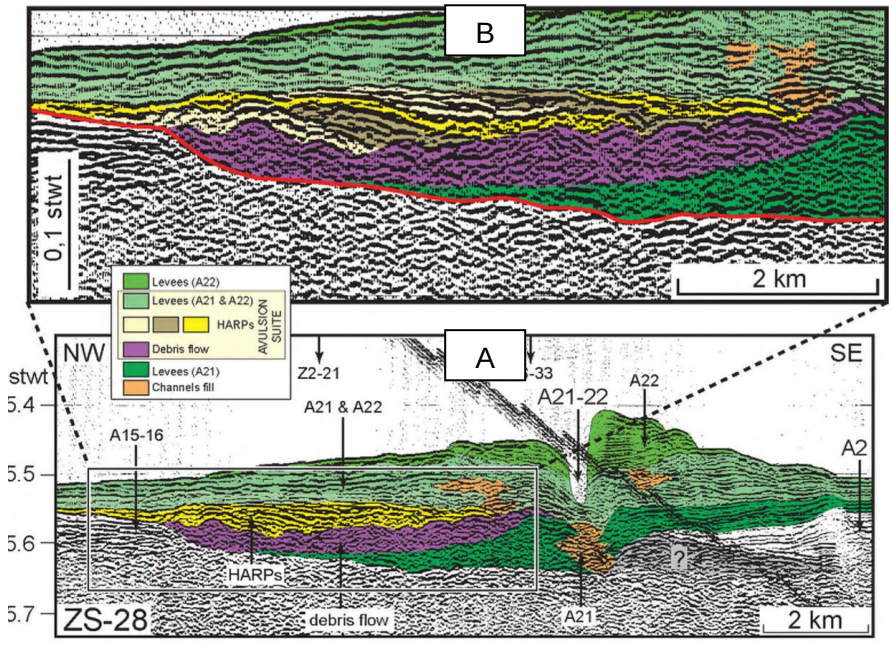

Figure V.4: Architecture of the avulsion point A21/A22 in the Zaïre Fan (Droz et al., 2002; submitted). A: High-resolution single channel seismic section upstream from the bifurcation point. B: zoom of A on the avulsion suite.

This avulsion point was later on studied with higher resolution seismic data that showed that the A21/A22 avulsion has been a complex series of events, probably of relatively long

duration. These events include several successive avulsions deposits along a segment of some kilometers on the levee of the ancient channel, before a new channel begins to aggrade (Droz et al., 2002)(Figure V.4).

General results from these high-resolution data emphasized that the A21/A22 avulsion zone exhibits a series of seismic units, called the "avulsion suite" (Droz et al., 2002) that separate the parent system from the new channel-levee system. This avulsion suite is composed of

- A transparent unit that truncates the levee of the ancient channel,
- A high-amplitude unit, that is partly interpreted as HARPs on which the new channel-levee system downlaps,
- Levee facies originating from both the ancient and new channels.

3 IS THE ZAÏRE FAN COMPARABLE TO THE AMAZON FAN ?

When referred to the classification of Reading and Richards (1994)(see Chapter I, Figure I.6), the Amazon and Zaïre Fans belong both to the same type, defined as river fed (point source), mud-rich submarine fans. Their sizes (surface area more than 300 000 km^2) are also comparable. However, a major difference is that the Zaïre Fan is a still active, in contrast to the Amazon Fan (inactive since ~10 ka cal B.P.).

I summarize in Table V.1 the major architectural characteristics of the Zaïre Fan compiled from Savoye et al. (2000), Babonneau (2002), Babonneau et al. (2002), Droz et al. (2003), Marsset et al. (in press), Savoye et al. (in press) and of the Amazon Fan compiled from Damuth et al. (1983, 1984, 1985, 1988), Flood et al. (1991), Lopez (2001) and dos Reis et al. (submitted) completed for the Amazon Fan by observations from this study (Chapter IV).

By comparing the architectural characteristics for both fans, I observe that:

- If I extrapolate the 13 Amazon channels that were built during the last 42 ka to the 210 ka and compare them with channels active over the same time interval in the Zaïre Axial Fan, the estimated number of channel-levee systems of the Amazon Fan (about 65 channels) is higher than in the Zaïre Fan (about 38 channels). This is a very simple approximation as turbidite sedimentation is highly discontinuous and the fans are not active in the same way (''on-off'' functioning for the Amazon Fan, always active for the Zaïre Fan).
- The seafloor morphology is quite different for the two systems, with a very good preservation of the seafloor expression of the channel-levee systems of the Zaïre

Fan, and mainly buried systems for the Amazon Fan.

- Regional MTDs are absent in the Zaïre Fan, while they are at least 5 of them in the Amazon Fan.
- Both systems show channel-levee systems with comparable seismic expressions. High-amplitude reflections have been reported as a common feature at the base of the channel-levee systems of both fans. However a particularity has been shown for the Zaïre Fan with small mass-transport deposits at the base of most of the high-amplitude units. Local, small transparent units have so far not been associated to avulsions in the Amazon Fan.
- The main seismic characteristics of HARPs are similar for both fans and their downfan extension is comparable (some hundreds of kilometers). Seismic facies similarities between the Zaïre's high-amplitude units and the Amazon's high-amplitude reflection packets include parallel and onlapping internal configuration, and presence of small erosional channels at the top. However, a seismic particularitiy has been observed for some of the HAUs in the Zaïre Fan: a possible convex-upward lens shapes of the Zaïre's units, suggesting the contribution of aggradation processes at the units' tops (Droz et al., 2003). For the HARPs of the Amazon Fan, a facies analysis in my study revealed internal erosional features and chaotic patches as well as a few transparent patches.
- Zaïre channels are incised, Amazon channels aggrade.

This comparison provides evidences of strong similarities for the seismic facies and architecture of the Zaïre and Amazon Fans. The major differences concern the morphology and channel activity (regional MTDs, distribution of channel-levee systems, channel entrenchment, distribution of sandy deposits, Figure V.5). These differences are so far suggested to be a result of different behaviors of flow dynamic (Babonneau, 2002) or space compensation (Droz et al., 2003).

	Zaïre Fan	Amazon Fan
Number of channel-levee systems	About 80 channel-levee systems in 780 ka including an activity during the Holocene and probably older interglacial periods (Droz et al., 2003; Marsset et al., in press).	13 systems for the last 40.28 cal. ka (this study, Chapter IV.1).
Morphology of channel-levee systems	Channel-levee systems are still visible and well-expressed on the seafloor, probably resulting of a combination of favorable conditions (sufficient available space, absence of big mass-transport deposits that would rework the channel-levee systems or buried them) (Droz et al., 2003).	Most of the channels or at least main upfan parts of the channels are buried. Most of the avulsion points are deeply buried and no more visible on bathymetry. This is probably a result of restricted available space, favoring overlapping systems in confined areas. Also huge mass-transport deposits cover the systems.
Channel-levee association	Avulsion suite separating the parent and new channel (basal local MTDs, HARPs, levees overbank from both channels) in avulsion zone A21/A22 (Droz et al., 2002, submitted).	No local MTD observed to be associated to avulsion zone. Period of synchronous activity of the parent and new channel has not been observed..
Channel activity	Frequent channel entrenchement (Babonneau, 2002, Babonneau et al., 2002; Droz et al., 2003)	Channel aggradation (Pirmez, 1994; Pirmez et al., 2003)
Other occurence of HAR	Thick and widespread high-amplitude facies Possible channel-mouth lobes Babonneau (2002)	This study (Chapter IV)

Table V.1: Table of main architectural characteristics of the Zaïre and the Amazon Fans.

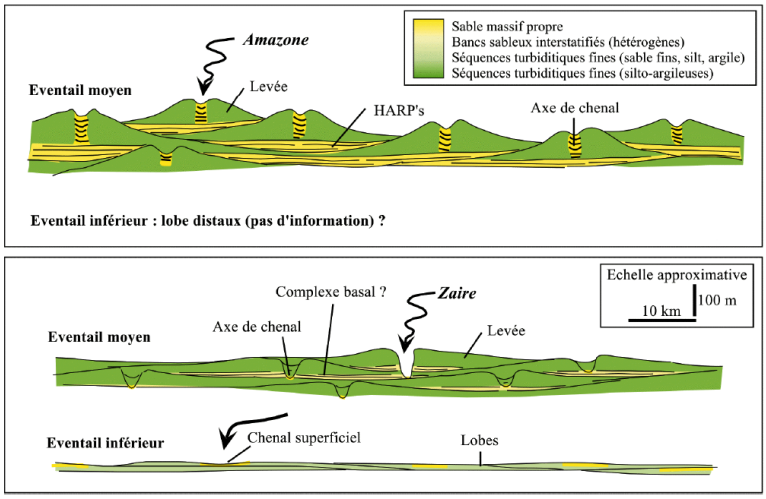

Figure V.5: Schematic cross sections in the Amazon (above) and Zaire (below) middle and lower fans (Babonneau, 2002; Babonneau et al., 2005).

4 INPUTS OF THE ZAÏRE FAN TO THE KNOWLEDGE OF THE AVULSION PROCESS

Previous studies of the Zaïre Fan have pointed out evidence of well-preserved crevasse splays on the right levee of channel A16 and levee breach by sliding from the right levee of channel S3 (see below), possibly offering the opportunity to image and characterize the first steps of an avulsion (Droz, pers. com.). Besides, the avulsion zone A21/A22 (see below) reveals synchronous activity of the parent and new channel. While the stacking pattern of the HARPs of this avulsion point had been described with details (Droz et al., 2002, submitted), the synchronous activity remained poorly studied. Being an eventual late step in the channel avulsion event, even if not generalized to other avulsion point, I decided to study in detail the stacking pattern of the levees of the parent and new channels to emphasize the pattern with which the overbanking activity is transferred from the parent to the new channel.

4.1 LOCATION OF THE STUDIED CHANNEL-LEVEE SYSTEMS

The A16 and A21 channel-levee systems belong to the Axial Fan, the youngest of the 3 individual fans that constitute the Quaternary Zaïre Fan (Figures V.2, V.6). Channel S3 is among the oldest channels of the previous Southern Fan.

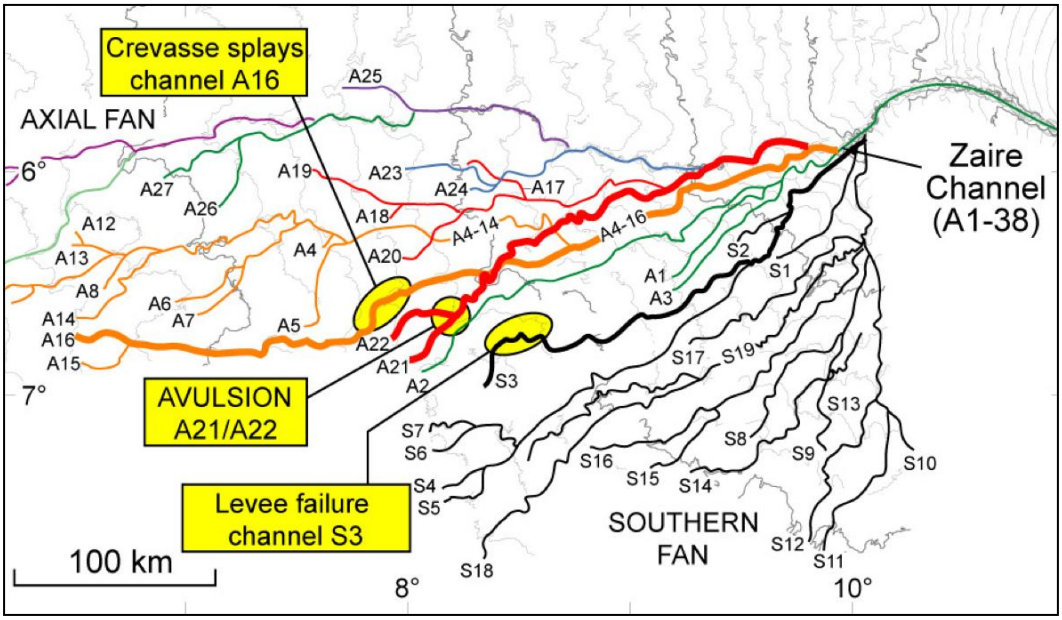

Figure V.6: Map showing the localizations of the portions of channel A16 and channel S3 and of the avulsion point A21/A22 that have been studied (modified from Droz and Marsset, submitted). The colored channels are Axial Fan channels; the black channels are Southern Fan channels.

Both the S3 and A16 channels have been mapped with EM12 data along their whole length.

The studied portion of channel S3 is located near its end, about 10 km from the entry of its termination where no channel-mouth lobe is known, and 300 km from the S2/S3 bifurcation point.
The analyzed portion of Channel A16 is situated approximately in the middle of the channel course, about 100 km from the A14/A15-16 bifurcation point and from the entry of the channel-mouth lobe that terminates this channel.

Bifurcation point A21/A22 is the latest bifurcation point identified in the ancient Axial Fan (Droz et al., 2003). The previous avulsion A20/A21 is situated about 125 km upstream, while the next avulsion (A22/A23) that resulted from the abandonment of channel A22 and aggradation of channel A23 is located about 150 km upstream (Figure V.6).
The parent and new channel were mapped with EM12, only along 20 to 30 km downstream from the bifurcation point, and the termination of these channels and, in particular, the possible occurrence of other avulsion zones and terminal lobes, are unknown.

4.2 DATA SET

The seismic dataset available on the Zaïre Fan consists mainly of processed 6- and 96-channel seismic lines (ZaïAngo 1 and 2 cruises), with about 14 km spacing, mostly oriented NNW-SSE with some additional dip lines (Figure V.7).

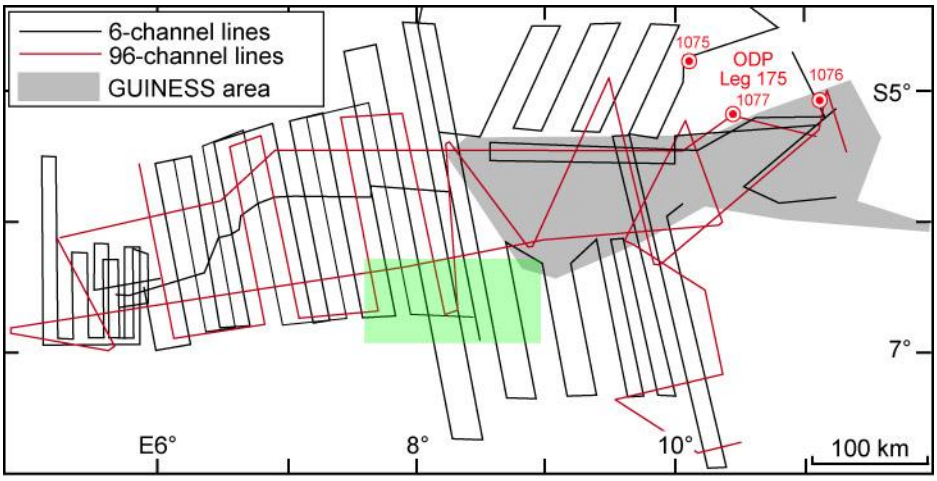

Figure V.7: Map of the HR multichannel seismic lines on the Zaïre Fan. The green box indicates the location of the studied area (modified from Droz et al., 2003).

In addition, high-resolution single channel seismic data (ZaïSar cruise) were available on the A21/A22 bifurcation point. These seismic data consists of NW-SE strike lines perpendicular

to successive parts of the systems (Figure V.8): the common part of channel A21-22 (ZS-30 and ZS-29), the bifurcation point (ZS-28), the downstream parts of the systems (ZS-27 and ZS-26) and the distal part of channel A22 (ZS-34). Profiles ZS-26 to ZS-30 are spaced by 2-3 km. A complementary dip profile (ZS-31-32-33) was acquired along the right levee of common channel A21-22 and parent channel A21, successively. A complementary E-W, very high-resolution deep-towed 3.5 kHz profile (ZS-35), was acquired obliquely across channel/levee system A21.

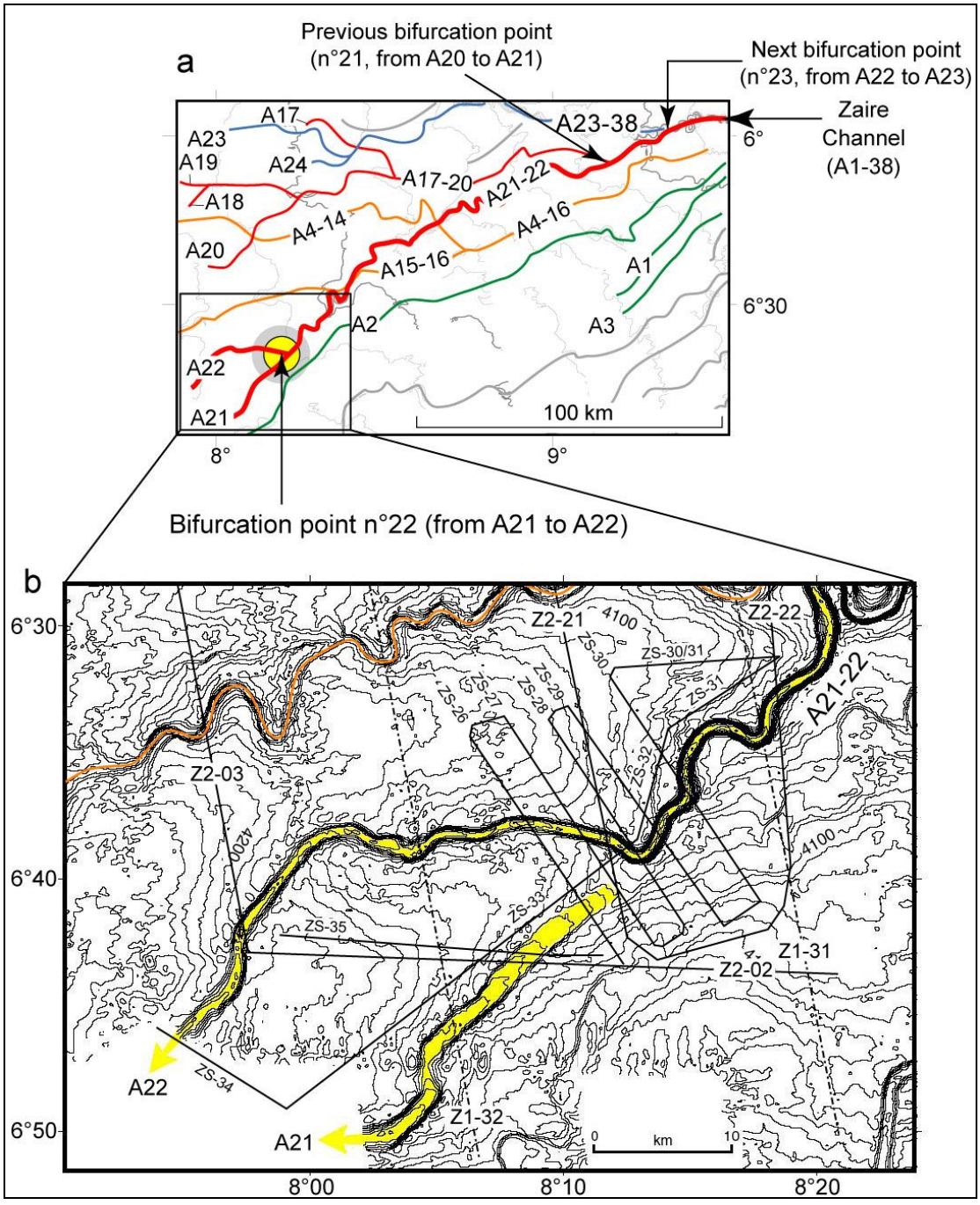

Figure V.8: Map of the HR multichannel (Z1- and Z2-) and single channel (ZS-) seismic lines available on the avulsion zone A21/A22 (Droz et al., submitted).

4.3 MORPHOLOGY OF THE CHANNEL-LEVEE SYSTEMS

The studied area is characterized by water depth ranging from 4050 to 4250 m, sloping towards the southwest (Figure V.9). The channels S3, A16, A21 and A22 are topographically well-expressed. A more subdued channel, A2, is also visible on the southeastern side of channel A21 (green doted line in Figure V.9).

- Channel A22 shows the best-expressed morphology with a meandering course upstream from the avulsion point and a more linear course downstream. Channel A21, the parent channel of A22 is very straight with a subdued morphology close to the avulsion area and becomes more sinuous and deepens at ~15-20 km downstream.
- Channel A16, which is under the A21-22 channel and therefore badly-expressed in the east of the area (orange doted line in Figure V.9), appears sinuous to meandering and deep in its upper part and becomes less deep and more linear downstream.
- Channel S3 is rather linear and deeply incised in the studied portion.

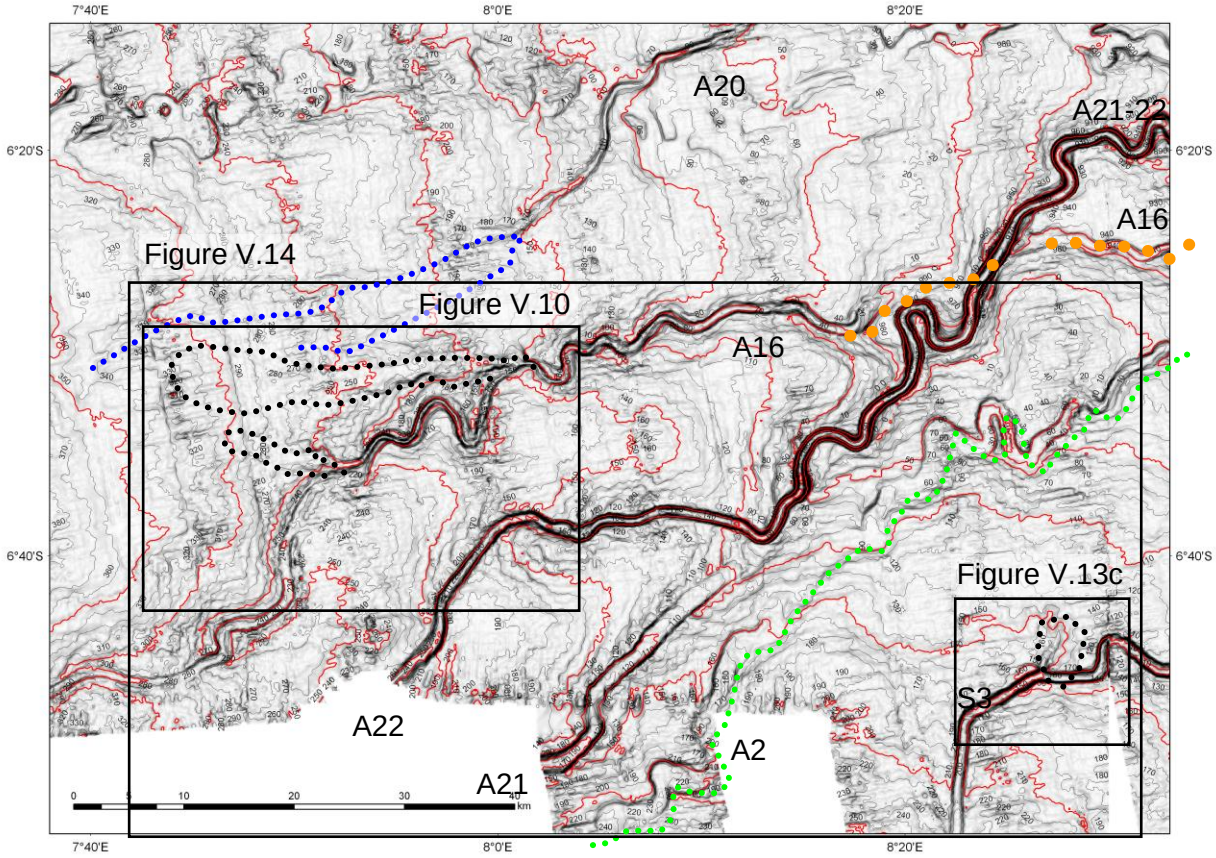

Figure V.9: Shaded slope map of the studied area, showing the 3 channel-levee systems S3, A16 and A21-A22 (contours are in meters). The orange doted line corresponds to the portion of A16, which is buried under A21-22. The green doted line marks the course of channel A2, which is buried under the left levee of channel A21. The blue doted lines are channels that could be distal prolongation of A20 channel. The black doted features along the A16 and S3 channels represent the lobate features discussed in text.

4.4 THE FIRST STEPS OF AN AVULSION

4.4.1 Crevasse splays on the right levee of A16

The channel-levee system A16 is affected on its right levee by lobate features that are connected headward to channel A16 via a narrow thalweg, which are comparable to crevasse splays of Posamentier and Kolla (2007) (see Chapter I). I called these features Splay 1 and Splay 2 and the portions of A16 limited by these splays are called A16c upstream from Splay 1, A16b between Splay 1 and Splay 2, and A16a downsteam Splay 2 (Figure V.10).

The feeding thalwegs of both splays are in continuity with A16, indicating that A16a is an old branch and that Splay 1 and Splay 2 are the youngest sedimentary events that occurred in this part of the A16 channel.

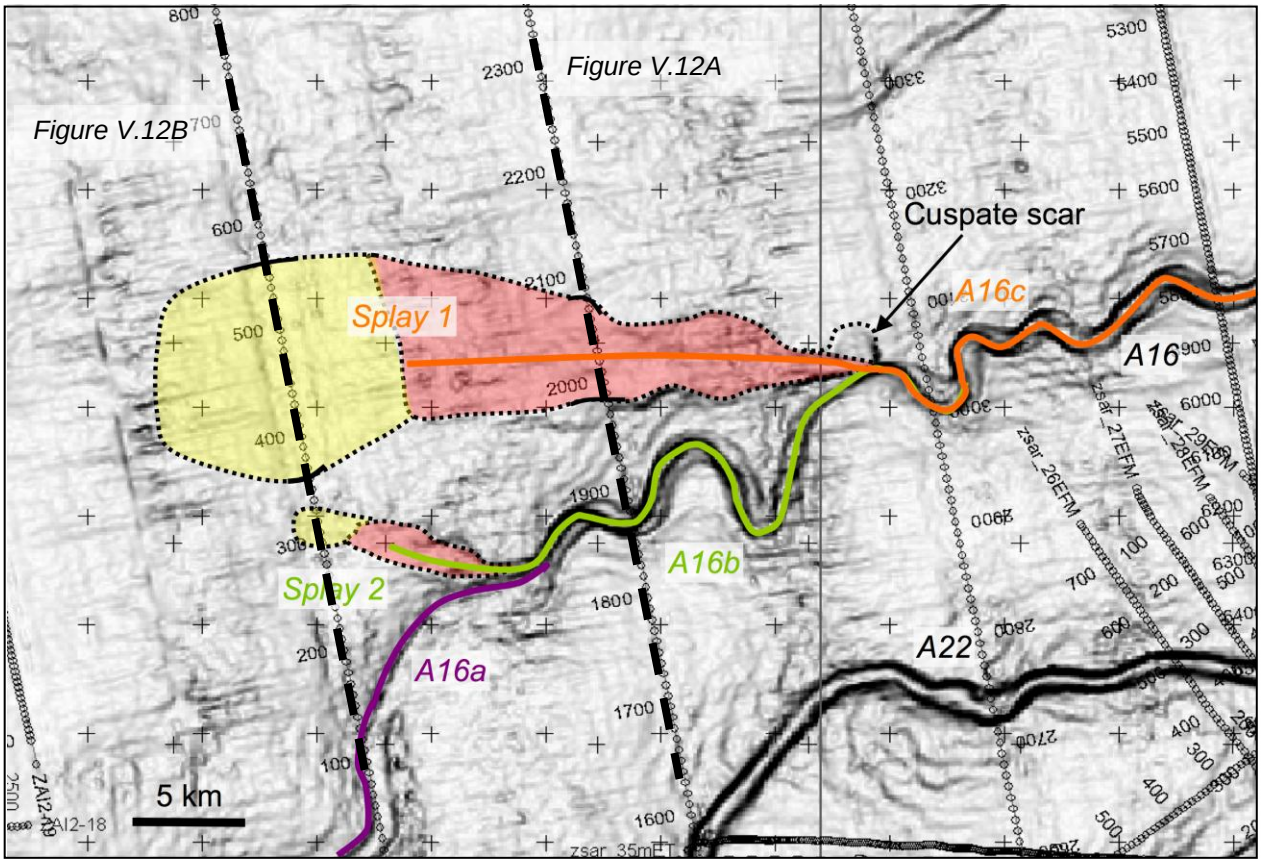

Figure V.10: Zoom on the two crevasse splays of A16. Splay 2 is older than Splay 1. Red areas are portions of the splays that are mainly erosional. Yellow areas are portions of the splays where transparent deposits are accumulated. For visualization of whole length of the A16 channel and position in the chronological relationship see Figure V.6. The dashed black lines are the location of seismic profiles shown in Figure V.12.

The along-channel depth profile of channel A16 (Figure V.11) reveals a very irregular thalweg floor, with numerous changes of slope, especially at the junction area between the

splays and the channel A16. The connection of branches A16c and A16b is marked by a clear 20 m shallowing of the thalweg from 4190 m to 4170 m water depth. A similar thalweg shallowing is observed at the junction point of branches A16a and A16b, with 20 m of relief between the two thalwegs.

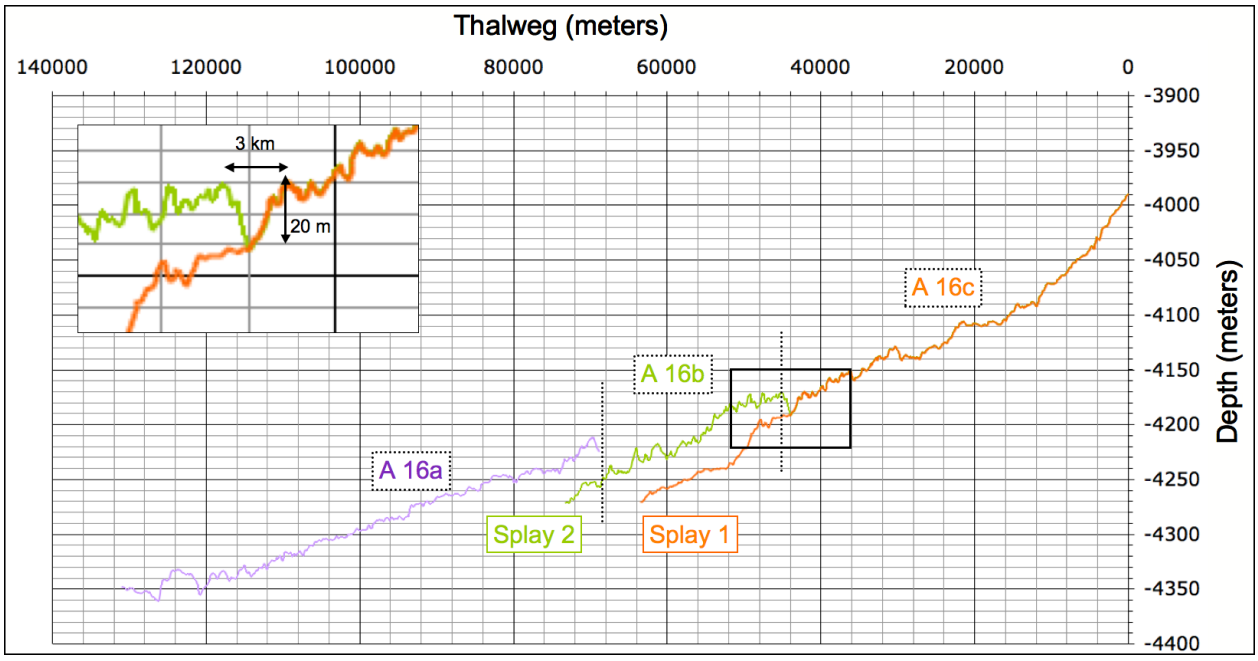

Figure V.11: Thalweg measurements for the channel A16 branches and the splays. The measurements on the splays have been realized arbitrarily at their middle. Note that the distal parts of Splay1 and Splay 2 are projected. The gray curve is the hypothetical slope of the A16 channel before the splay process occurred (upfan prolongation of A16a).

Seismic lines crossing the splays (Figure V.12) show that Splay 1 is constituted of:

- An upper zone that is mainly erosional, with up to 40 ms of A16 levee deposits that have been removed (Figure V.12A). The slope map (Figure V.10) shows that the lateral limits of the headward part of this erosional zone are sinuous break of slopes, more or less continuous, evoking slump scars. Note the cuspate shaped break in slope that affected the levee at the head of the splay, near the junction to channel A16.
- A lower zone characterized by transparent deposits (Figure V.12B) that accumulated in a preexisting depression between the A16 levee and a small channel levee system that could be a prolongation of channel A20 (Figure V.9). However, some evidence of truncations of the underlying seismic units are observed. The origin of this basal erosion is suspected to relate to the erosional first stage of the splay. The transparent deposits of Splay 1 are 50 ms thick and have a lateral extension of 11 km.

Transparent deposits are also observed at the distal part of Splay 2. No seismic data is available to illustrate the headward part of this splay, however, owing to similar lateral limits n

the slope map (Figure V.10), I suspect similar erosional features. Splay 2 is smaller than Splay 1, with a thickness of 50 ms and a width of 1.5 km.

The transparent deposits are inferred to be the sediments eroded from the A16 levee.

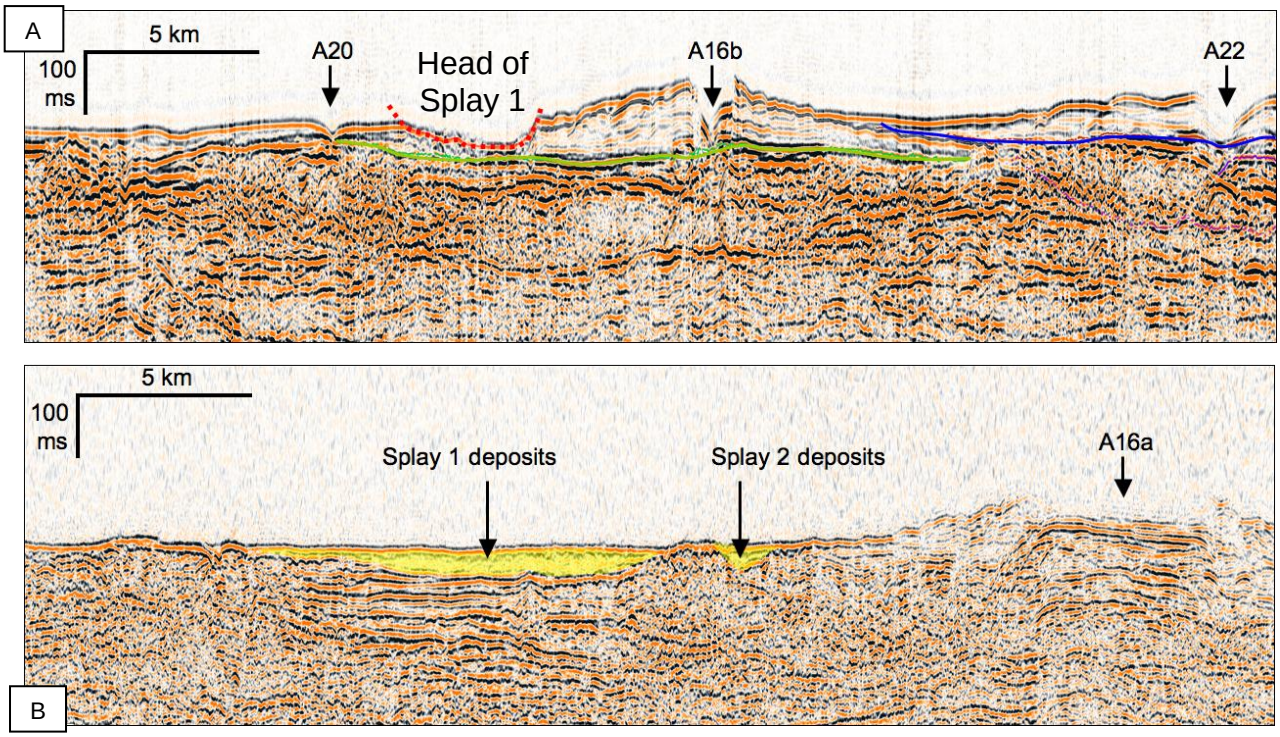

Figure V.12: Multichannel seismic lines crossing the splays that affect the right levee of channel A16 (see Figure V.10 for location).

4.4.2 Levee breach by local MTD on the right levee of Channel S3

Another lobate but smaller feature has been observed on the right levee of Channel S3 (Figures V.9 and V.13A) near a slight change in direction of the channel.

On seismic sections (Figure V.13) this feature is characterized by a 50 ms twt thick accumulation of transparent to chaotic facies bounded by scarps on the levee and associated to V-shaped incisions. The maximum lateral extension the chaotic facies is 3 km. This feature is interpreted as a levee failure that deposited a local MTD and led to the breaching of the levee.

Surprisingly, the lobate deposit and its associated incisions are oblique to channel, extending in the upfan direction, i.e. towards lower depths. This “abnormal” orientation led us to conclude that this levee breach is a local failure event that, in contrast to the above described splays, have probably primarily not been provoked by repeated overflows from the channel. However, the existence of the incisions seems to prove that, once the breach was created, overflows from S3 occurred and flowed on short distances in this upfan direction.

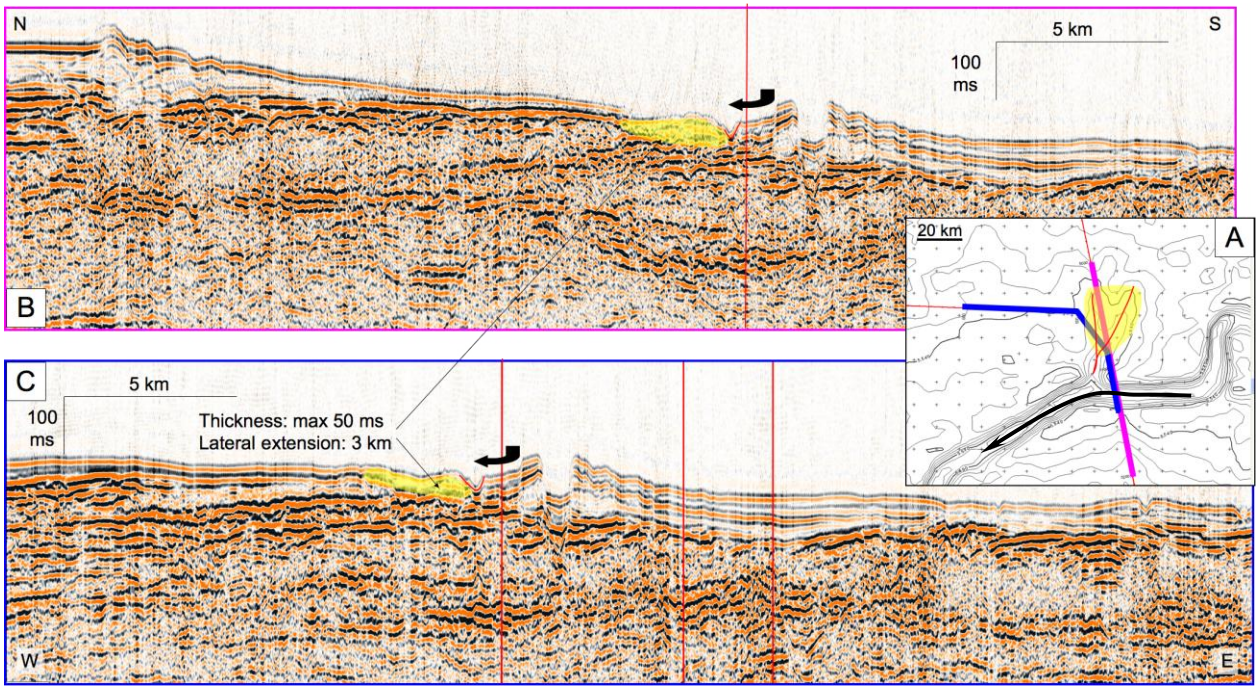

Figure V.13: Levee breach on the levee of channel S3 by local MTD. A: Bathymetric map of the MTD (yellow) and associated incisions (red lines). The black arrow indicates the direction of flows inside channel S3. B and C: Seismic lines crossing the channel-levee system S3 showing the scar (blue arrows) on the levee, the reworked levee deposits and a small incision.

The incisions remained unconnected to the channel (Figure V.13A), indicating that flows were only sporadic and did not lead to an avulsion. However, the levee was breached and I suspect that repeated overflows would probably have connected the incisions to the channel thalweg, and finally would have diverted the flows permanently, if Channel S3 had not been abandoned by avulsion higher on the Southern Fan.

It should be noticed in addition that Splay 1 on the levee of channel A16 (see Figure V.10), shows a similar cuspate-shaped morphology at its head, on its northern side near the levee crest. Seismic data are not available to show the internal structure of this feature, but, comparing with S3 feature, I think it could represent the initial levee failure that evolved, by repeated overflows inside, to the final connection with the A16 thalweg.

This levee failure by local MTD observed on the levee of S3 channel, and possibly at the head of Splay 1 on the levee of A16 channel, can therefore be considered as the earliest stage of an avulsion that open the way to turbidity currents to escape from the confinement of levees.

4.5 THE ONSET OF THE NEW CHANNEL

The avulsion A21/A22 has already been studied by Droz et al. (2003; submitted) showing

that after the HARP deposition of A22, levee aggradation occurs simultaneously from both the parent and new channels A21 and A22 before A21 is definitively abandoned.
I revisited this avulsion point, to investigate in more detail the evolution of the channel levee aggradation during and after the HARPs deposition.

The present-day morphology of the avulsion point and of the parent and new channels is shown on Figures V.8 and V.9. Channels A21 and A22 are located in an intersystem low, between two ancient channels, A2 to the southeast and A15-16 to the northwest. Channel A21-22 (common part of the channel upstream from the bifurcation point), and the new channel (A22) which presently connects to A21-22, are deeply incised. The total incision depth is about 100 m in the upstream common part and about 50 m in A22. The longitudinal slope of channel A21-A22 and its extension in A22 is rather smooth, with a steady gradient of 0.2 %, suggesting that the new channel floor is in an equilibrium state. However, locally at the bifurcation point, a 19 m-deep low could have resulted from the avulsion process. Close to the bifurcation point, channel A21 is disconnected from the common upstream part and appears as an elevated, nearly flat area, due to infill of the former channel by overbank deposition from new channel A22. A channel axis between two narrow levees of channel A21 progressively reappears about 2 km downstream, and becomes more and more incised, reaching a depth of 50 m.
My seismic interpretation confirms the simultaneous levee aggradation of A21 and A22 downfan the avulsion point (Figure V.14B) and I determined the following succession of units, from the oldest to the youngest:

- The A21 channel levee system
- The overlying simultaneous levee deposits of A21 and A22 and basal HARPs for A-22 at the localization of the future A22 channel.
- The A22 channel-levee system alone

A similar stacking pattern is observed on the seismic cross line situated 15 km downfan (Figure V. 14C).

In more details, only the lower part of the A21 post-avulsion levee (i.e belonging to the simultaneous levee A21-22) is deposited synchronously to HARPs A22. Following the end of HARPs deposition, the A22 levee begins to aggrade in the same time as A21 levee keeps on to deposit.
As observed on the downfan profile (Figure V.14C) (and in the upfan profile, Figure V.14B, but more badly expressed), the initial A22 channel-levee system is characterized by very high-amplitude levees. This high-amplitude basal levees possibly results from the absence of sufficient confinement of sandy basal parts of the flows.

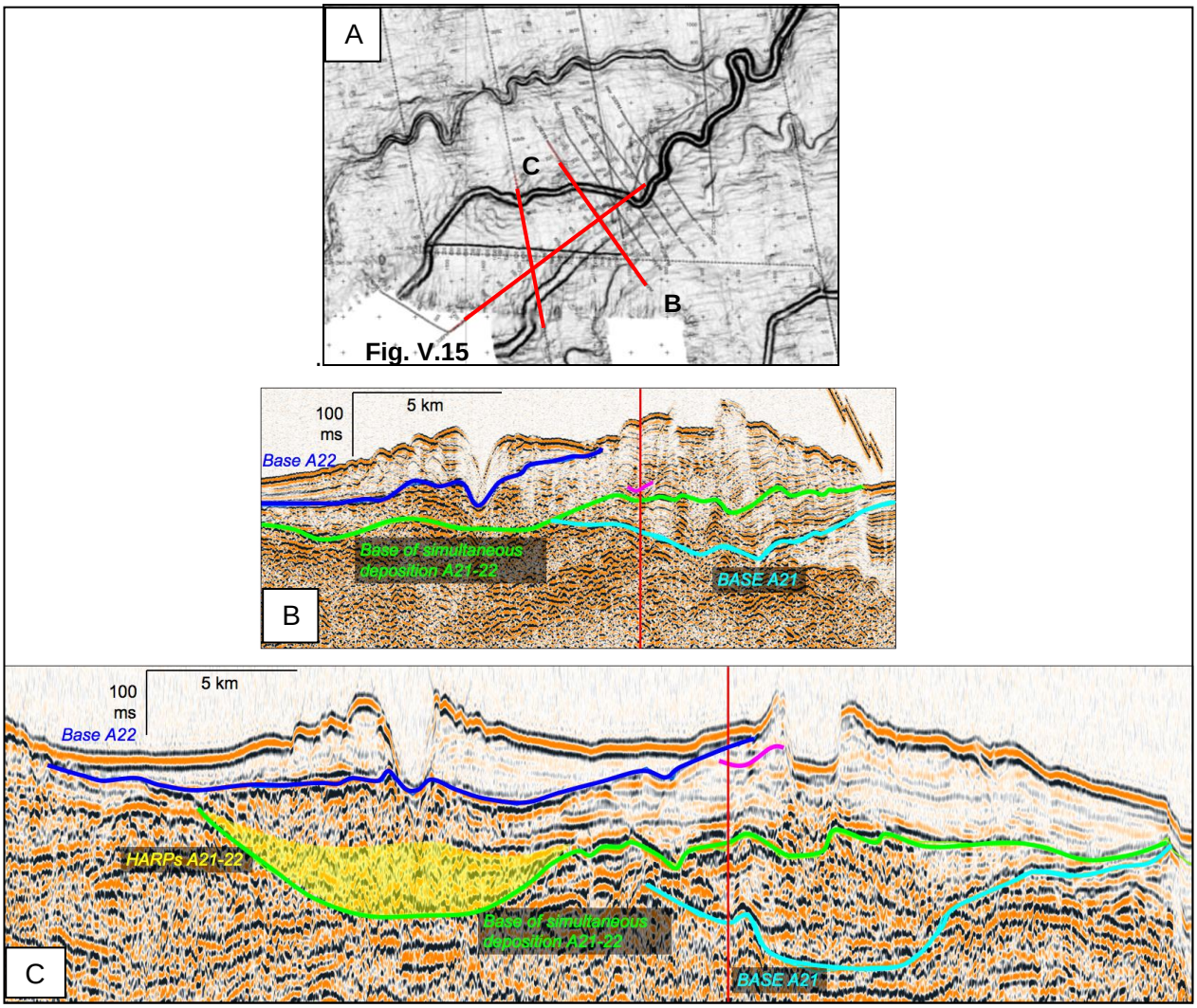

Figure V.14: Avulsion zone A21/A22. A: Slope map with location of available seismic data. The red lines indicate the position of lines shown in B and C, and in Figure V.15. A: Single channel strike line (ZS-26) 4 km downstream from the bifurcation point (location in A). B: Multichannel strike line (Z1-32) about 15 km downstream from the bifurcation point (location in A). Light blue horizon: base of A21 channel-levee system; light green horizon: base of simultaneous deposition of the levees A21 and A22 and of the HARPs A21-22 (in yellow); blue horizon: base of channel-levee system A22. The red vertical lines indicate the crossings with dip seismic line shown in Figure V.15. Note the pink marks discussed in text.

The longitudinal profile ZS-33 on the right levee of A21 (Figure V.15), allowed to evidence a particular architecture of the levee common to A21 and A22, characterized by successive upfan downlaps, i.e. by a clear backstepping pattern.

This stacking pattern results in a variation, from up to downstream, of the thickness of the seismic units of the levees, well evidenced by the pink horizon (Figure V.15) that is situated near the base of the common levee A21-22 on the upfan line (green horizon, Figure V.14B) and near the base of the levee of A22 on the downfan profile (blue horizon, Figure V.14C).

I interpreted this backstepping pattern as the result of the progressive transfer of activity from A21 to A22 during the period of simultaneous activity, until the definitive abandonment of A21, as schematized in Figure V.16.

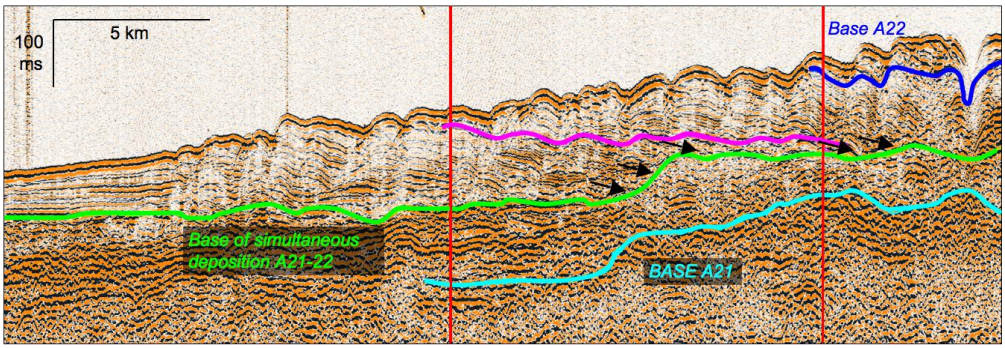

Figure V.15: Single channel dip line (ZS-33) on the right levee of the parent channel A21, downstream from the bifurcation point (location in Figure V.14A). Light blue horizon: base of A21 channel-levee system; light green horizon: base of simultaneous deposition of the levees A21 and A22 and of the HARPs A21-22; blue horizon: base of channel-levee system A22. The red vertical lines indicate the crossings with strike seismic lines shown in Figure V.14B and C. The pink horizon is a marker of the backstepping pattern discussed in text. Red arrows are downlaps of reflectors.

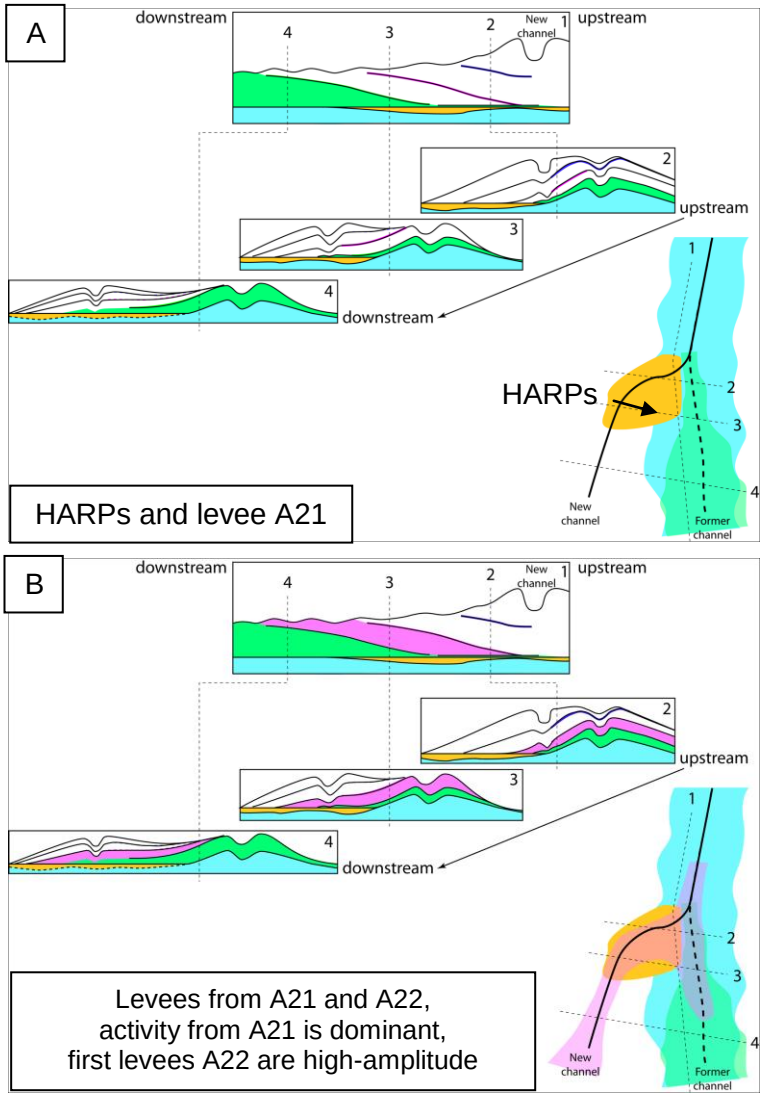

Figure V.16: Schematic sketches showing the evolution of the levees deposition during the A21/A22 avulsion characterized by a progressive transfer of the activity from A21 to A22 until the definitive abandonment of A21. A: Simultaneous deposition of HARPs and levees from A21. B: Simultaneous deposition of levees from both A21 and A22.

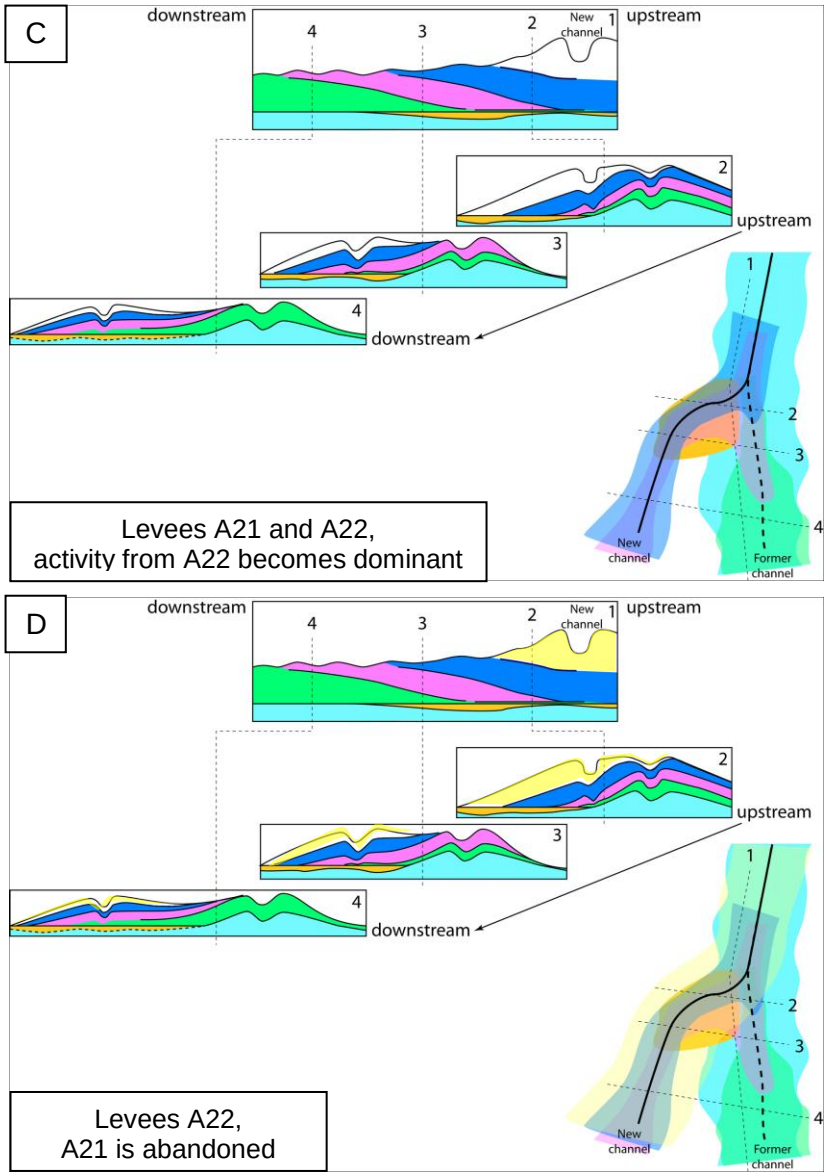

Figure V.16, continues: C and D: The activity is progressively decreasing from A21 in favor of A22, until the definitive abandonment of A21

4.6 CONCLUSIONS

Because of its very well preserved paleo-morphology on the seafloor, the Zaïre Fan provided, at three locations on the levees of channels A16 and S3, evidences of unconformable seismic bodies linked to levee rupture processes that are the earliest steps in the series of events that characterize an avulsion.

- The initial step (levee breach) has been observed on the levee of S3. In the case of S3, the breaching was realized by levee failure that deposited a small MTD. The breaching did not evolved in a true pathway for turbidity currents, possibly because S3 was abandoned a short time later. The head of Splay1

on channel A16 possibly kept the trace of cuspate scars that could result from similar levee failure.

- A second step (crevasse splays) was observed twice on the levee of A16. These small erosional/depositional unconformable bodies and their direct connection to the A16 thalweg indicate that the turbitidy flows have been more permanently escaping from the channel and flowed unconfined towards interchannel lows. The transparent deposits at the mouth of the thalwegs of the splays are probably sediments eroded upfan, inside the channel upstream the avulsion point and on the levees downstream the avulsion point.

Should these unconformable bodies (local MTDs and crevasse splays) evolve to a complete avulsion, they will be probably amalgamated in the HARPs and should be difficult to identify. However, they could be the equivalent of the unchannelized flat-laying sub-units of the HARPs, the change from transparent to the high-amplitude facies being related to compaction.
In contrast, if they do not evolve to a complete avulsion, and if the channel is not abandoned (as it was the case for A16 and S3), I can assume that they will be buried under further levee deposition of the former channel and will be possibly preserved as the transparent wedge-shaped bodies bounded by unconformities observed in the levees of the Amazon channels (Chapter IV.1).

The A21/A22 channel avulsion shows an example where the HARPs of the new channel are partially deposited while the parent levees continue to aggrade. The onset of the new channel then occurs, but again, the parent channel keep on aggrading some times simultaneously with levee deposition from the new channel. This stage records a progressive transfer of the main activity from the parent to the new channel. This progressive transfer of activity is at the origin of the longitudinal backstepping architecture the levee of A21, and ends by the definitive abandonment of the parent channel.

-Chapter VI-

Synthesis and conclusions

1 MAIN CONCLUSIONS AND DISCUSSION

The study of the Amazon Fan highlighted the great complexity of the HARPs architecture (at the scale of multi-channel high-resolution seismic data) and their lithological heterogeneity.
The study of some specific zones within the Zaïre Fan allowed to reveal both the earliest stages of an avulsion process related to levee breaches and first splays linked to unconfined flows on the levee, and the latest stage of this process, with the first levee deposition and evolution following the HARPs deposition.

From this study, I illustrated and described in details:

-A possible triggering mechanism of the avulsion and the first HARP deposits

The triggering mechanism, i.e. the event that allowed the turbidity currents to escape from the levee confinement, has been shown to be a levee failure, in the examples I found (channel S3, and possibly initial stage of splay 1 of channel A16). In the case of S3 it did not evolve. In the case of splay 1 the levee failure progressively evolve to erosive pathway where overflow processes became concentrated and deposited reworked products of upfan erosion of the channel and levee.
The A16 splays of the Zaïre Fan shows that levee breaches allowed the following flow inside the channel or at least part of it to incise deeper than the downfan part of the older channel. This retrogressive incision further headward in the upfan part of the older channel allows creating an obstacle to the downfan part of the channel and can probably lead to its abandonment if the flows are thinner than the height of the obstacle.

From literature, alignment of erosional scours due to successive erosional overflow processes has also been described as a triggering mechanism of levee breach (e.g. Monterey Fan: Figueiredo et al, 2007).

-The HARPs architecture and associated processes

The channel avulsion process in the Amazon Fan is characterized by the deposition of HARPs, 30 to 40 km (for the Brown and 1D HARP deposits respectively) from the avulsion point at the base of the newly formed channel-levee system. The location and the three-dimensional geometry of the HARPs is directly controlled by the degree of confinement of the gravity currents and thus by the pre-existing morphology.
The HARP deposits represent a stacking of several nested predominantly sandy sedimentary bodies, in which flows evolve in a complex manner. Numerous angular contacts and

erosional features are observed. They allow dividing the HARP bodies into internal elementary sub-bodies, revealing the existence of several depositional processes that contributed to build the HARPs. The different sub-units can be associated either to mainly depositional pattern (flat-lying reflectors, transparent patches) or erosional features (U- or V-shaped reflectors) or to a mix of depositional/erosional pattern (chaotic patches) in analogy to channel-infills (from seismic facies similarities and as well from lithologic facies similarities). No regular lateral and longitudinal migrations have been observed.
Therefore the HARPs, besides mainly constituted by homogeneous massive deposits resulting from sandy unconfined flows (flat-lying sub-units), are also zones of by-pass of flows that are confined by previous deposition (chaotic patches and erosive features).

-The evolution of levee aggradation consecutive to an avulsion up to the abandonment of the parent channel

The Zaïre avulsion A21/A22 showed an example where, during a transition time, the turbidity currents have been maintained along the pathway of the older channel, while the HARPs of the new channel were still being deposited, shortly followed by the onset of the new levees (new channel). This simultaneous activity of both pathways was accompanied by a progressive transfer of the activity from the parent channel to the new channel, until the definitive abandonment of the parent channel.
These seismic observations were made only for this example and I cannot generalize them to other avulsion in the Zaïre Fan, nor to other fans. However, the examination of the ages provided in the Amazon Fan (see Chapter IV.3) suggested a possible time interval of synchronous activity of the Brown and Nouveau systems, that could support the observations made in the A21/22 avulsion zone of the Zaïre Fan.
I suspect that the occurrence of this transitional phase of synchronous activity depends on the capacity of the flow to incise the new channel. Rapid aggradation of the splays thalwegs will create a barrier between the upfan and downfan branch of the old channel. Depending on their sizes, the following flows will be either deflected in the downfan direction along the splay (barrier height > flow height) or partly maintained in the parent channel (barrier height < flow height).
The capacity to incise of the currents flowing into the new channel depends on:

- The slope of the underlying morphology: high slope angle favors rapid and strong erosion,
- The nature of the substrate in relation to the erosional capacity of the flow.

In any case, I propose that, during the initial stages of the avulsion (splay time), unless levee breach had completely destroyed the levee, the barrier is not high enough to confine the

flows and the first currents that flow into this new geometry will probably be thick enough to overcome the obstacle and maintain the activity of the parent channel for a while. Depending on the erosional capacity of the flows, the duration of this phase of synchronous activity will be variable, possibly too short to be observable at the seismic scale.

2 SYNTHESIS: TOWARDS A CONCEPTUAL MODEL

These results provide new insights for the understanding of the processes involved during an avulsion (levee breach, HARPs accumulation, levee aggradation) and clues to refine the previous conceptual models and to reach a higher resolution knowledge of this process, by describing the inter-relationship of the different architectural sub-bodies of the HARPs and giving details on both the earliest and latest stages of the avulsion (Figure VI.1).

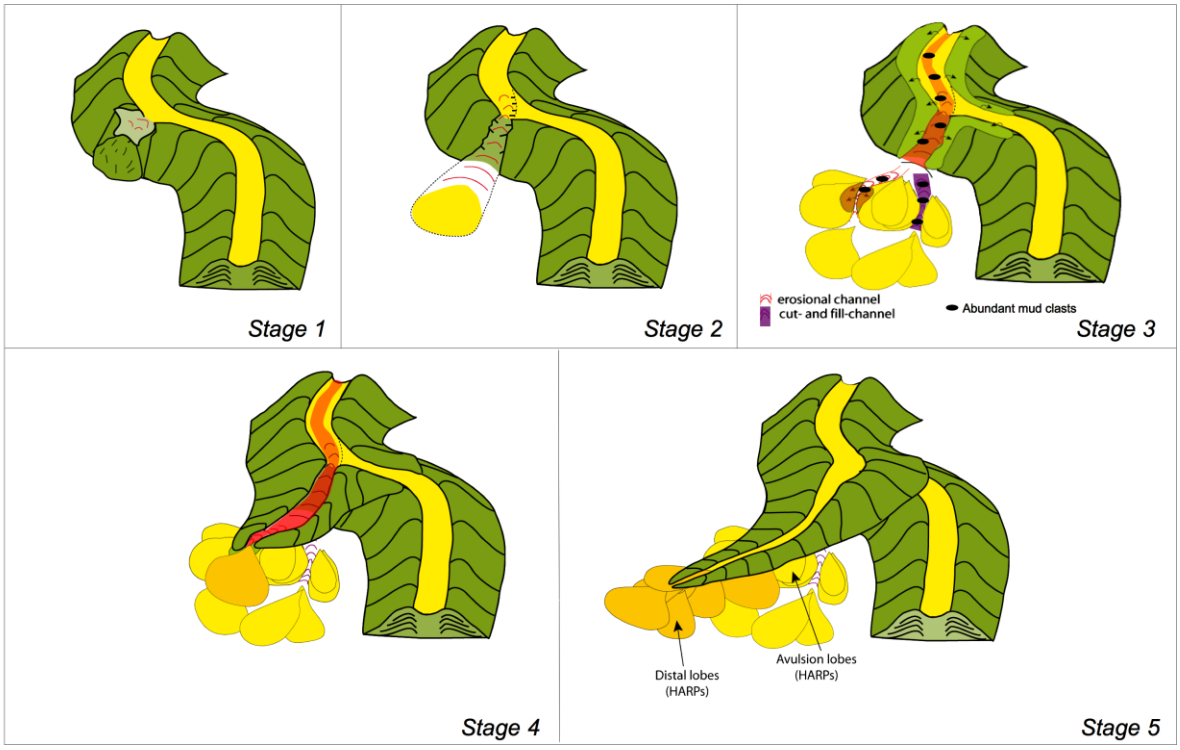

Figure VI.1: Schematic view of the different steps describing an avulsion process, built on observation and interpretation in this study.

The initial stage of the avulsion process is related to a breach of the levee (Figure VI.2) as observed on levees of the Zaïre Fan.).

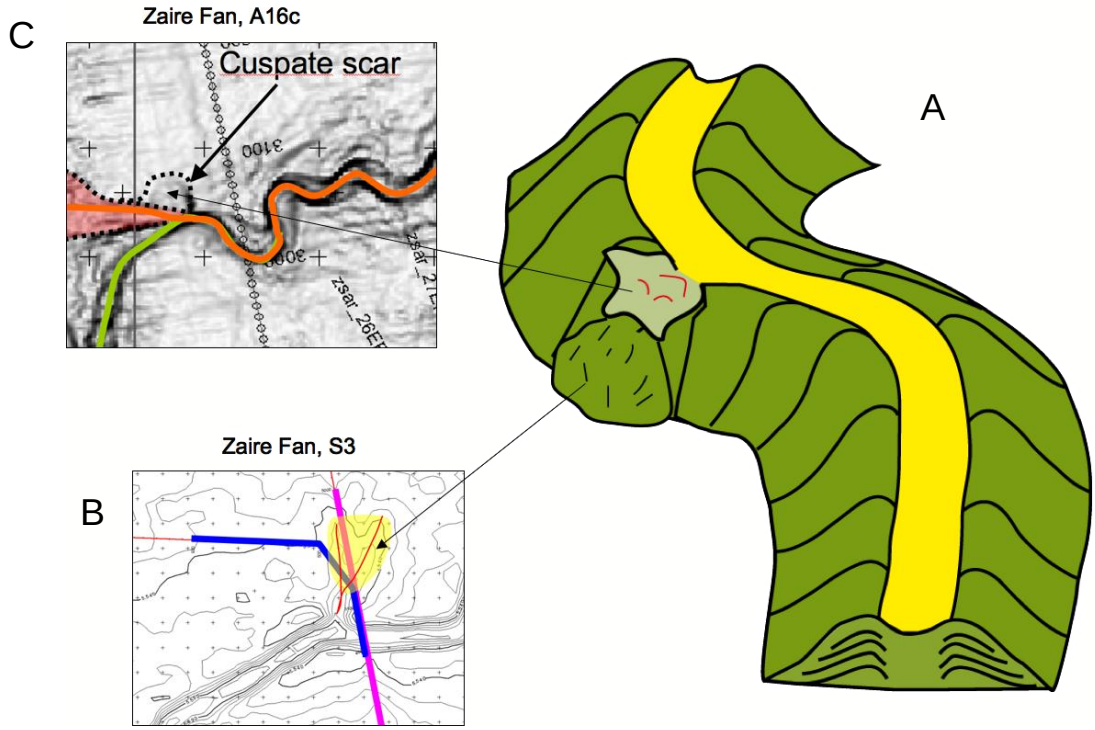

Figure VI.2: Initial stage of the avulsion. A: Levee breach can be provoked by levee failure, as observed on (B) the levee of S3 channel (see Figure V.13) and (C) possibly A16 channel (see Figure V.10) in the Zaïre Fan.

Stage 2: HARPs initiation *(Figure VI.2)*

A new pathway for the turbidity currents has been created from the breach at the levee crest towards the adjacent outer levee morphologic low (see Figure V.10). The new erosional pathway connects downfan to transparent splays, and is incised 20 to 25 m deeper than the thalweg of the main channel (see Figure V.11). This feature is composed of an erosional part and a depositional part further downfan (yellow depositional lobate feature on Figure VI.2). I suspect that these features are analogues to the crevasse splays observed in time slices of 3D seismic data (Posamentier and Kolla, 2007; Chapter I).

Crevasse splays can either evolve to a channel avulsion or just be recorded as an unconformable depositional feature inside the levees of the channels.

The crevasse splays observed on the Zaïre Fan sea-floor (Figure VI.2B), could be the analogues of the buried features observed inside the Amazon Fan levees (see Chapter IV.2), where erosional parts of plaeo-crevasse splays could be preserved as internal erosional unconformities of the levees and their depositional parts could be recorded as wedge-shaped transparent features (slumps) or high-amplitude reflectors (sandy deposits) (Figure VI.2C).

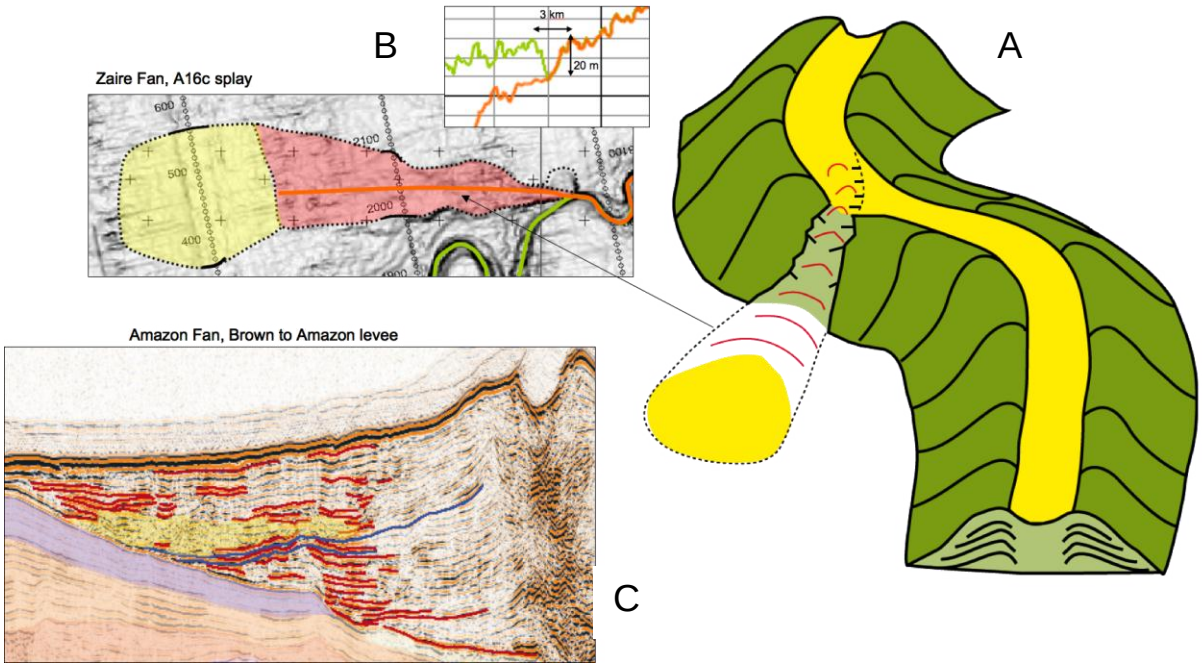

Figure VI.2: HARPs initiation stage. A new pathway is now available for turbidity currents that flow unconfined and deposit reworked material on the outer levee (A) as observed on the Zaïre Fan (B) (see Figures V.10 and V.11). In the case the avulsion continues, upward erosion finally results in the possible formation of a morphologic barrier inside the channel that will prevent the turbidity currents to keep on flowing in the down-avulsion point part of the initial channel. In the case the avulsion did not finally occur, splays can be recovered inside the levee deposits as interpreted in the Amazon Fan levees (Figure IV.9) (C).

Stage 3: HARP deposition *(Figure VI.3)*

If the activity of the crevasse splay, initiated during stage 2, persists, i.e. the following flows use the pathway of the crevasse splays, further depositional lobes will be accumulated down-levee. The depositional lobes are accumulated through successive lobe deposits of unconfined flows. They are probably stacked up close to each others, filling probably the lowest parts of the local area accessible by the currents. By filling-up one area, the morphology is modified and the following flow will be diverted resulting in a probably braided system (Figures IV.46 and VI.3A).

The sandy lobes have been associated (see Chapter IV.4) to the high-amplitude flat-lying seismic facies within the HARPs. Note that one lobe defined on the seismic data (i.e. one high-amplitude flat-lying reflector) probably corresponds to several succesive flow events.

The inter-lobe lows are relatively confined areas, allowing local channelizing of flows (Figure VI.3B, C) that will incise and create micro-channels as observed as U-or V-shaped features within the HARPs of the Amazon Fan. U-or V-shaped features are exclusively erosional, whereas chaotic patches can represent cut- and fill features (from other studies and due to their resemblance to the HARs of the Amazon Fan).

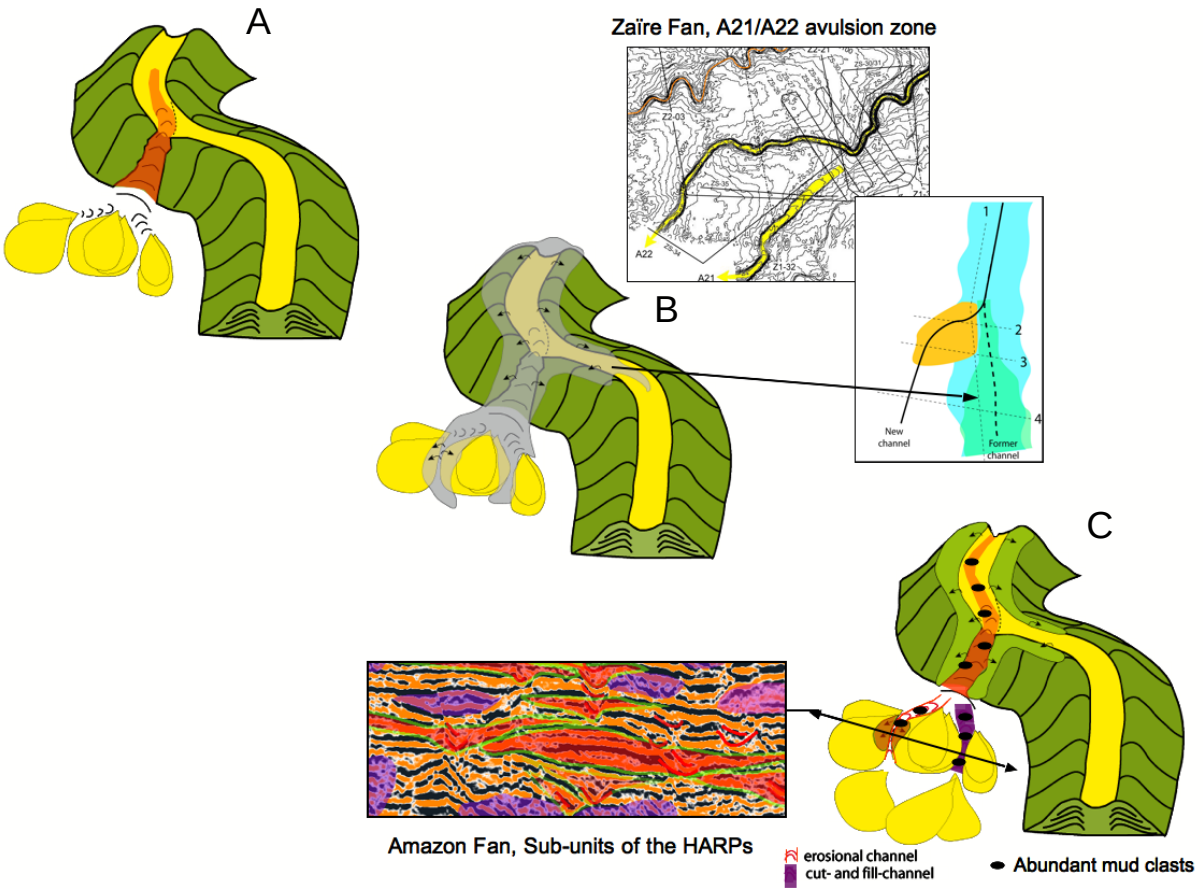

Figure VI.3: HARPs deposition stage. Shifting depocenters evolve from diverted turbidity currents due to permanently modified topography in the HARPs deposition zone (A), compare Figure IV.46. Turbidity currents (marked in transparent gray) can be divided at the avulsion point and maintain the synchronous activity along the downfan pathway of the older channel and along the new pathway into adjacent lows where the unconfined flows deposit HARPs as observed for the A21/22 avulsion in the Zaïre Fan (Figure V.16A) (B). In the HARPs deposition zone, turbidity currents can be channelized through inter-lobe lows (B). The depositional features associated to the channelized flows within the HARPs are recorded on seismic as U- or V-shaped features (marked by red incisions) with eventually associated overflow deposits (flat-lying reflectors colored in red), and cut- and fill structures (chaotic patches colored in purple). The channelized deposits show in the correlated lithologic intervals zones of abundant mud-clasts (compare Chapter IV.2.4.1.) (C).

During the deposition of the different sub-units of the HARPs, because retrogressive erosion inside the channel upstream from the avulsion point is not yet sufficient, turbidity flows continue to feed the parent channel and to build levees, as observed in the avulsion zone A21/A22 of the Zaïre Fan (Figure VI.3B).

Stage 4: onset of the new channel-levee system (Figure VI.4)

During this stage, a new channel will develop over the lobe-shaped deposits and micro-channels.

I propose that the transition from HARP deposits to overlying channel-levee system could be an autocyclic process: the levees at the new channel-mouth continue to develop and prograde and progressively reach the depocenters of the HARPs. At one moment the flows

could be captured by an existing micro-channel within the HARPs and eventually develop into a major channel in continuation of the upfan channel.

I think, even though I did not observe it, that a channel-mouth lobe can eventually develop at the termination of the newly created proto-channel-levee system.

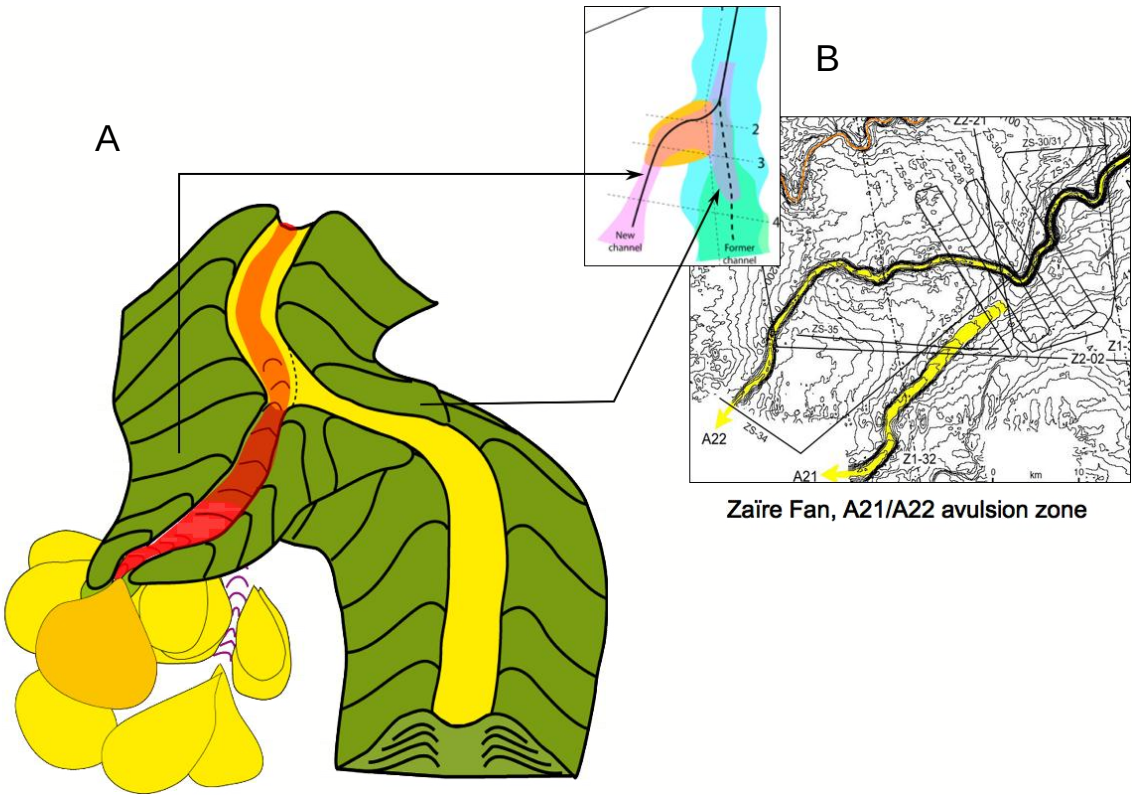

Figure VI.4: Onset of the new channel-levee system. A: Levees of the new pathway are developing. Aggradation of the levees results in the confinement of the flows that allows the system prograding onto the HARPs sub-units, the new channel eventually occupying the course of a micro-channel formed at stage 3.B, as observed in the Zaïre Fan, both channels are synchronously active (Figure V.16).

At this time, the parent channel can still be active as observed in the Zaïre Fan (avulsion A21/A22), receiving turbidity currents and building levees (Figure VI.4B). However these levees are progressively less and less developed while those of the new channel becomes thicker and thicker.

Stage 5: Abandonment of the parent channel (Figure VI.5)

The latest stage is characterized by the definitive abandonment of the parent channel, probably in response to a deep incision inside the channel upstream the avulsion point, and to the barrier effect that it provokes on the turbidity currents. This definitive abandonment results in the infilling of the parent channel by overbank deposits from the new channel.

I cannot exclude the possibility that channel-mouth develop at the termination of the newly

created channel. However the transition between the HARPs related to the avulsion and channel-mouth lobes has not been observed.

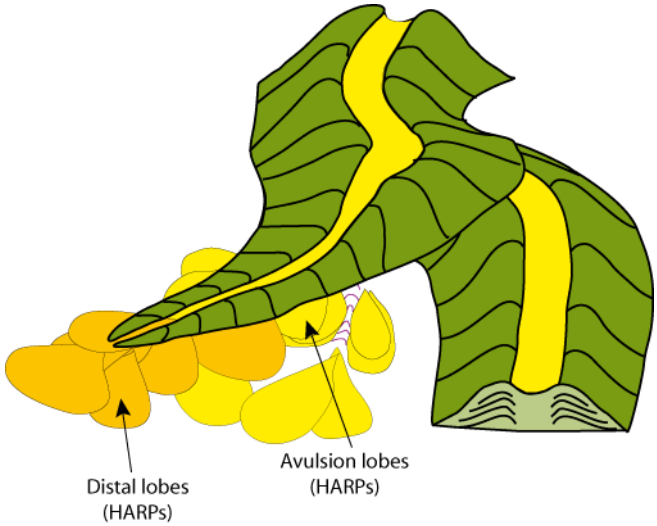

Figure VI.5: The new channel is a single active channel prograding over its HARPs.

3 LIMITS OF MY MODEL AND PERSPECTIVES

This refined conceptual model is based on several hypotheses that should be confirmed if possible. One of these hypothesis concerns the lithological nature of the splays observed on the levee of channel A16 of the Zaïre Fan. Ground truthing with conventional corings should bring needed lithological information.

Although I showed that the avulsion process do not provoke abrupt changes, but is a long-lived process that is responsible for the accumulations of several successive specific deposits, I think it would be necessary to give a timing and measure durations of the successive stages of the avulsion, by corings and dating sediments. Further sampling of sediments drilled in the Amazon Fan also could be achieved in order to obtain new datations and eventually confirm the problematic ages (particularly the dates that indicate a synchronous activity of Brown and Aqua systems).

Finally, my study suggests that the underlying morphology played an important role on the avulsion process, including impacts of slope gradient on the behaviour of the flows, on the rapidity of the incision creating a barrier for flows to the downfan branch of the parent channel, and on the distance between the HARPs and the avulsion point.
This autogenic morphological influence needs to be quantified by a detailed analysis of the

topographic evolution during the avulsion. The avulsion A21/22 (Zaïre Fan) would be a good example to conduct this detailed analysis based on the already interpreted horizons. This together with the timing information would allow quantifying volumes of sediments generated at each step of the avulsion. Future data acquisitions (seismic and corings, Reprezaï cruise) are planned on the downfan prolongation of these channels and will provide the knowledge of the entire systems, including additional avulsions and terminal lobes, necessary to measure total sediment volumes involved.

-References-

Allen, J.R.L., 1971. Mixing at turbidity current heads, and its geological implications. Journal of Sedimentary Petrology, 41: 97-113.

Appi, C.J., Kowsmann, R.O., Flood, R.D., Manley, P.L., and Pirmez, C., 1988. Evoluçao Quaternária Pós-Glacial do cone submarino do Amazonas: um modelo retrogradante. Avais XXXV Congr. Brasileriro Geol. 2, pp. 451-465.

Arz, H.W., Pätzold, J. and Wefer, G., 1998. Correlated millennial-scale changes in surface hydrography and terrigenous sediment yield Inferred from last-glacial marine deposits off Northeastern Brazil. Quaternary Science Reviews, 50: 157-166.

Babonneau, N., 2002. Mode de fonctionnement d'un chenal turbiditique méandriforme: Cas du système turbiditique actuel du Zaïre; Thèse de doctorat, Université de Bordeaux I, 308 pp.

Babonneau, N., Savoye, B., Droz, L., Morash, A. and Bez, M., 2005. Large modern deep-sea fans: the Amazon Channel versus the Zaire Channel. In: A.A. Convention (Editor), Calgary, Canda, 19-22 June, Abstracts Volume, p. A9.

Bellaiche, G. et al., 1983. Morphologie au sea-beam de l'éventail sous-marin profond du Rhône (Rhône deep-sea fan) et de son canyon afférant. Comptes Rendus de l'Academie des Sciences - Series II, 296: 579-583.

Bonnel, C., Dennielou, B., Droz, L., Mulder, T. and Berné, S., 2005. Architecture and depositional pattern of the Rhône Neofan and recent gravity activity in the Gulf of Lions (western Mediterranean). Marine and Petroleum Geology, 22: 827-843.

Bouma, A.H., 1962. Sedimentology of some flysch deposits: A graphic approach to facies interpretation. Elsevier, 168 pp.

Bowen, A.J., Normark, W.R. and Piper, D.J.W., 1984. Modelling of turbidity currents on Navy submarine Fan, California continental borderland, Sedimentology, pp. 161-185.

Brandão, J.A.S. and Feijó, F.J., 1994. Bacia da Foz do Amazonas. Boletim de Geociências da Petrobrás, 8: 91-99.

Britter, R.E. and Simpson, J.E., 1978. Experiments on the dynamics of a gravity current head. Journal of Fluid Mechanics, 88: 223-240.

Bukry, D., 1973. Low-amplitude coccolith biostratigraphic zonation. In: Edgar, N.T., Saunders, J.B., et a., Initial Reports DSDP, 15: Washington (U.S. Govt. Printing Office), 685-703.

Bukry, D., 1975. Coccolith and silicoflagellate stratigraphy, northwestern Pacific Ocean, Deep Sea Drilling Project Leg 32. In: Larson, R.L., Moberly, R., et al., Initial Reports DSDP, 32: (U.S. Govt. Printing Office), 677-701.

Bukry, D., 1978. Biostratigraphy of Cenozoic marine sediment by calcareous nannofossils, Micropaleontology, 24:44-60.

Castro, J.C., Miura, K. and Braga, J.A.E., 1978. Stratigraphic and structural framework of

the Foz do Amazonas Basin, 10th Annual Offshore Technology Conference, pp. 1843- 1847.

Cisowski, S., 1995. Synthesis of magnetic remanence correlation, Leg 155. In: R.D. Flood, D.J.W. Piper and A. Klaus (Editors), Proceedings of the Ocean Drilling Program, Initial Reports, 155. College Station, TX (Ocean Drilling Program), pp. 701-702.

Cisowski, S. and Hall, F., 1997. An examination of the paleointensity record and geomagnetic excursions recorded in Leg 155 cores. In: R.D. Flood, D.J.W. Piper, A. Klaus and L.C. Peterson (Editors), Proceedings of the Ocean Drilling Program, Scientific Results, 155. College Station, TX (Ocean Drilling Program), pp. 231-244.

Cobbold, P.R., Morgues, R. and Boyd, K., 2004. Mechanism of thin-skinned detachement in the Amazon Fan, assessing the importance of fluid overpressure and hydrocarbon generation. Marine and Petroleum Geology, 21: 1013-1025.

Damuth, J.E., 1973. The western equatorial Atlantic: morphology, quaternary sediments, and climatic cycles, Columbia University, 358 pp.

Damuth, J.E. and Kumar, N., 1975. Amazon cone: morphology, sediments, ages and grow pattern, Geological Society of America Bulletin, 86: 863-878.

Damuth, J.E. and Embley, R.W., 1981. Mass-transport processes on the Amazon Cone: western equatorial Atlantic. AAPG Bulletin, 65: 629-643.

Damuth, J.E., Kolla, V., Flood, R.D., Kowsmann, R.O., Monteiro, M.C., Gorini, M.A., Palma, J.J.C., and Belderson, R.H., 1983a. Distributary channel meandering and bifurcation patterns on Amazon deep-sea fan as revealed by long-range side-scan sonar (GLORIA), Geology, 11: 94-98.

Damuth, J.E., Kowsmann, K.O., Flood, R.D., Belderson, R.H. and Gorini, M.A., 1983b. Age relationships of distributary channels on Amazon deep-sea fan: implications for fan growth pattern. Geology, 11: 470-473.

Damuth, J.E. and Flood, R.D., 1984. Morphology, sedimentation processes, and growth pattern on the Amazon deep-sea fan. Geo-Marine Letters, 3: 109-117.

Damuth, J.E. and Flood, R.D., 1985. Amazon Fan, Atlantic Ocean. In: A.H. Bouma, W.R. Normark and N.E. Barnes (Editors), Submarine Fans and Related Turbidites Systems. SpringerVerlag, NewYork, pp. 97-106.

Damuth, J.E., Flood, R.D., Kowsmann, R.O., Belderson, R.H. and Gorini, M.A., 1988. Anatomy and growth pattern of Amazon deep-sea fan as revealed by long-range side-scan sonar (GLORIA) and high-resolution seismic studies. American Association of Petroleum Geologists Bulletin, 72: 885-911.

Dennielou, B. and Jouanneau, J.M., submitted. Ages and duration of sedimentary objects and sediment accumulation rates.

Devroey, E., 1941. Le bassin hydrographique congolais spécialement celui du Bief maritime: Institut Royal Colonial Belge, Section des Sciences Techniques. Mémoire Collection N° 8,

tome III, fasc. 3: 3-160.

Driscoll, N.W. and Karner, G.D., 1994. Flexural deformation due to Amazon Fan loading: A feedback mechanism affecting sediment delivery to margins. Geology, 22: 1015- 1018.

Droz, L. and Bellaiche, G., 1991. Seismic facies and geologic evolution of the central portion of the Indus Fan. In: P. Weimer and M.H. Link (Editors), Seismic Facies and Sedimentary Processes of Submarine Fans and Turbidite Systems. Springer Verlag, New York, pp. 383-402.

Droz, L., Marsset, T., Savoye, B. and Spy-Anderson, F.-L., 2002. Channel Transfer Processes in the Zaïre Turbidite System (ZaïAngo Project), AAPG Annual Meeting, Houston, March 2002, Poster, Abstract book, P. A45.

Droz, L., Marsset, T., Ondréas, H., Lopez, M., Savoye, B., Spy-Anderson, F.-L., 2003. Architecture of an active mud-rich turbidite system: The Zaire Fan (Congo-Angola margin southeast Atlantic): Results from ZaïAngo 1 and ZaÄngo 2 cruises. AAPG Bulletin, 87: 1145-1168.

Droz, L. and Marsset, T., submitted. New insights on avulsion processes, Chapter 7. In: N. Babonneau, B. Savoye and A. Morash (Editors), Key results of the integrated study of the modern Zaïre/Congo Fan (ZaïAngo Project). Edition Total-Ifremer.

Ericson, D.B., 1961. Pleistocene climatic record in some deep-sea sediment cores. Ann. N.Y. Acad. Sci., 95: 537-541.

Ericson, D.B. and Wollin, G., 1968. Pleistocene climates and chronology in deep-sea sediments. Science, 162: 1227-1234.

Figueiredo, A.G., Hoorn, C., van der Ven, P. and Soares, E., 2009. Late Miocene onset of the Amazon River and the Amazon deep-sea fan: Evidence from the Foz do Amazonas Basin. Geology, 37: 619-622.

Fildani, A. and Normark, W.R., 2004. Late Quaternary evolution of channel and lobe complexes of Monterey Fan. Marine Geology, 206: 199-223.

Flood, R.D., Manley, P.L., Kowsmann, R.O., Appi, C.J. and Pirmez, C., 1991. Seismic facies and late Quaternary growth of Amazone submarine fan. In: P. Weimer and M.H. Link (Editors), Seismic facies and sedimentary processes of submarine fans and turbidite systems. Springer-Verlag, New York, pp. 415-433.

Flood, R.D. and Damuth, J.E., 1987. Quantitative characteristics of sinuous distributary channels on the Amazon deep-sea fan. Geological Society of America Bulletin, 98: 728-738.

Flood, R.D. and Piper, D.J.W., 1997. Amazon Fan sedimentation: the relationship to equatorial climate change, continental denudation, and sea-level fluctuations. In: R.D. Flood, D.J.W. Piper, A. Klaus and L.C. Peterson (Editors), Proceedings of the Ocean Drilling Program, Scientific Results, 155, College Station, TX (Ocean Drilling Program), pp. 653-675.

Flood, R.D., Piper, D.J.W., Klaus, A. et al., 1995. Leg Synthesis, In: R.D. Flood, D.J.W.

Piper, and A. Klaus (Editors), Proceedings of the Ocean Drilling Program, Initial Reports, 155. College Station, TX (Ocean Drilling Program), pp. 17-21.

Flood, R.D., Piper, D.J.W., Klaus, A. et al., 1995. Explanatary Notes, In: R.D. Flood, D.J.W. Piper and A. Klaus (Editors), Proceedings of the Ocean Drilling Program, Initial Reports, 155. College Station, TX (Ocean Drilling Program), pp. 47-81.

Flood, R.D., D.J.W. Piper and A. Klaus (Editors), 1995. Proceedings of the Ocean Drilling Program, Initial Reports, 155. College Station, TX (Ocean Drilling Program), 1233 pp.

Flood, R.D., Piper, D.J.W., Klaus, A. and Peterson, L.C., 1997. Proceedings of the Ocean Drilling Program, Scientific Results, 155. College Station, TX (Ocean Drilling Program), 695 pp.

Flood, R.D., Pirmez, C. and Yin, H., 1997. The compressional-wave velocity of Amazon Fan sediments: calculation from index properties and variation with clay content. In: R.D. Flood, D.J.W. Piper, A. Klaus and L.C. Peterson (Editors), Proceedings of the Ocean Drilling Program, Scientific Results, 155. College Station, TX (Ocean Drilling Program), pp. 477-498.

Flower, B.P. and Kennett, J.P., 1900. The Younger Dryas cool episode in the Gulf of Mexico. Paleoceanography, 5: 949-961.

García, M., 1994. Depositional turbidity currents laden with poorly sorted sediment. Journal of Hydraulic Engineering, 120: 1240-1263.

Garcia, M. and Parker, G., 1989. Experiments on hydraulic jumps in turbidity currents near a canyon-fan transition. Science, 245: 393-396.

Garcia, M. and Parker, G., 1993. Experiments on the entrainment of sediments into suspension by a dense bottom current. Journal of Geophysical Research, 98: 4793- 4807.

Gartner, S., 1977. Calcareous nannofossil biostratigraphy and revised zonation of the Pleistocene. Marine Micropaleontology, 2:1-25.

Gervais, A., Mulder, T., Savoye, B., Migeon, S. and Cremer, M., 2001. Recent processes of levee formation on the Zaire deep-sea fan. Comptes Rendus de l'Academie des Sciences - Series IIA 332: 371-378.

Gervais, A. et al., 2004. Present morphology and depositional architecture of a sandy submarine system: the Golo turbidite system (Eastern margin of Corsica). In: S. Lomas and P. Joseph (Editors), Confined Turbidite Systems. Geological Society, Special Publication, London, pp. 59-89.

Hackbarth, C.J. and Shaw, R.D., 1994. Morphology and stratigraphy of a mid-Pleistocene turbidite leveed channel from seismic, core and log data, northeastern Gulf of Mexico. In: P. Weimer, A.H. Bouma and B.F. Perkins (Editors), Submarine fans and turbidite systems, Gulf Coast Society of the Society of Economic Paleontologists and Mineralogists Foundation, 15th Annual Research Conference, pp. 127-133.

Halbouty, M.T., 2001. Exploration into the new millennium. In: M.W. Downey, J.C. Threet,

W.A., Morgan (Editors), Petroleum provinces of the twenty-first century, AAPG memoir, 74, pp. 11-19.

Hay, A.E., 1987. Turbidity currents and and submarine channel formation in Rupert Inlet, British Columbia. 2. The roles of continuous and surge-type flow. Journal of Geophysical Research, 92: 2883-2900.

Heezen, B.C. and Ewing, M., 1952. Turbidity currents and submarine slumps, and the 1929 Grand Banks earthquake. American Journal of Science, 250: 849-873.

Heezen, B.C., Menzies, R.J., Schneider, E.D., Ewing, W.M. and Granelli, N.C.L., 1964. Congo submarine canyon, American Association of Petroleum Geologists Bulletin, pp. 1126-1149.

Hiscott, R.N., Hall, F.R. and Pirmez, C., 1997. Turbidity-current overspill from the Amazon channel: Texture of the silt/sand load, paleoflow from anisotropy of magnetic susceptibility and implication for flow processes. In: R.D. Flood, D.J.W. Piper, A. Klaus and L.C. Peterson (Editors), Proceedings of the Ocean Drilling Program, Scientific Results, 155. College Station, TX (Ocean Drilling Program), pp. 53-78.

Hübscher, C., Spiess, V., Breitzke, M. and Weber, M.E., 1997. The youngest channel-levee system of the Bengal Fan: results from digital sediment echosounder data. Marine Geology, 141: 125-145.

Imran, J., Parker, G. and Katopodes, N., 1998. A numerical model of channel inception on submarine fans. Journal of Geophysical Research, 103: 1219-1238.

Imbrie, J.M. et al., 1984. The orbital theory of the Pleistocene climate: support from revised chronology of the marine δ 18-O record. In: A. Berger, J. Imbrie, J. Hays, G. Kukla and B. Saltzman (Editors), Milankovitch and Climate (Pt. 1), NATO ASI Ser. C, Math Phys. Sci., pp. 269-306.

Jégou, I., 2008. Etude de la transition chenal-levées/lobes dans les syteèmes turbiditiques récents, Institut Universitaire de la Mer, Université de Bretagne Occidentale, 350 pp.

Jégou, I., Savoye, B., Pirmez, C. and Droz, L., 2008. Channel-mouth lobe complex of the recent Amazon Fan: The missing piece. Marine Geology, 252: 62-77.

Kenyon, N.H., Amir, A. and Cramp, A., 1995a. Geometry of the younger sediment bodies of the Indus Fan. In: K.T. Pickering, R.N. Hiscott, N.H. Kenyon, F. Ricci Lucchi and R.D.A. Smith (Editors), Atlas of deep water environments: architectural style in turbidite systems. Chapman & Hall, London, pp. 89-90.

Kenyon, N.H., Millington, L., Droz, L. and Ivanov, M.K., 1995b. Scour holes in a channel-lobe transition zone on the Rhône cone. In: K.T. Pickering, R.N. Hisccott, N.H. Kenyon, F.R. Lucchi and R.D.A. Smith (Editors), Atlas of Deep-water Environments: Architectural Styles in Turbidite Systems, pp. 212-215.

Kenyon, N.H., Klaucke, I., Millington, L. and Ivanov, M.K., 2002. Sandy submarine

canyon- mouth lobes on the western margin of Corsica and Sardinia, Mediterranean Sea. Marine Geology, 184: 69-84.

Klaucke, I., Masson, D.G., Kenyon, N.H. and Gardner, J.M., 2004. Sedimentary processes of the lower Monterey Fan channel and channel-mouth lobe. Marine Geology, 206: 181- 198.

Kneller, B., 1995. Beyond the turbidite paradigm: physical models for deposition of turbidites and their implications for reservoir prediction. In: A.J. Hertley and D.J. Prosser (Editors), Characterization of Deep Marine Clastic Systems, Geological Society Special Publications, 94, pp.31_49.

Kneller, B.C. and Buckee, C., 2000. The structure and fluid mechanics of turbidity currents: a review of some recent studies and their geological implications. Sedimentology, 47: 62-94.

Kolla, V., 2007. A review of sinuous channel avulsion patterns in some major deep-sea fans and factors controlling them. Marine and Petroleum Geology, 24: 450-469.

Komar, P.D., 1971. Hydraulic jumps in turbidity currents, Geological society of America Bulletin, pp. 1477-1488.

Komar, P.D., 1973. Continuity of turbidity current flow and systematic variations in deep-sea channel morphology, Geological Society of America Bulletin, pp. 3329-3338.

Kuehl, S.A., 1986. Nature of sediment accumulation on the Amazon continental shelf. Continental Shelf Research, 6: 209-225.

Kuenen, P.K. and Magliorini, C.I., 1950. Turbidity currents as a cause of graded bedding. Journal of Geology, 58: 91-127.

Leduc, G. et al., 2007. Moisture transport across Central America as a positive feedback on abrupt climatic changes. Nature, 445: 908-911.

Lopez, M., 2001. Architecture and depositional pattern of the Quaternary deep-sea fan of the Amazon. Marine and Petroleum Geology, 18: 479-486.

Lowe, D.R., 1982. Sediment gravity flows: II-depositional models with special reference to the deposits of high-density turbidity currents. Journal of Sedimentary Petrology, 52: 279-297.

Mahaffie, M.J., 1994. Reservoir classification for turbidite intervals at the Mars discovery, Mississippi Canyon 807, Gulf of Mexico. In: P. Weimer, A.H. Bouma and B.F. Perkins (Editors), Submarine Fans and Turbidite Systems, Gulf Coast Society of the Society of Economic Paleontologists and Mineralogists Foundation, 15th Annual Research Conference, pp. 233-244.

Manley, P.L. and Flood, R.D., 1988. Cyclic sediment deposition within Amazon deep-sea fan. American Association of Petroleum Geologists Bulletin, 72(8): 912-925.

Marsset, T., Droz, L., Dennielou, B. and Pichon, E., submitted. Cycles in the architecture of the Quaternary Zaire Turbidite System: a possible link with climate. SEPM Special Publication - Society for Sedimentary Geology, 92.

Martinson, D.G. et al., 1987. Age dating ad the orbital theory of the ice ages: development of a high-resolution 0 to 300,000-year chronostratigraphy. Quaternary Science Reviews, 27: 1-29.

Maslin, M., Vilela, C.G. and Mikkelsen, N., 2005. Causation of the Quaternary catastrophic failures of the Amazon Fan deduced from stratigraphy and benthic foraminiferal assemblages. Quaternary Science Reviews, 24: 2180-2193.

Maslin, M., Knutz, P.C. and Ramsay, T., 2006. Millennial-scale sea-level control on avulsion events on the Amazon Fan. Quaternary Science Reviews, 25: 3338-3345.

Mello, M.R., Mosmann, S.R.P., Maciel, R.R. and Miranda, F.P., 2001. Foz do Amazonas area: The last frontier for elephant hydrocarbon accumulations in the South Atlantic realm. In: J.C.T. Downey and W.A. Morgan (Editors), Petroleum provinces of the twenty-first century: AAPG Memoir, pp. 403-414.

Menard, H.W., 1955. Deep-sea channels, topography, and sedimentation. AAPG Bulletin, 39: 236-255.

Miall, A.D., 1999. In defense of facies classifications and models. Journal of Sedimentary Research, 69: 2-5.

Middleton, G.V., 1966. Experiments on density and turbidity currents: I Motion of the head, Canadian Journal of Earth Sciences, pp. 523-546.

Middleton, G.V. and Hampton, M.A., 1973. Turbidites and deep water sedimentation, SEPM Pacific Section.

Migeon, S., 2000. Dunes géantes et levées sédimentaires en domaine marin profond: approches morphologique, sismique et sédimentologique. Implications pour la reconnaissance des processus de transport et de dépôt des sédiments et pour la formation de corps sableux en domaine profond; Thèse de doctorat, Université de Bordeaux I. 288 pp.

Migeon, S., Savoye, B. and J.-C., F., 2000. Quaternary development of migrating sediment waves in the Var deep-sea fan; distribution, growth pattern, and implication for levee evolution. Sedimentary Geology, 133: 265-293.

Migeon, S., Savoye, B., Babonneau, N. and Andersson, F.L.S., 2004. Processes of sediment-wave construction along the present Zaïre deep-sea meandering channel: role of meanders and flow stripping. Journal of Sedimentary Research, 74: 202-208.

Mikkelsen, N., Maslin, M., Giraudeau, J. and Showers, J.W., 1997. Biostratigraphy and sedimentation rates of the Amazon Fan. In: R.D. Flood, D.J.W. Piper, A. Klaus and L.C. Peterson (Editors), Proceedings of the Ocean Drilling Program, Scientific Results, 155. College Station, TX (Ocean Drilling Program), pp. 577-594.

Moguedet, G., 1988. Les relations entre le fleuve Congo et la sédimentation récente sur la marge continentale entre l'embouchure et le sud du Gabon: Etude hydrologique, sédimentologique et géochimique, Doctorat d'Etat, Univeristy of Angers, Angers.

Molinier, M., Guyot, J.L., de Oliveira, E., Guimarães, V., Chaves, A., 1993. Hydrologie du bassin de l'Amazone. Grands Bassins Fluviaux, Paris, 22-24 novembre, pp. 335-344.

Morris, W.R., Kenyon, N.H., Limonov, A. and Alexander, J., 1998. Donstream changes of large-scale bedforms in turbidites around the Valencia channel mouth, north-west Mediterranean: implications for paleoflow reconstruction. Sedimentology, 45: 365- 377.

Mulder, T. and Syvitski, J.P.M., 1995. Turbidity currents generated at river mouths during exceptional discharges to the world oceans, Journal of Geology, pp. 285-299.

Mulder, T. and Cochonat, P., 1996. Classification of offshore mass movements. Journal of Sedimentary Research, 66: 43-57.

Mulder, T. and Alexander, J., 2001. The physical character of subaqueous sedimentary density flows and their deposits. 2001, 48: 269-299.

Murray, J. and Renard, A.F., 1891. Report on deep-sea deposits based on specimens collected during the voyage of HMS Challenger in the years 1873-1876: In 'Challenger' Reports. HMSO, London, 525 pp.

Mutti, E. and Ricci Lucchi, F., 1972. Le torbiditi dell' Appennino Settentrionale: introduzione all'analisi di facies. Memoria Società Geologica d'Italia, 11: 161-199.

Mutti, E. and Normark, W.R., 1987. Comparing examples of modern and ancient turbidite systems: problems and concepts. In: J.K. Leggett and G.G. Zuffa (Editors), Marine Clastic Sedimentology. Graham and Trotman, London, pp. 1-38.

Mutti, E. and Normark, W.R., 1991. An integrated approach to the study of turbidite systems. In: P. Weimer and M.H. Link (Editors), Seismic Facies and Sedimentary Processes of Submarine Fans and Turbidite Systems, pp. 75-107.

Nittrouer, C.A., Sharara, DeMaster, D.J., 1983. Variations of sediment texture on the Amazon continental shelf. Jour. Sed. Petrol, 53: 179-191.

Nittrouer, C.A., Kuehl, S.A., DeMaster, D.J., Kowsmann, R.O., 1985.The deltaic nature of Amazon shelf sedimentation. Geological Society of America Bulletin, 97: 444-458.

Nittrouer, C.A. and Kuehl, S.A., 1995. Geological Significance of sediment transport and accumulation on the Amazon Continental Shelf. Marine Geology, 125: 175-400.

Nittrouer, C.A. and DeMaster, D.J., 1996. The Amazon Shelf setting: tropical, energetic, and influenced by a large river. Continental Shelf Research, 16: 553-573.

Normark, W.R., 1970. Growth patterns of deep-sea fans. American Association of Petroleum Geologists Bulletin, 54: 2170-2195.

Normark, W.R., Piper, D.J.W. and Hess, G.R., 1979. Distributary channels, sand lobes, and mesotopography of Navy submarine fa,; California Borderland, with applications to ancient fan sediments. Sedimentology, 26: 749-774.

Normark, W.R. and Piper, D.J.W., 1984. Navy Fan, California Borderland: grwoth pattern and depositional processes. Geo-Marine Letters, 3: 101-108.

Normark, W.R., Damuth, J.E. et al., 1997. Sedimentary facies and associated depositional elements of the Amazon fan. I In: R.D. Flood, D.J.W. Piper, A. Klaus and L.C. Peterson (Editors), Proceedings of the Ocean Drilling Program, Scientific Results, 155. College Station, TX (Ocean Drilling Program), pp. 611-651.

Normark, W.R., Piper, D.J.W. and Hisccott, R.N., 1998. Sea level controls on the textural characteristics and depositional architecture of the Huneme and associated fan systems, Santa Monica Basin, California. Sedimentology, 45: 53-70.

Okada, H. and Bukry, D., 1980. Supplementary modification and introduction of code numbers to the low-latitude coccolith biostratigraphic zonation (Bukry, 1973; 1975). Marine Micropaleontology, 5: 321-325.

Payton, C.E., 1977. Seismic Stratigraphy-applications to hydrocarbon exploration. AAPG Memoir 26, 516 pp.

Peakall, J., McCaffrey, B. and Kneller, B.C., 2000. A process model for the evolution, morphology, and architecture of sinuous submarine channels. Journal of Sedimentary Research, 70: 434-448.

Peterson, R.G., Stramma, L., 1991. Upper-level circulation in the South Atlantic Ocean. Progress in Oceanography, 26: 1-73.

Pettinghill, H.S. and Weimer, P., 2002. Worldwide deepwater exploration and production: Past, present, and future. The Leading Edge, 21: 371-376.

Piper, D.J.W. and Normark, W.R., 1983. Turbidite depositional patterns and flow characteristics, Navy Submarine Fan, California Borderland, Sedimentology, pp. 681- 694.

Piper, D.J.W., Normark, W.R. and Hiscott, R.N., 1995. Holocene sand body geometry, Huneme Fan, California Borderland. In: K.T. Pickering, R.N. Hiscott, N.H. Kenyon, F.R. Lucchi and R.D.A. Smith (Editors), Atlas of Deep-water Environments: Architectural Styles in Turbidite Systems, pp. 203-206.

Piper, D.J.W. et al., 1997. Synthesis of stratigraphic correlations of the Amazon Fan. In: R.D. Flood, D.J.W. Piper, A. Klaus and L.C. Peterson (Editors), Proceedings of the Ocean Drilling Program, Scientific Results, 155. College Station, TX (Ocean Drilling Program), pp. 595-610.

Piper, D.J.W., Deptuck, M..E., 1997. Fine-grained turbidites of the Amazon Fan; facies chracterization and interpretation. In: R.D. Flood, D.J.W. Piper, A. Klaus and L.C. Peterson (Editors), Proceedings of the Ocean Drilling Program, Scientific Results, 155. College Station, TX (Ocean Drilling Program), pp. 79-108.

Piper, D.J.W., Hisccott, R.N. and Normark, W.R., 1999. Outcrop-scale acoustic facies analysis and letest Quaternary development of Huneme and Dume submarine fans, offshore California. Sedimentology, 46: 47-78.

Pirmez, C., 1994. Growth of a submarine meandering channel-levee system on the Amazon

fan. PhD Thesis, Columbia University, 587 pp.

Pirmez, C., Hiscott, R.N. and Kronen, J.D.J., 1997. Sandy turbidite successions at the base of channel-levee systems of the Amazon fan revealed by FMS logs and cores: unravelling the facies architecture of large submarine fans. In: R.D. Flood, D.J.W. Piper, A. Klaus and L.C. Peterson (Editors), Proceedings of the Ocean Drilling Program, Scientific Results, 155. College Station, TX (Ocean Drilling Program), pp. 7-33.

Pirmez, C., Beaubouef, R.T., Friedmann, S.J. and Mohrig, D.C., 2000. Equilibrium profile and baselevel in submarine channels; examples from late Pleistocene systems and implications for the architecture of deepwater reservoirs. In: P. Weimer et al. (Editors), Deep water reservoirs of the world. GCSSEPM Foundation, Houston, pp. 782-805.

Pisias, N.G. et al., 1984. High resolution stratigraphic correlation of benthic oxygen isotopic records spanning the last 300,000 years. Marine Geology, 56: 119-136.

Popescu, I., Lericolais, G., Panin, N., Wong, H.K. and Droz, L., 2001. Late Quaternary channel avulsions on the Danube deep-sea fan, Black Sea. Marine Geology, 179: 25- 37.

Popescu, I., 2002. Analyse des processus sédimentaires récents dans l'éventail profond du pp. 282.

Posamentier, H., Erskine, R.D. and Mitchum, R.M., Jr., 1991. Models for submarine fan deposition within a sequence stratigraphic framework. In: P. Weimer and M.H. Link (Editors), Seismic Facies and Sedimentary Processes of Submarine Fans and Turbidite Systems. Springer-Verlag, New York, pp. 127-136.

Posamentier, H. and Kolla, V., 2003. Seismic geomorphology and stratigraphy of depositional elements in deep-water settings. Journal of Sedimentary Research, 73.

Posamentier, H., 2007. Deep-water turbidites and submarine Fans. SEPM Special Publication - Society for Sedimentary Geology, 84: 399-520.

Postma, G., Nemec, W. and Kleinspehn, K.L., 1988. Large floating clasts in turbidites: a mechanism for their emplacement, Sedimentary Geology, pp. 47-61.

Prell, W.L. et al., 1986. Graphic correlation of oxygen isotope stratigraphy: application to the late Quaternary. Paleoceanography, 1: 137-162.

Pujos, A. and Giraudeau, J., 1993. Réparation des Neolaerhabdacas (nannofossiles calcaires) dans le Quaternaire moyen et supérieur des océans Atlantique et Pacifique. Oceanologica Acta, 16: 349-362.

Raffi, I., Backman, J., Rio, D., Shackleton, N.J. 1993. Plio-Pleistocene nannofossil biostratigraphy and calibration to oxygen isotope stratigraphies from Deep Sea Drilling Project Site 607 and Ocean Drilling Program Site 677. Paleoceanography, 8: 387-408.

Reading, H.G. and Richards, M., 1994. Turbidites systems in deep-water basin margins classified by grain size and feeder system, American Association of Petroleum Geologists Bulletin, pp. 792-822.

Reading, H.G., 1996. Sedimentary Environments: Processes, Facies and Stratigraphy. Blackwell Science, 688 pp.

Reis, A.T., Perovano, R., Silca, C.G., Vendeville, B.C., Araújo, E., Gorini, C., Oliveira, V., submitted. Multi-scale gravitational collapse in the Amazon Deep-sea Fan: a coupled system of gravity tectonics and mass wasting processes. Journal of the Geological Society of London.

Rossetti, D.F. and Valeriano, M.M., 2007. Evolution of the lowest amazon basin modeled from the integration of geological and SRMTD topographic data. Catena, 70: 253-265.

Savoye, B. et al., 2000. Structure et évolution récente de l'éventail turbiditique du Zaire; premiers résultats scientifiques des missions d'exploration Zaiango 1 & 2 (marge Congo-Angola). Comptes Rendus de l'Academie des Sciences, Serie II. Sciences de la Terre et des Planetes, 331: 211-220.

Savoye, B., Babonneau, N., Denneliou, B. and Bez, M., in press. Geological overview of the Angola-Congo margin, the Congo deep-sea fan and its submarine valleys. Deep-Sea Research II.

Schwenk, T., Spiess, V., Hübscher, C. and Breitzke, M., 2003. Frequent channel avulsions within the active channel-levee system of the middle Bengal Fan, an exceptional channel-levee development derived from Parasound and Hydrosweep data. Deep Sea Research, PART II 50: 1023-1045.

Schwenk, T., Spiess, V., Breitzke, M. and Hübscher, C., 2005. The architecture and evolution of the Middle Bengal Fan in vicinity of the active channel-levee system imaged by high-resolution seismic data. Marine and Petroleum Geology: 637-656.

Shanmugam, G., 2000. 50 years of the turbidite paradigm (1950s--1990s): deep-water processes and facies models--a critical perspective. Marine and Petroleum Geology, 17: 285-342.

Shipboard Scientific-Party, 1995a. Site 935. In: R.D. Flood, D.J.W. Piper, A. Klaus et al. (Editors), Proceedings of the Ocean Drilling Program, Scientific Results, 155. College Station, TX (Ocean Drilling Program), pp. 273-319.

Shipboard Scientific-Party, 1995b. Site 936. In: R.D. Flood, D.J.W. Piper, A. Klaus et al. (Editors), Proceedings of the Ocean Drilling Program, Scientific Results, 155. College Station, TX (Ocean Drilling Program), pp. 321-382.

Shipboard Scientific-Party, 1995c. Site 944. In: R.D. Flood, D.J.W. Piper, A. Klaus et al. (Editors), Proceedings of the Ocean Drilling Program, Scientific Results, 155. College Station, TX (Ocean Drilling Program), pp. 591-633.

Shipboard Scientific-Party, 1995d. Site 945. In: R.D. Flood, D.J.W. Piper, A. Klaus et al. (Editors), Proceedings of the Ocean Drilling Program, Scientific Results, 155. College Station, TX (Ocean Drilling Program), pp. 635-655.

Shipboard Scientific-Party, 1995e. Site 946. In: R.D. Flood, D.J.W. Piper, A. Klaus et al. (Editors), Proceedings of the Ocean Drilling Program, Scientific Results, 155. College Station, TX (Ocean Drilling Program), pp. 657-693.

Shipboard-Scientific-Party, 1995f. Site 940. In: R.D. Flood, D.J.W. Piper, A. Klaus et al. (Editors), Proceedings of the Ocean Drilling Program, Scientific Results, 155. College Station, TX (Ocean Drilling Program), pp. 463-501.

Shepard, F.P., McLoughlin, P.A., Marshall, N.F. and Sullivan, G.G., 1977. Current-meter recordings of low speed turbidity currents. Geology, 5: 297-301.

Showers, J.W., Schneider, R., Mikkelsen, N. and Maslin, M., 1997. Isotopic stratigraphy of Amazon Fan Sediments, Proceedings of the Ocean Drilling Program, Scientific Results, pp. 281-304.

Siddall, M., Rohling, E.J., Almogi-Labin, A., Hemleben, C., Meischner, D., Schmelzer, I. and Smeed, D.A., 2003. Sea-level fluctuations during the last glacial cycle. Nature, 423: 853-858.

Silva, S.R.P., Maciel, R.R. and Severino, M.C.G., 1999. Cenozoic tectonics of Amazon Mouth Basin. Geo-Marine Letters, 18: 256-262.

Simpson, J.E., 1969. Effects of the lower boundary on the head of a gravity current. Journal of Fluid Mechanics, 53: 759-768.

Smith, D.G. and Sandwell, D.T., 1997. Global seafloor topography from satellite altimetry and ship depth soundings. Science, 277: 1957-1962.

Sommerfield, C.K., Nittrouer, C.A. and Figueiredo, A.G., 1995. Stratigraphic evidence of changes in Amazon shelf sedimentation during the late Holocene. Marine Geology, 125: 351-371.

Stow Dorrik, A.V. and Shanmugam, G., 1980. Sequence of structures in fine-grained turbidites: comparison of recent deep-sea and ancient flysch sediments. Sedimentary Geology, 25: 23-42.

Stow Dorrik, A.V., Reading, H.G. and Collinson, J.D., 1996. Deep Seas. In: H.G. Reading (Editor), Sedimentary Environments. Blackwell Science pp. 395-454.

Stow, D.A.V. and Mayall, M., 2000. Deep-water sedimentary systems: New models for the 21st century. Marine and Petroleum Geology, 17: 125-135.

Stuiver, M. and Grootes, P.M., 2000. GISP2 oxygen isotope ratios. Quaternary Science Reviews, 53: 277-284.

Tiedemann, R., Sarnthein, M. and Shackleton, N.J., 1994. Astronomic timescale for the Pliocene Atlantic δ 18-O and dust flux records of ODP site 659. Paleoceanography, 9: 619-638.

Turakiewicz, G., 2004. Mécanismes forçants dans les éventails turbiditiques de marges matures - Exemple de l'éventail Quaternaire du Congo; Thèse de doctorat, Université

Montpellier II, 367 pp.

Twitchell, D.C., Schwab, W.C. and Kenyon, N.H., 1995. Geometry of sandy deposits at the distal edge of the Mississippi Fan, Gulf of Mexico. In: K.T. Pickering, R.N. Hisccott, N.H. Kenyon, F.R. Lucchi and R.D.A. Smith (Editors), Atlas of Deep-water Environments: Architectural Styles in Turbidite Systems, pp. 282-286.

Vail, P.R., Mitchum, R.M. and Thompson, S., 1977. Seismic stratigraphy and global changes of sea level, part 3: relative changes of sea level from coastal onlap. In: C.E. Peyten (Editor), Seismic Stratigraphy - Applications to Hydrocarbon Exploration. American Association of Petroleum Geologists, pp. 63-81.

Van Weering, T.C.E. and Van Iperen, J., 1984. Fine-grained sediments of the Zaire deep-sea fan, southern Atlantic Ocean. In: D.A.V. Stow and D.J. Piper (Editors), Fine-grained sediments: deep-water processes and facies. Blackwell Scientific Publications, London, pp. 95-113.

Vilela, C.G. and Maslin, M., 1997. Benthic and planktonic foraminifers and stable isotopic analysis of mass-flow sediments in the Amazon Fan. In: R.D. Flood, D.J.W. Piper, A. Klaus and L.C. Peterson (Editors), Proceedings of the Ocean Drilling Program, Scientific Results, 155. College Station, TX (Ocean Drilling Program), pp. 335-352.

Walker, R.G., 1978. Deep-water sandstone facies and ancient submarine fans: models for exploration for stratigraphic traps. AAPG BUlletin, 62: 932-966.

Wang, X. et al., 2004. Wet periods in northeastern Brazil over the past 210 kyr linked to distant climate anomalies. Nature, 432: 270-273.

Weaver, P.P.E., 1993. High-resolution stratigraphy of marine Quaternary sequences. In: E.A. Hailwood and R.B. Kidd (Editors), High resolution stratigraphy. Geol. Soc. Special Publication, pp. 137-153.

Wefer, G., H.W. Berger and C. Richter (Editors), 1998. Proceedings of the Ocean Drilling Program, Initial Reports, 175. (Ocean Drilling Program), College Station, TX (Ocean Drilling Program), 1477 p.

Wefer, G, H.W. Berger and C. Richter (Editors), 2002. Proceedings of the Ocean Drilling Program: Scientific results, 175. (http://www-odp.tamu.edu/publications/175_SR/175sr.htm) accessed September 4, 2009.

Weimer, P., 1990. Sequence stratigraphy, seismic geometries and depositional history of the Mississippi Fan, deep Gulf of Mexico. AAPG Bulletin, 74: 425-453.

Weimer, P. and Link, M.H., 1991. Seismic Facies and Sedimentary Processes of Submarine Fans and Turbidite Systems, 447 pp.

Wynn, R.B., Kenyon, N.H., Masson, D.G., Stow, D.A.V. and Weaver, P.E., 2002. Characterization and recognition of deep-water channel-lobe transition zones. AAPG Bulletin, 86: 1441-1462.

Zaragosi, S. et al., 2000. Physiography and recent sediment distribution of the Celtic Deep-Sea Fan, Bay of Biscay. Marine Geology, 169: 207-237.

-ANNEX-

Sites	Environment	System	Time top (s)	Time base (s)	Thickness time (s)	Depth top (m)	Depth base (m)
930	levee	Aqua	4.1983	4.2605	0.0622	0.00	45.64
	levee	Purple	4.2605	4.3170	0.0565	45.64	89.28
	levee	Orange-1 A	4.3170	4.4316	0.1146	89.28	184.18
	channel-infill	Orange-1 B	4.4316	4.5255	0.0939	184.18	268.30
940	levee	Brown	4.2723	4.3968	0.1245	0.00	95.25
	levee	Nouveau	4.3968	4.4700	0.0732	95.25	154.86
	levee	Aqua	4.4700	4.5702	0.1002	154.86	240.79
	HARPs	Aqua	4.5702	4.5913	0.0211	240.79	259.52
935	levee	Brown	4.6465	4.6878	0.0413	0.00	30.53
	levee	Aqua	4.6878	4.7726	0.0848	30.53	96.33
	HARPs	Aqua	4.7726	4.8065	0.0339	96.33	123.81
	levee	Orange-1 B	4.8065	4.8354	0.0289	123.81	147.77
	HARPs	Orange-1 B	4.8354	4.8658	0.0304	147.77	173.49
	debris flow	URMTD	4.8658	4.9727	0.1069	173.49	268.23
934	Channel-infill	Brown	4.5641	4.7390	0.1749	0.00	138.06
936	levee	Brown	4.7666	4.8436	0.0770	0.00	59.09
	levee	Brown	4.8436	4.8584	0.0148	59.09	70.74
	HARPs	Brown	4.8584	4.8919	0.0335	70.74	97.48
	levee	Orange-1 B	4.8919	4.9153	0.0234	97.48	116.44
	HARPs	Orange-1 B	4.9153	4.9615	0.0462	116.44	154.59
	debris flow	URMTD	4.9615	5.1073	0.1458	154.59	281.11
943	levee	1D	4.9171	4.9772	0.0601	0.00	45.27
	HAR	1D	4.9772	5.0385	0.0613	45.27	93.89
	levee	1D	5.0385	5.0687	0.0302	93.89	118.74
	levee	Brown	5.0687	5.0935	0.0248	118.74	139.59
944	levee	1D	4.9265	5.0402	0.1137	0.00	87.25
	levee	Brown	5.0402	5.0810	0.0408	87.25	120.06
	HARPs	Brown	5.0810	5.1225	0.0415	120.06	154.23
	HARPs	HARPs X	5.1225	5.1656	0.0431	154.23	190.60
	URMTD	URMTD	5.1656	5.2347	0.0691	190.60	250.74
945	HAR	1B	5.4980	5.5209	0.0229	7.03	16.66
	HARPs	1D	5.5209	5.5318	0.0109	0.00	24.90
	HARPs	HARPs X	5.5318	5.6195	0.0877	24.90	98.18
946	levee	1B	5.4593	5.4800	0.0207	0.00	15.53
	levee	1C	5.4800	5.4915	0.0115	15.53	24.12
	levee	1D	5.4915	5.5174	0.0259	24.12	43.91
	HARPs	1D	5.5174	5.5427	0.0253	43.91	63.60
	HARPs	HARPs X	5.5427	5.6142	0.0715	63.60	121.07

ANNEX III.1a: Seismic units and depositional systems at sites 930, 940, 935, 934, 936, 943, 944, 945 and 946 from up to downfan from interpretation in this study. Limits of seismic units are indicated in ms twt and converted after the time-depth chart of Flood et al. (1997) (see Chapter III).

Sites	Environment	Systems	Time top (s)	Time base (s)	Thickness time (s)	Depth top (m)	Depth base (m)	Thickness (m)	ODP units	Sub-units	Depth top (m)	Depth base (m)	Thickness (m)
935 A	HARPs	Aqua	4.7726	4.8065	0.0339	96.33	123.81	27.48	IIIA	IIIAa	98.5	113.08	14.58
935 A	Levee	Orange -1 B	4.8065	4.8354	0.0289	123.81	147.77	23.96	IIIA	IIIAb	113.08	132	18.92
										IIIAc	132	135.77	3.77
										IIIAd	135.77	151.67	15.90
									IIIB	IIIBa	151.67	171.5	19.83
935 A	HARPs	Orange -1 B	4.8354	4.8658	0.0304	147.77	173.49	25.72		IIIBb1	171.5	173.4	1.9
										IIIBb2	173.4	178.87	5.47
										IIIBc	179	189.6	10.6
										IIIBd	189.6	199.3	9.7
936 A	HARPs	Brown	4.8584	4.8919	0.0335	70.74	97.48	26.73	IIIA	IIIAa	72.10	99.40	27.30
										IIIAb	99.40	106.30	6.9
936 A	levee	Orange -1 B	4.8919	4.9153	0.0234	97.48	116.44	18.97	IIIB	IIIBa	106.30	112.30	6.00
										IIBb	112.30	117.00	4.70
936 A	HARPs	Orange -1 B	4.9153	4.9615	0.0462	116.44	154.59	38.15	IIC		117.00	154.5	37.50
944 A	HARPs	Brown	5.0810	5.1225	0.0415	120.06	154.23	34.18	IIC	IICb	124.00	130.00	6.00
										IICc	130.00	140.63	10.63
944 A	HARPs	Brown and HARPs X	5.1225	5.1656	0.0431	154.23	190.60	36.36		IICd	140.63	182.00	41.37
944 A	HARPs	HARPs X	5.1225	5.1656	0.0431	154.23	190.60	36.36	IID		182.00	191.60	9.60
945 A	HARPs	1D	5.5209	5.5318	0.0109	16.66	24.90	8.23	III upper part below 8 m		8	75.26	73.80
945 A	HARPs X	facies on URMT D	5.5318	5.6195	0.0877	24.90	98.18	73.28	III basal part				
946 A	HARPs	1D	5.5174	5.5427	0.0253	43.91	63.60	19.68	IIIC	IIICb	45.00	67	22
946 A	HARPs	HARPs X	5.5427	5.6142	0.0715	63.60	121.07	57.47	IV	IIICb basal part	67.00	128.72	61.72

ANNEX III.1b: HARPs seismic units correlated to ODP lithologic units or sub-units in this study. The limits of seismic units converted in mbsf match generally well with the lithological units (variances less than 10 m). The most important variance has been observed for the top of the Orange-1 B HARPs (values marked in red).

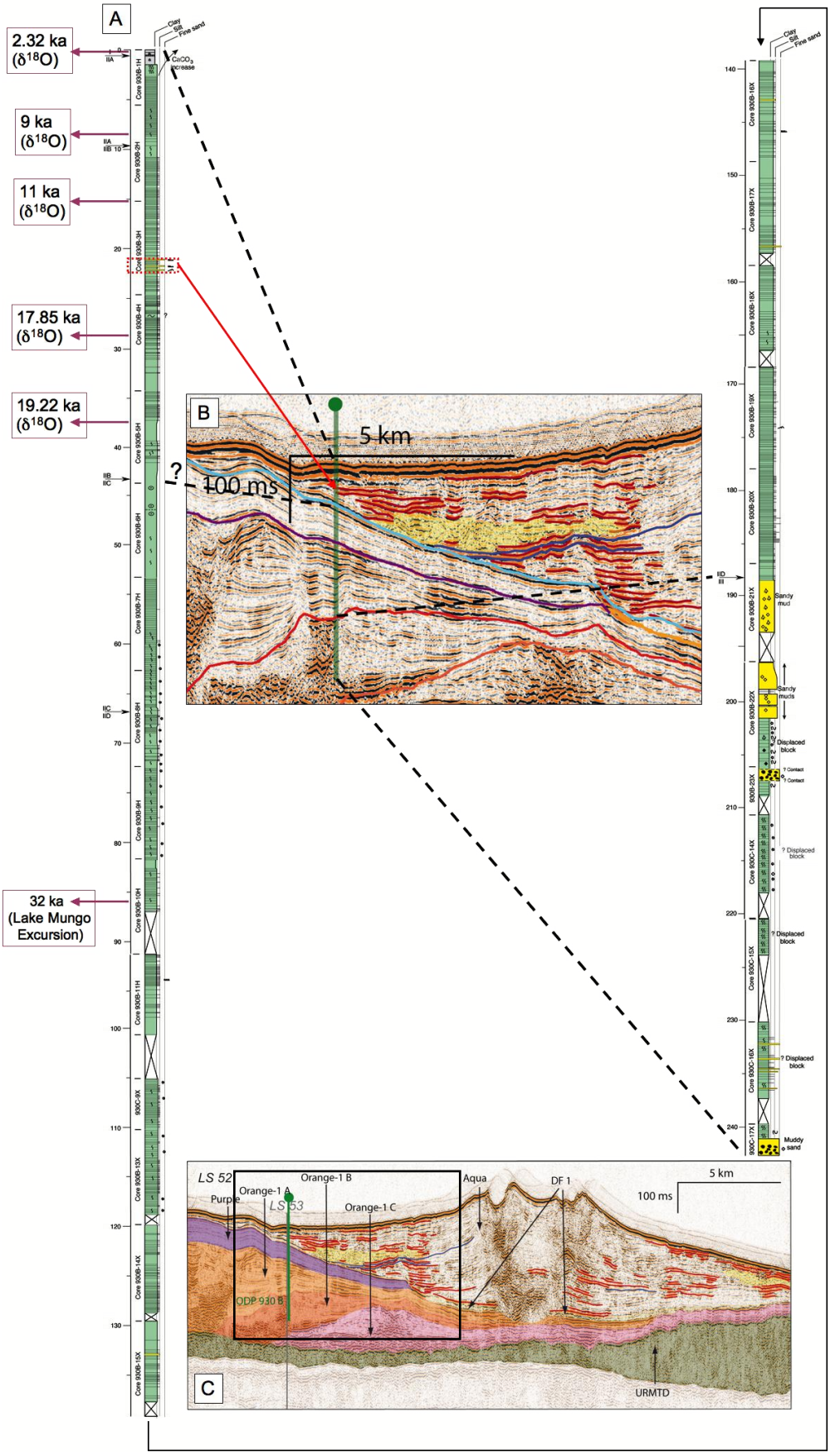

ANNEX III.2a: A: Synthetic log at site 930 with indicated datations. B: Zoom on cored facies. C: Interpreted seismic line showing localization of site and deposition systems.

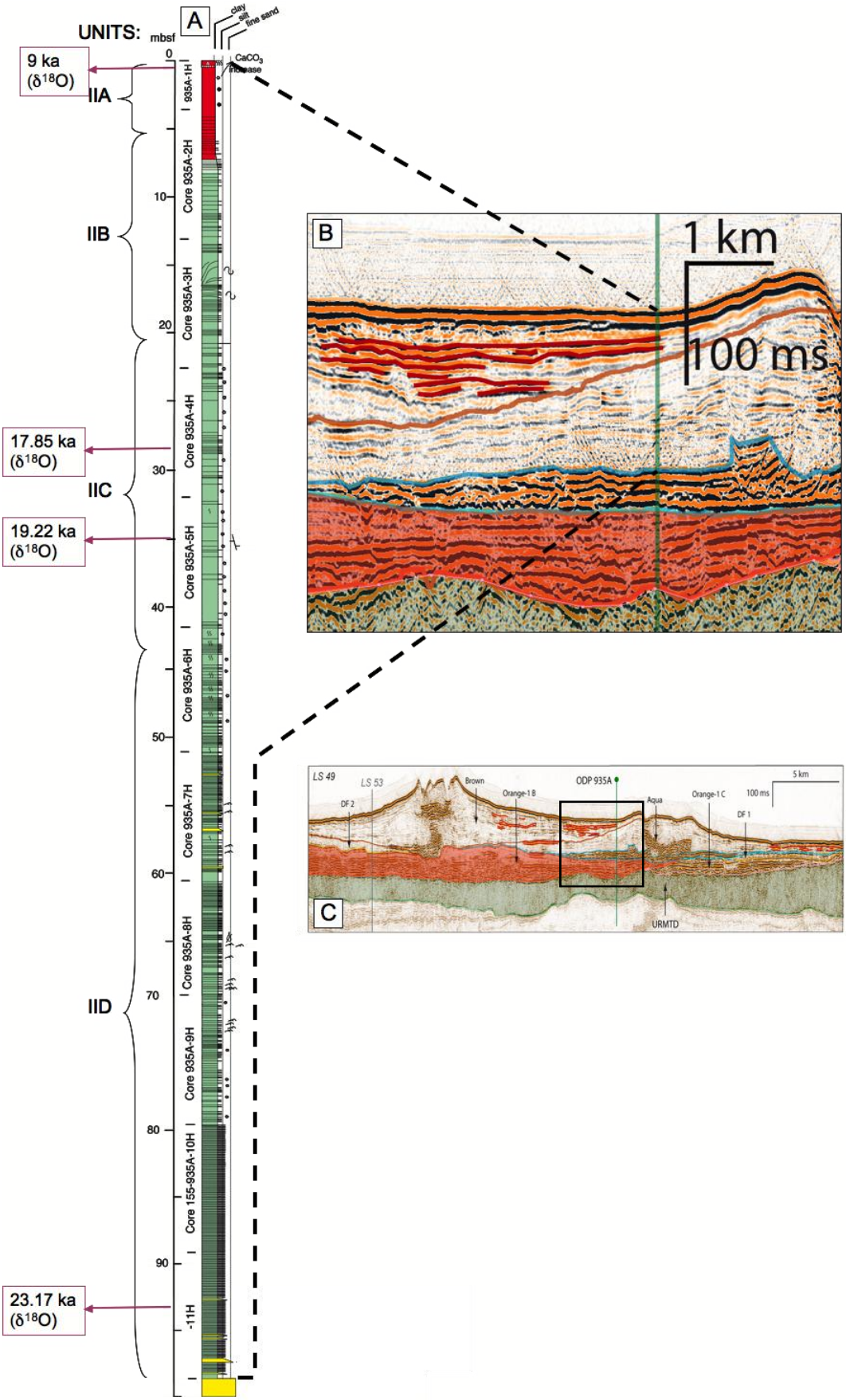

ANNEX III.2b: A: Synthetic log for the levee deposits at site 935 with indicated datations. B: Zoom on cored facies. C: Interpreted seismic line showing localization of site and deposition systems.

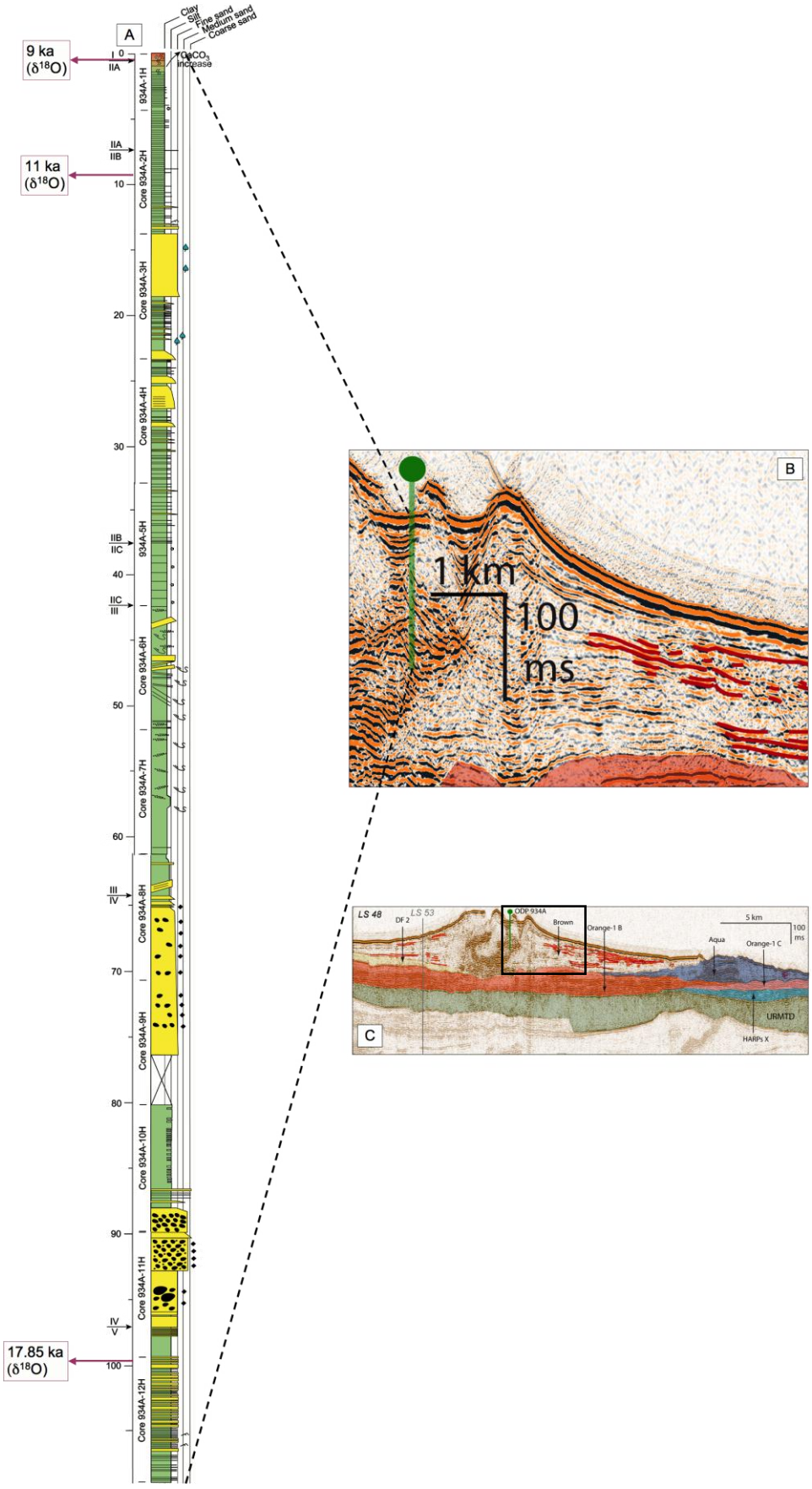

ANNEX III.2c: A: Synthetic log at site 934. B: Zoom on cored facies. C: Interpreted seismic line showing localization of site and deposition systems.

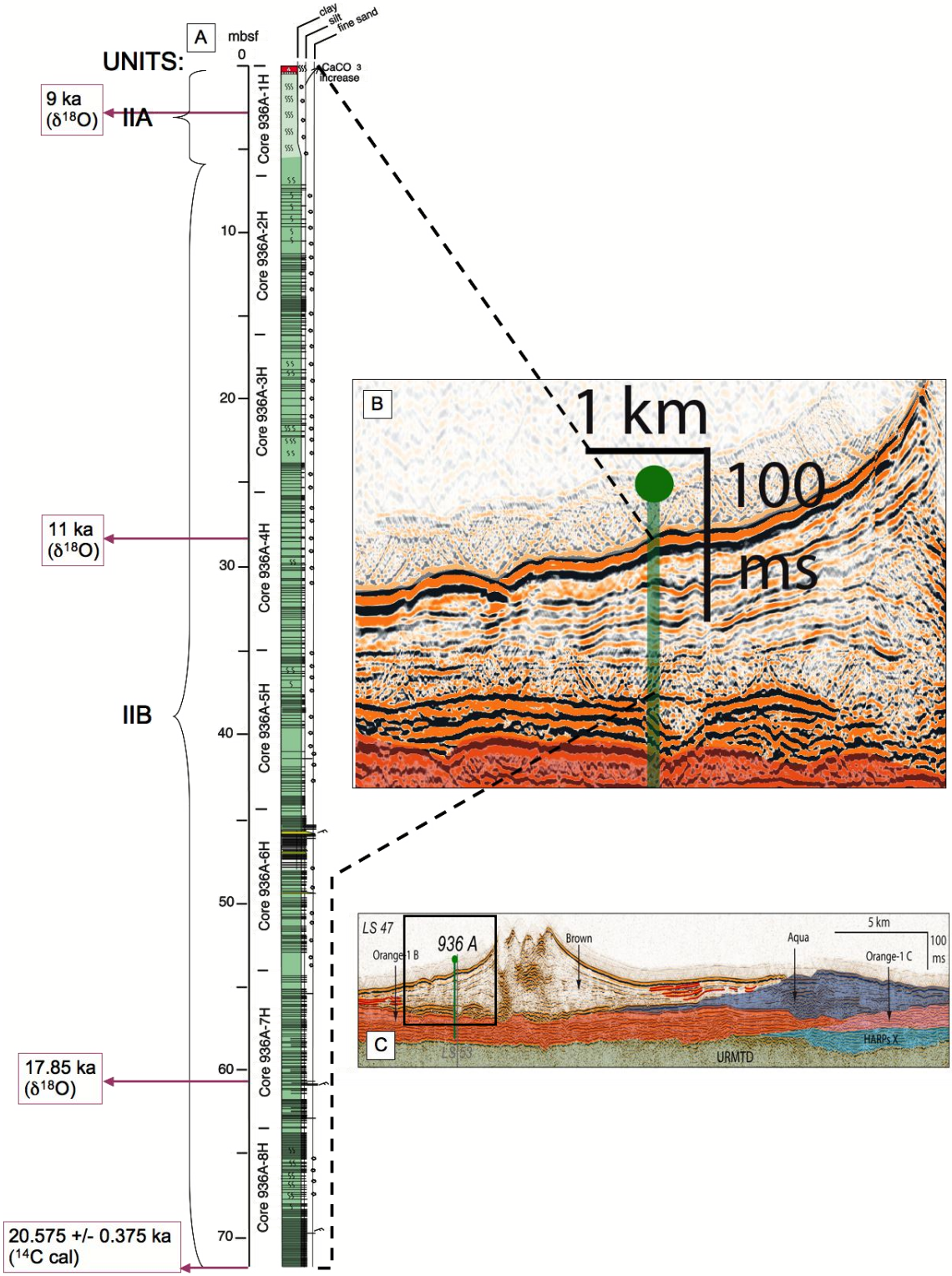

ANNEX III.2d: A: Synthetic log for the levee deposits at site 936. B: Zoom on cored facies. C: Interpreted seismic line showing localization of site and deposition systems.

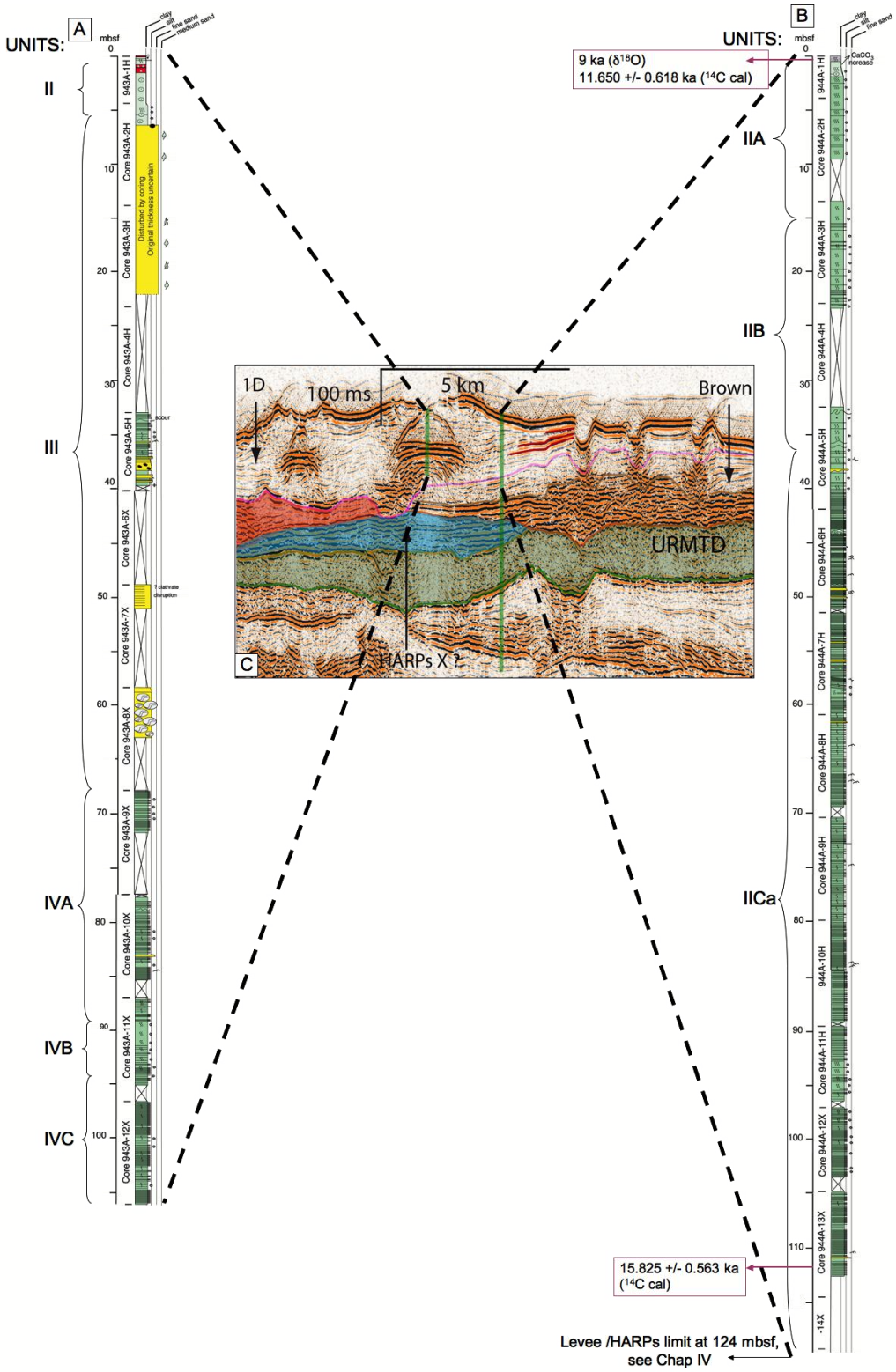

ANNEX III.2e: A: Synthetic log at sites 943 and 944. B: Zoom on cored facies. C: Interpreted seismic line showing localization of site and deposition systems.

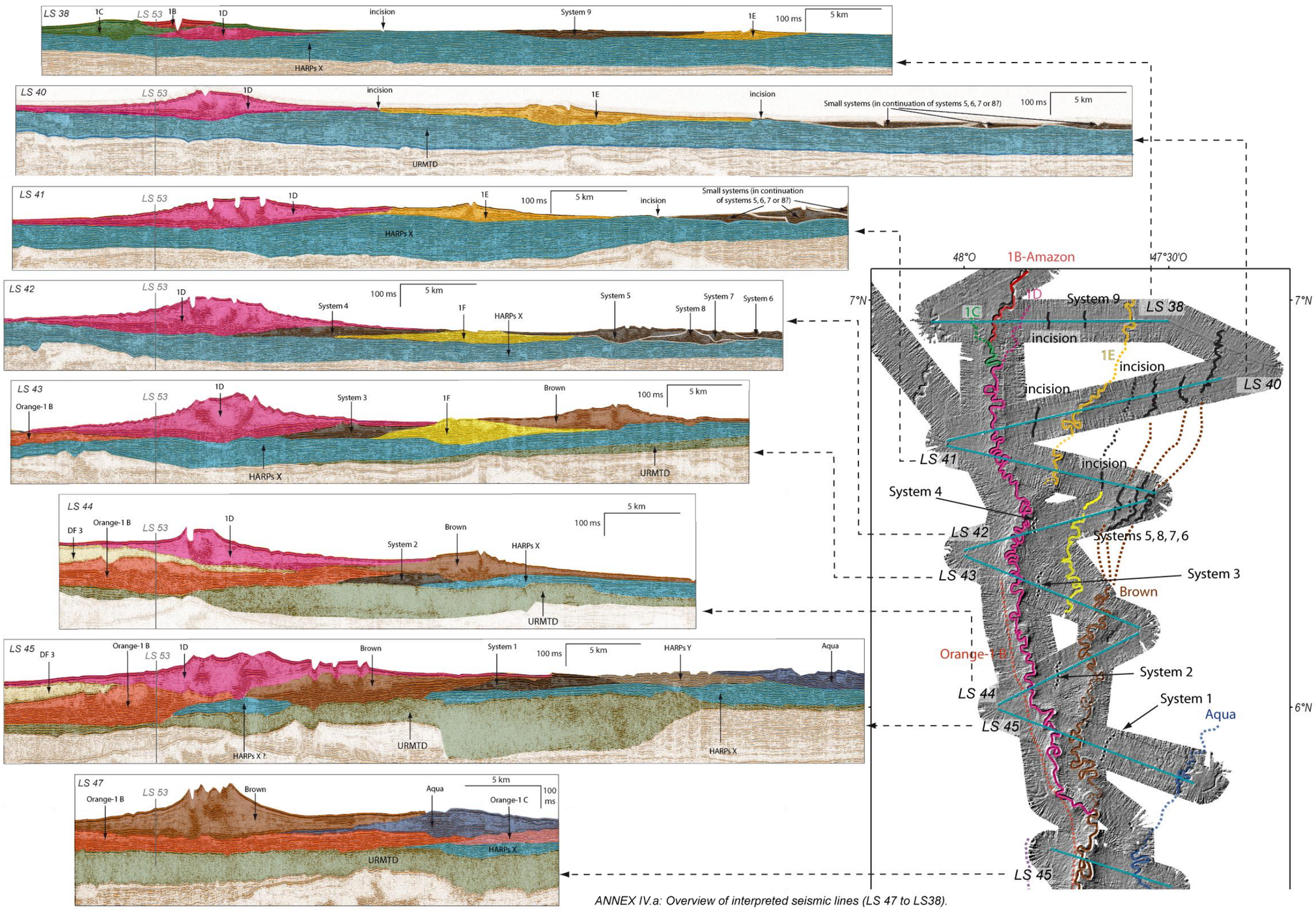

ANNEX IV.a: Overview of interpreted seismic lines (LS 47 to LS38).

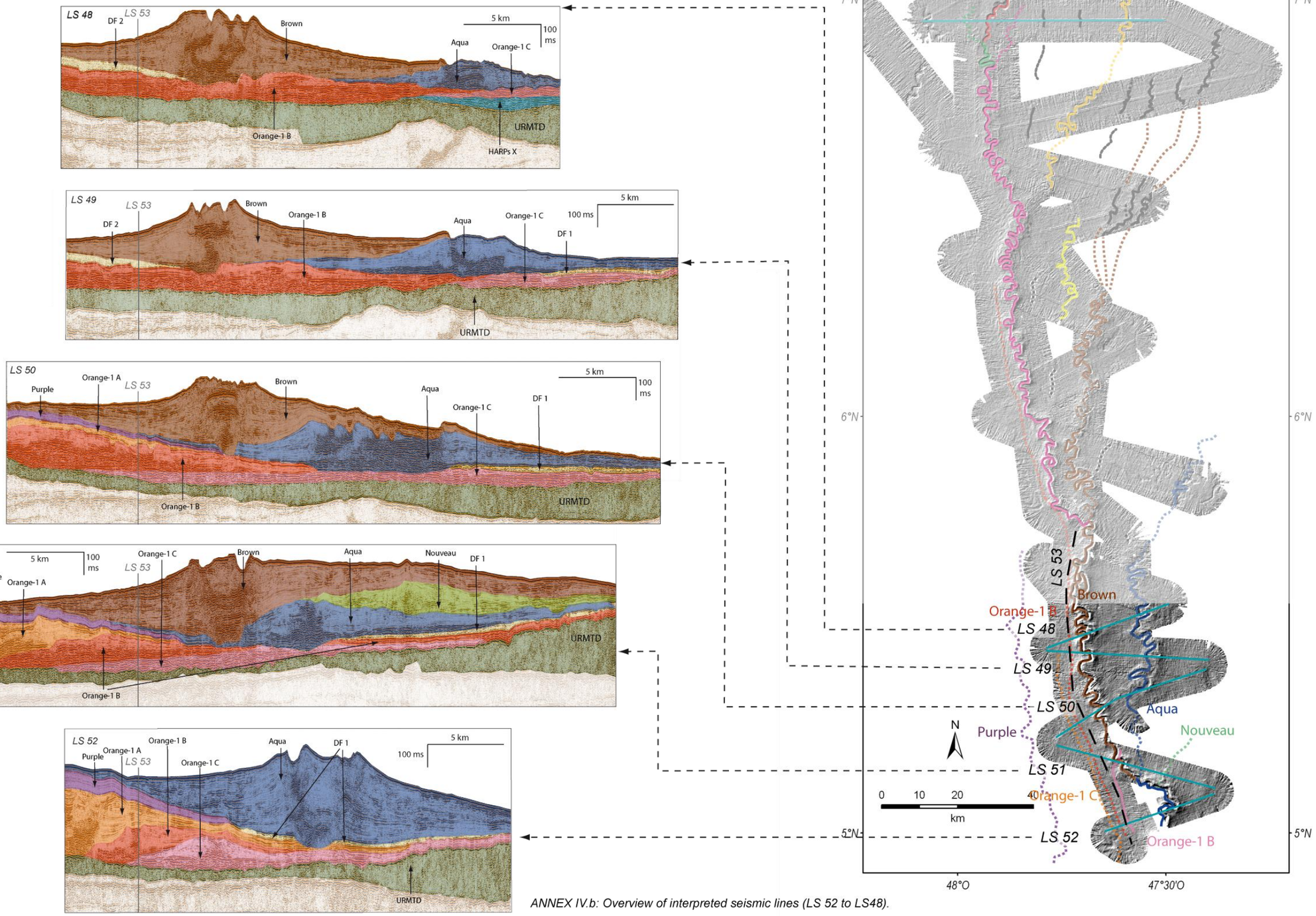

ANNEX IV.b: Overview of interpreted seismic lines (LS 52 to LS48).

Summary : Our study focuses on the avulsion process, the key for the depocenter migration of stacked channel-levee systems in the deep-sea. To present, the avulsion process has been explained as the abandonment of a channel (parent channel) and the birth of a new one (new channel). A true indice of avulsion has been given by the detection of the HARPs, a seismic term known since the 80s for high-amplitude reflection packets at the base of new channel-levee systems. The HARPs are suggested, in analogy to the studies from ODP Leg 155 of the Amazon Fan, to be sandy deposits in lows adjacent to breached parent channels.

Our present work, by re-visiting the Amazon Fan, highlights the great complexity of the HARPs architecture (at the scale of multi-channel high-resolution seismic data) and their lithological heterogeneity. The study of some specific zones within the Zaïre Fan allowed to reveal both the earliest stages of an avulsion process related to levee breaches and first splays linked to unconfined flows on the levee, and the latest stage of this process, with the first levee deposition and evolution following the HARPs deposition.

These results provide new insights for the understanding of the processes involved during an avulsion (levee breach, HARPs accumulation, levee aggradation) and clues to refine the previous conceptual models and to reach a higher resolution knowledge of this process, by describing the inter-relationship of the different architectural sub-bodies of the HARPs and giving details on both the earliest and latest stages of the avulsion.

Résumé : Grâce aux données de forages ODP du Leg 155, corrélées aux coupes sismiques haute résolution de la campagne Lobestory d'Ifremer, l'éventail géant de l'Amazone est devenu une zone privilégiée pour étudier l'évolution des systèmes chenaux-levées.

Les travaux antérieurs ont montré que le processus d'avulsion est un des processus fondamentaux de la construction des édifices turbiditiques. Il aboutit au changement brutal de cours d'un chenal et à son abandon en aval du point d'avulsion. Ce processus et les phénomènes qui en découlent (courants non-confinés, rupture de profil d'équilibre du chenal, …) ainsi que les conditions topographiques spécifiques sont à l'origine d'une distribution sédimentaire particulière, avec des dépôts grossiers (HARPs) en semelle des chenaux.

Dans le travail présenté, les paquets de réflecteurs de fortes amplitudes (HARPs) situés à la base de ces systèmes fortement aggradant, ont pu être caractérisés lithologiquement comme une amalgamation de petits unités sableuses et chenalisées probablement mises en place par une succession de courants de turbiditié de haute densité et très sableux.

Ces travaux ont été complétés par l'étude sismique et bathymétrique des premiers et derniers stades d'une avulsion, c.à.d. brêche de la levée chenal père et aggradation/progradation de levées après dépôts des HARPs, aux localisations spécifiques de l'éventail du Zaïre.

Ces résultats permettent de proposer un modèle d'évolution pour un système chenal-levées depuis les premiers stades de l'avulsion qui lui a donné naissance.